ANALYSIS OF RR LYRAE STARS OF THE NORTHERN SKY VARIABILITY SURVEY

By

KAREN KINEMUCHI

A DISSERTATION

Submitted to
Michigan State University
in partial fulfillment of the requirements
for the degree of

DOCTOR OF PHILOSOPHY

Department of Physics and Astronomy

2004

ABSTRACT
ANALYSIS OF RR LYRAE STARS OF THE NORTHERN SKY VARIABILITY SURVEY

By

KAREN KINEMUCHI

RR Lyrae variable stars are important astronomical objects for the investigation of the structure and evolution of the Milky Way Galaxy. These pulsating stars are known to be found in old populations in our Galaxy and have the useful feature that we can readily derive distances from them. With a large survey of the Galaxy, the RR Lyrae stars can be used to map Galactic structures.

The Northern Sky Variability Survey (NSVS), whose data was obtained through the Robotic Optical Transient Search Experiment (ROTSE-I) telescope, provides an opportunity to study RR Lyraes found near the Sun. The RR Lyrae stars can be detected up to 7-9 kiloparsecs from the Sun and can probe the inner halo and thick disk component of the Galaxy. This survey is an excellent complement to other Galactic surveys of the bulge and halo components.

We have found that almost 90% of the RR Lyraes in the NSVS survey are not included in the General Catalog of Variable Stars (Kholopov 1985). Our sample of RR Lyraes consists of approximately 1430 ab-type RR Lyrae and 375 c-type RR Lyrae candidates. We have determined the periods and amplitudes, and have derived phased light curves for these stars. Metallicity ([Fe/H]) of these stars was derived from the photometric data using empirical methods developed by Jurcsik & Kovacs (1996) and Sandage (2004). To derive distances, we made use of an M_V-[Fe/H] relation from Cacciari & Clementini (2003). We have also found that our sample of c-type RR Lyraes close to the plane is contaminated by other types of short period variable

stars.

RR Lyrae stars of both Oosterhoff I and II groups are present in the field population of RR Lyraes, but we find that the Oosterhoff I is dominant. A metal-rich group of stars was found in our ab-type RR Lyrae sample. These metal-rich stars were identified as belonging to the thick disk population. This metal-rich group was used to find the scale height of the thick disk. The result is approximately 0.4 kpc, which is lower than many estimates of the thick disk scale height. Our low value may indicate that a thin disk component may be present in our metal-rich sample. We have also found evidence for a mix of halo and disk populations for the metal-poorer ([Fe/H] < -1) RR Lyraes sample.

There is a need for additional kinematic information for these stars. The kinematics can help clearly associate the stars with their parent Galactic component population. The sample of the ab-type RR Lyraes used for analysis was restricted to a magnitude brighter than the actual limit of NSVS. The consequence of using this magnitude limit is the removal from this study of stars found 5 kpc or further from the plane of the Galaxy. The fainter RR Lyrae candidates need to be included in future work for a more complete analysis of the inner halo regions.

DEDICATION

This Ph.D dissertation is dedicated to Dr. Horace A. Smith, my advisor. He is the best role model for any graduate student. Not only is he a wonderful teacher and researcher, but a very caring and kind individual. He is the best possible mentor any student could ever wish to have. Horace has shown me that not all people in this field are rotten bastards, and that nice people do exist. I only hope that I grow up to be just like him.

ACKNOWLEDGEMENTS

This publication makes use of data products from the Two Micron All Sky Survey, which is a joint project of the University of Massachusetts and the Infrared Processing and Analysis Center/California Institute of Technology, funded by the National Aeronautics and Space Administration and the National Science Foundation.

This research has made use of the SIMBAD database, operated at CDS, Strasbourg, France.

This research has made use of NASA's Astrophysics Data System.

A big thank-you to Timothy McKay and the University of Michigan for providing a version of the NSVS database. Without their kindness, there would be no thesis. Thanks also go to Eli Rykoff and Don Smith at University of Michigan for all their help in the navigation of the dataset and in running their IDL routines. Thanks to Carl Akerlof, the principal investigator for the ROTSE projects, for spear heading this ambitious project.

I thank the ROTSE collaborators at the Los Alamos National Laboratory for allowing me to work on the ROTSE-I/NSVS dataset. Thanks to Katherine McGowan for graciously letting me stay with her during one of my visits. Thanks to Przemyslaw Wozniak and his energy to keep this project going.

I would like to thank Kem Cook and Anthony Miceli allowing me to use the Supersmoother period searching algorithm, as well as their helpful advice for running this code and interpreting the results.

Thanks go to Peter Stetson for his advice on the variability index used in this work. Without his clarity, the variable star catalog would still be a work in progress!

Thanks also go to Alex Schwarzenberg-Czerny for providing a version of his Analysis of Variance period searching program and prompt diagnosis to problems I encountered with this method.

Thanks to Joern Wilms and Sara Benlloch for providing the Lomb-Scargle period searching code for IDL.

Thanks to Brian Sharpee for supplying versions of his spline fitting routine to derive amplitudes and mean magnitudes.

Thanks to Timothy Beers for supplying the magnitude standard calibration relation and useful science discussions about the results.

Thanks to Christopher Waters for helping me produce figures 2.2 and 4.11, and for the useful discussions of statistical analysis.

And now the special thank you's....

Thanks to the thesis committee members: Dr. Horace A. Smith, Dr. Jack Baldwin, Dr. Timothy Beers, Dr. Wayne Repko, and Dr. S.D. Mahanti. Thanks for reading my funny "little" thesis. You missed my pirate joke! Thanks to Dr. Horace Smith for reading, re-reading, re-re-reading, and $n\times$re-reading the many drafts of the thesis and all the helpful comments.

Thanks to the Astronomy Group in the Physics & Astronomy Department at Michigan State University. Without their support and the pizza/relativistic-croquet-bbq/bad science fiction movie parties and their general sense of fun, I would not have had such a good graduate school experience. Thanks for putting up with my practical jokes and sense of humor.

Thanks to Amparo Alvarado, Shawna Prater, Debbie Simmons and all the secretaries in the department. I know who is really in charge of things around here!

Thanks to astronomy graduate students for being such a fun group of people. The sense of community we have is special and hopefully it will continue long after I am gone. And 1) write your thesis early, 2) save some money for the graduation process (there are a lot of hidden costs!), and 3) see you sometime at some conference somewhere.

Thanks to my office mates, Mike Davis, Aaron "Cluze" LaCluyze, Brian Marsteller, and Christopher Waters. Thanks for putting up with my Hello Kitty obsession, my swearing, and all my crap precariously balanced on my desk, ready to fall at a moment's notice.

Thanks to the people who made Freecell. The 12642 games helped keep my sanity while I was waiting for code to finish running.

Thanks to the professors who did NOT believe in me, who thought I was not graduate school material, who thought I would never make it in astronomy because I did not know how to program and the general bastards who tried to make me quit this field. Without your negativity, I would not have pulled myself up by my bootstraps and motivated myself to achieve getting a Ph.D. I suppose this thesis is proof to myself that I can do it.

Thanks to John Martin and Christopher Waters for their support throughout the whole Ph.D experience. A special thanks to Chris for making me understand being happy is the most important thing.

Okaasan to Otousan ni, arigatou gozaimasu. Yatto dekita nee!

Table of Contents

List of Tables

List of Figures

Chapter 1

Introduction

Variable stars provide valuable information, not only of the objects themselves, but of their parent systems, such as globular clusters. Stellar characteristics of variable stars give clues to physical processes within the stars. These stars have intricate stellar astrophysical properties that can describe the surroundings in which they are found (i.e. the structure of a galaxy). Analysis of the chemical composition of these variable stars also gives information about their histories.

All variable stars are interesting objects for study, and some have particularly important uses in different fields of astronomy. This dissertation will focus on one kind of variable star, RR Lyrae stars. Key to their importance is the ability to determine their distances from their apparent brightness (or magnitude). We will use the RR Lyraes from an all sky survey and investigate the stellar properties of these variable stars. From the properties, we investigate the history, or evolution, of the Milky Way Galaxy.

1.1 The Project

The Robotic Optical Transient Search Experiment (ROTSE-I) was originally designed to look for the optical counterparts to gamma ray bursters (Akerlof et al. 1999, 2000a). The telescope for this experiment sweeps the entire sky from Los Alamos, New Mexico, and tries to capture the optical flashes of the gamma ray bursters. While searching for these flashes, the telescope collects vast amounts of data by taking images of the sky continuously. This particular operation is referred to as "patrol" mode. The ROTSE team of scientists divided the observable sky from Los Alamos into 209 areas, which corresponds to $-30°$ in declination (δ) to $+90°$. This telescope was online 365 days a year, except during inclement weather.

Preliminary results on a variable star survey have been published in Akerlof et al. (2000b). These results were obtained from only five fields out of the 209, which corresponds to about 5% of the total sky surveyed by ROTSE-I. Their analysis of the five fields yielded 299 probable RR Lyraes, of which 89% were not listed in the General Catalog of Variable Stars (Kholopov 1985). Of these RR Lyrae candidates, some may have been misidentified (for example, some c-type RR Lyraes could be δ Scuti variable stars or other types of variable stars (Jin et al. 2003)). Nonetheless, any program with the potential to have such large numbers of newly discovered RR Lyraes can have the potential to reveal important information regarding the structure and history of our Galaxy.

1.2 Goals of the Dissertation

A large catalog of variable stars can be produced from the Northern Sky Variability Survey (NSVS), which is created from the observations of ROTSE-I. These variable stars, in turn, can be used as probes of the Galaxy. The variable star properties can tell us much about the structure, evolution, and kinematics of the Galaxy. For this project, RR Lyraes will be used as the diagnostic tool in the investigation of a 5 kiloparsec (kpc) region of the Milky Way Galaxy, centered near our Sun. The actual limit defined by the RR Lyraes in the survey may extend to 7 or 9 kpcs.

There are two main scientific objectives to this project. The first goal is to produce a catalog of the RR Lyraes found within the regions ROTSE-I observed. This part of the project is a collaborative effort with the ROTSE team at both the University of Michigan and Los Alamos National Laboratory. The second objective for this dissertation is to use the RR Lyraes from the catalog to probe the disk and inner halo components of the Galaxy.

One important advantage of the dataset obtained by the ROTSE-I telescope is its well sampled light curves. This is due to the observations being made from night to night for a span of a year (1999 to 2000). Most of the variable star candidates in the northern fields of the ROTSE-I survey have plenty of observations, and thus good quality light curves. Stars found in the southern fields or near the Galactic plane have fewer observations. The stars in the southern skies are more sparsely observed because the southern fields were not up in the sky as long as the northern fields. Stars in the Galactic plane tend to be underobserved because they have near neighbors or crowding issues so that photometry could not be cleanly determined.

Once light curve information has been produced for all the candidate variable stars, several steps must be taken in order to analyze the information the RR Lyraes can tell us. Due to the size of the dataset, automated methods (written in IDL and C) were preferred and used. The first major task is to identify all the variable stars

within the survey limits. The second task is to pick out the RR Lyraes from all the variable stars. Once the RR Lyraes are identified, the properties of these stars such as periods, brightnesses, and metallicities, must be determined.

The ROTSE-I dataset complements well other surveys. The OGLE and MACHO surveys cover the Galactic bulge, whereas QUEST and SDSS study the more distant halo of our Galaxy. The ROTSE-I survey fits in between these surveys of the bulge and the halo. Because of its coverage of the Galaxy, the ROTSE-I dataset can allow one can look at the stars in the transition region from bulge to halo, as well as the thick disk. The properties of those stars should help to clearly associate the stars with particular galactic populations.

With such a wealth of information locked in the survey, many questions can be answered, as well as generated, about the Galaxy, specifically about its field population, and about the stars themselves. Do we find support for one particular galaxy formation scenario over another? Do we find different populations of RR Lyraes within the region of the NSVS survey? The RR Lyraes should provide tantalizing clues about the nature of the thick disk and inner halo component of the Galaxy.

The dissertation is organized in the following manner. Chapter 2 will provide an overview of the RR Lyraes, astronomical terms, and a brief description of the galaxy formation scenario we will be investigating. The instrumentation and data acquisition of the ROTSE-I telescope will be described in Chapter 3. Chapter 4 will discuss the work done to calibrate and to determine the parameters of the RR Lyraes. Chapter 5 will focus on the some of the basic results from the RR Lyraes of the NSVS survey. Chapter 6 contains an in depth discussion of the results and their implications for Galactic structure. Suggestions of future projects stemming from this dissertation as well as problems encountered in the analysis are presented in Chapter 7.

Chapter 2

Background on RR Lyrae Stars

2.1 RR Lyrae Variable Stars

RR Lyrae variable stars are very important objects to study in astronomy. They are excellent distance indicators since these stars are both luminous and ubiquitous in the Galaxy. These stars have a periodic change in brightness which makes RR Lyraes easy to find. RR Lyraes are pulsating stars, which means as there are changes in brightness, size and temperature of the star.

A Hertzsprung–Russell (HR) diagram, which plots brightness (or magnitude) versus temperature (or color), shows where RR Lyrae stars are in relation to other types of stars, both variable and non-variable. Figure 2.1 shows a simple color-magnitude diagram (CMD), which is a version of an HR diagram. The diagram depicts the evolutionary sequences found in a globular cluster or other old population of stars. RR Lyraes are low mass ($\sim 0.7 M_{\odot}$) Population II objects, which means they represent an older population of stars (Smith 1995).

In evolutionary terms, these stars have stopped fusing hydrogen in their cores and

are burning helium for the main energy generation. Some amount of energy is also being produced in a shell of hydrogen burning surrounding the helium burning core. Generally, if a low mass star is burning helium in the core, this places the star in the horizontal branch on the CMD. Furthermore, RR Lyraes are only found in one specific part of the horizontal branch. This location is the "instability strip", a zone that crosses the horizontal branch and that contains pulsating stars.

RR Lyrae stars are found in all components of the Galaxy: the bulge, disk, and halo. They are also found in globular cluster systems as well as extragalactic objects of the Local Group such as the Magellanic Clouds, dwarf spheroidal galaxies, and M31. RR Lyrae stars trace the old parent population in which they are found. In this dissertation, we will be investigating RR Lyraes of the field population (not associated with a globular cluster) of the thick disk and inner halo in the vicinity of the Sun.

2.1.1 Subtypes of RR Lyraes

The period of the pulsation cycle can be determined from the time evolution of the light variation, i.e. the "light curve". From the light curves, we can also obtain the amplitude of the change in brightness. These two properties (period and amplitude), along with temperature and other characteristics are used to classify the RR Lyraes into subtypes. RR Lyraes can be divided into three main groups: RRab, RRc, and RRd.

The "ab" and "c" divisions of RR Lyraes are called Bailey types (Bailey 1902). "RRab" RR Lyraes are the most abundant form of these stars. There are small differences between Bailey type "a" and "b", but these stars are usually lumped

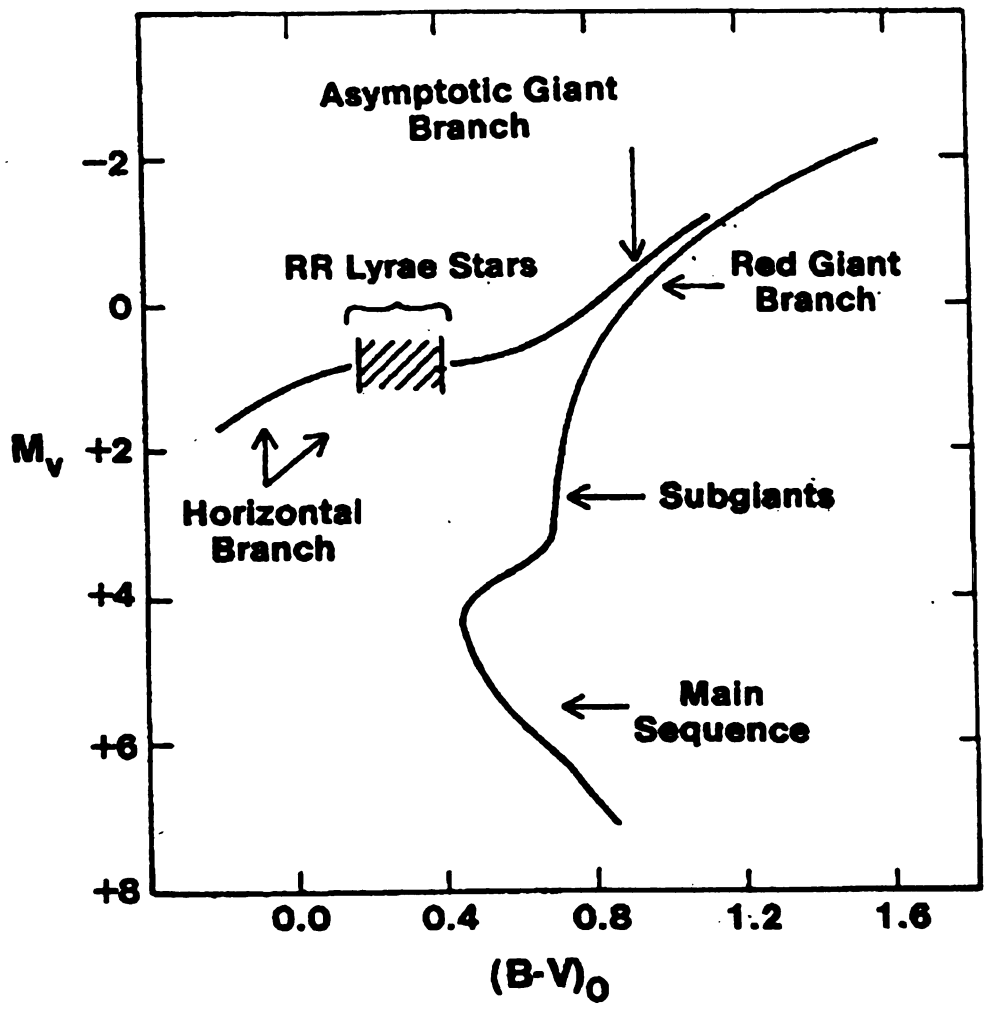

Figure 2.1 Example Hertzsprung-Russell diagram (Smith 1995).

Table 2.1. RR Lyrae properties (Smith 1995)

Property	RRa	RRb	RRc
Period (days)	0.5	0.6	0.3
Temperature (Kelvin)	6300	6100	7400

together as "ab". A Bailey type "a" RR Lyrae has a period around 0.5 days and an asymmetric light curve shape. The amplitude of the light curve is approximately 1 magnitude in the V passband. The "b" type RR Lyrae periods are slightly longer, averaging 0.6 days. The light curves are also asymmetric, except the amplitude is shallower, ranging between 0.5 and 0.8 magnitudes (Petit 1987, Smith 1995). It has been observed that shorter period RRab stars have larger amplitudes whereas the longer period ones have smaller amplitudes.

Both the RRa and RRb stars are pulsating in the fundamental radial mode. The fundamental pulsational mode has a single node in the center of the star. The best analogy would be an oscillating string attached at one end while the other end is free. This mode is often referred to as the "breathing" mode. However, the pulsation is actually negligible at the star's core and is significant only in the star's outer envelope.

Bailey type c RR Lyraes have a shorter average period near 0.30 days. The RRc light curves are more sinusoidal in shape than the RRab light curves, but usually display some asymmetry. The amplitude of the light curve averages to about 0.5 magnitudes in V. The pulsational mode for RRc stars is the first overtone radial mode. This mode is characterized as having a node in the center of the star and another somewhere in the stellar atmosphere. Table 2.1 summarizes the important properties of RR Lyraes.

The third major type of RR Lyrae is the double mode RR Lyrae or "RRd". These

are not as numerous as the RRab or the RRc types. The RRd stars pulsate in both the fundamental and first overtone modes. Hence, their light curves appear to have more scatter than normal when they are plotted with any single period. One can deconvolve the light curves to find the corresponding light curves of the fundamental and first overtone modes. RRd first overtone periods range from 0.390 to 0.429 days (Smith 1995), and they are often lumped together with the RRc stars.

Another category of RR Lyraes has been recently proposed, the second overtone RR Lyraes, or "RRe" type (Clement & Rowe 2000, Clement et al. 2001). These RR Lyraes are even more rare than the RRd stars, and astronomers have disputed whether they exist or not. They are characterized by short periods, smaller amplitudes than the RRc stars, and sinusoidal light curve shapes. Because of their low amplitudes and light curve shapes, it is often difficult to distinguish RRe stars from other types of short period, low amplitude variable stars.

The MACHO consortium (Alcock et al. 2000) has advocated a new naming convention for the RR Lyraes. Rather than using the Bailey type nomenclature of RRab and RRc, the new system refers to them as "RR0" and "RR1", respectively. Double mode RR Lyraes are designated as RR01, and the second overtone RRe stars as RR2 (Clement et al. 2001). We will not be using this new naming convention for RR Lyraes.

In the history of observing RR Lyrae variables, a long term secondary modulation of the light curve has been detected for some of these stars. This phenomenon is called the Blazhko Effect, after S. Blazhko, who first discovered it in RW Dra (Blažko 1907). The Blazhko effect can easily be seen in the shape of the light curve. The period of the star remains the same, but the amplitude of maximum changes. Often it is revealed because it produces noisy looking light curves when the curves are plotted according to just the primary period. The period of this secondary modulation can be anywhere

from 11 to 533 days (LaCluyzé et al. 2004). This effect is predominantly seen in RRab type RR Lyraes, but also has been observed in RRc types. The Blazhko effect appears to affect roughly 20-30% of the known RR Lyraes in our Galaxy (Kovács 2001) and stars exhibiting the Blazhko effect are found in the field population, in Galactic globular clusters, and in other nearby galaxies. Unfortunately, the mechanism for the Blazhko effect is unknown. It has been speculated that the cause of the Blazhko effect could be related to either magnetic fields or resonance with non-radial pulsation (Cousens 1983, Moskalik 1986, Kolenberg 2004).

In the CMD, the RRab and RRc stars appear in different regions within the intersection of the instability strip and the horizontal branch. This is determined by the temperature of the RR Lyraes. The RRab stars have an effective temperature of approximately 6100 K whereas the RRc stars are hotter at 7400 K (Smith 1995). Thus, the RRab stars are located in the red end of the instability strip and the RRc type stars in the blue end. It has been speculated that RRd stars are those RR Lyraes evolving from one side of the instability strip to the other. This could explain the existence of the double mode pulsation observed in RRd stars. However, RRd type stars are not observed ubiquitously. Some systems contain these stars, while in others they are absent.

2.1.2 Pulsation Mechanism

The pulsation of a variable star, such as an RR Lyrae, can be described by Ritter's relation:

$$Q = P\sqrt{\rho} \tag{2.1}$$

This relation relates the pulsational period (P) with the density ρ of the star. Q is

the pulsational constant. If the constant Q is known (for example, from theory) and the pulsational period is also known, parameters such as radius, temperature, and mass of the star can be determined.

Many pulsating variable stars can be best described as driven by the κ mechanism. For this mechanism to work, the star must have a partial ionization zone of an abundant element at the right depth in the stellar envelope. This partial ionization zone is often referred to as the "Eddington Valve" after Arthur Stanley Eddington, who first noted the need of such a "valve" to maintain stellar pulsation. This zone can be comprised of either neutral hydrogen (HI) and singly ionized hydrogen (HII) or singly and doubly ionized helium (He II). An ionization zone that contains the HI to HII transition will have a characteristic temperature of 10000 to 15000 K. An He II ionization zone is found deeper in the atmosphere and has a characteristic temperature of 40000 K (Carroll & Ostlie 1996).

The κ mechanism can be described starting with a star being perturbed away from hydrostatic equilibrium. Usually, such perturbations will damp out in a star in a relatively short time scale. In order to keep this perturbation, or pulsation, going some kind of driving mechanism is necessary. Eddington's valve is just such a driving mechanism. For the "valve" to work effectively, it must block off the outflow of energy when the star is at maximum compression. This then leads to a pressure maximum after the star reaches maximum compression. This provides the star the necessary "kick" to start it expanding again. At this point, the valve must open and release the energy. The star then expands and cools.

The opacity (κ) in the partial ionization zone contributes to the Eddington valve driving mechanism. Opacity is a quantity that describes the cross section for photons (of a particular wavelength) to be absorbed by a given mass of stellar material.

Usually, in stellar envelopes, the opacity can be described by Kramer's opacity law:

$$\kappa = \rho T^{-3.5} \tag{2.2}$$

where T is the temperature and ρ is the density. Kramer's opacity law can explain the usual case where the star is most transparent when it is compressed and at its hottest. However, this is not what we want for the valve. Rather, the partial ionization zone should follow an opacity law that scales as ρT^{-s}, where s is smaller than 3.5 or even negative (King & Cox 1968). Thus, back in the pulsation scenario, as the star contracts and compresses, the opacity increases in the ionization zone, and the radiation is essentially blocked. When the stellar envelope expands and cools, the partial ionization becomes less efficient at blocking the radiation. At this expanded state, the hydrostatic equilibrium is not balanced. The star will contract again to achieve this state. Thus, this sets up the cycle for pulsation.

Another way for the partially ionized zone to act as an Eddington Valve is through the γ-mechanism (King & Cox 1968). Essentially, the partial ionization zone will absorb heat during the compression phase of the pulsation cycle. This phenomenon can happen because the heat energy going into the zone does not raise the temperature of the material. Rather, this energy goes into ionizing the gas in the zone. Thus, the ionization zone can absorb more heat/energy during the compression. Then, at this point in the pulsation cycle, the pressure in this zone will again approach a maximum after the minimum volume is achieved from compression. This provides a "kick" to the outer layers and drives the pulsation.

2.1.3 RR Lyraes as Distance Indicator

One of the most important characteristics of RR Lyraes is that we can readily derive their distances. These stars are distance indicators called "standard candles". The distance to the objects are calculated from the distance modulus:

$$m - M = 5 \times Log_{10}d - 5 \tag{2.3}$$

Magnitudes are a logarithmic scale of brightness, where the fainter the object, the larger the magnitude value. Bright objects can even have negative values. In Equation 2.3, to determine the distance (in units of parsecs), one must have the difference in the apparent magnitude, m, and the absolute magnitude, M (or M_V if in the Johnson V filter system). The apparent magnitude is simply the observed brightness. The absolute magnitude is the brightness an object would have if it were placed 10 parsecs away from the observer. RR Lyraes are an excellent distance indicator because there is a narrow range of absolute magnitudes for these objects and because they are comparatively bright stars, visible to very large distances.

Unfortunately, the absolute magnitudes of RR Lyraes are dependent on at least one quantity, metallicity. Metallicity, or [Fe/H], of a star or celestial object refers to the relative amount of heavy elements (elements other than hydrogen or helium) compared to the amount found in the Sun. The value of [Fe/H] is actually a logarithmic ratio of the iron to hydrogen abundance of the star to the iron to hydrogen abundance in the Sun.

$$[Fe/H] = \log(\frac{N_{Fe}}{N_H}) - \log(\frac{N_{Fe}}{N_H})_\odot \tag{2.4}$$

For example, if a star has an [Fe/H] of -2, the Sun has 100 times more iron than this star. [Fe/H] is often used as a proxy for the overall heavy element abundances of a star. If the metallicity of a collection of stars in a star cluster or dwarf galaxy is

known, that metallicity is often assigned to that parent object as its own metallicity. For the case of this study, the metallicity of the individual RR Lyraes are determined from an empirical relation, which is discussed in detail in Chapter 4.

Several different methods are used to derive the absolute magnitude as a function of metallicity and it is, unfortunately, still an issue of some contention. Different methods of obtaining M_V have various uncertainties and different systematic errors. Thus, the published values of M_V have a range from as bright as 0.45 magnitudes to as faint as 0.77 magnitudes for a metal-poor RR Lyrae population (Layden et al. 1996, Popowski 2001).

The average absolute magnitude of RR Lyrae stars is usually parameterized as

$$\langle M_V \rangle = a + b[Fe/H] \tag{2.5}$$

which may be oversimplified. Thus, there are two parameters that need to be determined: the zero point and the slope of the relation. There is a general agreement that the more metal rich stars have fainter M_V values. Some M_V-[Fe/H] relations are discussed in Bono et al. (2003), Chaboyer (1999), and Cacciari & Clementini (2003).

Some of the methods of finding M_V include: trigonometric parallax, statistical parallax, the Baade-Wesselink method, and the usage of the double-mode RR Lyrae properties (Benedict et al. 2002). The trigonometric parallax is the simple geometric measurement of the distance to a star, using the orbit of the Earth around the Sun as a baseline. Statistical parallax is a more difficult measurement since it needs kinematic information on these stars, namely proper motions and radial velocities. The Baade-Wesselink method uses the varying color, light and radial velocity information to obtain distances and absolute magnitude (Carretta et al. 2000). Other versions of the Baade-Wesselink method include the surface brightness method and the use of

infrared flux (Cacciari et al. 1992). Double-mode RR Lyraes, although rare, can also be used to determine M_V from the ratio of their fundamental to first overtone mode periods. This ratio is related to the mass and using a mass-luminosity relation, absolute magnitudes can be derived (Carretta et al. 2000).

For this dissertation, I will use the M_V-[Fe/H] relation of Cacciari & Clementini (2003), which is consistent with most recent results. The Cacciari-Clementini relation is given below:

$$M_V = (0.17 \pm 0.04)[Fe/H] + (0.80 \pm 0.10) \quad \text{for} \quad [Fe/H] < -1.5 \tag{2.6}$$

$$M_V = (0.27 \pm 0.06)[Fe/H] + (1.01 \pm 0.12) \quad \text{for} \quad [Fe/H] > -1.5 \tag{2.7}$$

2.2 Galactic Structure

The luminous part of the Milky Way Galaxy can be broken up into three main components: the central bulge, the disk, and the halo. Each component has its own distinguishing characteristics, as defined by its stars and the stellar systems. Numerous surveys have been conducted to investigate the components and their properties (such as metallicity or rotational velocity). Some notable Milky Way Galaxy variable star surveys are the OGLE and MACHO surveys of the Galactic bulge, and the SDSS and QUEST surveys of the outer halo. These surveys produced catalogs of RR Lyraes found in each component of the Galaxy. This dissertation will focus in the region of the inner halo and thick disk centered around the Sun, which is a region intermediate to those covered in other surveys. More details about the ROTSE-I

survey and its database are presented in Chapter 3. Here, we will briefly discuss each Galactic component, and the reader is directed to Figure 2.2 for a rough diagram of the Galaxy.

2.2.1 The bulge

The central bulge is often a difficult Galactic component to observe in the optical wavelengths due to dust obscuration. Often, studies of the bulge, where it is close to the Galactic center, must be done in the radio or infrared wavelengths, in which dust is more transparent. Stars of the bulge have a spheroidal distribution, like the halo component, though studies have shown that a bar may exist in this region as well. Astronomers have found that the bulge stars are also quite metal rich, averaging around $[Fe/H] = -1$. The range in metallicity for the bulge has been observed to be between [Fe/H] $= -1.25$ and 0.5 (Binney & Merrifield 1998).

2.2.2 The disk

The disk can be considered to be comprised of two components: the thin disk and the thick disk. The stars in both the thin and thick disk have a flattened distribution, with the former more flattened than the latter. Disk stars also generally have circular rotation around the Galactic center.The thin disk, with its scale height of roughly 300 parsecs, contains a mix of young and old stars. The thin disk is generally more metal rich (with $-0.5 < [Fe/H] < 0.3$) than the thick disk (Carroll & Ostlie 1996). It is generally believed that the thin disk may have had a different origin than the thick disk, but they have interacted with each other as they evolved.

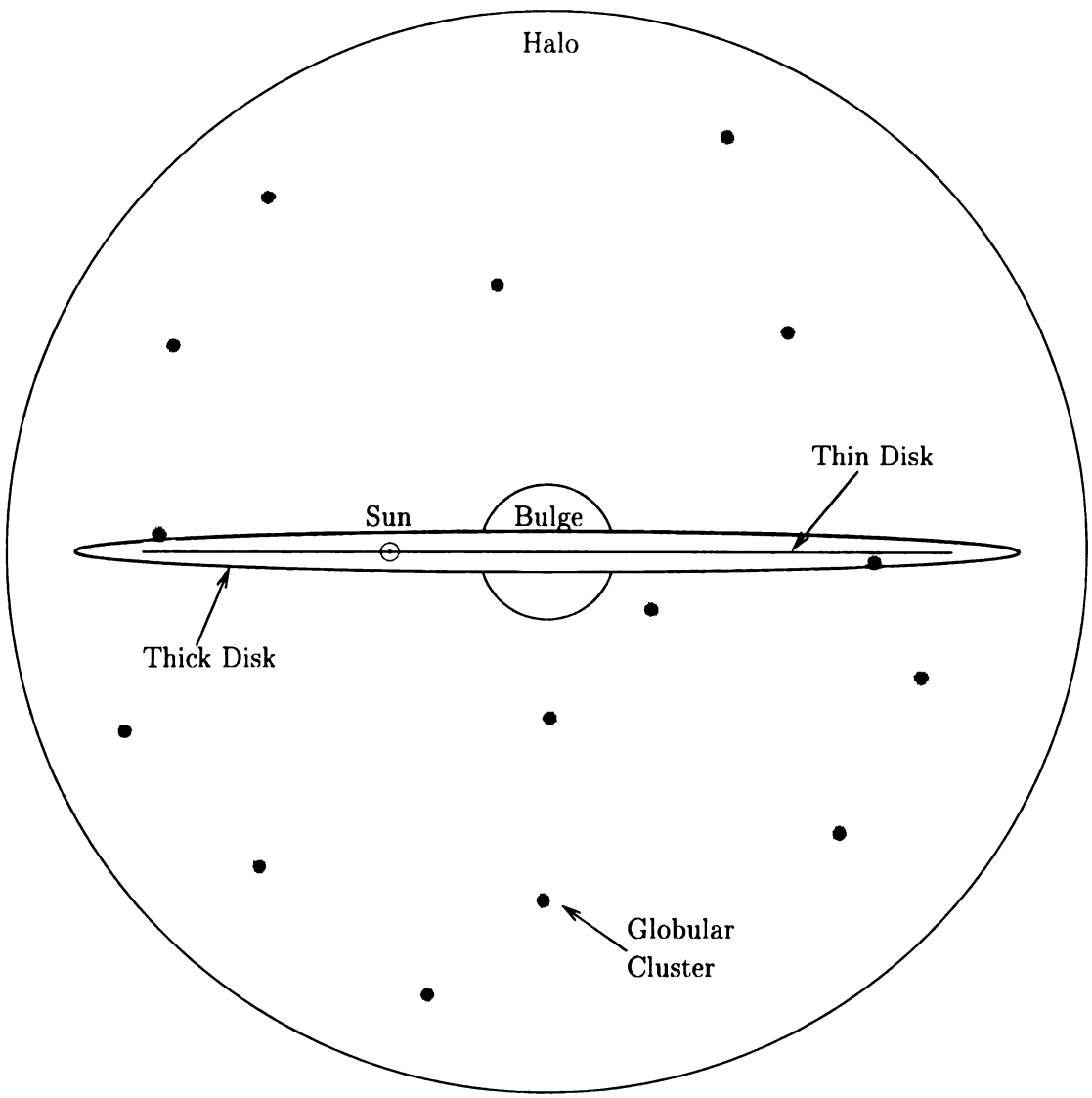

Figure 2.2 Diagram of the Milky Way Galaxy

The thick disk contains older and more metal poor stars. The thick disk has a scale height of approximately 1 kiloparsec. The thick disk stars have an average [Fe/H] of -0.6, but can range down to -2 (Chiba & Beers 2000 Beers, private communication). Several different scenarios have been developed to describe the formation of the thick disk. A brief outline of these possible scenarios are listed in King et al. (1990).

2.2.3 The halo

The halo component of the Galaxy is mostly composed of old stars in a roughly spherical distribution that is symmetric about the Galactic center. Studies have shown that the inner regions of the halo have a more flattened distribution than the outer regions (Hartwick 1987, Carney et al. 1996, Sommer-Larsen et al. 1997, Chiba & Beers 2000). Globular clusters and field stars found within the halo indicate a density fall off that can be described by a -3 or -3.5 power law with increasing distance from the Galactic center. The orbits of the halo stars have been observed to be highly eccentric. Overall, the halo stars appear to have a rotation about the Galactic center that is much smaller than the disk stars (but see the discussion in section 2.3.3). Studies of the halo objects have also shown the lack of a metallicity gradient beyond about 10 kpc from the Galactic center (Rich 1998, Suntzeff et al. 1991). The mean metallicity of the halo has been estimated to be around [Fe/H] = -1.6, with a spread of $\sigma \sim 1$ dex[1] (Carney et al. 1996). Compared to the disk, the halo must have had a very different origin and evolutionary processes.

[1]dex is an increment in base 10 logarithm.

2.3 Galactic Formation Models

One of the big questions in astronomy is how our Galaxy formed. Using the observations collected in catalogs and surveys, and results of theoretical simulations, two major models were produced in the early 1960s and late 1970s. Eggen, Lynden-Bell, & Sandage (1962) (hereafter referred to as "ELS") described the Milky Way Galaxy forming from a monotonic collapse of a large protogalactic cloud. Searle & Zinn (1978) (hereafter referred to as "SZ") advocated a chaotic merger/accretion scenario of small sub-galactic "fragments". Many observational results were used to develop these models for formation of the Galactic features.

However, the current picture of the Galaxy has made things complicated. Some astronomers have suggested the existence of a "dual halo" component of our Galaxy and have required a galaxy formation model that best explains this. Neither ELS nor SZ alone can explain this feature in the halo. One possibility that has been supported by many astronomers is a hybrid scenario of the two main models. This new composite model, coupled with the hierarchical assembly of cold dark matter (CDM) (Peacock 1999, Longair 1998), has emerged to describe the features found in the Galaxy's dual halo.

In this section, the two main "classical" galaxy formation models are discussed briefly. In the last subsection, a description of the hierarchical assembly scenario and observational evidence supporting the existence of a dual halo are presented.

2.3.1 Eggen, Lynden-Bell, and Sandage (ELS) Model

The ELS, or the "top-down", model envisions a proto-Galaxy as a large gas cloud with some angular momentum undergoing a systematic collapse. This monotonic

collapse was estimated to occur in a time span of $\sim 10^8$ years, which is a rather rapid collapse comparable to the free-fall collapse time of the proto-Galactic cloud. Stars formed early during the collapse episode became the observed metal-poor stellar halo population we see today. These early stars are now observed to have highly eccentric orbits. The more massive early stars have evolved to the supernova stage during the collapse episode and helped enrich the interstellar medium. In the radial direction, the collapse of the gas was stopped by rotation, but it continued in the z direction (using the sense of cylindrical coordinates). This latter collapse is believed to have formed the rotating disk. Thus, in the now denser disk, star formation is encouraged and increased.

The kinematically hot gas in this proto-Galaxy helped to dissipate the collapse energy and condensed into the central region (now the Galactic bulge). The gas, and any stars formed from this gas, began to orbit in a circular motion. Meanwhile, stars in the halo still follow the eccentric orbits from the collapse episode. The old population of stars observed in the bulge that are metal rich are stars formed from the enriched gas, due to supernovae deaths of halo stars formed even earlier in the collapse.

There are certain aspects of the ELS model that are no longer viable. One aspect is the observed motion of the halo stars and globular clusters. Many of the halo objects are moving with retrograde motion or have net 0 rotational velocity. Under the ELS description, all the halo stars and globular clusters should be moving in the same direction. Even if there were some chaos in the collapsing cloud of this model, the halo systems would be expected to still have a small net rotation in the same sense as the disk. Under this model, no substantial halo subsystem would have a net retrograde motion. The halo stars, under this model, also are expected to have a correlation between metallicity and the eccentricity of their orbits. As the cloud

dissipates and the orbits of these newly formed halo stars are less plunging, the cloud enrichment is also greater. The existence of this correlation has been disputed.

The globular clusters themselves also provide contradictions to the ELS model. Variations in chemical composition and cluster age have been observed in both the bulge and halo components. The bulge globular clusters are generally metal-rich and old (although there are exceptions), whereas the halo population, in general, has a wide variety of metallicities and a range of ages. The large range in age (several billion years) indicates that no rapid formation occurred.

2.3.2 Searle and Zinn (SZ) Model

In the SZ model, protogalactic cloud "fragments" gravitationally coalesce to form the Galaxy. These cloud fragments have masses on the order of 10^6 to $10^8 M_\odot$ and are assumed to be spherically distributed about the proto-Galaxy. This model assumes a rapid collapse for the central (and more mass concentrated) region of the proto-Galaxy. Globular clusters in this region should have roughly the same cluster age.

The outer halo, however, formed more slowly (longer than 10^9 years). From collisions and tidal disruptions of the cloud fragments, the outer halo globular clusters formed. These parent cloud fragments were still in the process of being chaotically accreted onto the Galaxy when these globular clusters were forming.

SZ proposed that the outer cloud fragments evolve independently of each other and of the proto-Galaxy. Supernovae self-enrich these fragments. Thus, these fragments would have their own unique chemical composition, globular cluster systems, and stars. These evolutionary processes in the fragments are slower than the similar processes that formed the bulge.

Kinematically, these cloud fragments become tidally disrupted and accrete onto the halo, or even the disk. The stars and clusters from the fragments are expected to retain the eccentric orbits of the parent fragments. The retrograde motions observed in some of the outer halo stars are best described by this scenario. The chaotic accretion/merger events also predict a range in age and chemical composition (but no metallicity gradient) for the stars and globular clusters of the outer halo, which has been observed. However, the SZ model does not adequately explain the observed metallicity gradient in the inner halo component. The ELS model with a dissipative collapse episode predicts this feature.

2.3.3 Hierarchical Galaxy Formation

As larger surveys become available for study of the kinematics and chemical abundances of the stellar population of the Milky Way Galaxy, questions arise over the results. One wonders which galaxy formation scenario can explain the trends in the observed properties of various tracer objects in each Galactic component (RR Lyraes, horizontal branch (HB) stars, etc.). Many investigators have called for a hybrid of the ELS and SZ models, since neither can completely explain all of the observed trends (Hartwick 1987, Carney et al. 1996, Sommer-Larsen et al. 1997). These observed trends, and the discrepancies will be discussed at the end of this section.

Recently, astronomers have tried to apply the hierarchical assembly of CDM model to explain the formation of the Milky Way (Bekki & Chiba 2001). Since this work focuses on the thick disk and inner halo of our Galaxy, the model developed by Bekki & Chiba (2001) is particularly apropos.

The hierarchical assembly of CDM (Peacock 1999, Longair 1998) requires that

the lowest mass objects form first. These objects, or "clumps" will cluster and coalesce. These processes are influenced by the underlying perturbations in the cosmic microwave background (CMB). It is expected that the large scale structures in the universe are built up by these clumps coalescing together. This model has conceptual similarities with the SZ model and can be applied in larger scales than the Milky Way Galaxy.

Bekki & Chiba (2001) apply this hierarchical assembly model in their numerical simulations for the formation of the Galaxy. They describe the Galaxy formation in the following manner. The proto-Galaxy starts off as in the ELS model, gravitationally collapsing. While this is occurring, subgalactic fragments that have relatively low mass form in large numbers. The clumps are predicted by the small-scale perturbations requisite in the CDM hierarchical assembly model. The clumps merge into our Galaxy with or without dissipation, and thus gradually build our Galaxy. In particular, the halo is constructed by these clumps without any dissipation. Different mechanisms are involved in the formation of the inner halo, but essentially, a dissipative merger of clumps and collapse is required. Additionally, stars will form in the clumps, and die, thus enriching the environment with metals. The clumps will merge and become progressively more massive. The largest central conglomeration will become the bulge. The subgalactic clumps and gas from the halo will continue to accrete into the bulge and help form the disk of the Galaxy. However, this model has not been fully tested to recreate all the observed structure, kinematics, chemical abundance properties, and explicit formation of the stellar Galactic halo.

The Bekki & Chiba (2001) model helps explain a possible dual halo nature in our Galaxy. Several studies have advocated the existence of a dual halo component (Hartwick 1987, Norris 1994, Carney et al. 1996, Sommer-Larsen et al. 1997, Chiba & Beers 2000). An important feature of this dual halo is the stellar distribution. It has

been observed that the inner halo ($R_{gc} < 15$ kpc) is flattened whereas the outer halo has a spherical distribution. This has been observed through surveys of RR Lyraes (Hartwick 1987), blue HB stars (Kinman et al. 1994), and metal-weak stars (Chiba & Beers 2000).

The inner halo, in addition to its flattened distribution, has interesting features that are clues to its formation history. A metallicity gradient has been observed for galactocentric distances less than 10 kpc (Zinn 1993, Sommer-Larsen et al. 1997, Suntzeff et al. 1991). Kinematically, Sommer-Larsen et al. (1997) report that the inner halo stars are moving in a more radial direction with respect to the Galactic center rather than tangentially. One proposed characteristic, a net prograde motion of the inner halo stars, has garnered some dispute. Norris (1994) found the inner halo stars to have disk-like properties and to be kinematically "hot" (i.e. having large velocity dispersions) with a prograde motion. Carney et al. (1996) argue that the inner halo stars observed in their survey were "cooler" kinematically than Norris's results and are rotating about the Galactic center more slowly than the metal-rich thick disk stellar population. Carney et al. also supported a prograde motion (average rotational velocity $\langle v_{rot} \rangle = +27 \pm 7$ km/s) for the inner halo stars. However, Chiba & Beers (2000) did not find this prograde motion in their kinematically unbiased sample of metal-weak stars.

Regardless of the kinematic disagreements, all the investigators agree that the inner halo stars come from a dissipative collapse episode. The gas in this region dissipates into the bulge and the inner halo distribution flattens. The local (solar neighborhood) halo stars studied by Sommer-Larsen et al. (1997) appeared to have similar angular momentum distributions as the bulge stars. This scenario also predicts the existence of a metallicity gradient for the inner halo, which has been observed.

The outer halo stellar distribution has been observed to be spherical. Metal-

weak (Chiba & Beers 2000) and blue HB (Sommer-Larsen et al. 1997) stars both trace out the spherical distribution. The best scenario that describes the formation of the outer halo may be an accretion/merger model similar to that of Searle & Zinn (1978). Several observed characteristics support this idea. The absence of a metallicity gradient has been reported by Norris (1994) and Sommer-Larsen et al. (1997). This absence is to be expected since each subgalactic fragment (or satellite galaxy) would evolve separately and have its own metallicity distribution before being accreted into the Galactic halo. The outer halo stars have a net retrograde motion ($\langle v_{rot} \rangle = -45 \pm 22$ km/s (Carney et al. 1996)), and Sommer-Larsen et al. (1997) report this population to have a tangential motion rather than a radial motion with respect to the Galactic center. Carney et al. (1996) also fit isochrones to the outer halo star population and found them to be generally younger than the inner halo stars. This also supports the idea that the merged systems should be younger than those formed from the dissipative collapse.

2.4 The Oosterhoff Dichotomy

Oosterhoff (1939, 1944) first discovered this unique phenomenon in the Galactic globular clusters (GGC) that contained RR Lyrae populations. His original work consisted of a study of five clusters, but today, many GGC's with RR Lyraes have been investigated. Oosterhoff noted that the observed properties of the RR Lyraes separated into two distinct groups. The Oosterhoff dichotomy is defined by the mean period of RRab and RRc stars ($\langle P_{ab} \rangle$ and $\langle P_{ab} \rangle$) and the number ratio of RRc stars to RRab (or all RR Lyraes) in the cluster. Later, other astronomers investigating the Oosterhoff dichotomy found correlations with metallicity (Arp 1955) and kinematics

Table 2.2. Properties of the Oosterhoff I and Oosterhoff II groups (Smith 1995)

Property	Oosterhoff I	Oosterhoff II
$\langle P_{ab} \rangle$	0.55	0.64
$\langle P_c \rangle$	0.32	0.37
$\frac{n_c}{n_{RRL}}$	0.17	0.44

(Lee & Carney 1999).

Oosterhoff type I is distinguished by an average period of $\langle P_{ab} \rangle \approx 0.55$ days, but can have a range of $0.52 < \langle P_{ab} \rangle < 0.58$ days (Catelan 2004). The number of first overtone pulsators (n_c) to the total number of RR Lyrae stars (N_{RRL}) is $\frac{n_c}{N_{RRL}} \approx 0.17$. Oosterhoff I GGC's tend to have more RRab's than RRc's or RRd's. Oosterhoff II type clusters have an average RRab period of 0.65 days, but can span from 0.62 to 0.66 days (Catelan 2004). The number fraction for Oosterhoff II clusters is $\frac{n_c}{N_{RRL}} \approx 0.44$, which shows more RRc stars are expected than in Oosterhoff I clusters. Studies with metallicity shows that [Fe/H] $\cong -1.7$ separates the two Oosterhoff groups. Oosterhoff I RR Lyraes tend to have [Fe/H] > -1.65 while Oosterhoff II have [Fe/H] < -1.6 (Catelan 2004). The zone where RR Lyraes do not populate in period space is often referred to as the "Oosterhoff gap". The current description of the Oosterhoff groups is summarized in Table 2.2.

The existence of the Oosterhoff dichotomy raises the question of its origin and how it is tied to the formation of the Galaxy. The Oosterhoff dichotomy has been searched for not only in GGC's, but in the field population of RR Lyraes (Suntzeff et al. 1991, Vivas et al. 2004), in the Large Magellanic Cloud (Alcock et al. 2004), and in dwarf spheroidal galaxies of the Milky Way.

Kinematically, the Oosterhoff I and Oosterhoff II clusters have been found to

have different rotational motion about the Galactic center. Lee & Carney (1999) found that the Oosterhoff I clusters have a slight retrograde rotational motion of $\langle v_{rot} \rangle = -68 \pm 56$ km/s, and for Oosterhoff II clusters, they found a prograde motion of $\langle v_{rot} \rangle = 94 \pm 47$ km/s. Layden et al. (1996) confirmed these kinematics for field RR Lyraes.

These results remind us of the studies of outer halo stars by Carney et al. (1996). Carney et al. (1996) found the outer halo stars tended to have a net retrograde rotational motion and associated this motion with the scenario of the accretion of small, subgalactic fragments into the Galactic halo as the Milky Way was forming. This implies that an Oosterhoff I population is more dominant in the outer halo. As for the Oosterhoff II, the prograde motions indicate an origin similar to the inner halo (Carney et al. 1996). Lee & Carney (1999) also found most of the Oosterhoff II clusters in their sample to populate closer to the disk. Thus, Oosterhoff II trends may be dominant in the inner halo.

What causes the Oosterhoff dichotomy to exist is not exactly known or clearly understood. One plausible solution was proposed by van Albada & Baker (1973). They propose that the existence of the two Oosterhoff groups depends on the evolution and morphology of horizontal branch stars within the globular clusters. They postulate that in the region where the RR Lyraes are found on the horizontal branch, a transitional zone for pulsational modes must exist. In their model, an RR Lyrae star evolves across this transitional region (or hysteresis zone) starting with one pulsational mode and evolves through the hysteresis zone before switching into the other mode. For example, if the RR Lyrae star starts from the red end of the instability strip, it will be pulsating in the fundamental mode. If it evolves toward the blue end, and thus becomes hotter, the star will keep pulsating in the fundamental mode until it has completely crossed the hysteresis zone. As the star moves out of the hysteresis

zone and enters the first overtone zone, the pulsational mode will switch. The opposite scenario works for an RR Lyrae star starting on the blue side of the instability strip and evolving toward the red (cooler) end. The pulsational mode initially starts out as the first overtone mode. The star will continue to pulsate in the first overtone mode as it crosses the hysteresis zone, and then change over to the fundamental mode once it moves out of this zone.

Furthermore, in the van Albada & Baker model, the RR Lyraes evolving from the red to the blue end will be distributed evenly across the horizontal branch. As the RR Lyraes evolve from the blue end to the red end, evolutionary processes proceed faster as the star evolves toward the asymptotic giant branch. Thus, most of the RR Lyraes should be strongly populating the blue side of the instability strip. This model was able to describe the number ratios observed in the Oosterhoff groups.

Briefly mentioned in van Albada & Baker (1973) is Sandage's conclusion that Oosterhoff II RR Lyraes must be more luminous. In Sandage et al. (1981), this result is revisited, and it was shown that, at a given effective temperature, the Oosterhoff II RR Lyraes must be more luminous than the Oosterhoff I stars. According to stellar pulsation theories, the fundamental period is related to the star's luminosity, mass, and effective temperature (i.e. equation 2.1, Ritter's relation). If we assume the stars of Oosterhoff I and II have the same masses, the Oosterhoff II stars with the longer periods have lower densities and larger radii than their Oosterhoff I counterparts of equal effective temperature. Then using the luminosity equation that relates effective temperature and radius, Sandage et al. were able to conclude that the Oosterhoff II stars are more luminous. This conclusion still holds if the masses of Oosterhoff I and II are not equal, but differ by the amounts suggested by stellar evolution theory. Thus, the Oosterhoff dichotomy not only shows up in the average quantities of globular clusters, but also on a star-by-star basis.

Lee, Demarque, & Zinn (1990) investigated this phenomenon of the Oosterhoff II stars being more luminous. With evolutionary simulations of the horizontal branch stars, they concluded that the Oosterhoff II stars are more evolved than the Oosterhoff I stars. To explain why the Oosterhoff II stars were more luminous than Oosterhoff I stars, they found that the Oosterhoff II stars must have evolved off of the zero age horizontal branch (ZAHB). The Oosterhoff II stars are evolving from initial positions on the blue horizontal branch toward the red with luminosities higher than their ZAHB values. The Oosterhoff I stars are closer to the ZAHB and are less evolved. However, there is some debate whether the Oosterhoff II systems can produce enough blue horizontal branch progenitors to become the observed number of RR Lyraes (see discussion in Catelan (2004)).

It should be mentioned here that a third Oosterhoff group has been introduced by Pritzl et al. (2000). This is based on two metal rich ([Fe/H] $\sim$ -0.5) GGC's, NGC 6388 and NGC 6441. These clusters are some of the most metal rich globular clusters to contain RR Lyraes. A peculiar feature of the RR Lyraes in these clusters is their very long periods - longer than that expected even from Oosterhoff II RR Lyraes. Particular details of this Oosterhoff class are presented in Pritzl et al. (2000).

An intermediate Oosterhoff class is needed when analyzing the RR Lyraes found in dwarf spheroidal galaxies of the Milky Way and M31. This intermediate Oosterhoff class is usually characterized by a average RRab period falling in between those that define Oosterhoff I and Oosterhoff II, in the Oosterhoff gap. However, Catelan (2004) emphasizes that this class should be determined by the properties of the individual RR Lyraes, and not just from average quantities such as $\langle P_{ab} \rangle$. The danger is that this class can be misinterpreted if the system has a mix of Oosterhoff I and II RR Lyraes rather than a true Oosterhoff intermediate population.

One issue we would like to address is whether the Oosterhoff properties can be dis-

tinguished among the field RR Lyraes. Whether we will see the Oosterhoff dichotomy or not is not entirely clear for this kind of RR Lyrae sample. In figure 8a of Suntzeff et al. (1991), an Oosterhoff gap appears in a plot of [Fe/H] versus log P for their sample of field RR Lyraes. However, Vivas et al. (2004)'s period-amplitude diagram for RRab stars from the QUEST survey does not show a clean separation between Oosterhoff I and II groups. We will return to this issue when we have selected our sample of solar neighborhood RRab stars based on the ROTSE-I observations.

Chapter 3

Instrumentation and Data Reduction

3.1 Robotic Optical Transient Search Experiment (ROTSE)

The Robotic Optical Transient Search Experiment (ROTSE-I) project's telescope collected the data used in this dissertation. This telescope is located at Los Alamos, New Mexico, and collected data from March 1998 until 2001. The telescope is maintained by the astrophysicists of Los Alamos National Laboratories and of the University of Michigan. This telescope was originally designed to capture the optical transients of gamma ray busters. Their only notable detected optical transient of a gamma ray burster was GRB 990123 (Akerlof et al. 1999).

Due to the daily data collection capabilities of this telescope, ROTSE-I provides a large photometric dataset. ROTSE-I covers all the sky down to declination (δ) of

$-30°$. Since this telescope has been in operation year round, all right ascension (α) positions have been observed.

3.1.1 Instrumentation

The ROTSE-I telescope is actually composed of 4 small telescopes arranged in a 2×2 array. These telescopes are mounted on a rapidly slewing platform. The entire telescope is housed inside a military surplus electronics enclosure with a clamshell cover, which is opened automatically on nights of good observing quality. ROTSE-I is located on Fenton Hill Observatory, which is part of the Los Alamos National Laboratory in Los Alamos, New Mexico. The telescope and the data acquisition are entirely automated.

Each telescope is equipped with a charge-coupled device (CCD) camera with a Thompson TH7899M chip (Kehoe et al. 2001). The chip contains 2048×2048 pixels, and each pixel is 14 microns on a side. The camera is thermoelectrically cooled, so removing any dark (thermally-generated) noise is important. The main optical element of each telescope is a Canon FD 200 mm f/1.8 telephoto lens. Figures 3.2 and 3.3 show the ROTSE-I telescope when it was operational.

The plate scale is 14.4"/pixel for the CCD chips and the setup of this robotic telescope. This corresponds to $16.4° \times 16.4°$ coverage of the sky or field-of-view. Each individual telescope had a field-of-view of $8.2° \times 8.2°$ (Akerlof et al. 2000b). Unlike most regular optical observing programs, this telescope system does not have a filter system installed. All observations were made without a standard filter set, with the unfiltered system perhaps being closest to the broad-band Johnson R filter. Calibration of the data to a standard filter system will be discussed in section 3.2.1. With

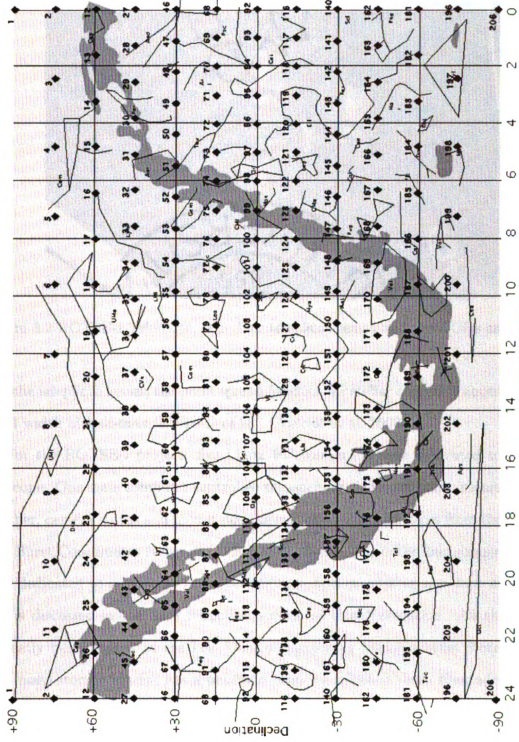

Figure 3.1 ROTSE-I Fields with constellations

Figure 3.2 ROTSE-I Telescope. The four telephoto lenses and the CCDs are shown.

just the telephoto lenses, the point spread function for stellar objects is approximately a full width at half-max (FWHM) of 20" (Akerlof et al. 2000b).

For the ROTSE-I project, five Linux PC computers were dedicated to run the telescope. One main computer controlled the opening of the enclosure, monitoring the weather, camera status and mount positioning, and received notices from the Gamma Ray Burst Coordinates Network (Kehoe et al. 2001). The other four computers were each dedicated to a camera. Some preliminary data processing was done at the site and is discussed in the data reduction section of this dissertation. All the data is currently being stored at the Los Alamos Computing Division Mass Store System. This mass storage system has a petabyte capacity, which is more than adequate for the amount of data generated for this project. The dataset used for this dissertation is approximately 4 terabytes, which includes the processing and calibration files.

Figure 3.3 ROTSE-I telescope enclosure at Los Alamos National Laboratory, Fenton Observatory

3.1.2 Observational Program

As mentioned previously, the ROTSE-I telescope was originally designed to observe the optical transients of gamma ray bursts (GRBs). GRBs are outside of the scope of this dissertation and will not be discussed in detail. Due to the short lifetimes of the optical counterparts to GRBs, a requisite of the telescope was an ability to slew quickly to the position of the detected GRB. GRBs were monitored from two satellites orbiting around the Earth. When a GRB was detected, this information was distributed throughout the GRB astronomy community by the the GRB Coordinates Network (GCN). ROTSE-I received the notices from the GCN and positioned itself to the GRB location, if it was visible from its Los Alamos site. This is the higher priority mode of the ROTSE-I telescope, as well as the next generation of this project, ROTSE-III.

The lower priority mode of ROTSE-I, which is basically the main observing program for most nights, was sky patrol mode. During sky patrol mode two images are taken of each part of the sky that is visible. The sky was divided up into 206 square fields (see Figure 3.1). On most nights, ROTSE-I was able to obtain two sets of field images, resulting in four images per field. Exposure times for the dataset obtained between April 1999 to March 2000 were 5, 20, and 80 seconds. Most of the calibration images have the shorter exposure times. The object images are taken at 80 second exposure times with a little over a minute between pairs. Sky patrol occurred on most nights except during precipitating weather or if mechanical maintenance was being performed.

From the sky patrol observations, the resulting dataset can be used in a survey of variable stars. This dataset is ideal for some kinds of variable stars since it spans a

year and there are multiple observations per night. For long period variables, often only part of the light curve can be observed. RR Lyrae variable stars can be picked out from this dataset from their distinct characteristics and light curve shapes. Other auxiliary stellar astronomy projects are being developed for a wide variety of objects ranging from supernovae to flare stars (Akerlof et al. 2000b).

3.2 Data Reduction

Observations obtained from ROTSE-I go through two iterations of reductions before the data can be used. The first data reduction step is done on-line and automatically at the telescope. In this first step a bias, dark, and flat field correction are performed. Additionally astrometry and calibration are also done. Details of the first reduction step are outlined in the following subsection. These "reduced" data are moved to the mass storage system. At a later date, a more thorough relative photometric correction is done, as described in subsection 3.2.2. The resultant data from the two reduction phases can then be used for variable star work. This section will outline and describe each of the reduction steps taken from the exposure at the telescope to the production of light curves.

3.2.1 First Pass Data Reduction

The raw data are processed through the basic data reduction steps each night. This online processing makes it possible to quickly find GRBs. For each night that observing was possible, multiple dark images are obtained. These are images taken at the same exposure time as the object images, but with the shutter, or in this

case the clamshell, closed. This will provide the mean level of thermal noise that is contaminating each object frame. Several of these darks are taken and averaged to create a reference dark frame to be used in reducing the data.

The next important calibration frame that must be created is the flat. These frames help correct for any sensitivity variations on the camera chip. The preferred method in creating a useful flat for ROTSE-I data is to use object frames that have the dark level subtracted out and have been median-averaged (Kehoe et al. 2001). These flat frames were most useful in correcting vignetting, as seen in the corners of each well exposed image. Vignetting is the obstruction of the light due to the instrument itself.

Once these processing steps are completed on the images, the data are run through an external software package called Source Extractor, or "Sextractor" (Bertin & Arnouts 1996). This program finds and classifies stellar or galactic sources from images. The resultant product from running Sextractor on the dataset is a list of objects, or "cobj files" for all the fields. After these steps are completed on the raw data, the calibrated data are moved to the mass storage system at Los Alamos.

ROTSE-I was operational and started observing in 1998, but it was determined that data obtained between April 1, 1999, and March 31, 2000, are the optimal dataset. Early in the life of ROTSE-I, many of hte images were not optimized for study. Later, after 2000, the telescope was beginning to degrade and the quality of the images became poorer. For this time interval's worth of data, the raw images were extracted from mass storage and was re-reduced carefully in 2001. The entire dataset was divided into thirds and distributed to three workers, including myself. The same basic reduction steps are completed – dark subtraction and flat-fielding correction. Sextractor is still used as the main software package to distinguish the stellar and galactic sources, as well as providing the calibrated object lists (cobj files). During

this reduction phase, it was noted that Sextractor had problems with fields near the Galactic plane, since there are many more stars in these regions. Another problem encountered in this phase, and flagged, is the misidentification of the cameras. This misidentification is known as "flipped" fields where camera A was identified as camera C and camera B as camera D. This error occurred mostly in fields near the Galactic North Pole.

Astrometry was also performed on the dataset. Astrometry is the science of accurately identifying the positions of astronomical objects. For the ROTSE-I dataset, the Tycho catalog of stars is used as the main calibration reference. The Tycho catalog is a product from the European Space Agency's Hipparcos Space Astrometry Satellite (Hoeg et al. 1997). The Tycho catalog was produced in conjunction with the Hipparcos catalog. It has been estimated that within one ROTSE-I field, one would expect roughly 1500 Tycho catalog stars.

The magnitude range of the Tycho catalog stars matched that of the ROTSE-I telescope, which is between an instrumental magnitude, $m_v = 9.0$ and $m_v = 15.0$ (Akerlof et al. 2000b). Another advantage in using the Tycho catalog is the additional photometric information of the stars. The Tycho stars have measurements in the Tycho magnitude system for B_T and V_T magnitudes and color, $(B_T - V_T)$. Cross referencing can be done to obtain standard Johnson magnitudes from the main Hipparcos/Tycho catalogs (van Leeuwen et al. 1997).

3.2.2 Second Pass Data Reduction

The second data reduction phase for the dataset is the relative photometry correction. For this step, a relative photometry correction factor is derived for each field.

The relative photometry correction factor scales each image of each field to the field template. This accounts for any clouds or unwanted external light-polluting sources that may affect the photometric measurements.

The relative photometry correction factors are derived by taking the residuals of the photometric measurements of a star to the same star found in the template field. Template fields were chosen with the criteria of good seeing and transparency. Each image of the field is compared to this template by dividing both images into macro-pixel boxes of a predetermined size. All the stars in the macro-pixel boxes are cross identified with the template stars. Their residuals, i.e. the difference between the instrumental magnitude of the image and the template image, are recorded. Those instrumental magnitude residuals are averaged to a value, which becomes the relative photometry correction factor for that macro-pixel box. This effectively scales the boxes to the same photometric level as the corresponding macro-pixel box of the template image.

In this portion of the data reduction, problems with the image are also identified. These are set as flags and stored in the headers of the each frame's file. Common problems identified are nearest neighbor stars that may contaminate photometric measurements of the target stars, blended stars (two stars overlapping in the image), saturation, and stars found near the edge of the frame. Typically, if these flags are set, their measurements can be thrown out for further analysis. Other problems flagged are related to errors occurring during relative photometry correction. Regardless, all measurements are kept, but corrupt or problem images can be excluded by checking these flags prior to analysis.

3.3 Data Analysis of ROTSE-I Observations

Once the relative photometry correction has been finished, and problem flags have been set, light curve information is available. For this portion of the data reduction, Interactive Data Language (IDL) software is used. All the data is stored in a FITS (Flexible Image Transport System) file format. This programming language is ideal for reading, writing, and manipulating FITS-format files. Throughout the reduction steps, all the data is stored in FITS format.

The program actually performs several analysis steps before light curves can be generated. First, the observation date and time must be converted from the modified Julian date to heliocentric Julian date. Next, the variability index is calculated for each star. And finally, for the variable star candidate, the period is determined. The variability index calculations will be discussed in the following subsections. Period searching algorithms are described in Chapter 4.

3.3.1 Heliocentric Julian Dates

For variable star work, the Julian dates must be corrected to *heliocentric* Julian dates. Originally, all observedd epochs were identified by a "modified" Julian date. This is the Julian date with a constant of 2400000.5 days subtracted. Essentially, we want all the epochs to reflect observations done as if at the Sun's position (hence heliocentric) rather than on the orbiting Earth. A correction is added to the Julian date to reflect this. The shift in time and location is calculated by using the star's positional coordinates (right ascension and declination) and other solar orbital elements (such as mean solar anomaly). These new dates are stored in the FITS header

files of each frame.

3.3.2 Variability Index

Estimating from the nine fields analyzed in Akerlof et al. (2000b), we extrapolated the approximate number of variable stars to be found in the total ROTSE-I dataset. The full survey has over 19 million objects for the fields observed by the ROTSE-I telescope. On the order of 30000 periodic variable stars are expected to be contained in these fields. For the RR Lyraes, we expected on the order of 3000 RR Lyraes from the entire ROTSE-I survey.

The variability index is a diagnostic tool for finding variable stars from photometric data. Those stars with large variability indices have a high likelihood of being a real variable star. This index also should not discriminate too much between pulsating and non-pulsating (eclipsing) variable stars. The algorithm used to calculate the variability index was incorporated into the light curve extraction program.

The variability index algorithm used for the analysis of the ROTSE-I dataset is a modified version of the Welch & Stetson method (Welch & Stetson 1993, Stetson 1996). All the variability indices described in Stetson (1996) are computed, but the Stetson L index is primarily used in this analysis. The L index is a composite of two other Stetson indices, J and K, which are described in detail in the following subsections. This particular method of finding variables was chosen because the variability index is optimized for pairs of observations. This method also allows us to weight spuriously bright or faint measurements and to avoid misidentifying non-variable stars.

J Index

The calculation of the index requires the computation of the weighted mean magnitude from each star's observations. The observational measurement (magnitudes) and their uncertainties are also necessary for the calculation. The first variability index calculated is the Stetson J index (Stetson 1996).

$$J = \frac{\sum_{k=1}^{n} w_k sgn(P_k)\sqrt{|P_k|}}{\sum_{k=1}^{n} w_k} \tag{3.1}$$

This is used for pairs of observations. For each observation, w_k is the weighting factor. The factor changes for the case of either a pair or single observation. In the case where both observations of a pair are good and included in the variability index calculation, the weighting factor for that pair is assigned a value of 1.0. If only one of the observations in the pair is of good quality and is used in the calculation, w_k is assigned a weight of 0.5. The expression P_k is a product of residuals of two observations, i and j (Stetson 1996). The function "sgn" is a sign function that returns either 1, 0 , or -1. If the numerical value or expression going into the sgn function is positive, the result is one. If the input is negative, the output value is -1.

$$P_k = \delta_{i_k}\delta_{j_k} \tag{3.2}$$

The residual or the "relative error" of each observation, δ_{i_k}, is defined (for a particular band pass, in this case the visual band, v) as:

$$\delta_i = \frac{v_i - \bar{v}}{\sigma_{v_i}}\left(\sqrt{\frac{n}{n-1}}\right) \tag{3.3}$$

where n is the total number of observations that go into the calculation of the weighted

mean magnitude, $\bar{v}$.

Most of these indices were designed for paired observations in two filter bandpasses. The indices can be adapted for observations taken in one filter. This is the case for the ROTSE-I survey and all the variability indices are modified for paired observations in one filter. For the J index, the P_k expression is different for the cases where a single or pair observation is good. If a pair of observations are used, then the P_k expression (Equation 3.2) is correct. For single observations, P_k is defined as (Stetson 1996),

$$P_k = \delta_{i_k}^2 - 1 \tag{3.4}$$

This expression comes from statistical arguments for a random dataset with single observations instead of pairs. This is fully explained in Stetson (1996).

K Index

The K index, or *kurtosis index*, can be used in place of the J index or used in conjunction with the J index to form the L index (see next subsection). This index is ideal for datasets where the number of observations is small and the number of bad data points can affect the outcome of any analysis (Stetson 1996). Again, the "relative error", δ, is used in the K index. It is constructed as follows:

$$K = \frac{\frac{1}{N}\sum_{i=1}^{N}|\delta_i|}{\sqrt{\frac{1}{N}\sum_{i=1}^{N}\delta_i^2}} \tag{3.5}$$

where N is the number of observations without regard to pairing of observations. For our analysis of the ROTSE-I dataset, the K index calculation is an intermediate step in the final determination of the main variability index.

L Index

As mentioned in the K index description, the combination of the J and K index gives a more robust variability index, L. The L index is:

$$L = \left(\frac{JK}{0.798}\right)\left(\frac{\sum w}{w_{all}}\right) \tag{3.6}$$

The value 0.798 in the denominator comes from the statistics of the K index. If we consider the K index in the limit where the range of the variable star's variation is larger than the $\sigma's$ of each observation, then for a Gaussian-like magnitude distribution, $K \rightarrow \sqrt{\frac{2}{\pi}} = 0.798$ (Stetson 1996). Thus, if the magnitude distribution is truly Gaussian, the L index reverts back to the definition of the J index with an additional weighting factor multiplied.

The weighting factor to the L index is included for the cases where the star does not appear in one of the images. This can be an important problem in survey work. Many spurious variable candidates can be found if the star happens not to be present on one or several frames. This "disappearance" of the star can be attributed to technical issues, such as the star being on the edge of the frame (it might be left off of the frame if the telescope moves and returns to the original field, but slightly offset) or it can be near a cosmetic blemish on the CCD chip. As the telescope moves from object to object or field to field, and cycles through again, there is no guarantee that the camera will be pointing in the same exact location of the sky. Thus, stars can "fall off" the edge of the frame or "fall into or out" of CCD blemishes.

However, in the case of the ROTSE-I survey, there is a reasonable amount of overlap between fields, so "edge dropoffs" are not a problem and potential candidates are not lost forever. Multiple observations of the same star can occur, if there are tiny

differences in the astrometry assignment. This particular problem was documented in Wils (2001).

In this analysis of the ROTSE-I survey, a flag system is instituted for various problems associated with the astrometry (Sextractor) and the photometry. For the calculation of the variability index, all these flags are checked for each star in all the frames. Thus, if the star is found near the edge of the frame or near a blemish on the CCD, it is flagged. Those flagged observations can be excluded from the variability index calculations. Therefore, the need for the weighting factor on the L index is unnecessary. All the "good" observations of the stars are used for the calculation, so the weighting factor will be unity. The set of optimal flags for the best data are described and listed in Woźniak et al. (2004).

Thus, the final variability index used in this work is a modified L index:

$$L = \frac{JK}{0.798} \tag{3.7}$$

In a previous, preliminary work on variable stars in the ROTSE-I survey (Akerlof et al. 2000b), Equation 3.7 was used to find the variable candidates. For the ROTSE-I fields in this study, this index also provided the greatest number of real variable star candidates. However, in early tests, this index also chose stars that would have one or two bright outlier observations. These could be possible flare stars, as described in Akerlof et al. (2000b), but may also be stars with undetected problems in the photometry. Periods were sought for these stars, but none were cleanly found. By our best guess, these stars are not the variable candidates we would like to include for a general variable star catalog and will be subsequently ignored.

To help weed out these spurious candidates, a special weighting factor was implemented (Stetson 1996, 1987). This weighting factor reduces the influence of any

outliers of a set of measurements. The weighting factor is:

$$w = \left[1 + \left(\frac{|\delta|}{a}\right)^b\right]^{-1} \tag{3.8}$$

where $a = b = 2$ (Stetson 1996). Again, δ is the relative error definition, Equation 3.3. This weighting factor is used in the calculation of the mean magnitude, which is then used in determining the variability indices. Those magnitude measurements with large uncertainties or that are unusually bright or faint, are given a smaller weight in the calculation of the mean. With the new weighted mean magnitude, the variability indices are less sensitive to the flare-type stars and pick out more small amplitude, short period variable stars. Equation 3.8 is iterated a minimum of five times in order for the mean magnitude to stabilize in value.

3.3.3 Identification of Candidate Variable Stars

To pick out the variable star candidates, a cutoff value had to be chosen for the range of L indices calculated. Those candidates with large L indices are generally considered to be highly probable in being a variable star. In Akerlof et al. (2000b), this cutoff value was determined from a Gaussian fit for the L indices per magnitude bin. The magnitude range of the ROTSE-I dataset was binned. For each magnitude bin, a Gaussian was fitted for the variability index values of the stars in that bin (McKay, private communication). A mean and standard deviation were calculated. The standard deviation was used to determine the L index cutoff value, which was 4.75σ.

However, this coefficient of 4.75 was chosen ad-hoc. Akerlof et al. (2000b) had chosen the best observed fields from ROTSE-I and only used paired observations

for analysis. Thus, this affects the quality of the light curves and the calculation of the variability index. For the analysis in this work, a more rigorous and conservative approach was used to determine the L index cutoff. Two test fields were used to check the validity of this method as well as the quality of the variable star candidates' light curves.

The variability index should have some dependence on magnitude and position in the sky (as opposed to position on the CCD chip) due to its dependence on the magnitude uncertainty. The positional dependence comes from the number of observations taken as well as from crowding in the Galactic plane. More observations of the ROTSE fields were done in the polar regions compared to the southern regions. The dependence on magnitude comes from the formal and systematic errors of each observation. Tests showed that the formal errors were overestimated for the brighter magnitudes (about 10th magnitude and brighter) and underestimated for the fainter (about 15th and fainter). This in turn, affects the resultant value of the L index. To account for both effects of the position and magnitude on the variability index, the cutoff values are determined for each field. Within each field, the cutoff value is calculated per magnitude. Breaking up the sky into the small fields helps to determine any local changes to the index rather than having a large global value, which may or may not be the optimal cutoff value.

All the stars in a test field, per camera, were binned by magnitude. The bin size was one magnitude, but the calculations overlapped the bins by 0.5 magnitudes. In each magnitude bin, the median and 95th-percentile of the variability index were calculated. The range of magnitudes is from 9th magnitude (bright end) to 16th magnitude (faint end), so 13 values were calculated. The 95th-percentile value of the L indices were then fitted by an IDL polynomial fitting routine (POLY_FIT.PRO). This provided the cutoff value for the L variability index with respect to magnitude.

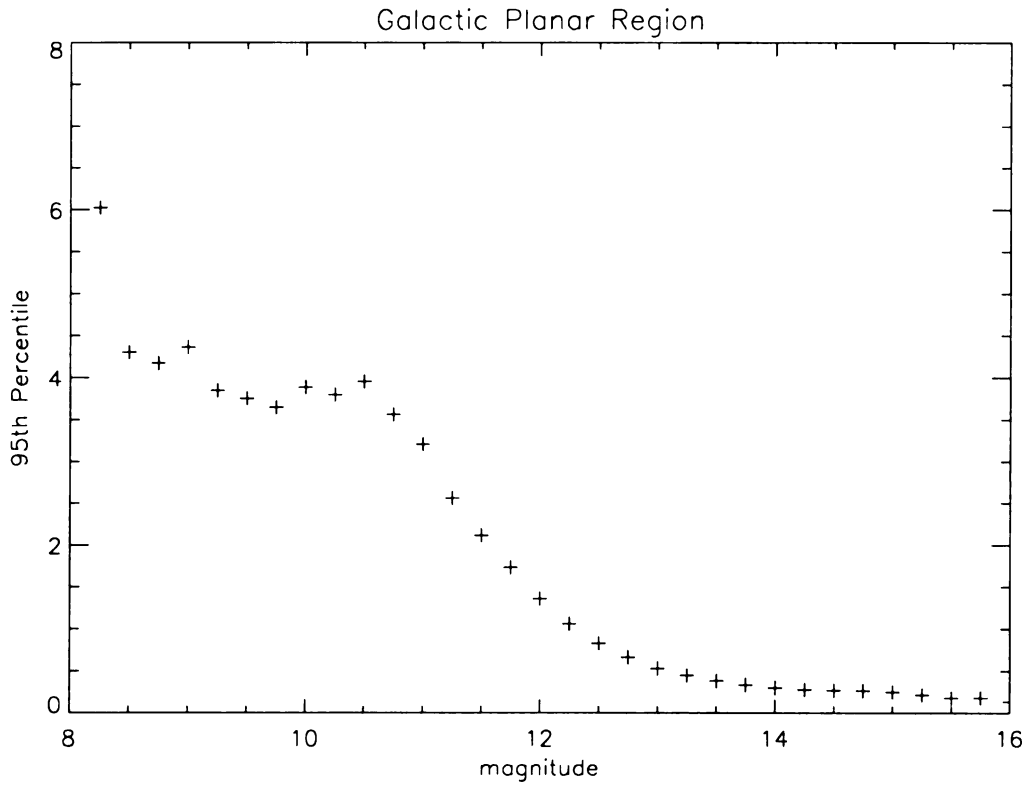

Figure 3.4 95th-Percentile L index trend with magnitude in the Galactic planar region.

Figure 3.4-3.6 show the trend of the cutoff value with respective low, mid and high latitude Galactic regions. One thing to note is that stars brighter than 10th magnitude were considered to be saturated. For stars found to be brighter than 10th magnitude, the cutoff value at 10th magnitude was used to determine whether the star was a variable candidate or not.

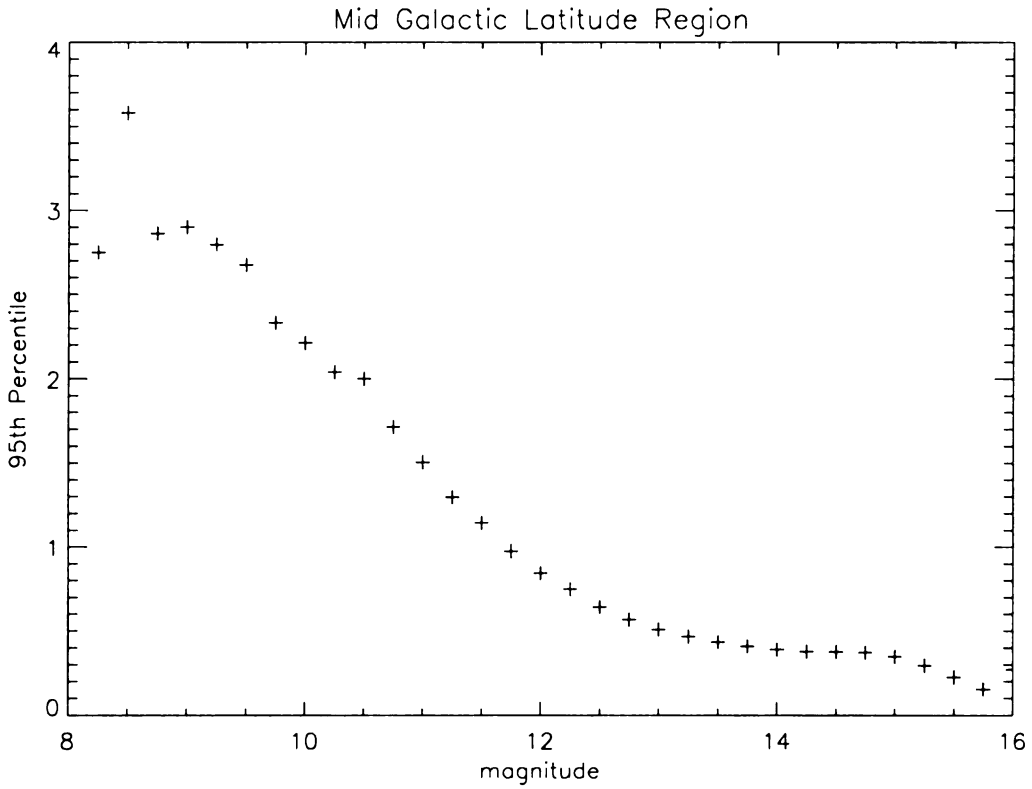

Figure 3.5 95th-Percentile L index trend with magnitude in the mid Galactic latitude regions.

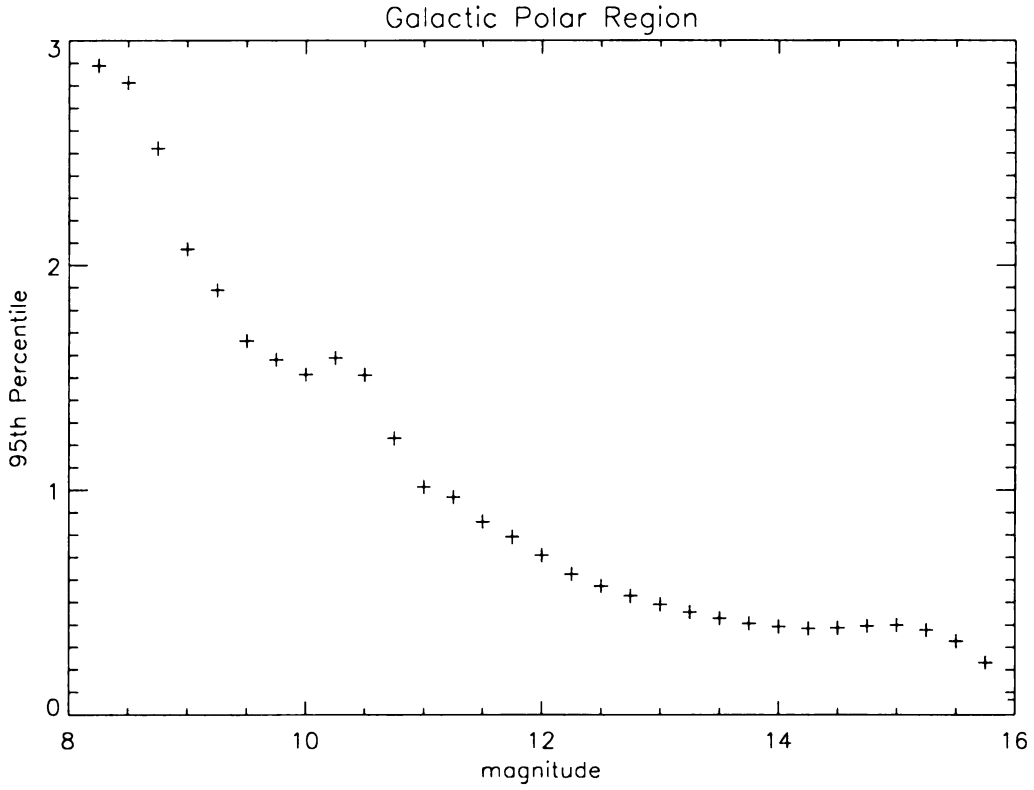

Figure 3.6 95th-Percentile L index trend with magnitude in the Galactic polar region.

Chapter 4

Determination of RR Lyrae Properties

This chapter will focus on the determination and calibration of various properties of the RR Lyraes. For many of the quantities, several different algorithms or methods were tested for facility in use for the ROTSE-I dataset. Explanations are given concerning which method(s) were preferred for the analysis. No one method is really always better than another, rather the choice of method is dependent on the characteristics of the dataset. Starting from this chapter, the dataset will be referred as the Northern Sky Variability Survey (NSVS) (Woźniak et al. 2004) rather than the ROTSE-I dataset.

4.1 Period Searching Algorithm

In variable star research, one of the desired goals is to find the period of the light

variation. There are many different algorithms available currently to find the periodic variations. For the NSVS dataset, five methods were tested, but one algorithm appeared to be most suited for this particular survey. This section will describe each of the methods briefly along with advantages and disadvantages of the algorithm. Regardless, no one algorithm is perfectly ideal, and the best one can do is to adapt it for one's dataset.

Phased light curves are an easy way to see immediately if the period solution is correct. Phasing the observations assigns each observation the corresponding point in the pulsational cycle of the variable star. To do this, one needs all the heliocentric corrected Julian dates and the period for a particular variable star. All the Julian dates are divided by the period. Those values are then subtracted by their respective integer portion. The formulae which describe these steps are:

$$d = \text{Heliocentric Julian Dates/Period (days)} \tag{4.1}$$

$$phase = d - (\text{integer portion of d)}) \tag{4.2}$$

One of the major criteria used to choose the optimal period searching routine was its ability to distinguish period aliases from the correct period of the RR Lyraes. The alias problem can be significant in some methods, whereas in others, it is clear that some period solutions do not give the best phased light curves. Often, these aliases will be a subharmonic to the correct frequency (or period). In some cases, when phased light curves are produced with the period alias, the light curve will appear as good as that phased from the correct period. For those cases in the NSVS sample of RR Lyraes, both period aliases were kept, as the correct period could not be determined.

4.1.1 Phase Dispersion Minimization

An old reliable algorithm readily available through IRAF[1], although a stand-alone version does exist, is the Phase Dispersion Minimization (PDM) method (Stellingwerf 1978). This method is actually a minimization of the scatter of the data in phase space. The phase space mentioned here refers to the ordering of the observed points according to where they should be in the varying light cycle. A range of periods is tested, usually set within the task by the individual. Thus if the actual period is found, its phased light curve should have the least amount of scatter in a PDM periodgram. The measurement of this scatter in the phased light curve is called the Θ-statistic. A better description of this statistic and the method is provided in Stellingwerf (1978).

PDM has been used often in variable star research. However, for this dataset, PDM is not efficient and requires a great deal of user interaction. The NSVS dataset has millions of objects, of which it is estimated that there will be thousands of variable stars. The ideal period searching algorithm needs to be non-interactive and fairly automated for these thousands of stars. Since PDM requires one to check minima of the Θ-statistic for the correct period, period searching can become time consuming. This is especially true if there are many period aliases. A period alias can easily be confused with the actual period because the alias may produce an acceptable phased light curve. For the reasons of efficiency and difficulty in distinguishing the minima (i.e. the correct period versus all the aliases), PDM is not an ideal period searching algorithm for this dataset.

[1]IRAF is distributed by the National Optical Astronomy Observatories, which are operated by the Association of Universities for Research in Astronomy, Inc., under cooperative agreement with the National Science Foundation.

4.1.2 Lomb-Scargle Periodgram

Another often used period searching algorithm is the Lomb-Scargle Periodgram. According to Reimann (1994), periodgrams and many least-squares methods are employed to find frequencies (or periods, i.e. $\nu = 2\pi/P$) assuming the light curve of a variable star can be described by a simple harmonic model. The Lomb-Scargle periodgram is actually a least-squares method (Lomb 1976, Scargle 1982). The periodgram is calculated at equally-spaced frequency intervals via a fast Fourier transform (Press & Rybicki 1989). This method requires a computation of the Fourier power series over frequency intervals. The major periodicities refer to frequencies where the Fourier power is maximized (Akerlof et al. 1994).

The version of the Lomb-Scargle periodgram that was tested for the NSVS survey was written in IDL (Wilms, private communication). After choosing test candidate variable stars, several period searching runs were done using this method. Two input parameters can be changed with each run of the program. The parameters are *pmax* and *pmin* which define the maximum and minimum period search range. I found that if these input parameters changed (for example, pmax from 80000 seconds to 100000 seconds), different solutions would be returned for the same candidate variable. Thus, depending on the adequacy of the chosen search range, potentially incorrect values for period will be derived. To complete a wide range search of periods for different types of variable stars in the NSVS survey, this method could provide many spurious results unless finely tuned. To use this method, the search period range must be set for each type of variable star, and the search must be run several times through the list of variable candidates to ensure complete coverage. This method, in light of the results of the test runs, is not very efficient.

Other disadvantages include poor detection of multimodal stars or eclipsing binaries (Reimann 1994). The Lomb-Scargle periodgram also does not use weights on good versus poor observations. All observations are treated equally. The dataset at this point should have most of the problem observations omitted for any calculation. However, there are those outliers with small observational errors that are included in the light curve information. Thus, the Lomb-Scargle periodgram algorithm, as well as the other period searching methods described in this chapter, can become confused by these sharp dips or peaks. Another disadvantage with this method is that it assumes the data have a uniform distribution of the variance (Akerlof et al. 1994). One loses statistical confidence for those light curves that have non-sinusoidal shapes, such as is the case for RRab type stars. Thus, this method was not chosen as a viable period searching algorithm.

4.1.3 Cubic Spline

The cubic spline method was used for the variable star candidates in the original analysis of the ROTSE-I test fields published in Akerlof et al. (2000b). The basic idea behind the cubic spline method is to fit a function, preferably a cubic polynomial, between "knots". These knots are placed in equally-spaced intervals in a phased light curve. A least-squares fit of the sum of the cubic spline functions is calculated. The best frequency (or period) for the phased light curve is found when the χ^2 is minimized.

One of the advantageous things about this method is how easily this algorithm can be implemented automatically. However, as reported in Akerlof et al. (1994), this method has problems in determining periods for RR Lyraes. Also, the cubic

spline method expects the data to be equally spaced in phase space, when in reality, this is not true. Tests were done with candidate variable stars where the period had been determined by at least one other method. It was found that the cubic spline could pick out the correct frequency. However, this was dependent on what inputs were used when the cubic spline was run. Revising the number of knots and the maximum frequency changed all the results. In some cases, the correct frequency was not even listed. Again, this can be a problem with running this algorithm on the NSVS dataset. The periods of all the candidate variable stars are unknown ab initio nor are the data expected to be evenly spaced.

When the test fields were analyzed, as described in Akerlof et al. (2000b), an IDL graphical interface was used to check each frequency choice as determined from this algorithm. This method needs a person to check if the program is correctly finding the frequency/period. Since now this algorithm must be applied to over 200 fields and not just the 9 test fields, this may not be the most ideal period searching routine. However, there still will be some user interface necessary to see if any algorithm is choosing the correct period or an alias. The human element cannot be totally removed from the variable star analysis.

4.1.4 Analysis of Variance (AoV)

A successful period-searching algorithm called the Analysis of Variance (Schwarzenberg-Czerny 1989) was extensively used in variable star analysis of the OGLE survey (Schwarzenberg-Czerny 1998, Mizerski & Bejger 2002). This particular period algorithm is designed to be used for large survey projects. In the literature, AoV has been cited to be highly successful in finding periods for candidate variable stars.

The AoV method is based on the F-distribution. The F-distribution uses two independent χ^2 random variables, U and V, with a and b degrees of freedom, respectively. A χ^2 random variable, U, has a chi-squared distribution with one degree of freedom, which is described by $U = Z^2$. Z is a standard Gaussian random variable (Rice 1995). The F-distribution is constructed as follows:

$$W = \frac{\frac{U}{a}}{\frac{V}{b}} \tag{4.3}$$

Schwarzenberg-Czerny (1989) constructed the AoV statistic based on the formula of the F-distribution:

$$\Theta_{AoV} = \frac{\frac{1}{(r-1)} \sum_{i=1}^{r} n_i (\bar{x}_i - \bar{x})^2}{\frac{1}{(n-r)} \sum_{i=1}^{r} \sum_{j=1}^{n_i} (x_{ij} - \bar{x}_i)^2} \tag{4.4}$$

The U variable is assigned the summed function in the numerator of Equation 4.3 and V is the summed function in the denominator. The degrees of freedom are $a = \frac{1}{r-1}$ and $b = \frac{1}{n-r}$ in this statistic.

The number of observations, n, is divided into r bins. In each bin there are n_i observations, where $\bar{x}_i$ is the average of those observations. The average of all the observations is $\bar{x}$, and x_{ij} is the j^{th} individual observation in the i^{th} bin. One thing to note here is that the uncertainty in each observation (merr) is not used as a weight in the statistic. Good and bad observations are both used.

The AoV statistic is used to check the validity of a solution for a given periodgram. As in the Fourier methods (such as the Lomb-Scargle algorithm), a maximum power is assigned to the correct frequency. This statistic checks this solution validity of being the correct frequency of the periodgram. The AoV statistic can also be used

to check alias solutions. A nice feature of this method is its use for non-sinusoidal light curves. The Fourier series methods are the best method for light curves with sinusoidal shapes.

The AoV code has two separate subroutines which calculate the AoV statistic. The slower calculation of the AoV statistic, "saov", uses bins with a fixed number of observations. The advantage with saov is its insensitivity to the sampling of the observations. The faster calculation of the statistic, "faov", uses bins of fixed phase width. Although the subroutine runs faster than saov, if the phase bins are underpopulated, spurious results are more likely to occur in the periodgram (Schwarzenberg-Czerny, private communication). Another subroutine was developed which took the best attributes of saov and faov, which produced consistent results (Schwarzenberg-Czerny, private communication).

The advantage of this period-searching algorithm is that it is easily automated and fast. Again, this method is designed for large survey projects, which is ideal for the NSVS database. However, this method is not entirely free of user interaction. In some tests, the alias frequencies can be confused easily with the correct frequency. An example of this problem can be seen in Figure 4.1. This may be a problem if the candidates have poor time coverage, as is the case for some of the southern fields of NSVS. One would need to check the results of AoV by inspection of the phased light curves.

Another one of the advantages with AoV is that one can easily control the frequency interval steps for the period search. The bin sizes can also be readily changed. However, the output files (which contain the periodgrams) can be large compared with the outputs from other methods. Regardless, AoV can easily be adapted to the current software to find periods of variable candidates. For a more complete description of this method see Schwarzenberg-Czerny (1989).

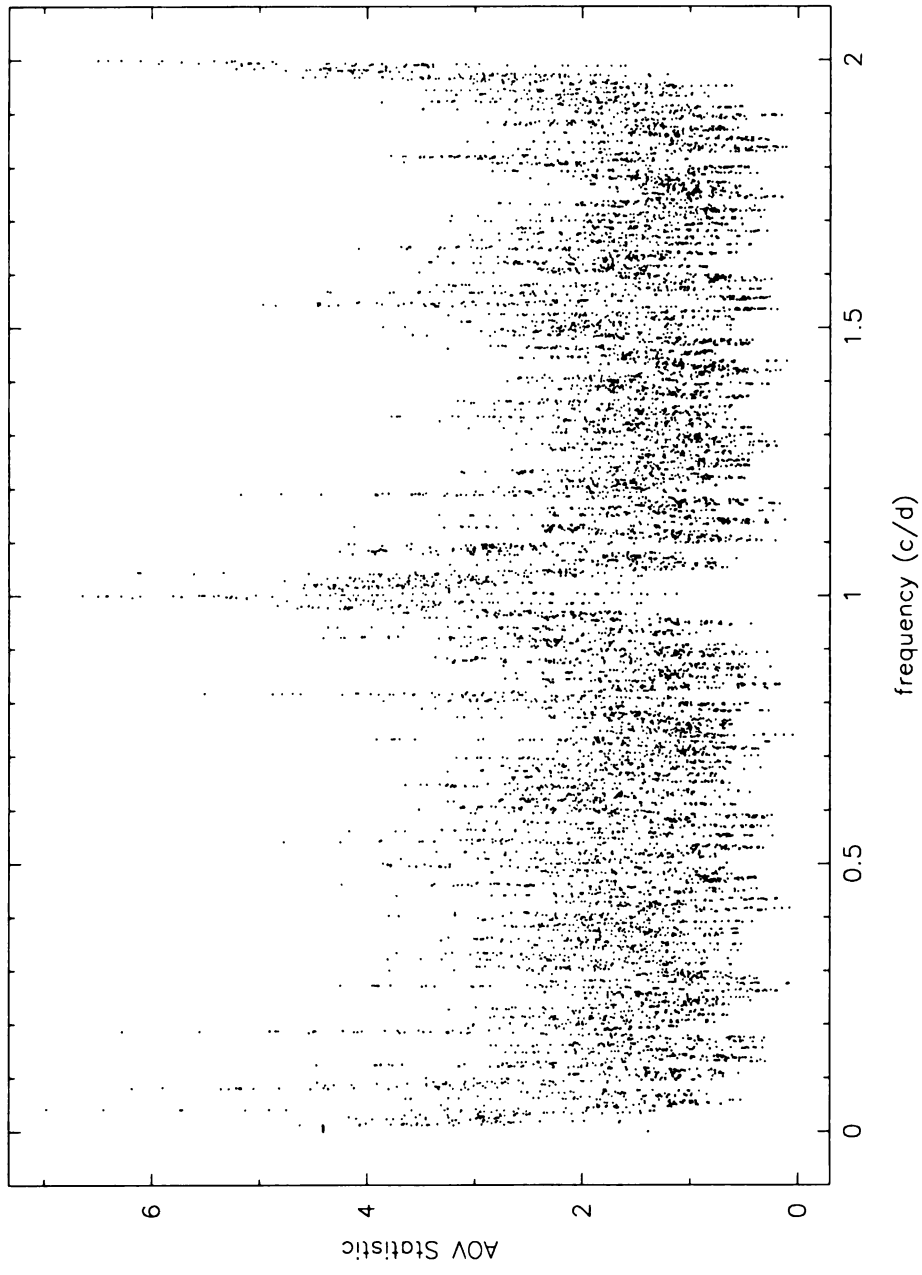

Figure 4.1 Aliasing problem with AoV

4.1.5 Supersmoother

Another new period searching algorithm proved to be both efficient and non-interactive in determining periods for candidate variables in the NSVS survey. "Supersmoother" (Miceli, private communication, Reimann (1994)) is different in its approach to finding periods compared to the other methods, but is slightly similar to the cubic spline method. Supersmoother was originally used in the variable star analysis in the MACHO dataset (Alcock et al. 1995).

The general idea behind Supersmoother (and all smoothing routines) is to fit the observations as the function of phase for a particular frequency (Reimann 1994). Algorithms that are considered smoothers use this principle. Some example smoothers are algorithms that use a running mean or running linear regression on the data. Supersmoother uses a "variable-span" method. There are three running linear smoothers with three different relative span lengths (short, medium, and long). These three different spanned smooths are run on the data in phase space. To check which span interval is appropriate to the phased observation, a "local cross-validation" is done. This is where the fitted value is compared to the observed value at each span interval and checked if the residual is minimized. The calculation of the cross validation is done by using the following formula, called the sum of absolute residuals (SAR) (Reimann 1994):

$$SAR_n(v) = \sum_{j=1}^{n} \frac{1}{s_j} |y_j - \hat{y}_{j,v}| \tag{4.5}$$

For this statistic, v is the frequency, s_j is the sample variance, y_j is the magnitude from the dataset, and $\hat{y}_{j,v}$ is the fitted calculated magnitude. This statistic is summed over all n observations. To find the best period, the global minimum of the SAR statistic

is determined.

Reimann (1994) conducted exhaustive tests comparing how supersmoother fared against other period searching algorithms. Reimann compared the PDM, Lomb-Scargle algorithm, cubic spline and Fourier methods against the supersmoother method. All the advantages and disadvantages are discussed in depth in his thesis. One of his conclusions was that the supersmoother method was found to work well for all kinds of light curves (i.e. all kinds of variable stars). This algorithm is self-adjusting and does not need the light curve shape to be inputted for the calculation. This feature makes this method particularly attractive for use in large variable star survey projects.

However, one of the problems discussed in Reimann (1994) is that the fitted curve can be discontinuous to the phased points. If the frequency is changed, the phase will also change, and this will affect the fit. Reimann (1994) did cite that in this case, the SAR may become discontinuous, but the changes will be small.

In the tests conducted on the NSVS dataset, supersmoother was able to find the periods quickly. The correct frequency/period was usually found within the first 15 guesses or less. This program also was easy to implement and to include in programs used to find the variable star candidates. The program contains algorithms using a trigonometric polynomial or a cubic spline routines to fit phased points for period searching. Often the trigonometric polynomial is used for fitting longer period variables (period $> 50^d$), and the cubic spline is good for the shorter period variables.

Again, as with the other period searching algorithms, one cannot totally eliminate the human factor in this analysis. One must see if the period choice is correct or if it is an alias or subharmonic. For pulsating variables, the "cycles" number from the Supersmoother output provided a clue to the best period for the data. The cycles refer to the number of times the Supersmoother curve crosses the mean value divided

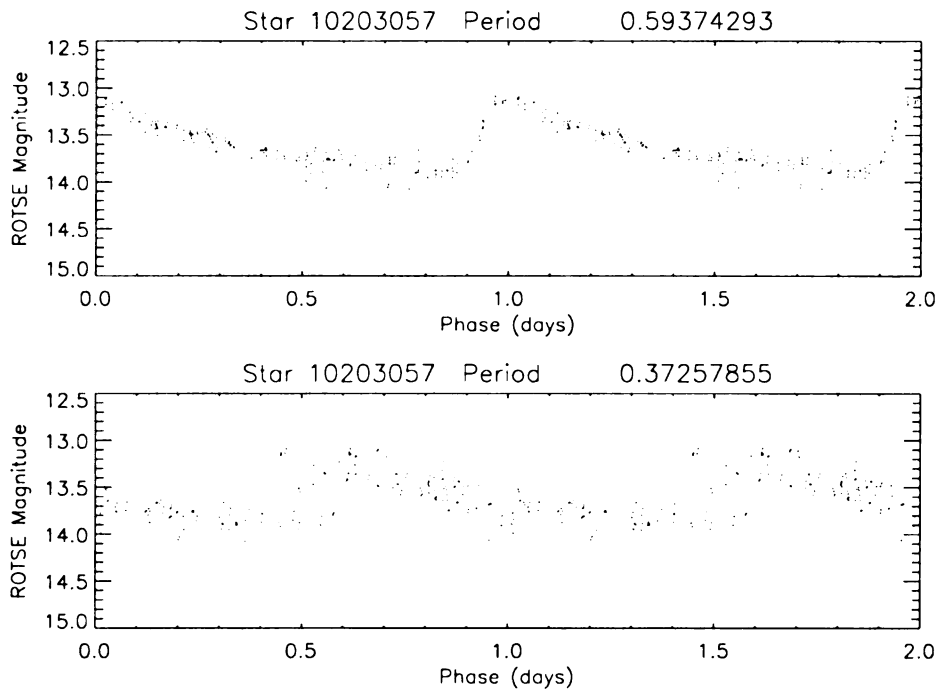

Figure 4.2 Supersmoother phased light curves. Upper plot: correct period. Lower plot: alias period.

by two (K. Cook, private communication). Thus one should look for a cycles value of 1 for the best period guess of a pulsating variable star. Any more than that, the choice is most likely an alias. However, one runs into ambiguity problems with W Ursa Majoris (W Uma) stars or other eclipsers (particularly if the two minima are of similar minimum depth). Then the cycles value should be equal to 2.

For the period determination of the NSVS RR Lyraes, Supersmoother was the main period searching algorithm used. The phased light curve for each star was inspected by eye to ensure the correct period was recorded for the RR Lyrae candidate. An example of phased light curves for a period and an alias from Supersmoother is shown in Figure 4.2. All the Supersmoother period solutions were also compared with a solution from the cubic spline method (Akerlof et al. 1994). This was particularly useful when multiple Supersmoother solutions gave reasonable looking phased light curves. In cases where Supersmoother and the cubic spline method produced two different period solutions, PDM was used to determine which is the correct period and which is the alias period. At most, for certain stars, periods were derived from three different methods to arrive at the correct solution. In cases where PDM could not distinguish between the alternatives, both periods were kept for analysis, even though one of them is surely the alias period. Often these alternative periods corresponded to the frequencies near 2 cycles/day or 3 cycles/day.

4.2 Amplitude Work

With periods for all the RR Lyrae candidates, phased light curves are produced. Figure 4.3 and 4.4 show some typical phased light curves of NSVS RRab and RRc stars, respectively. Note that the fainter stars have larger photometric errors than

the brighter stars, regardless of how well observed the stars are. The number of observations were as few as 15 and as many as over 300.

With phased light curves, one can start analyzing light curve shapes. The first step is to determine the amplitude of the light curves. To find amplitudes, two different methods were employed. One was a spline fitting routine which also calculated the mean magnitude. The second method performed a template fit to the observed light curve. Each method and its results are described in the following subsections.

4.2.1 Amplitudes from Spline Fitting

The spline fitting method is based on a Numerical Recipes algorithm (Press et al. 1992). The program (written in perl) uses the subroutines *spline* and *splint* (Sharpee, private communication). The results from this program include the minimum and maximum magnitude of a spline fit to a set of observations for a star, the amplitude (which is just the difference of the previous quantities), and the mean magnitude (magnitude and intensity weighted). Figure 4.5 shows an example of the spline fit to one of the program stars.

4.2.2 Amplitudes from Template Fitting

This template fitting method was developed by and described in Layden (1998) and in Layden & Sarajedini (2000). The computer code can be obtained from Andy Layden's website,

`physics.bgsu.edu/~layden/ASTRO/DATA/EXPORT/progs.htm`

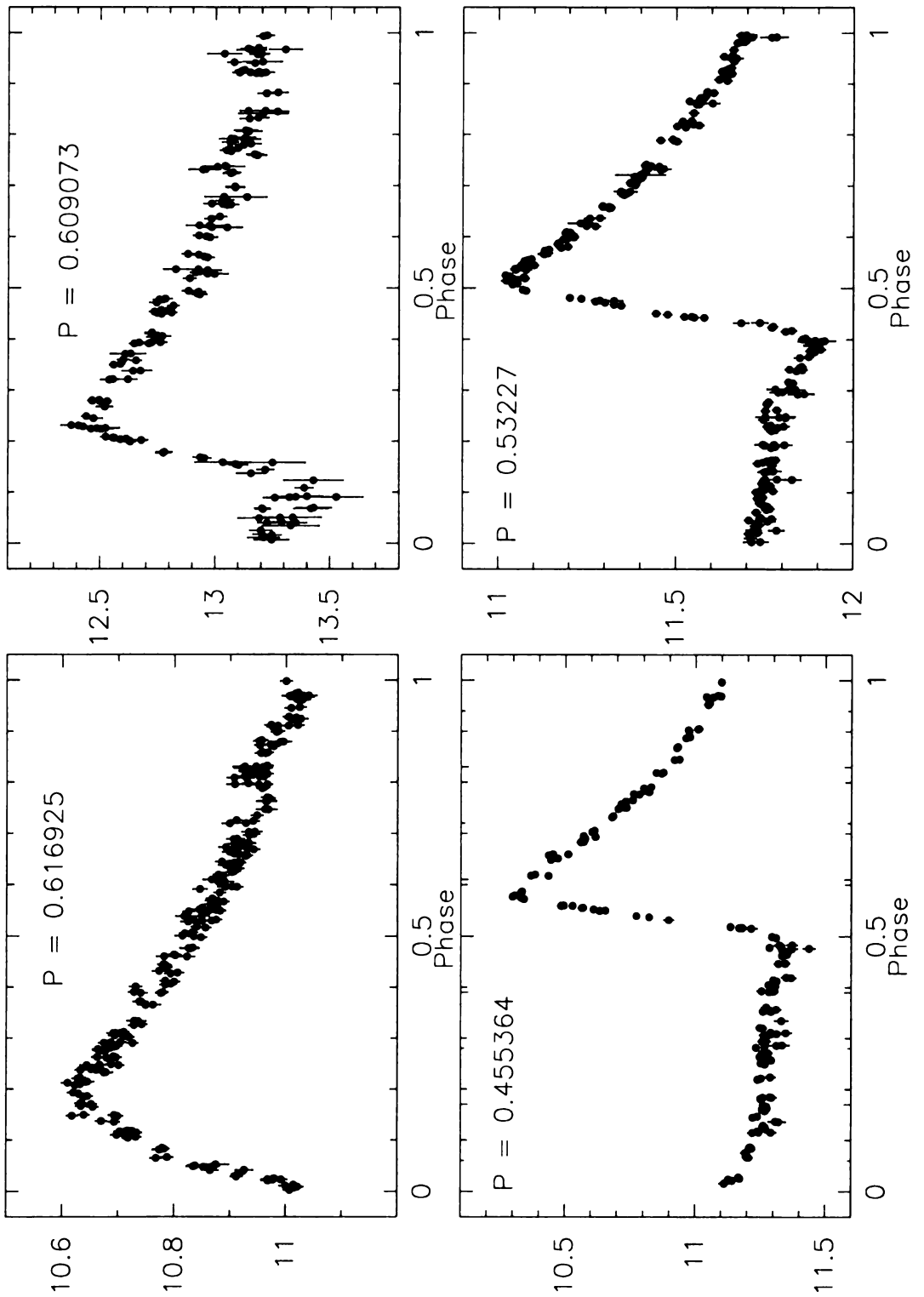

Figure 4.3 RRab phased light curves from the ROTSE-I survey. The ROTSE magnitude is the Y-axis quantity. The periods are in units of days.

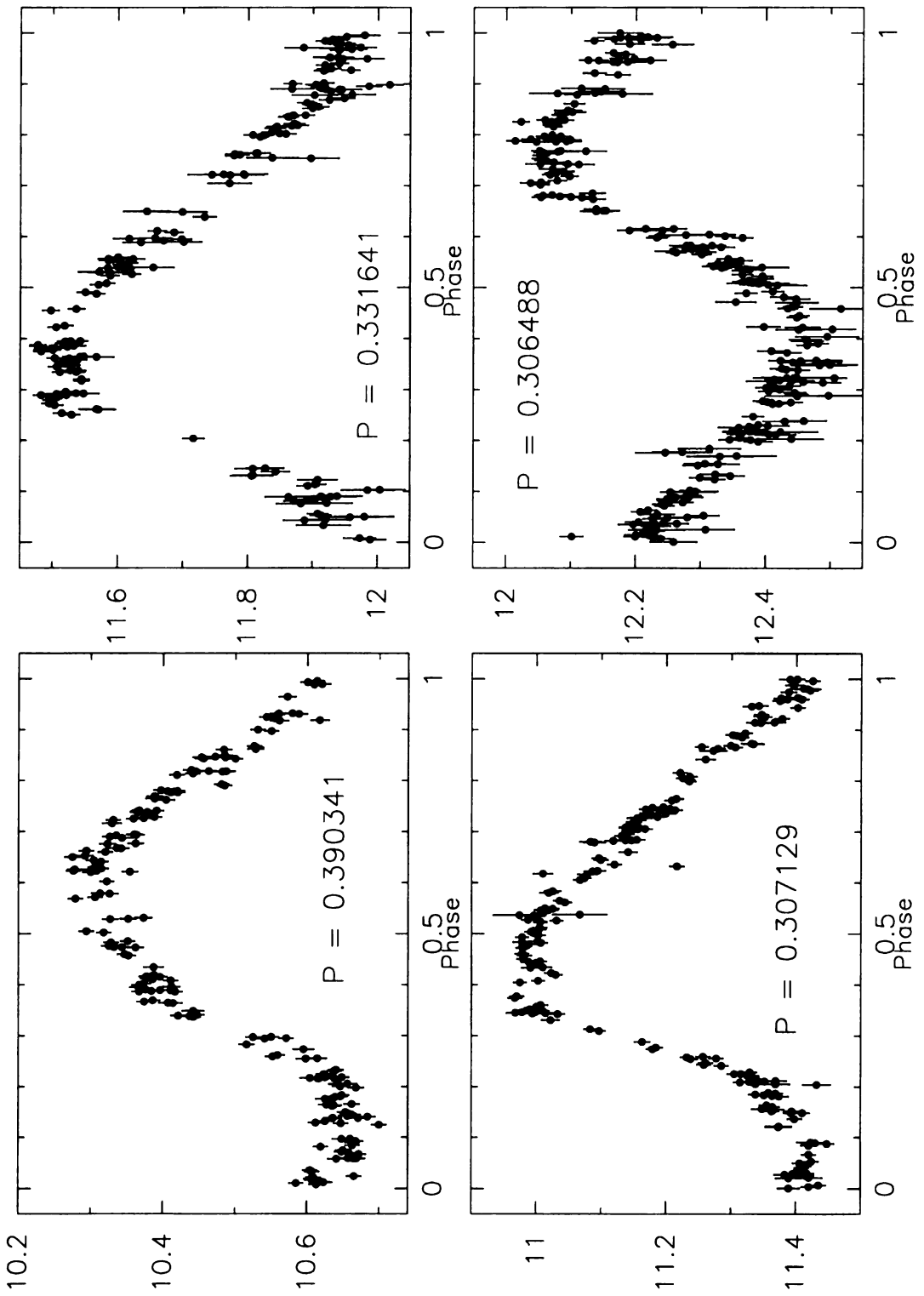

Figure 4.4 RRc phased light curves. The ROTSE magnitude is the Y-axis quantity. The periods are in units of days.

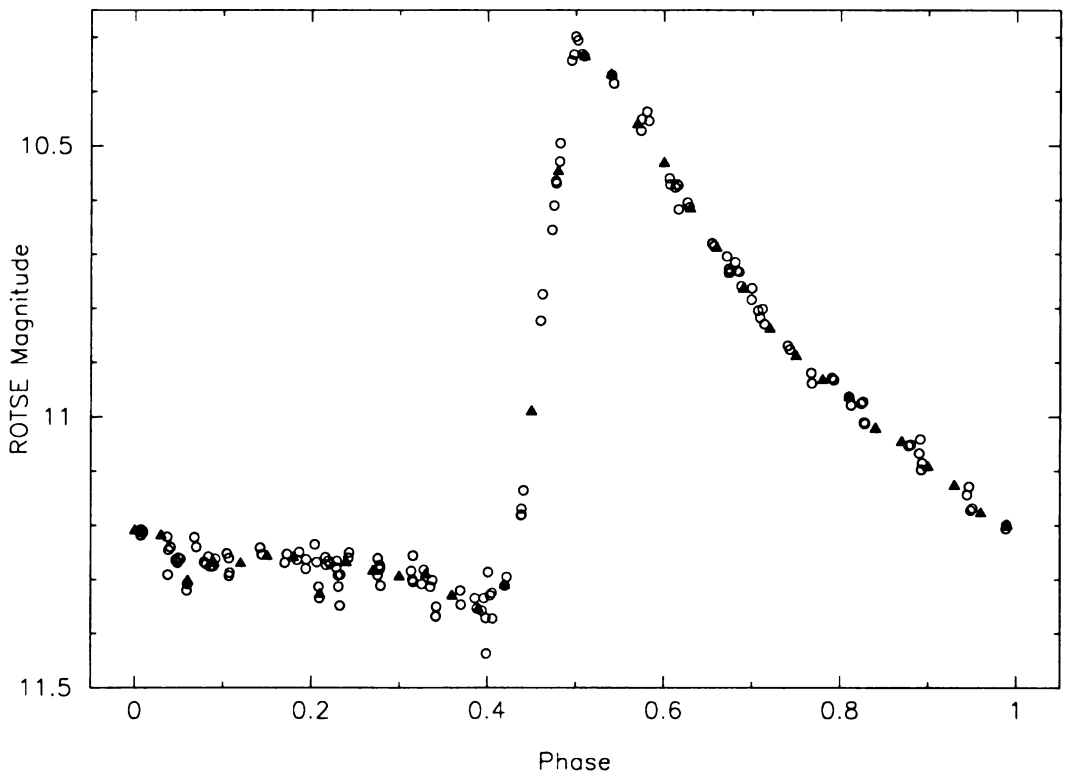

Figure 4.5 Spline fitting method. Filled triangles are values from the spline fit. Circles are the actual NSVS data.

This template fitting routine is based on well sampled light curves and should perform well for many of the RRab candidates in this sample. However, what was found was that some stars that lacked observations in the rising branch part of the light curve had problems with the template fit. The correct template would not be chosen and a spurious result would occur. Tests were made with a subsample of "standard" RRab stars that have been well observed (Sandage 2004).

The average residual from the spline fit, 0.087 ± 0.013, was tighter than from the template fit. The average residual for the template fit is 0.113 ± 0.024. Both values are based on 55 RRab stars that had well sampled light curves and for which the average uncertainty in the observations is about 0.02 magnitudes. Figure 4.6 and 4.7 show the results from the template fitting routine.

Comparisons were also made with published amplitudes (Bookmeyer et al. 1977) for the set of 55 RRab stars. The amplitudes derived from the NSVS data needed to be scaled into a "standard" system. All the NSVS observations were obtained from a filterless ROTSE-I telescope, so the best approximation is a Johnson R for the data. As one goes redder in the Johnson filter set, the shape of the light curve flattens. This effect can be explained by a Planck blackbody radiation distribution. The bluer filters of the Johnson system (UBV) are near the peak of the blackbody radiation curve, whereas the redder filters are near the tail of the curve. The flux at the visible portion of this radiation distribution has a T^4 dependence whereas in the infrared end, it is more of a $T^{1.6}$ dependence (Jameson 1986). As the temperature changes during the RR Lyraes' pulsational cycle, there will be a greater change in flux at the bluer end than in the redder end. Hence, the amplitudes derived from observations in a bluer filter will be relatively larger than those from a redder filter. Therefore, the ROTSE amplitudes are expected to be slightly smaller than what we would find if the stars were observed through a Johnson V filter.

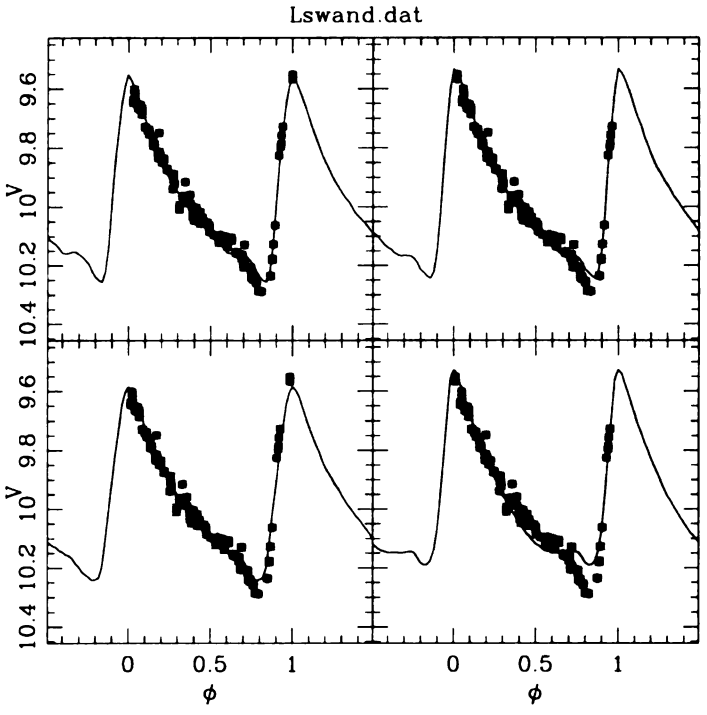

Figure 4.6 Example of output from the Template fitting method for SW And. These are the 4 best template fits (smallest RMS values).

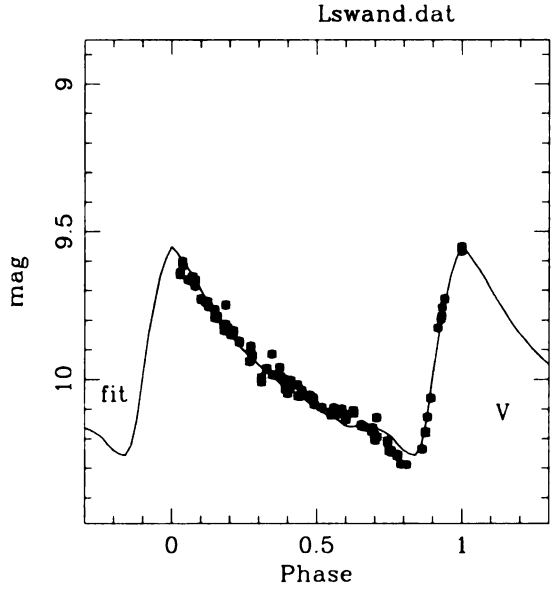

Figure 4.7 Example of output from the Template fitting method for SW And. This plot shows the best fitted light curve to the NSVS data.

To calibrate our ROTSE amplitudes to amplitudes in the standard Johnson V filter system, the standard V amplitude values were taken from Bookmeyer et al. (1977) and Simon & Teays (1982). Some discrepancies were found between the amplitude values of Bookmeyer and those published in Simon & Teays. Bookmeyer's observations were done in the Johnson system, and in their publication, light curve data are provided as an additional check. For the Simon & Teays published amplitudes, the values were obtained from Lub (1977), whose observations were done in the VBLUW Walveran system. Lub does provide a conversion of the observations from the Walveran to the Johnson system (Lub 1977). However, for those discrepant amplitude values, a third source was checked (the General Catalog of Variable Stars (Kholopov 1985)). Ultimately, it was decided to use the Bookmeyer amplitudes for our calibration to avoid any discrepancies.

In addition to the RRab sample from Sandage (2004), a sample of well observed RRc stars was also used for the calibration of NSVS amplitudes. These RRc stars were selected mainly from Bookmeyer et al. (1977), but a few RRc stars amplitude values were taken from other more recent publications (Pena et al. 1990, Fernley et al. 1990, Skillen et al. 1993, Heiser 1996).

Using a set of 55 well observed field RRab stars and 12 field RRc stars, the scaling relation for the amplitudes is:

$$A_V = 1.185 A_{NSVS} + 0.065 \tag{4.6}$$

Figure 4.8 shows the calibration for the amplitudes of the 55 RRab stars. With this scaling relationship, we can now produce period-amplitude diagrams. This result will be discussed in chapter 5.

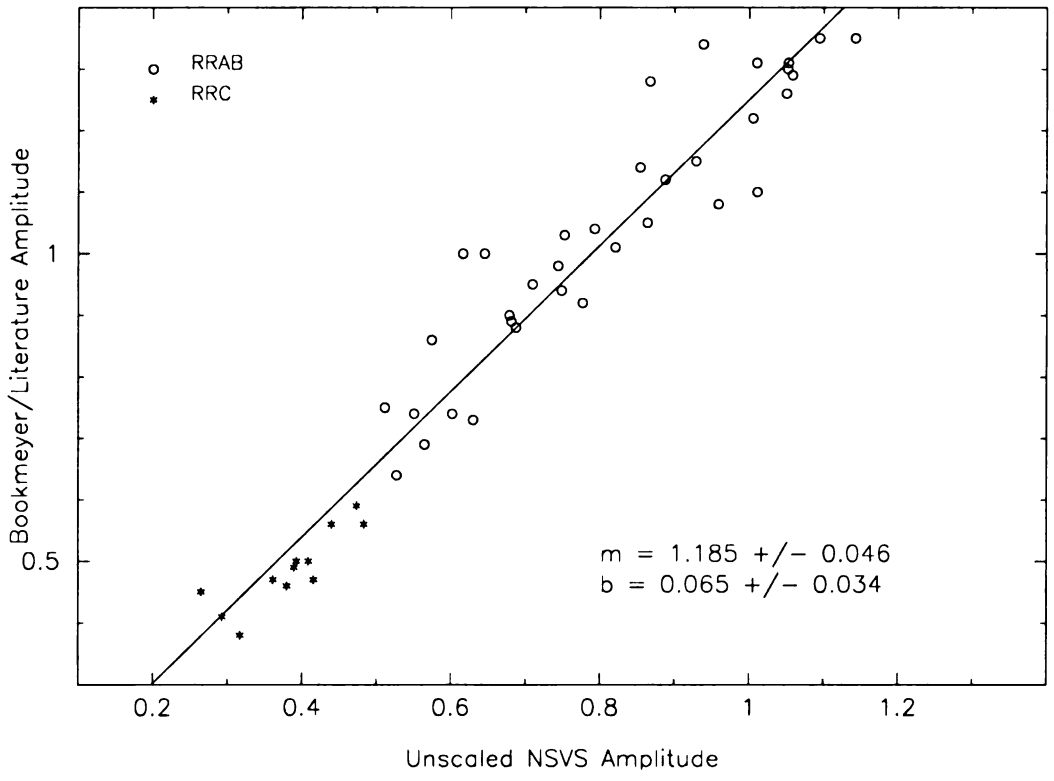

Figure 4.8 Amplitude calibration for RRab and RRc stars. Slope and Y-Intercept of the fitted line are also shown.

4.3 Magnitude Calibration

Since all the observations are on the V magnitude system of the Tycho catalog, more work needs to be done to put the NSVS observations onto the standard Johnson V system. The main reason to do this is for easy comparison to quantities in the literature, which is usually cited in Johnson V. To calibrate the data, we can use the Landolt standard stars (Landolt 1992).

The first selection criterion for Landolt standard stars was location. Most of the standard stars are located near the celestial equator, but we excluded those far in the southern celestial hemisphere. The second selection criterion is based on the color $(B-V)$ of the Landolt standard star. For the RR Lyraes, a representative $B-V$ color is 0.4. Thus, Landolt standard stars with a $B-V$ between 0.0 and 1.0 should be used. In this analysis, the entire range of $B-V$ was used ($-0.3 < B-V < 2.0$), but emphasis was made to cover the $B-V$ range from 0.0 to 1.0.

A search was conducted for the Landolt standard stars in the NSVS catalog. A number of the standard stars were not found in this catalog due to a crowded field or a bright, near neighbor that made identification difficult. A search radius cone of $0.1'$ to $0.8'$ was used. In the end, a total of 147 Landolt standard stars were used for magnitude calibration.

For the calibration, a linear regression fit was performed. The fit took into account the $B-V$ and V magnitude provided in Landolt (1992). The regression fit produced the following relation (T. Beers, private communication):

$$V_{NSVS} = 0.692(0.072) + 0.981(0.006)V_{standard} - 0.549(0.015)(B-V)_{standard} \quad (4.7)$$

The quantities in parentheses are the uncertainties in the coefficients. This equation was rearranged so that the input is the NSVS magnitude and the output is the standardized magnitude. A color term exists for the calibration, as can be seen in Figure 4.9. This color term was taken into account in the transformation and the results can be seen in Figure 4.10. For the RR Lyrae standard magnitudes, we chose a $(B-V)$ color of 0.35.

4.3.1 Absolute Magnitude of RR Lyraes and Distances

To derive photometric distances, the absolute magnitude of the object of interest must be well known. However, obtaining this value can be a difficult endeavor. RR Lyraes are an ideal distance indicator for old stellar populations since they are found in all components of the Galaxy and in extragalactic sources, such as the Magellanic Clouds and M31. The absolute magnitudes of the RR Lyraes are however, still not as well defined as one would want. Different methods used to obtain RR Lyrae absolute magnitudes, though now yielding similar results, still show some discrepancies.

For this project, many of the results depend on some distance measurement of the NSVS RR Lyraes. The absolute magnitude was obtained through a M_V-[Fe/H] relation first (see section 2.1.3), and then the distances were calculated. To derive the distance, the distance modulus was employed:

$$m - M = 5 \log_{10} d - 5 + A \tag{4.8}$$

The parameters are defined as: apparent magnitude (m), absolute magnitude (M), distance in parsecs (d), and some extinction (A). The extinction parameter must be

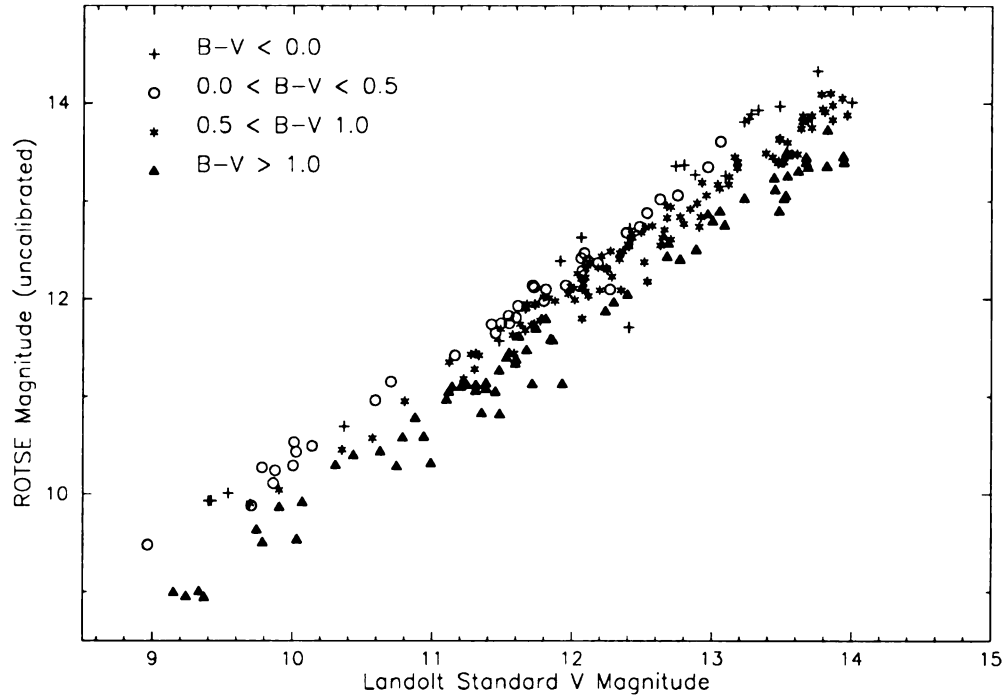

Figure 4.9 Tycho calibrated ROTSE magnitude versus the Landolt standard magnitude. Note the color term dependence.

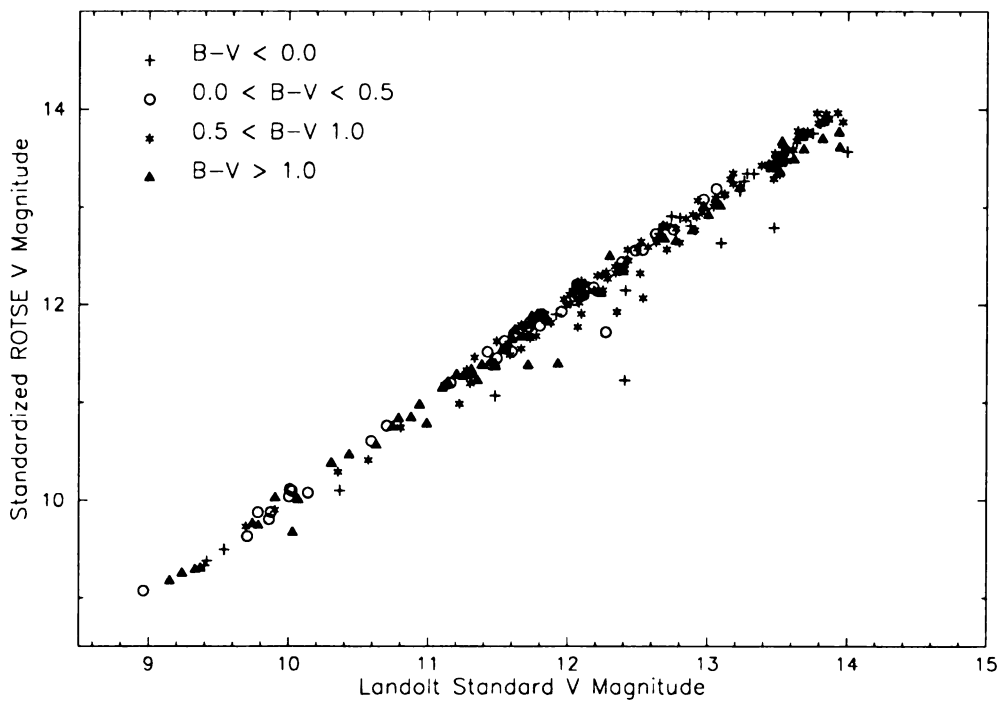

Figure 4.10 V magnitude calibration with Landolt standard stars. Note the same symbols are used for each color range as in Figure 4.6.

used to account for any diminishing of the brightness due to any interstellar dust found between the observer and the star. To determine the extinction, the Schlegel dust maps were used to find A for each RR Lyrae candidate.

The Schlegel dust maps are an ideal resource to derive the extinction since the maps have direct measurements of reddening from dust in the Galaxy. The Schlegel dust maps were produced from COBE/DIRBE and IRAS/ISSA maps of the Galaxy with all of the zodiacal light and cosmic infrared background removed (Schlegel et al. 1998). A fuller description of the process of creating these maps and converting the information into absorption information is provided in their paper and is beyond the scope of this dissertation.

To access this information, the entire Schlegel dust maps were downloaded as well as programming tools to access it. To retrieve the reddening information in the form of $E(B-V)$, the galactic coordinates (l,b) are needed. Using the relation $A_V = 3.2E(B-V)$ for Johnson V, the absorption correction is obtained.

Once the absorption correction is known, the distance to the RR Lyraes in the sample can be determined. In addition to finding the distance of the RR Lyraes from the Sun, a *Z distance* was calculated. This is the distance above or below the Galactic Plane ($Z = 0$) in parsecs. The Z distance is a simple geometric relation between the galactic latitude (b) and the distance from the distance modulus (d):

$$Z = d \sin b \tag{4.9}$$

For the distance from the Galactic center (R), simple geometric relations are used. Figure 4.11 is a diagram showing all the distances and angles used for these calculations. Since we now know the distance (d) in parsecs from the sun for an object, the galactic coordinates (which are really angles) are related to find R. Galactic

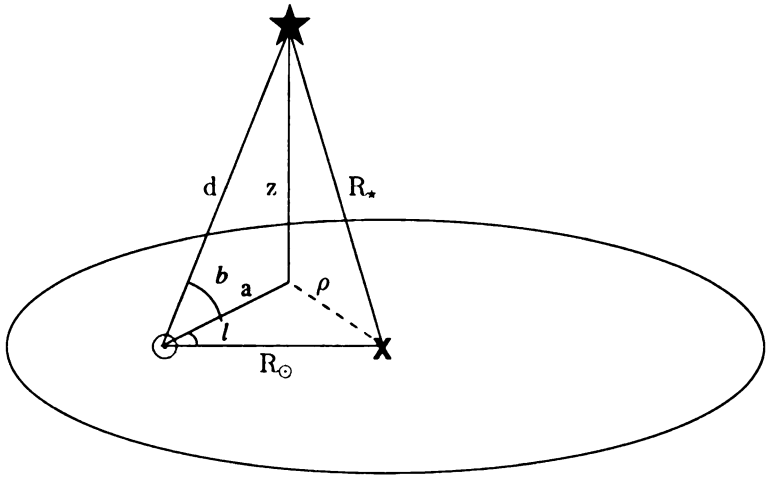

Figure 4.11 Diagram of the the geometry to determine the distances. The solar distance ($R_\odot$ was assumed to be 8.5 kpc). The **X** in the diagram is the center of the Galaxy or where there is buried treasure.

longitude is l and the galactic latitude is b. The projection of the distance to the RR Lyrae candidate from the Sun onto the Galactic plane is:

$$a = d\cos b \tag{4.10}$$

Then, on the plane of the Galaxy, we can determine the projected distance, ρ, of the RR Lyrae candidate to the Galactic center by using the law of cosines:

$$\rho = \sqrt{(d\cos b)^2 + R_\odot^2 - 2dR_\odot \cos b \cos l} \tag{4.11}$$

where $R_\odot$ is 8.5 kpc (the distance of the Sun from the center of the Galaxy).

We assume the additional z distance of the Sun from the Galactic plane to be negligible compared to $R_\odot$ or to z. This z distance is about 8 pc from the Galactic plane. Therefore, the distance of the star from the Galactic center is found from the Pythagorean theorem:

$$R_\star = \sqrt{z^2 + \rho^2} \tag{4.12}$$

Furthermore, the relative x and y projections on the Galactic plane can be calculated, and graphically show the distribution of the RR Lyrae candidates about the Galactic center. Figure 4.12 shows this distribution.

$$x = RCos(l) \tag{4.13}$$

$$y = RSin(l) \tag{4.14}$$

4.4 Photometric Metallicities

Traditionally, metallicities of RR Lyraes are derived from spectroscopic observations. In the case of large surveys where there are many thousands of stars, obtaining spectra for each of these stars may take more than the lifetime of a graduate student! Instead, metallicities can be derived from empirical relations based on photometric observations. Two empirical relations were used, and they are described in the following subsections.

4.4.1 The Jurcsik & Kovacs [Fe/H]-ϕ_{31}-P relation

Jurcsik & Kovacs (1996) introduced a method using the period and the Fourier decomposition parameters of the light curve to determine the metallicity. This method

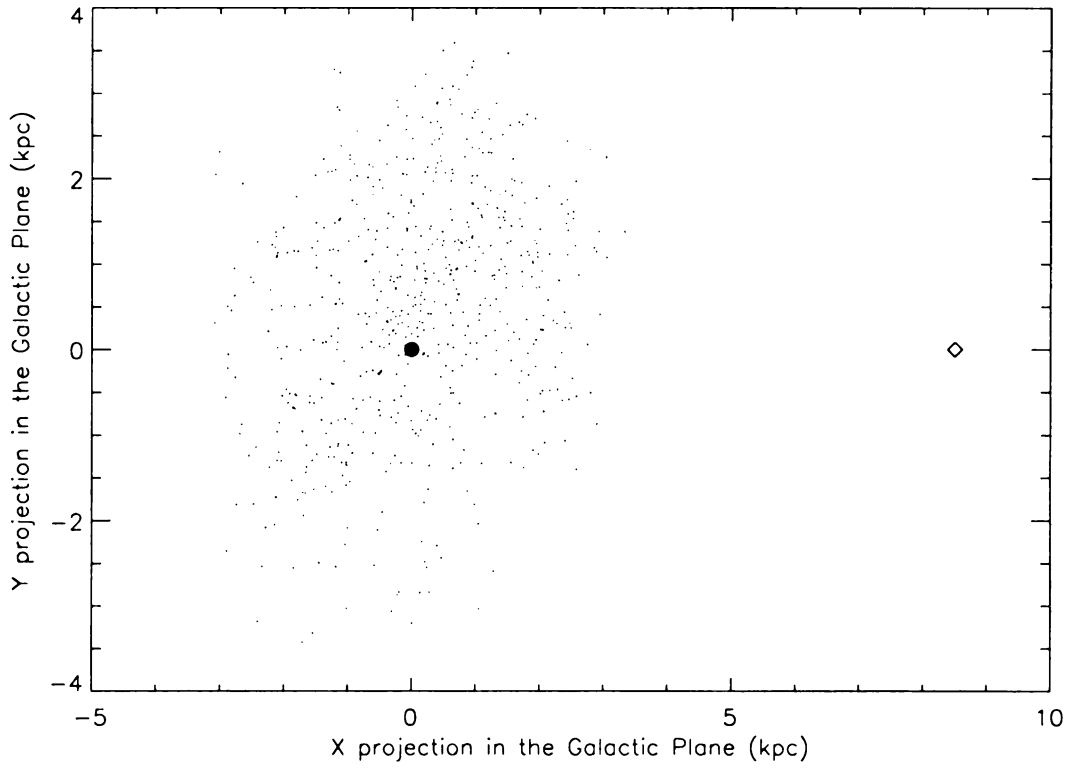

Figure 4.12 Distribution of the 660 RRab stars projected into the plane of the Galaxy. The solid circle is the Sun, at location (0,0) kpc. The Galactic center is at 8.5 kpc from the Sun. The open diamond at (8.5,0) kpc identifies its location.

is based on a set of well observed field RRab stars. They were careful not to include field stars that are experiencing the Blazhko Effect, as this affects the shape of the light curve, and hence the Fourier parameters. They performed a 15th order Fourier decomposition using *sine* functions on their sample of RRab stars. To accurately determine the Fourier parameters, it is necessary to have well sampled light curves, since the parameters are derived from the shape of the phased light curve. Lower quality light curves often have gaps in various parts of the light curve which can cause spurious values of the Fourier parameters.

The Fourier parameters can be calculated from fitting a sine or cosine Fourier series to the observed light curve:

$$m = A_0 + \sum_i A_i \cos(i\omega(t - t_0) + \phi_i) \qquad \text{where i} = 1, 2, \ldots \tag{4.15}$$

or

$$m = A_0 + \sum_i A_i \sin(i\omega(t - t_0) + \phi_i) \qquad \text{where i} = 1, 2, \ldots \tag{4.16}$$

In both equations, m is the observed magnitude or brightness of the variable star, and the A_i and ϕ_i are the coefficients of the fit. For this dataset, the FORTRAN program MINFIT was used to calculate up to an 8th order fit (Simon 1979).

$$R_{ij} = \frac{A_i}{A_j} \tag{4.17}$$

$$\phi_{ij} = i\phi_j - j\phi_i \tag{4.18}$$

An important thing to note here is that for the ϕ_{ij} terms, different factors of π need to be added or subtracted depending on whether one uses a sine or cosine Fourier series. Table 4.1 shows the correct factors that must be added/subtracted. The output files from MINFIT provide all the coefficients of the Fourier series up to

Table 4.1. Factors of π to add for the ϕ_{ij} Fourier parameters

Conversion direction	Factor	Fourier Parameter
COSINE to SINE	$-\pi/2$	ϕ_{21}
	$+\pi$	ϕ_{31}
	$-3\pi/2$	ϕ_{41}
SINE to COSINE	$+\pi/2$	ϕ_{21}
	$-\pi$	ϕ_{31}
	$+3\pi/2$	ϕ_{41}

8th order ($i = 8$) and the corresponding Fourier parameters. MINFIT uses a *cosine* Fourier series. To use the Jurcsik & Kovacs (1996) metallicity relation, the ϕ_{ij} terms must be converted to a *sine* Fourier series. The Fourier parameter of interest for the RRab metallicity relation is ϕ_{31}, so a factor of $+\pi$ was added.

The ϕ_{31} parameter is a shape parameter that best identifies the RR Lyrae variable stars. Other Fourier parameters have been used for analysis, but were not as distinctive as the ϕ_{31} parameter. Specifically, the ϕ_{31} parameter appears to be correlated with period and metallicity. Jurcsik & Kovacs (1996) found that this relation is actually a linear one.

Jurcsik & Kovacs derived a linear relationship with [Fe/H], period (P), and the Fourier phase parameter ϕ_{31}. This relation and the uncertainty in the [Fe/H] value are reproduced here. The uncertainty equation comes from Jurcsik & Kovacs (1996), their equation 4 and 5. This uncertainty relation is rather complex due to the circumstances that the regression variables (period and ϕ_{31}) were not completely independent from each other.

$$[Fe/H] = -5.038 - 5.394P + 1.345\phi_{31} \tag{4.19}$$

$$\begin{aligned}\sigma^2_{[Fe/H]} = & \\ & 1.809\sigma^2_{\phi_{31}} + 2(-0.01753)\phi_{31} + 2(-0.00289)P\phi_{31} \\ & +0.08910 + 0.02529P^2 + 0.00374\phi^2_{31}\end{aligned} \tag{4.20}$$

For comparison, a set of well observed field RR Lyraes (Bailey type ab) were processed to check this relation. These 55 RRab stars were among those used by Sandage (2004) for his work on the period shift and the Oosterhoff phenomenon. Sandage had compiled values for both ϕ_{31} and [Fe/H] from the literature. We cross referenced those stars from NSVS and obtained all the stars' photometric data.

We found that the NSVS ϕ_{31} values had to be scaled into a "standard" system, specifically the one Sandage had used. The reason for this scaling is similar to the one described in section 4.2 for the amplitudes. The Fourier parameter was derived from the light curves obtained with the filterless ROTSE-I telescope. To derive Fourier parameters as would be obtained with Johnson V observations, the NSVS ϕ_{31} values (ϕ'_{31} in equation 4.21) must be scaled. The scaling relation is :

$$\phi_{31} = 0.855(0.046)\phi'_{31} + 0.063(0.105) \tag{4.21}$$

Once the ϕ_{31} value is scaled, the Jurcsik & Kovacs (1996) metallicity formula can be used. Figure 4.13 shows our ϕ_{31} values compared with published values (Sandage

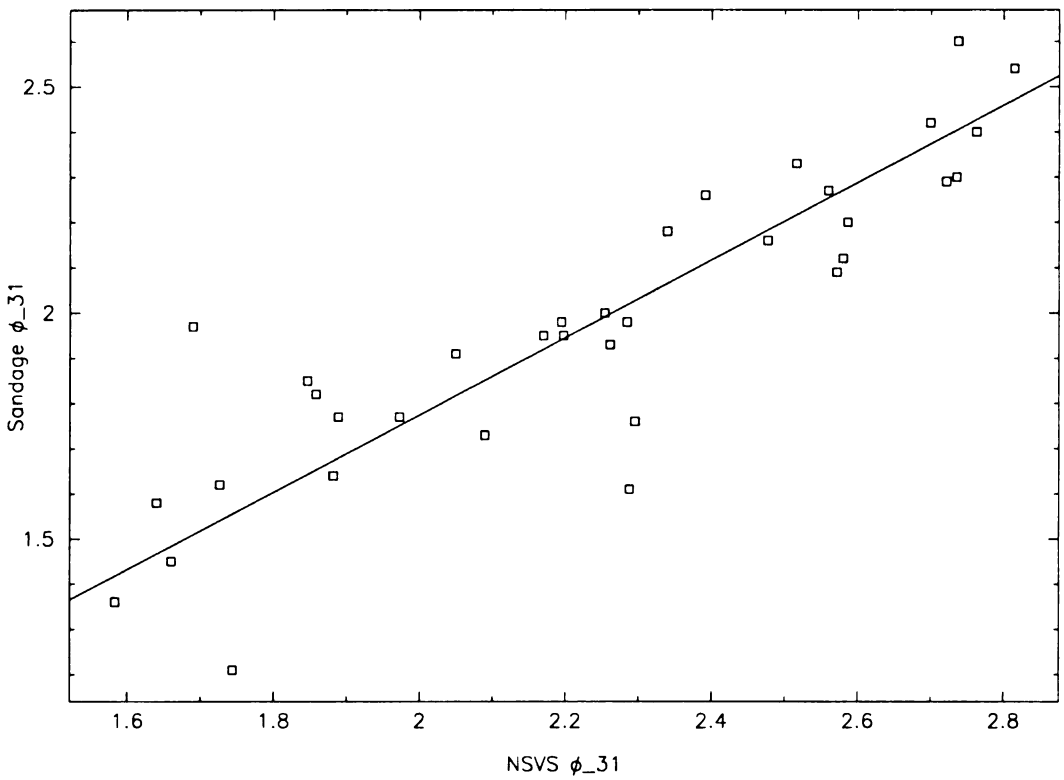

Figure 4.13 Calibration of the ϕ_{31} values to the published values (Sandage 2004).

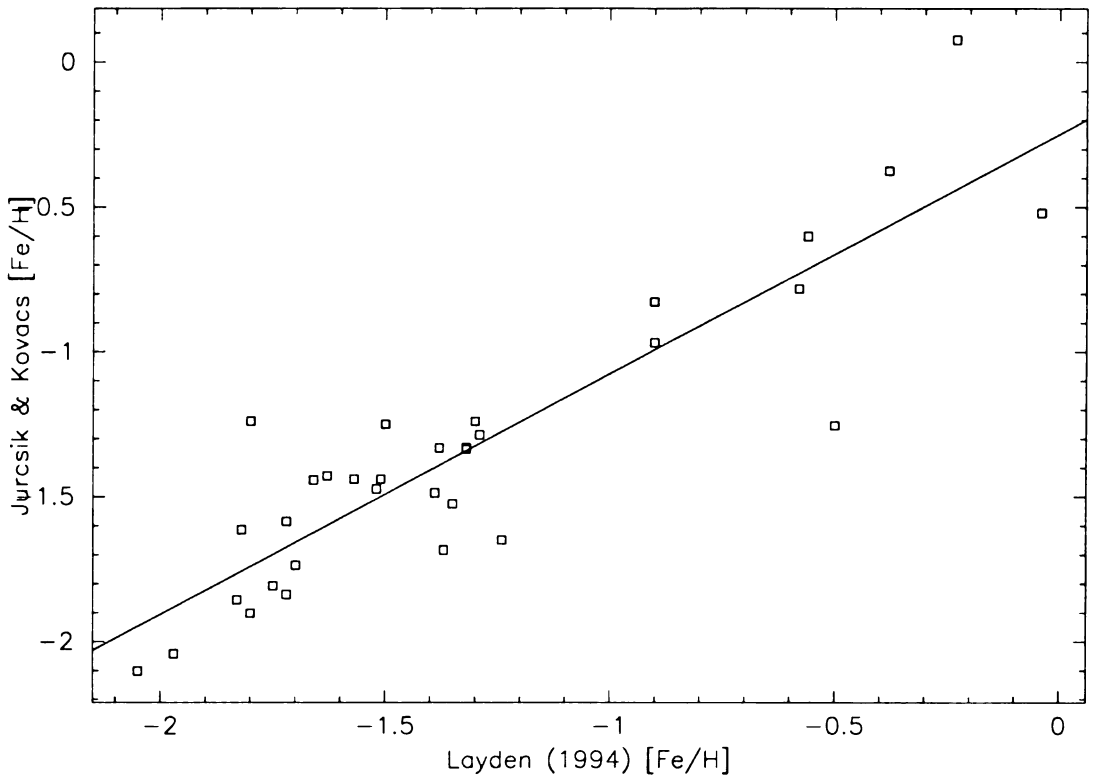

Figure 4.14 Calibration for the metallicities derived from Jurcsik & Kovacs (1996) method on to metallicity system adopted by Sandage and used by Layden (1994).

2004). However, Sandage noted that the metallicity from the Jurcsik & Kovacs relation should be scaled when it is used with other metallicity systems that have been published in the literature. Specifically, Sandage's and our [Fe/H] scale is the [Fe/H] scale used by Layden (1994), which in turn is based on the Zinn & West scale (Zinn & West 1984). The plot of the calibration of the Jurcsik & Kovacs [Fe/H] with published values is presented in Figure 4.14. The Jurcsik & Kovacs metallicity was scaled onto the Zinn & West system by using Sandage (2004)'s relation:

$$[Fe/H] = 1.05[Fe/H]_{Jurcsik\&Kovacs} - 0.20 \tag{4.22}$$

In order to check if a given RR Lyrae star's light curve is adequate for the metal-

licity calculation, Jurcsik & Kovacs developed a compatibility test. They construct a "deviation parameter", D_F, to check the Fourier parameters. It is defined as:

$$D_F = \frac{|F_{obs} - F_{calc}|}{\sigma_F} \tag{4.23}$$

where F_{obs} are the Fourier parameters, a set of R_{ij} and ϕ_{ij}, from the observations. The theoretical values of F_{calc} and σ_F were updated by Kovacs & Kanbur (1998) (see their table 2). Specifically, F_{calc} are the corresponding theoretical values of the set of Fourier parameters. The σ_F are the uncertainties for F_{calc} determined from their calculations. In Jurcsik & Kovacs (1996), they state that the compatibility test is satisfied when D_m (the maximum of the set of D_F parameters) is less than 3.0. For the sample of RRab stars, a majority of the stars did not pass the compatibility test. However, for stars that did pass this test, their light curves were very well sampled and did not contain any large gaps in the phased light curve. Therefore, we did not use the D_m parameter to obtain a clean sample of RRab stars, since most of the stars are known to have adequate, but not high quality, light curves.

4.4.2 Sandage's [Fe/H]-log P-A_V relation

In addition to the Jurcsik & Kovacs method of deriving photometric metallicities, Sandage himself developed a way to obtain this quantity using different observational parameters. Sandage (2004) investigated the Jurcsik & Kovacs relation and its correlation to the period shift of the Oosterhoff groups. Sandage defines a period shift, ΔLog P, with respect to RR Lyraes found in M3, which is an Oosterhoff I globular cluster. The period shift can be calculated by comparing an RRab star to its counterpart of equal amplitude in M3. Sandage found that the ϕ_{31} parameter is indeed

correlated with the period shift, ΔLog P, in the same manner as the amplitude or color (see Sandage et al. (1981) for the complete period shift explanation). He argues that ϕ_{31} is correlated with metallicity, just as the period shift and the luminosity of RRab stars are. Therefore, using his results from Sandage et al. (1981), the derived metallicity is no longer dependent on ϕ_{31}, but rather another parameter correlated with the period shift. In this case, the parameter was amplitude.

Sandage's $\log P$-amplitude relation is reproduced here:

$$[Fe/H] = -1.453(\pm 0.027)A_V - 7.990(\pm 0.091)\log P - 2.145(\pm 0.025) \qquad (4.24)$$

To determine the uncertainty of the [Fe/H] value from this relation, we assume the largest source of error comes from the amplitude measurement. Since the true uncertainty of the amplitude is unknown and we have only calculated the external error, we adopt an uncertainty of [Fe/H] to be ≈ 0.32 dex. This was determined empirically by comparing the spectroscopic [Fe/H] from Layden (1994) to the [Fe/H] derived from Equation 4.24, subtracting in quadrature the uncertainty Layden attributed to his [Fe/H] values. Figure 4.15 shows how well the [Fe/H] from the $\log P$-amplitude relation compared with Layden's values.

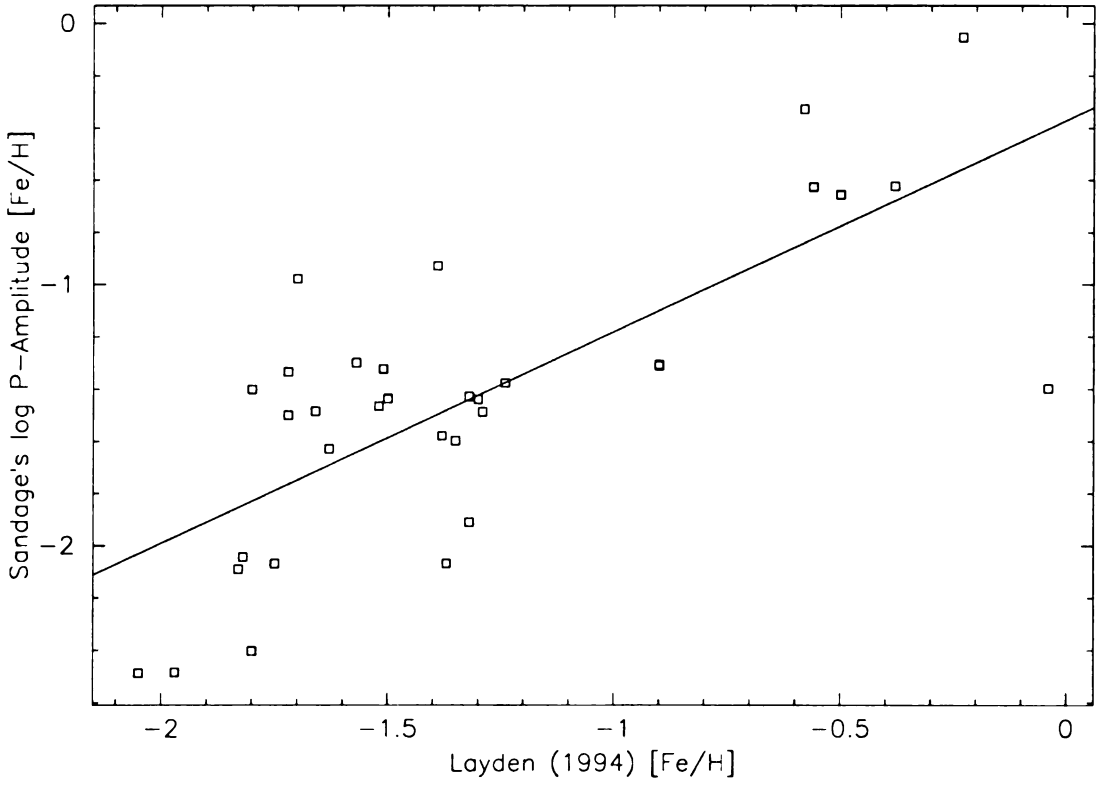

Figure 4.15 Comparison of [Fe/H] from the Sandage relation using amplitude and log period with Layden (1994) [Fe/H] values.

Chapter 5

Results from the Analysis of the NSVS RR Lyraes

Most of the results presented in this chapter are for the RRab candidates from the NSVS survey. The sample used for this dissertation was obtained from a copy of the full database at the University of Michigan. Two samples were extracted: one for the RRab stars and another for the RRc candidates. Many problems were encountered with the analysis of the RRc stars (see section 5.6). As for the RRab stars, the number of candidates shrank with certain cutoffs used to get a clean sample of stars. We will also discuss in the sections below some of the basic analysis tools constructed from the observed parameters. A more in depth discussion of the implications of these RRab results is deferred to Chapter 6.

5.1 Criteria for RR Lyrae Selection

5.1.1 Description of the Selection Criteria

For the sample obtained through the University of Michigan, two sets of criteria were used to extract a subsample of RRab and RRc candidates. It was assumed there would be some contamination of other types of variable stars in our RR Lyrae candidate sample. These criteria sets were designed to mine almost all of the RR Lyraes.

The criteria for the RRab candidates are listed in table 5.1. The period and amplitude range were set from the known general observational properties of RRab stars. The "ratio" is defined as a function of the brightest and faintest measurement with the median magnitude of the star. This parameter identifies whether a star spends most of the time brighter or fainter than its median magnitude. The ratio was originally developed to find contact binaries in the NSVS survey (T. McKay, private communication).

$$ratio = \frac{\text{max magnitude} - \text{median magnitude}}{\text{max magnitude} - \text{min magnitude}} \tag{5.1}$$

The ratio criterion depends on the period of the RRab stars. Since the period and amplitude are correlated to each other, the ratio is also correlated to the period. In Figure 5.1, the ratio is plotted against the period range of 0.0 to 1.2 days for all the stars in the database. A clump of stars appears in the period range between 0.4 and 0.8 days. This clump is believed to contain the majority of the RRab candidates. The stars below this clump are other types of variable stars. A shallow sloped line was fit to include these RRab candidates. This limit is used as one of our filters to

Table 5.1. RRab candidate criteria for selection from the NSVS survey.

Parameter	Range of Values
Period	0.30 to 0.95 days
Amplitude	0.20 to 1.5 magnitudes
Ratio	$> -0.625 Period + 0.719$
$J - H$	-0.1 to 0.5
$H - K$	-0.1 to 0.25

obtain the RRab sample.

Furthermore, the NSVS survey was cross correlated with the 2MASS catalog by the ROTSE team at the University of Michigan (T. McKay, private communication). This now gives us infrared color ($J - H$ and $H - K$) information on all the NSVS stars. To check if the color criteria range was adequate, a sample of known RRab from the General Catalog of Variable Stars (Kholopov 1985) was found in the 2MASS catalog. The average $J - H$ color was 0.219 and 0.063 for $H - K$. Thus, the color criteria was broad enough to ensure the RRab stars could be chosen.

For the RRc sample, the criteria set changed slightly. Table 5.2 lists the RRc criteria. Two regions were needed for the ratio criterion. This ensured that the previously selected RRab stars and short period, non-RR Lyrae variable stars (e.g. eclipsing binaries and δ Scuti stars) would not be included in this sample. Figure 5.2 shows the regions in ratio-period space where the RRc stars were expected to exist.

Again, the period and amplitude criteria were based on the known general observational parameters of RRc stars. The 2MASS color ranges were kept the same. As with the RRab stars, the average 2MASS colors of RRc stars were obtained and found to be within the given range. The average $J - H$ color was calculated to be 0.164 and the average $H - K$ color was 0.04. Thus, the color range was broad enough

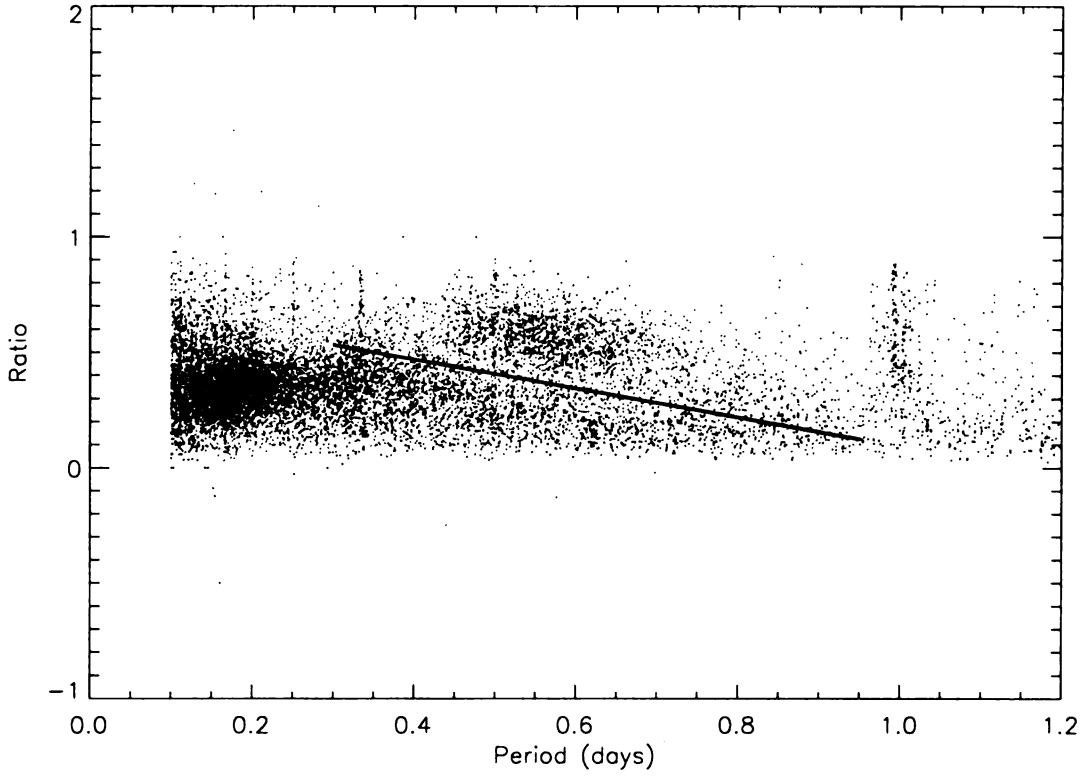

Figure 5.1 This plot was used to determine the appropriate ratio range to select the RRab candidates. Note the clump of stars between 0.4 and 0.8 days. The line is the function for the ratio parameter.

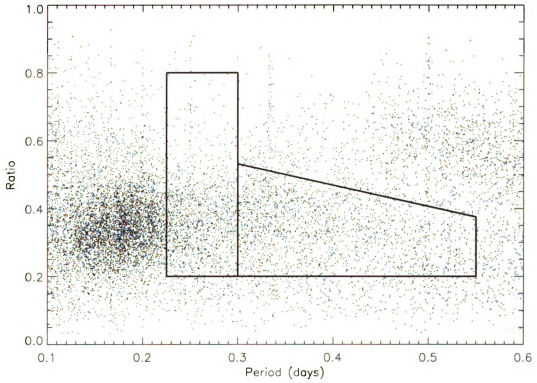

Figure 5.2 Ratio distribution with period. The boxed regions are where the RRc candidates were selected.

Table 5.2. RRc candidate criteria for selection from the NSVS survey.

Parameter	Range in Triangular region	Range in Rectangular region
Period	0.225 to 0.3 days	0.3 to 0.55 days
Amplitude	0.2 to 0.7 magnitudes	0.2 to 0.7
Ratio	0.2 to 0.8	> 0.2 and $< (-0.625 Period + 0.719)$
$J - H$	-0.1 to 0.5	-0.1 to 0.5
$H - K$	-0.1 to 0.25	-0.1 to 0.25

to select RRc stars.

5.1.2 Cutoffs for a Clean Sample of RR Lyraes

In total, we obtained 2196 RRab and 2558 RRc candidates using these sets of criteria. One of the first cutoffs for extracting the RR Lyraes stars from the sample was to remove all the duplicate entries of the stars. This particular problem was noted by Wils (2001). These "duplicate" stars have multiple entries in the NSVS database due to the way the star entries were created. Each star has its own unique position. However, the NSVS positions for an individual star occasionally can vary as much as 10 arcseconds. When this happens, another separate entry is made for the star. The duplicates were removed by comparing the equatorial coordinates (right ascension and declination), the period of the star, and the number of observations. A duplicate was found if the difference in equatorial coordinates was less than 10 arcseconds. Due to the small differences in photometric zero point, the observations for multiple identifications of the same star were not combined. Instead, we chose the entry with the most observations for the analysis. Using these requirements, 228 duplicate RRab and 205 RRc candidates were removed from our sample.

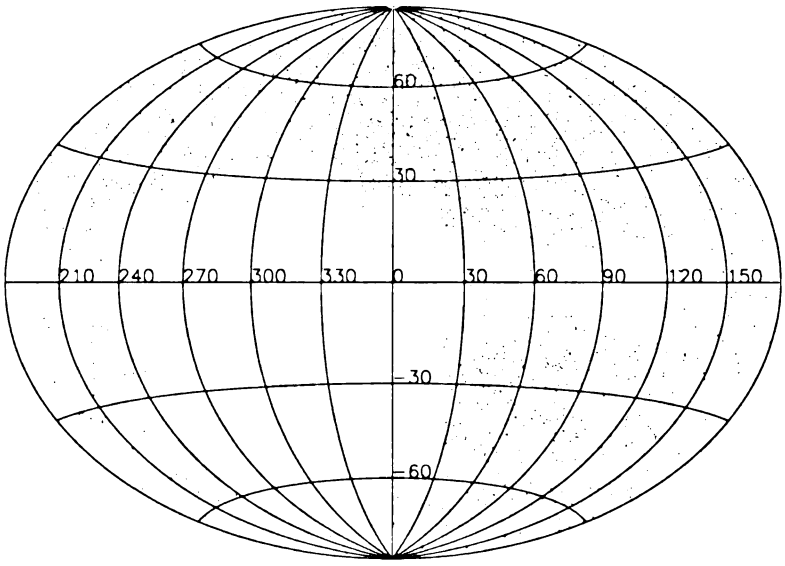

Figure 5.3 1430 RRab candidates selected from the NSVS survey. The coordinate system is in Galactic l and b.

In addition to these duplicate entries, stars whose light curves were clearly not of an RR Lyrae type were removed. These stars were often found to be eclipsing binary stars. Ten RRab stars were found in the RRc sample and 17 RRc stars were in the RRab sample. These stars were placed in the respective samples. With these results and the identification of the duplicate stars, the RRab sample was reduced to 1430 candidates. The RRc sample shrank to 1446 candidates. Figure 5.3 and 5.4 are the Aitoff plots of the RRab and RRc samples at this point.

Furthermore, a second cutoff was applied after the duplicates and the obvious non-RR Lyraes were removed. We noticed the fainter RR Lyrae candidates had noisy phased light curves. With such light curves, it becomes difficult to determine accurate parameters such as amplitude or the Fourier parameter ϕ_{31}. Therefore, we instituted a cutoff in magnitude in order to obtain a clean sample of RR Lyrae stars. Stars

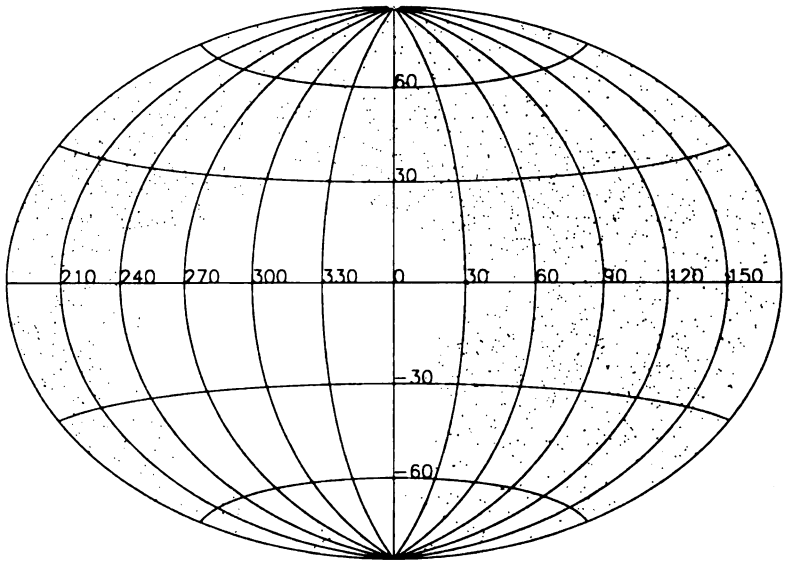

Figure 5.4 1471 RRc candidates selected from the NSVS survey. The coordinate system is in Galactic l and b.

fainter than 14th magnitude (in ROTSE's Tycho magnitude system) were omitted. The star's intensity weighted mean magnitude[1] was used for this cutoff.

Also in consideration of determining the observational parameters, stars with fewer than 40 observations were omitted from the analysis. Often the light curves of these stars exhibited large gaps, and in some cases, missing maximum or minimum of the light curve cycle. The combination of these two cutoffs reduced the size of our samples further. The RRab sample now has 660 stars where the RRc sample contains 375 stars. Figure 5.7 and 5.8 show the Aitoff projection of the RR Lyraes for these reduced samples.

[1]Intensity weighted mean magnitude is calculated by simply taking the magnitude measurements and converting them to fluxes via the luminosity equation. The fluxes are then averaged and this value is converted back into a magnitude.

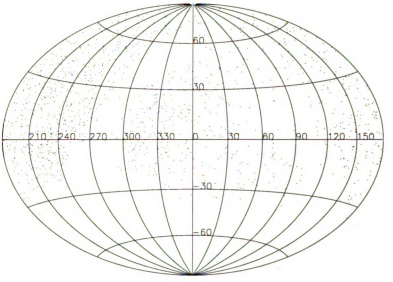

Figure 5.5 1430 RRab candidates selected from the NSVS survey. The coordinate system is in the equatorial system (right ascension and declination).

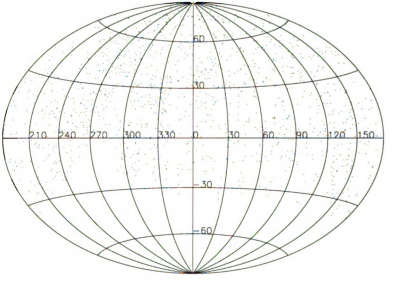

Figure 5.6 1471 RRc candidates selected from the NSVS survey. The coordinate system is in the equatorial system (right ascension and declination).

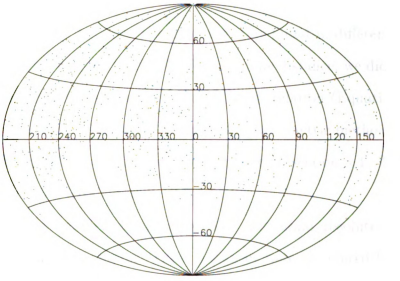

Figure 5.7 RRab sample of 660 stars in Aitoff projection (in equatorial coordinates).

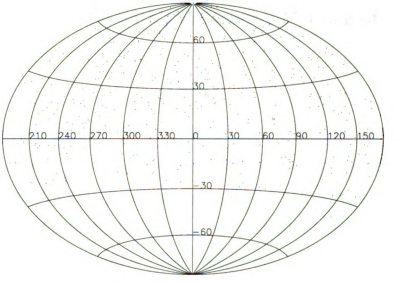

Figure 5.8 RRc sample of 375 stars in Aitoff projection (in equatorial coordinates).

5.1.3 Absolute Magnitudes and Distances for the RRab Stars

For some of our results, we wished to compare stars found in different regions of the thick disk/inner halo covered by NSVS. To determine distance, we did not use an average absolute magnitude, but rather the M_V-[Fe/H] relation (Equations 2.6 and 2.7). The metallicities were all obtained through the photometric methods described in section 4.4. The metallicity results will be discussed in section 5.4. The average M_V for our sample of 660 RRab stars is 0.58 ± 0.15.

Each star's distance was determined from their individual absolute magnitudes derived from the M_V-[Fe/H] relation. These distances were calculated by the usual way with the distance modulus (Equation 4.8) and applying extinction corrections as described in section 4.3.1. All distances are in units of kiloparsecs.

5.1.4 Cross-correlation with the General Catalog of Variable Stars

As a check, we searched for the 1430 NSVS RRab candidates in the General Catalog of Variable Stars (GCVS) (Kholopov 1985). We had to consider that many of the stars in the GCVS have poor positions, with errors of up to one arcminute. Nonetheless, to match the NSVS RRab stars in the GCVS, we had to use the positions. The search grid limit was varied from 1 and 2 arcminutes and down to 3 arcseconds. For 2 arcminutes, there were 312 matches whereas for 1 arcminute, 291 stars were matched. In the smallest search grid size of 3 arcseconds, 133 NSVS RRab stars were found in the GCVS. Out of approximately 1400 RRab stars used in the analysis, between 80 and 90% of the stars found in the NSVS survey are not found in the

GCVS catalog. The RRc stars were not matched with the GCVS since a final clean sample of RRc stars can not be produced at this time (see discussion in section 5.6).

5.2 Period of the RRab Stars

The periods of the RRab candidates were derived from the supersmoother method or from the cubic spline routines (see Section 4.1). The original database contained the periods determined through the cubic spline methods described in Akerlof et al. (2000b). Supersmoother was run on all of the candidates, deriving periods independently from the cubic spline routines. In most cases, the periods from supersmoother agreed with the cubic spline result to about 0.001 days. For 111 stars, the periods from the two different methods had a difference of more than 0.01 days. These period discrepant stars had a third pass in determining their periods using the IRAF task PDM. If the PDM period solution agreed with one of the two period choices, that period was chosen.

However, there are cases where the PDM solution did not resolve the period alias. Often the aliases were at a third or half day periods. For this situation, both supersmoother and the cubic spline solutions were kept, but not used for any analysis involving periods. This applies to six RRab candidates. Of the 111 stars checked with PDM, PDM suggested a third period solution for four stars. With three different period solutions from the three methods, the phased light curve shape was examined to determine which period was correct. In this situation, the PDM solution was chosen. Uncertainties in the periods are roughly at the level of 10^{-4} days. This was determined from an examination of the period aliases close to the true period, as seen by the solutions from supersmoother and from PDM.

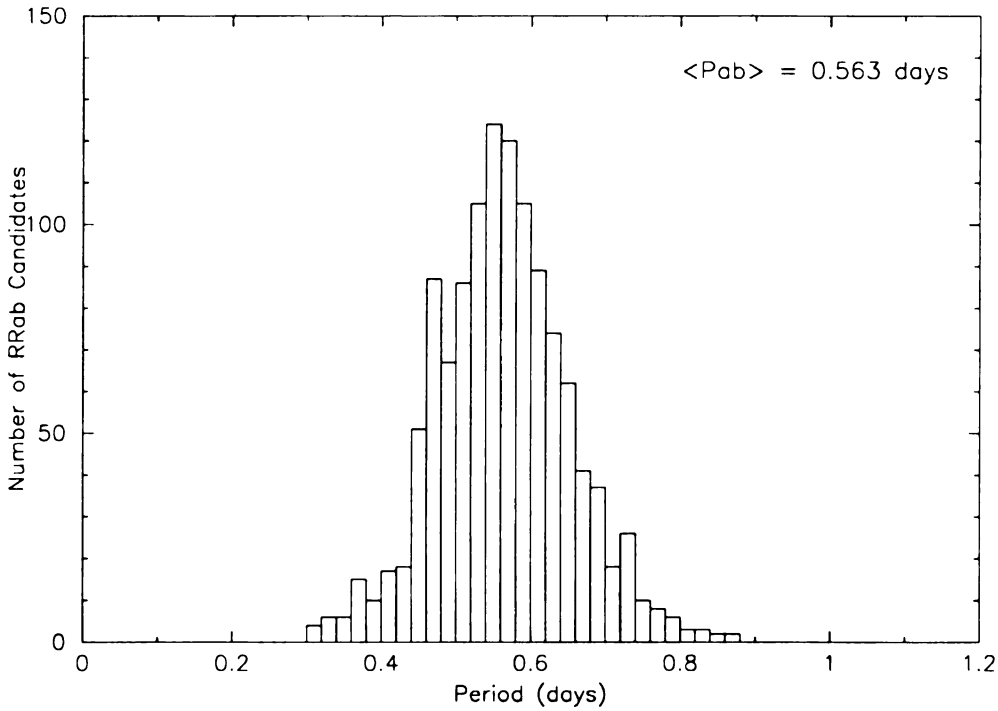

Figure 5.9 Period distribution histogram for RRab candidates from the NSVS survey.

To graphically show the range of periods of the NSVS RRab sample, a histogram was produced. Figure 5.9 shows the periods for the RRab stars, and Figure 5.10 shows how the periods are distributed by zones of $|Z|$ distance.

The average period in each zone is close to the value of an RR Lyrae population from an Oosterhoff I globular cluster. There does seem to be a tail into the longer periods, which would indicate a population of RR Lyraes similar to those found in an Oosterhoff II population. We see from the histogram that the Oosterhoff I signature is dominant for the RRab stars in the solar neighborhood, but there is still a contribution from Oosterhoff II. We will demonstrate later that the short period RRab stars in the low $|Z|$ zone also indicates the presence of a thick disk population.

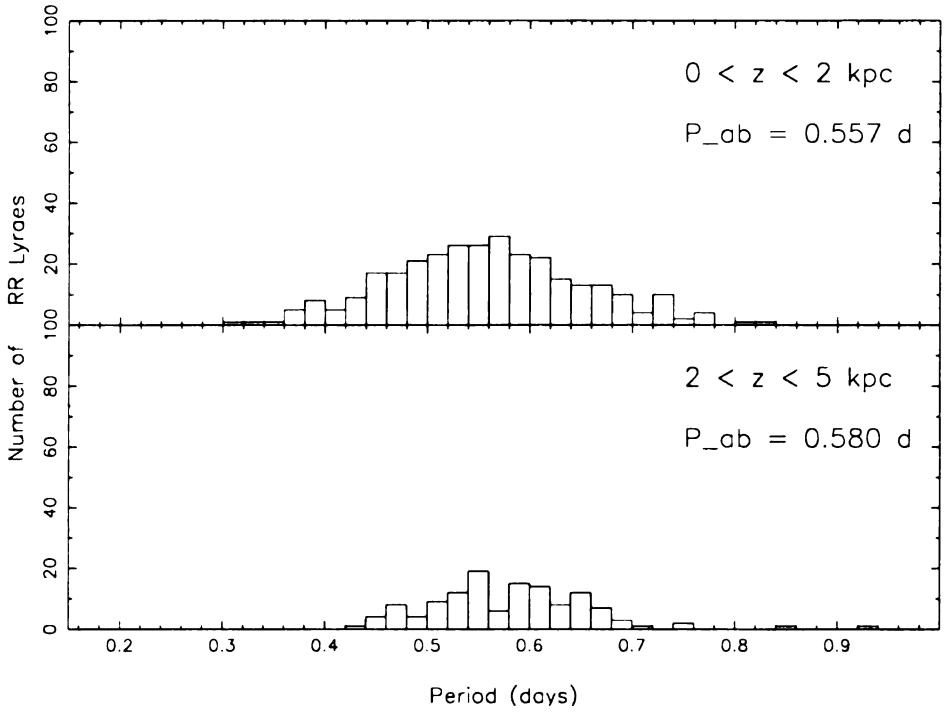

Figure 5.10 Period distribution histogram for 608 RRab's, divided by $|Z|$ distance zones.

5.3 RRab Amplitudes

The amplitudes of the RRab stars were the next observational parameter calculated for this project. The amplitude can be used with other parameters to investigate trends in the population. Section 4.2 described the important step of calibrating the amplitudes onto the Johnson V filter system. This calibration was performed for the sample of 660 RRab stars. After this calibration, the light curves were checked for quality and completeness. In some cases, the light curves were not complete, i.e. the maximum or minimum of the light cycle was not observed. Fifty-two stars with questionable amplitudes were omitted from the study and our sample is now at 608 stars.

It should be mentioned here that the intrinsic uncertainty of the amplitude is un-

known since it was determined from either the spline fit or a template fit. The fitting routines did not return a useful formal error to the amplitudes. However, inspection of the phased light curves indicates that the amplitudes have an uncertainty of ~ 0.1 magnitudes. This is assuming the star was well observed with many data points. The calibration uncertainty was calculated from the scaling relation onto the Johnson V filter system (see Equation 4.6). This uncertainty from the calibration of the NSVS amplitudes onto the V amplitude system is on average about 0.02 magnitudes.

5.3.1 Period-amplitude diagram

One of the diagnostic tools to investigate the Oosterhoff dichotomy is the period-amplitude diagram. Clement & Rowe (2000) confirmed earlier results that in a period-amplitude diagram, RRab stars from the Oosterhoff I and II groups lie in two different regions. A trend line for both groups was determined by Clement & Rowe based on the RR Lyraes found in M3 (an Oosterhoff I cluster) and ω Cen (an Oosterhoff II cluster). These trend lines can shift with metallicity in these diagrams, but the general locations of the Oosterhoff I and Oosterhoff II locii do not change.

In order to use the Oosterhoff trend lines developed by Clement & Rowe, the log base 10 of the periods was calculated and plotted with the scaled amplitudes. Figure 5.11 shows the NSVS RRab stars with the Oosterhoff trends overplotted. One should note that the RRab stars do not all fall on one or the other trend line. It appears that a majority of stars fall near the Oosterhoff I trend line, which is in agreement with the result from the period histograms. However, there are stars populating the region where Oosterhoff II stars reside in the period-amplitude diagram. This presents a stronger case for the existence of an Oosterhoff II population in the region covered

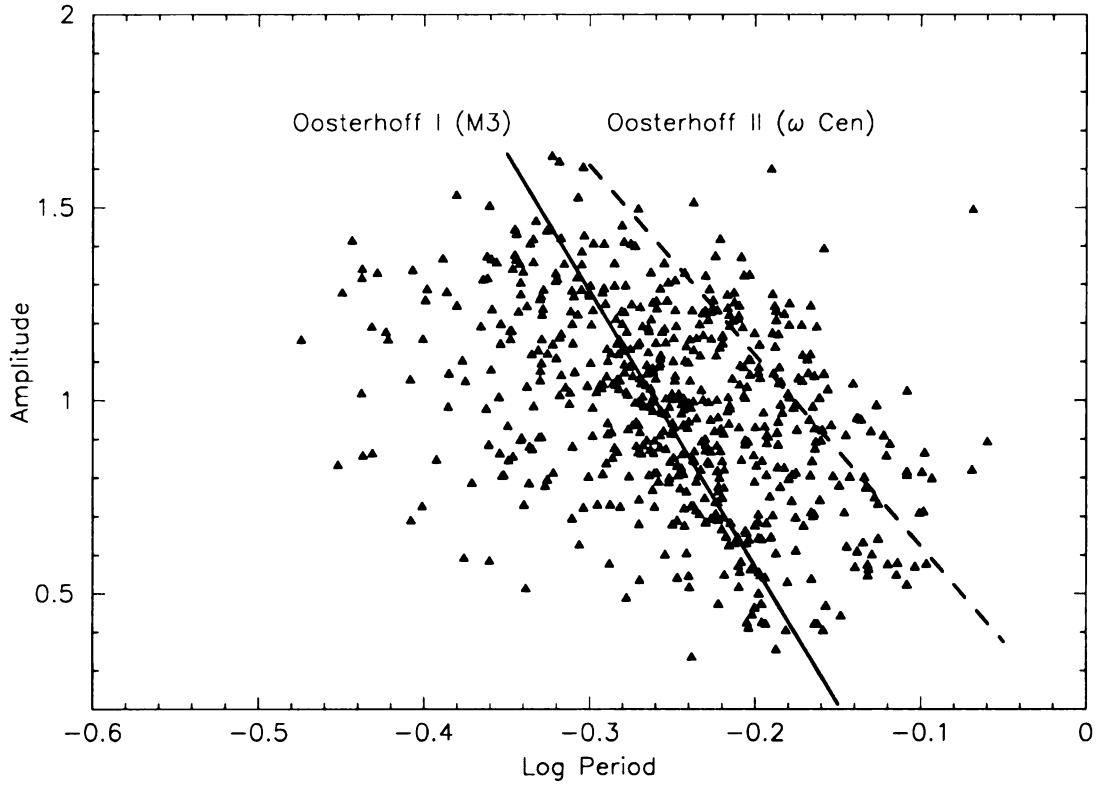

Figure 5.11 Period-Amplitude diagram for 608 RRab's. The Oosterhoff trend lines are from Clement & Rowe (2000). The solid line is Oosterhoff I and the dashed line is the Oosterhoff II trend line.

by the NSVS survey.

5.3.2 Interesting outliers

Not only does the period amplitude diagram show the Oosterhoff I and II population, interesting stars show up in the plots as outliers. In a few instances, there were legitimate reasons to omit these outlier stars. Usually the reason was that the light curve was too poor for accurate amplitude measurements. However, one long period outlier was found to be a possible anomalous type II Cepheid variable star. Other shorter period variables were found to be possible thick disk RR Lyraes or

long period RRc stars not yet excluded from the RRab sample. The RRc stars were omitted from the RRab sample, but placed in the RRc sample (see discussion of RRc stars in section 5.6). In the period-amplitude diagram presented here, the thick disk candidates were left in the plot. In section 6.2, we will revisit these thick disk stars.

5.4 Metallicities

Traditionally, metallicities of RR Lyraes are derived from spectroscopic observations. In the case of large surveys where there are many thousands of stars, obtaining spectra for each of these stars may take more than the lifetime of a graduate student! Instead, metallicities can be derived from empirical relations based on photometric observations. Two empirical relations were used to obtain photometric metallicities, which are described in the following subsections.

5.4.1 [Fe/H] from Jurcsik & Kovacs' Method

The Jurcsik & Kovacs method (see section 4.4.1) was used to derive photometric metallicities in the cases where the uncertainty in ϕ_{31} was less than 0.2. We found that if the uncertainty is large, unrealistic or very uncertain metallicities were determined. This particular cutoff in ϕ_{31} uncertainty reduced the number in the RRab sample from 608 to 433 stars. Figure 5.12 shows the metallicity derived from this method as a function of $|Z|$ distance.

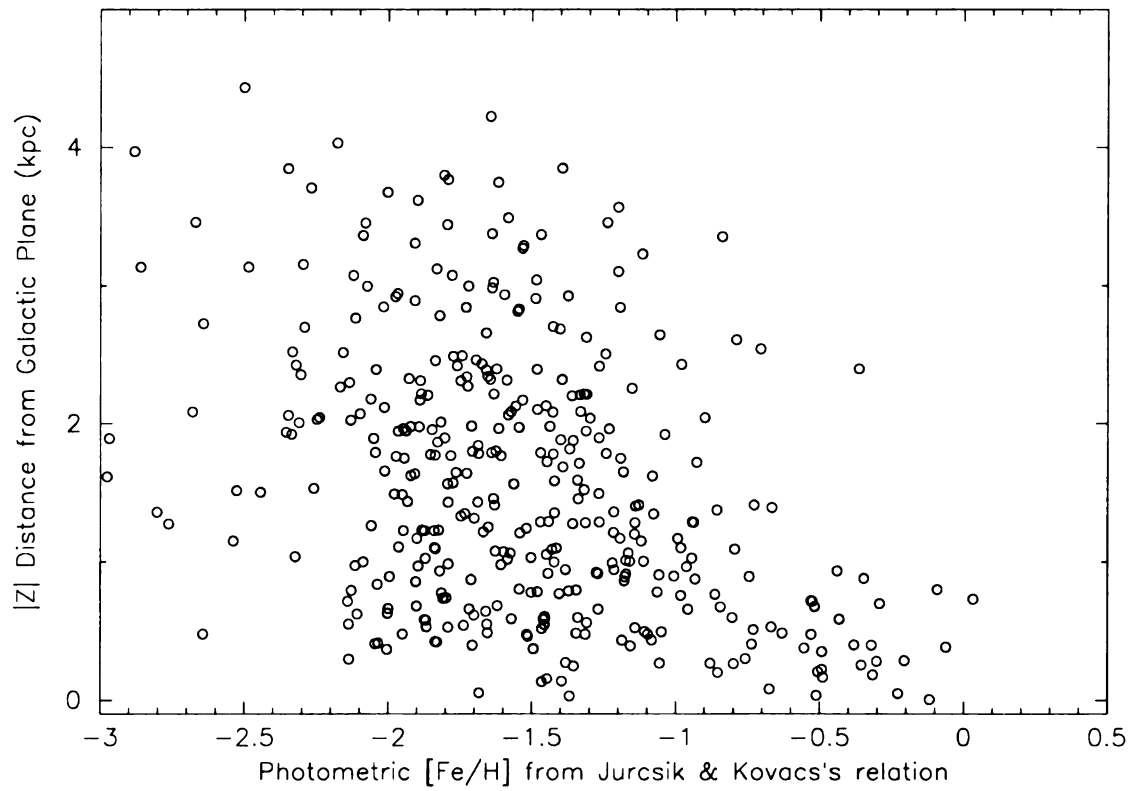

Figure 5.12 Distribution of the metallicities as a function of distance from the Galactic Plane. Note the clump of stars at high metallicity and low $|Z|$ distance. This may be the thick disk component. These stars have [Fe/H] values determined only from the Jurcsik & Kovacs (1996) method.

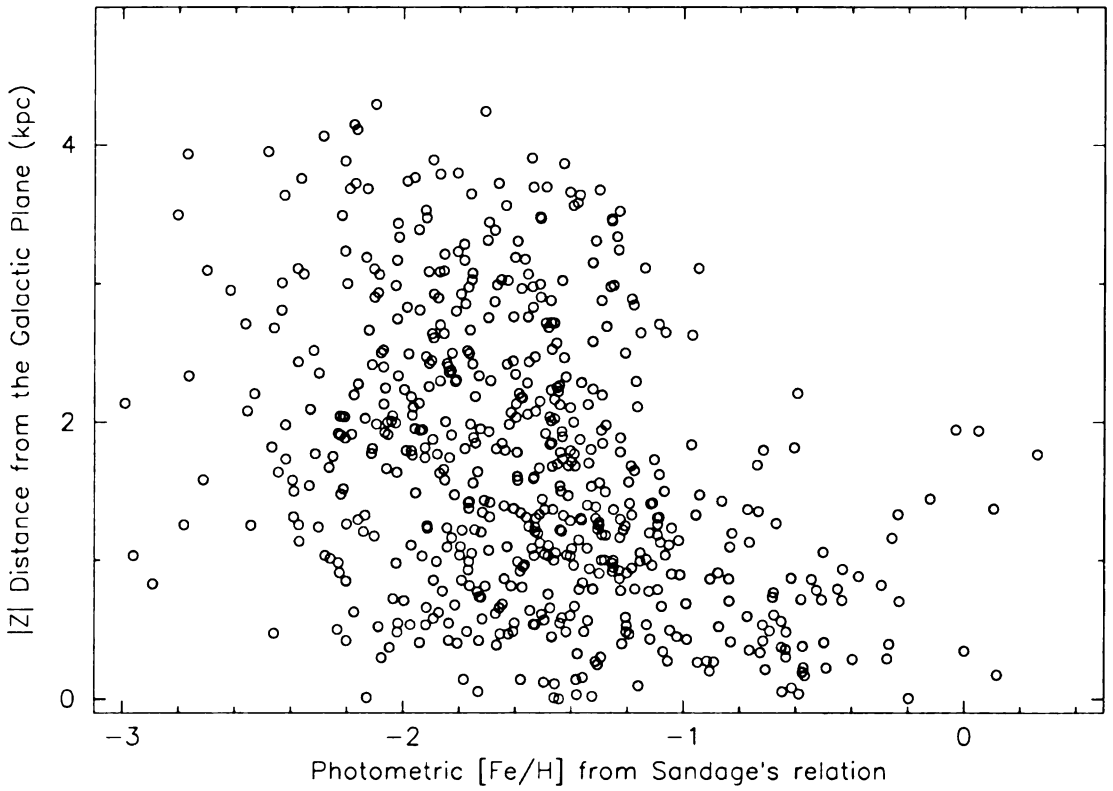

Figure 5.13 Distribution of metallicity from Sandage's method as a function of $|Z|$ distance.

5.4.2 [Fe/H] from Sandage's Method

A second metallicity calculation was made by the method of Sandage (2004) (section 4.4.2). This method was applied to the RRab stars with good amplitude measurements. While the Jurcsik & Kovacs method reduced our sample to 433 stars, the Sandage method provides metallicities for the 608 stars. Figure 5.13 shows the metallicity distribution of the 608 stars with $|Z|$ distance. Again, we see a clump of stars at [Fe/H] > -1 and close to the plane. However, compared to Figure 5.12, this clump appears to be more scattered.

5.4.3 The Best Estimate of [Fe/H]

The [Fe/H] values from the two methods were compared to each other, since both methods seem to provide reasonable values of [Fe/H] for the calibrating RRab set. In some cases there were large discrepancies between two values of [Fe/H] for the same star. This difference could on rare occasion be as large as 3 dex. The light curves for these discrepant stars were checked, and it was found that the light curves often contained large gaps, which affect the ϕ_{31} value, or gaps that coincided with the maximum or minimum, which affects the amplitude value. Due to this result, 50 stars were omitted from the analysis, reducing our sample of RRab stars to 608. Figure 5.14 shows how well matched the two values of [Fe/H] are with respect to each other. The χ^2 of the fit is 6.01.

In the cases where there was adequate agreement between the two [Fe/H] values, a weighted average of the metallicity was calculated. This value is our "best estimate" for [Fe/H] of that star. In the cases where the Jurcsik & Kovacs method [Fe/H] was not calculated, the Sandage method [Fe/H] is our best estimate. A table of our best estimate [Fe/H] values for 608 NSVS RRab stars is given in Appendix A. Column 1 is the NSVS identification number, column 2 is the [Fe/H] from Sandage's relation, column 3 and 4 are the [Fe/H] and uncertainty from the Jurcsik & Kovacs method, and column 5 is the best estimate for the metallicity.

5.4.4 The Oosterhoff and Metal-Rich Groups

Three groups of RRab stars were identified from their location in the period-amplitude diagram. These groups are 1) the Oosterhoff I RRab stars, 2) the Ooster-

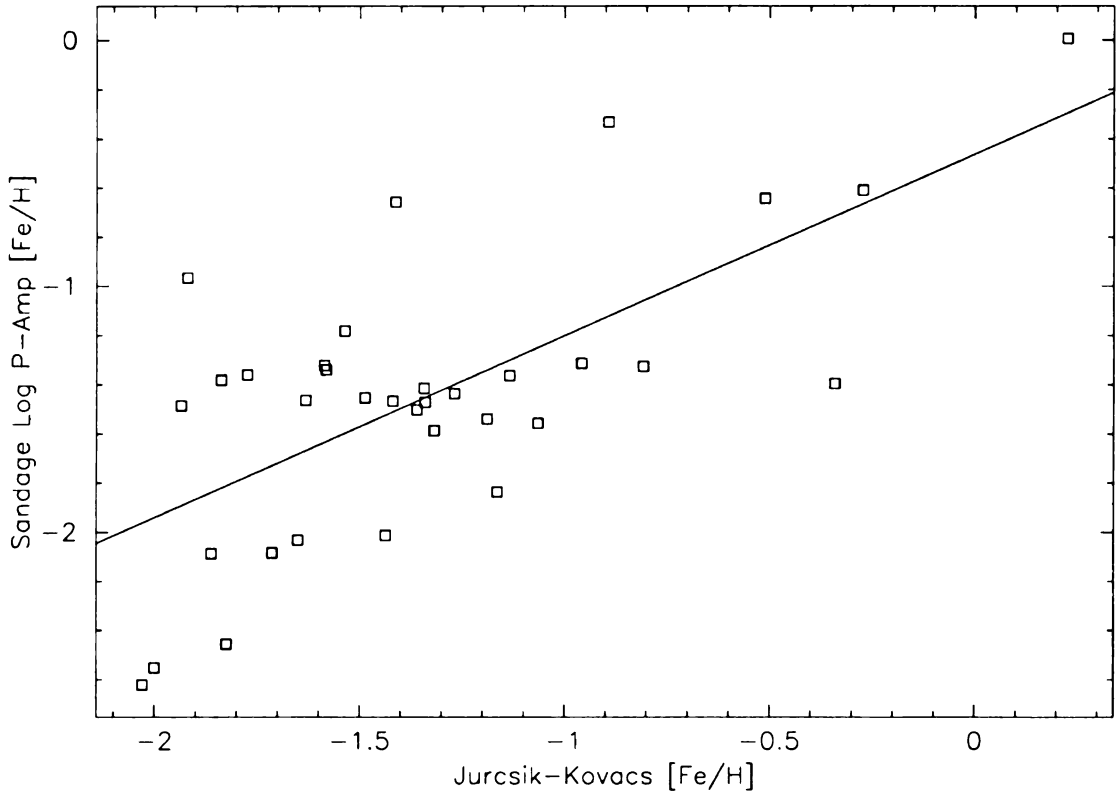

Figure 5.14 Comparison of the [Fe/H] from the Jurcsik & Kovacs method with the [Fe/H] value from Sandage's method.

hoff II RRab stars, and 3) a metal-rich group that we will discuss later in the context of a thick disk population. A more thorough discussion is presented in sections 6.1 and 6.2.

The period-amplitude diagram is reproduced here with the divisions for the three groups indicated (see Figure 5.15). The dotted line between Oosterhoff I and II is an arbitrary boundary between the two groups. The stars found to the right of this boundary are considered to be Oosterhoff II stars while those on the left of this boundary are associated with the Oosterhoff I class.

The region contained by the "metal-rich" box was carefully scrutinized for any RRc stars. Having found that stars within the box appear to be RRab types, we checked their photometric metallicity values. The stars in the box almost always have an [Fe/H] > -1. The right end boundary of the "metal-rich" box is defined by [Fe/H] $= -1$ based on the Sandage [Fe/H]-Log P-Amplitude relation. These stars are identified in the plot as an open circle with a solid square inside it. There are a few open circles in the "metal-rich" box. These stars have a Jurcsik & Kovacs [Fe/H] value but a Sandage [Fe/H] > -1. Note that some of the stars identified as metal-rich ([Fe/H] > -1) appear in the region occupied by Oosterhoff I stars. Those stars were for some purposes reclassified into our metal-rich group.

Layden (1995) suggests a metal-rich RRab population exists in the disk. As we will discuss in the next chapter, our metal-rich stars also appear to be associated with the disk population.

5.5 C-Type RR Lyraes

As discussed in section 5.1, the final sample of RRc candidates contained 375

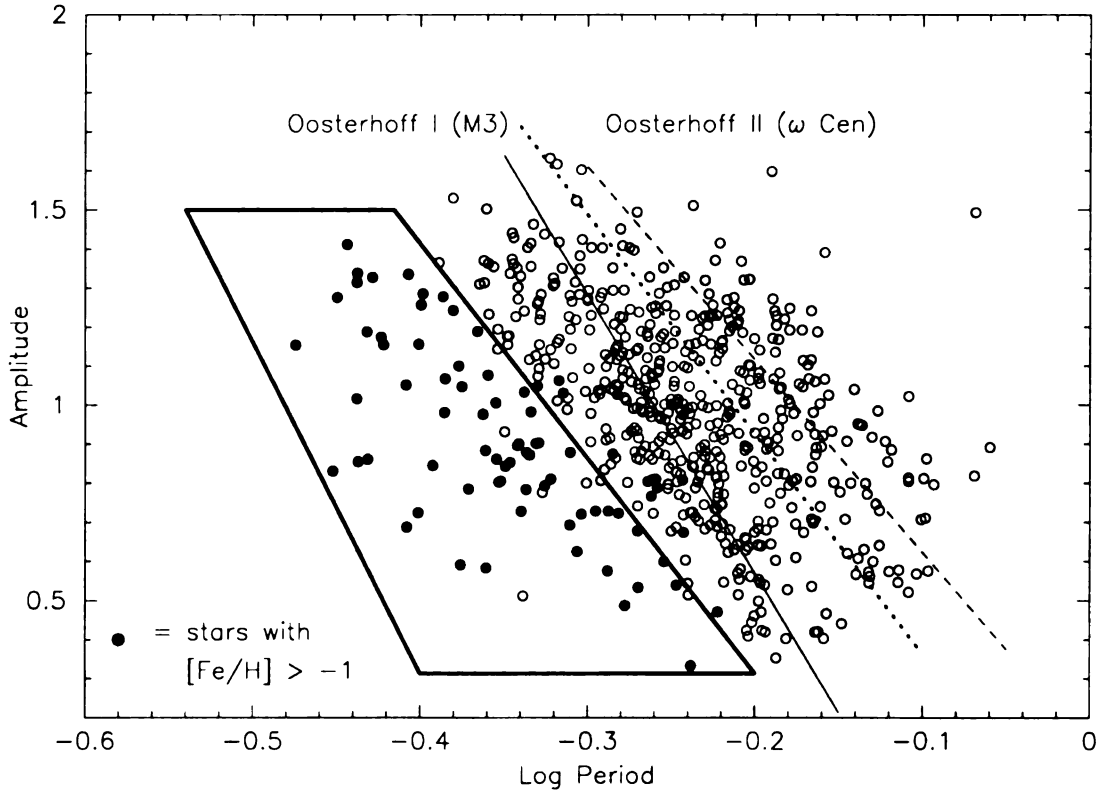

Figure 5.15 Regions in the period-amplitude diagram occupied by three groups of RRab stars. The dotted line separates the Oosterhoff I and II groups. The boxed area identifies the metal-rich RRab group in this sample. Note that most of these metal-rich stars have a comparatively shorter period than the Oosterhoff I group.

stars. Figure 5.16 shows the period distribution of these stars. The average period ($\langle P_c \rangle$) for this sample is ~ 0.309 days. We note that in this histogram, there appears to be a large number of short period stars between 0.2 and 0.3 days. Most likely the inflation of the numbers of stars in these bins are high amplitude δ Scuti stars. These δ Scuti stars are difficult to weed out by looking at the light curves (as opposed to the obvious eclipsers). Long period, high amplitude δ Scuti stars overlap with the shorter period RRc stars. A second histogram, divided by $|Z|$ distance, shows that these short period, non-RR Lyrae stars are concentrated close to the plane. A discussion on the attempts to obtain a clean sample of RRc stars is presented in section 5.5.2. Figure 5.17 shows the period distributions in $|Z|$ regions from 0 to 2 kpc and 2 to 5 kpc.

It should be mentioned here that the distances calculated for the RRc sample are not based on the M_V-[Fe/H] relation from Equations 2.6 and 2.7. Rather, a fixed value of $M_V = +0.6$ was chosen (Smith 1995), which may not be the best value for these stars. This was due to the fact that metallicities could not be derived for the RRc stars.

In the bottom histogram of Figure 5.17, we see less of a contamination of these short period, non-RR Lyraes. This indicates that the contaminating star may belong to a disk population. The mean period for the RRc stars found in $2 < |Z| < 5$ kpc is very close to what is expected for an Oosterhoff I system. The average period is typically $\langle P_c \rangle \approx 0.32$ days for an Oosterhoff I group. Therefore, we find that the RRc sample agrees in this respect with the RRab sample. However, there might still be some contamination from the δ Scuti population even in this $|Z|$ distance region.

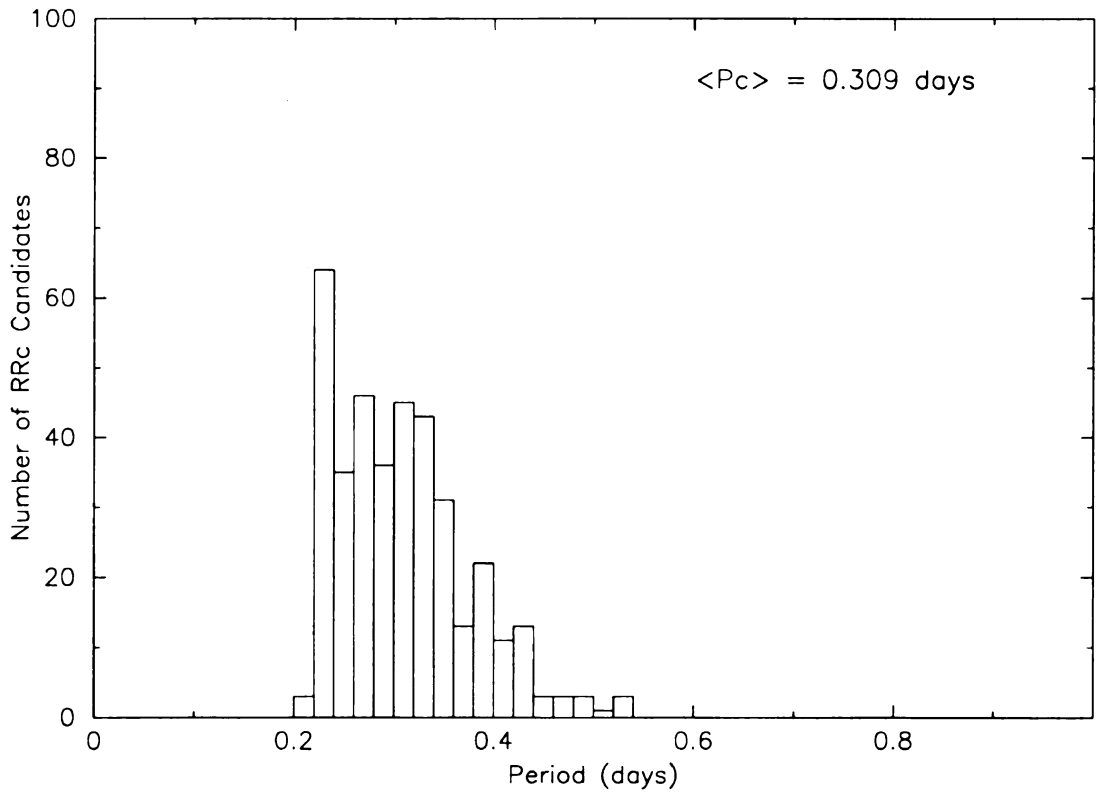

Figure 5.16 Period distribution histogram for 375 RRc candidates from the NSVS survey.

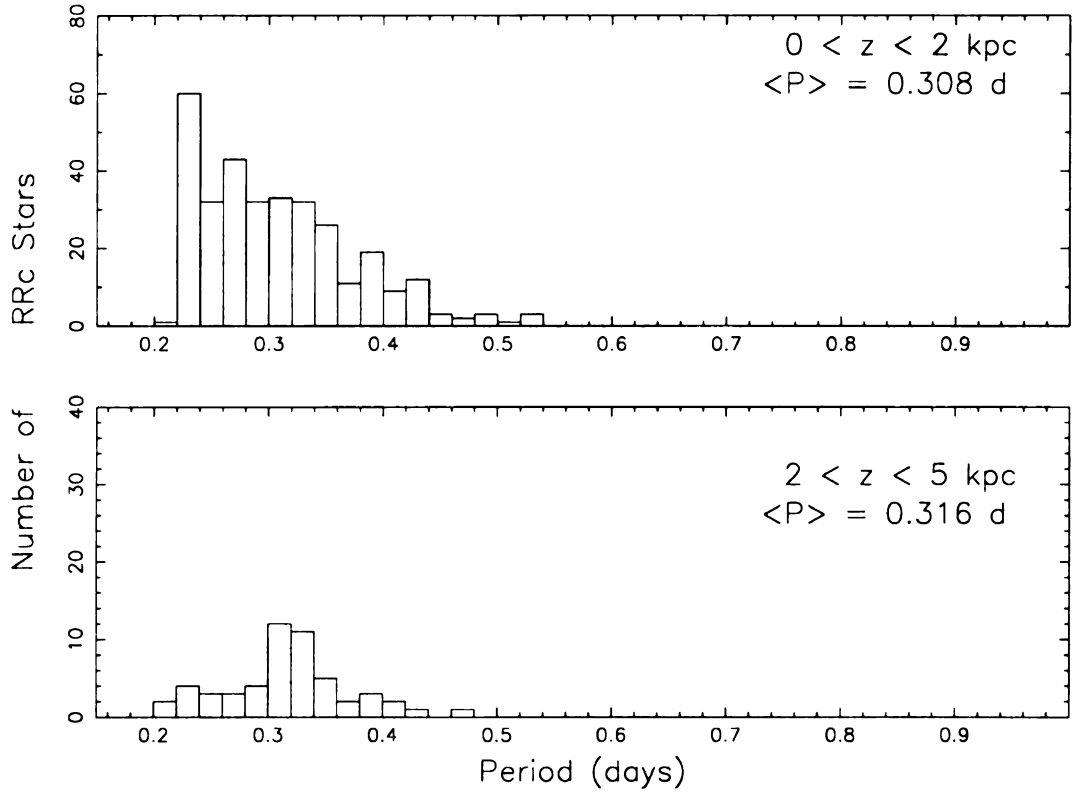

Figure 5.17 Period distribution histogram for 375 RRc candidate stars in $|Z|$ distance zones.

5.5.1 Period-Amplitude Diagram

Figure 5.18 is the period-amplitude diagram with the inclusion of the RRc stars. Unlike the RRab stars, clear linear trend lines for the Oosterhoff groups do not exist for the RRc stars. In Clement & Rowe (2000), parabolic trend lines were used for the RRc population. For this dataset, their trends were not used. It is difficult to discern any preferred trend in the region spanned by the RRc's in Figure 5.18. Again, it is noted that the very short period stars ($\log P_c < -0.65$ days) could be high amplitude δ Scuti stars. For complete assurance, all the stars with log periods less than -0.60 should all be carefully analyzed to see if they are all RRc stars or a mix of short period variables and the very short period RRc stars.

Based on our RRab period-amplitude diagram and period histograms, we would expect the RRc stars to exhibit strong Oosterhoff I characteristics. However, there should be a population of Oosterhoff II RRc stars as well. Furthermore, in Oosterhoff II systems, RRc stars are more common than in Oosterhoff I systems. We would then expect a stronger Oosterhoff II component among the RRc stars than for the RRab. As we noted for the RRc candidates in the $|Z|$ range between 2 and 5 kpc, the average period is very close to the value of $\langle P_c \rangle$ of Oosterhoff I RR Lyraes. However, until we eliminate the contamination in the RRc sample of the short period, non-RRc variable stars, we cannot draw any strong conclusions.

5.5.2 RRc Identification Problem

In an attempt to pick out the short period, non-RRc stars from our sample, three methods were used. The first method was the original variable star classification

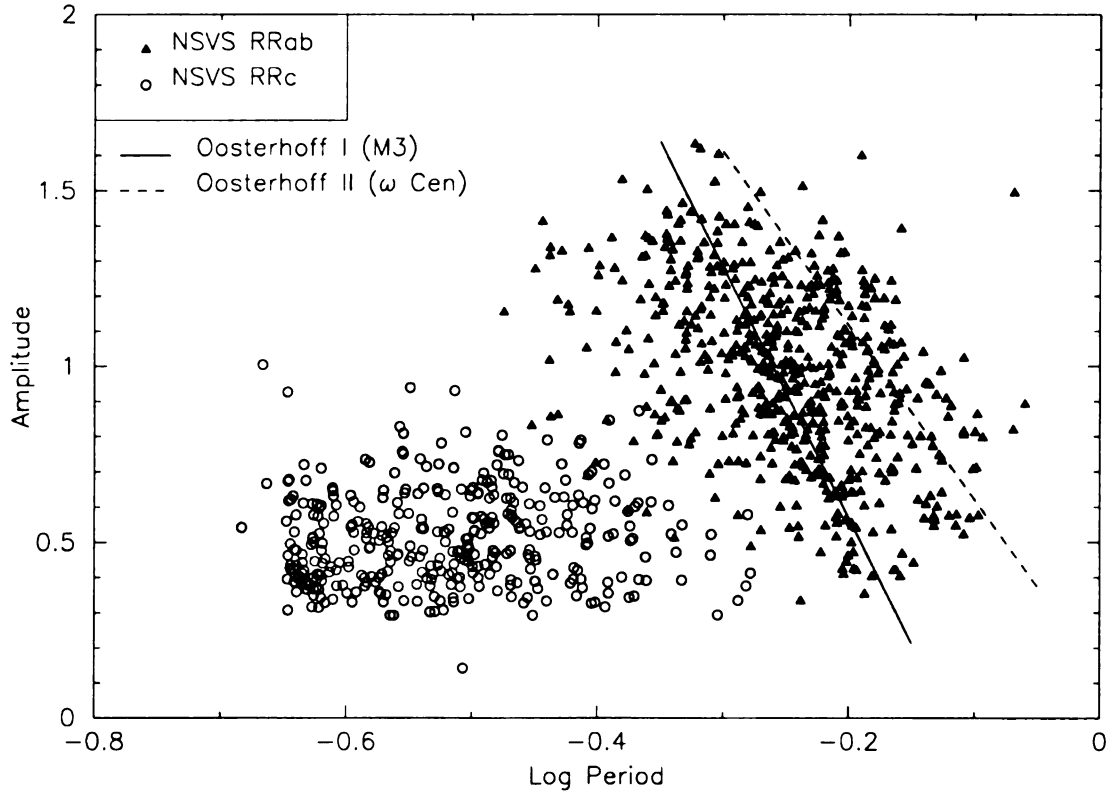

Figure 5.18 Period-Amplitude diagram with the inclusion of the RRc candidate stars.

scheme used on the ROTSE-I variables in Akerlof et al. (2000b). The second method is that of Poretti (2001), who showed that the OGLE variable stars separated into groups when the Fourier decomposition parameters were plotted against period. The third method was developed by Szymanski et al. (2001), who also used the Fourier decomposition parameters. Each method is described in depth in their respective papers, but is briefly summarized here.

Akerlof et al. (2000b)'s variable star classification scheme utilizes the Fourier decomposition of the light curves. The light curves were decomposed via:

$$\Delta m(t) = \sum_i p_i \cos(\frac{2\pi t}{\Gamma}) \tag{5.2}$$

where $\Delta m(t)$ is the phased light curve information in the Tycho magnitude system, and Γ is the derived period. The p_i coefficients, which are related to the a_i coefficients of the usual formula for Fourier decomposition) were combined to form the ratios:

$$r_1 = \frac{p_2}{p_1} \tag{5.3}$$

$$r_2 = \frac{p_3}{p_1} \tag{5.4}$$

$$r_3 = \frac{p_2}{p_3} \tag{5.5}$$

These ratios actually correspond to the Fourier decomposition parameters R_{21}, R_{31}, and R_{23}. With these ratios and a period range, the variable stars were classified into 8 categories: RRab, RRc, δ Scuti, Cepheid, contact and eclipsing binaries, Miras, and long period variables. For the RRab stars, the combination of parameters is listed in Table 5.3

These criteria were tested on the current sample of RRab candidates and almost

Table 5.3. RRab classification criteria (Akerlof et al. 2000b)

Parameter	Values
Period	$0.3 < \Gamma < 2.0$
r_1 ratio	$0.08 < r_1 < 1.0$
r_2 ratio	$0.01 < r_2 < 1.0$
r_3 ratio	$r_3 < 0.6$

Table 5.4. RRc classification criteria (Akerlof et al. 2000b)

Parameter	Values
Period	$0.2 < \Gamma < 1.0$
r_1 ratio	$r_1 < 0.16$
r_2 ratio	$r_2 < 0.24$

95% were returned as "RRab" under this method. For the RRc candidates, we expect a similar result in obtaining a clean sample of RRc stars.

The set of parameters for RRc stars is listed in Table 5.4. However, for RRc periods greater than 0.4 days, the criteria of $r_1 < 0.08$ and $r_2 < 0.24$, and amplitude greater than 0.35 magnitudes were required. To distinguish eclipsers from the RRc stars, the additional criterion of the sign of the largest deviation was taken into consideration. This "sign of the largest deviation" is determined from the mean magnitude of the variable star and depends upon whether most of the observed points are brighter or fainter than this mean. For eclipsers, this value is usually negative, whereas for RRc stars it is positive.

As applied here, the upper period was changed to a period of 0.6 days rather than 1.0 day. With the application of this variable star classification scheme, the final number of RRc candidates was 375 stars. We believe the bulk of the stars dropped

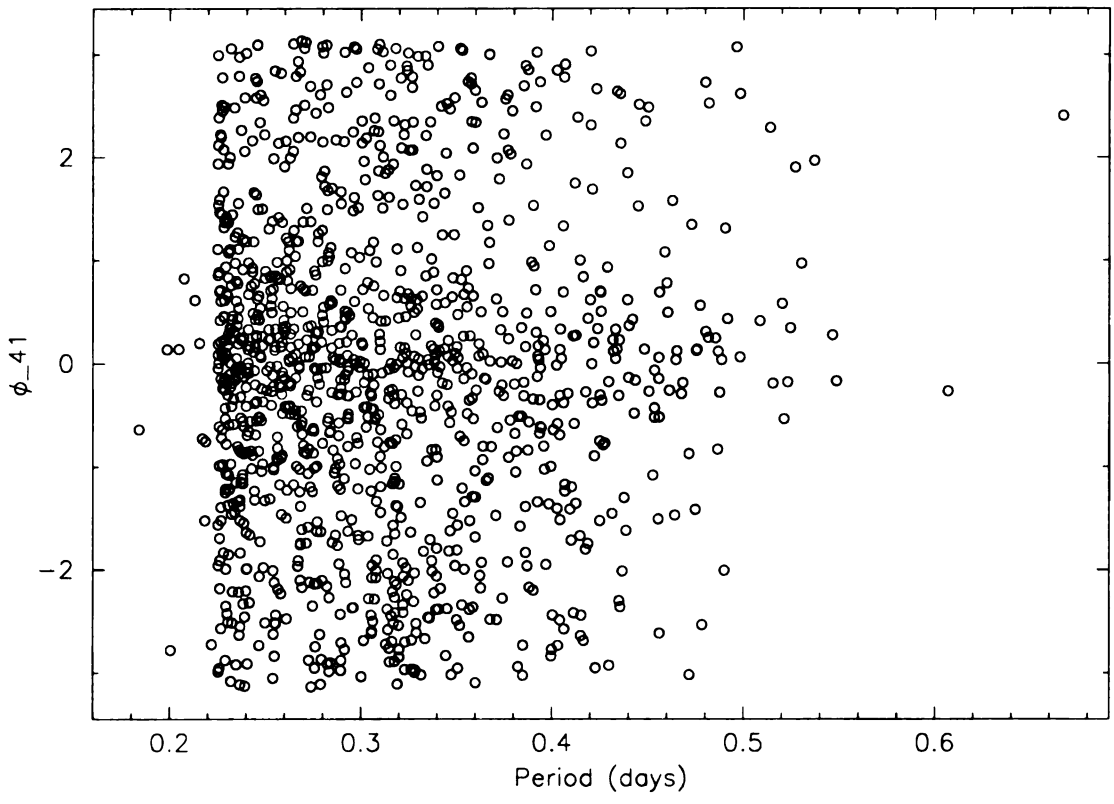

Figure 5.19 Fourier parameter ϕ_{41} vs. Period. In contrast to the similar diagrams in Poretti (2001), no clear separation is seen between δ Scuti and RRc stars.

from the original sample were either short period, non-RR Lyraes or eclipsers.

As a check, we used the analysis scheme of Poretti (2001), which compared Fourier decomposition parameters to period (see his Figure 4, 5, 6, and 7). For our RRc candidates, plots of ϕ_{41} versus period and R_{21} versus period were produced because the δ Scuti stars are expected to cleanly separate away from the RRc stars in these diagrams.

Despite our expectations, in Figures 5.19 and 5.20, a separation between the RRc candidates and our supposed contaminant population could not be seen clearly. One thing to note here is that the Fourier parameters R_{21} and ϕ_{41} were not scaled to a standard system as the ϕ_{31} parameter was for the RRab stars (see discussion in section 4.4). We could not produce an adequate calibration relation for the Fourier

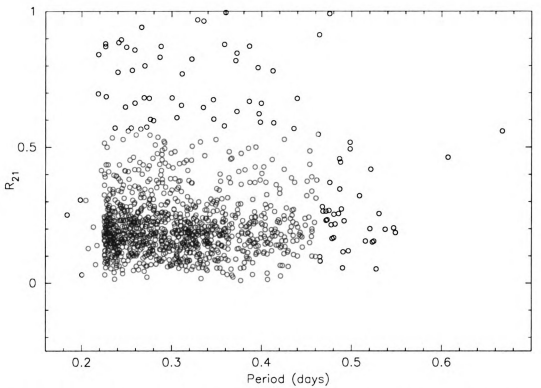

Figure 5.20 Fourier parameter R_{21} vs. Period. As with the ϕ_{41} plot, no clear separation is seen between the two types of short period variable stars.

parameters of the RRc stars to a standard V system equivalent. There were only a few well observed RRc stars in the literature for which we also had good observations from the NSVS survey. Most likely this is not the major reason why a separation was not observed since a general separation should occur regardless of the particular calibration on the Fourier parameters. Why the separation of δ Scuti and RRc stars was not observed is unknown at this time.

The third method was obtained from Szymanski et al. (2001), whose sample of stars came from the MACHO survey. In their method, again a Fourier decomposition was performed on the light curves. Their formula is reproduced here:

$$A(t) = a_0 + \sum_i a_i \cos(i\omega t + f_i) \tag{5.6}$$

A(t) is in magnitude units and is essentially the light curve information. The f_i terms are the phase terms, often shown as ϕ_i in the usual convention of the Fourier decomposition. The main impetus behind the development of this method was to weed out the pulsating variables and to get a clean sample of eclipsing stars. In our case, we desire to exclude the binary stars but keep the pulsators. Szymanski et al. found that a strong correlation between f_2 (or ϕ_2) and f_4 (or ϕ_4) phase term exists for eclipsing stars, but is weak for pulsators. This trend for the eclipsing binaries is:

$$f_2 - 2f_4 = 0 \tag{5.7}$$

Figure 5.21 shows the application of this method on the RRc sample. One could be convinced that the trends seen in Szymanski et al.'s figure 1 are present in our Figure 5.21. It may also be plausible that a majority of the eclipsing binaries have already been removed. Regardless, the strong trend Szymanski et al. had observed in their figure is not present in Figure 5.21. In any case, we have decided this method

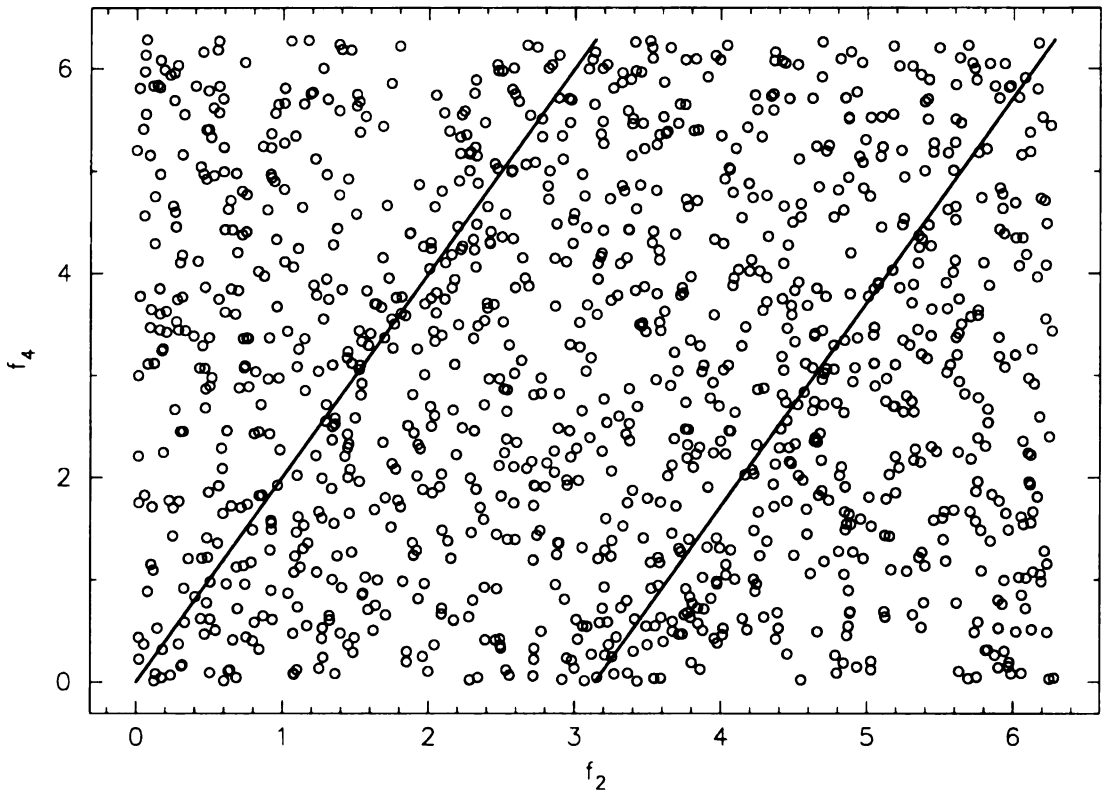

Figure 5.21 Szymanski et al. (2001) method of weeding out the eclipsers from the sample of RRc stars. The trend lines here are the location of Szymanski et al. (2001)'s relation (Equation 5.7). The right hand trend line was created by adding 2π to the left hand trend line.

was not useful in weeding out the eclipsers with very shallow and equal minima. Szymanski et al.'s method does not easily facilitate the separation of those types of eclipsers and the RR c stars with very sinusoidal looking light curves.

Another RRc separation method developed by Rucinski (1997, 1993) was not tested, but may be a promising technique. Akerlof et al. (2000b) proposed to use Rucinski's method for the full ROTSE-I/NSVS variable star catalog. The Rucinski method fits a cosine series function to the light curve data, which is in flux units. The coefficients of this fit are to be used to separate out, in particular, the binary stars from the pulsating stars. Until we can test this method on the NSVS sample of RR Lyraes, we can neither advocate nor oppose this use of Rucinski's method.

From the results of these three methods, extracting the RRc stars from the NSVS survey is no easy endeavor. There is an apparent contamination by some type of short period, non-RR Lyrae star near 0.2 days. These stars are most likely to be high amplitude δ Scuti stars that have sinusoidal looking light curves. These stars overlap in period space with the shortest period RRc stars. We find that the techniques used by Poretti (2001) and Szymanski et al. (2001) did not produce a clear separation of the RRc stars from the other variable stars. The ROTSE-I variable classification scheme (Akerlof et al. 2000b) caused the removal of a large portion of the RRc candidate sample. However, even this scheme did not remove all the shortest period non-RRc stars. At this point, either the Rucinski method or another technique is needed to obtain a clean sample of RRc stars from the NSVS survey.

Chapter 6

Discussion of the Results

In this chapter, aspects of our sample of NSVS RRab stars relevant to galactic structure are discussed. The implications of galaxy formation scenarios are addressed.

6.1 Oosterhoff Dichotomy and Galaxy Formation Implications

As discussed in section 5.4.4, three groups have emerged from the sample of RRab stars. Here, we take a closer look at the Oosterhoff I, Oosterhoff II, and the metal-rich group. The thick disk will also be discussed separately in section 6.2.

6.1.1 Contour Plots of the Period-Amplitude Diagram

An interesting test of the Oosterhoff groups is to overlay contours determined

by the density of stars for each locii. To produce this map, a grid with box sizes determined by the log period and amplitude was constructed. We assume a box size of the grid is 0.25 in log period space and 0.1 magnitudes in amplitude space. Next, the number of stars in each grid box was counted up. To determine the density, this number is divided by the area of the grid box. Once the density, or "concentration number" is determined, the IDL task CONTOUR can be used to produce the contour map of the period-amplitude diagram.

Figure 6.1 shows our contour plots at two different resolutions. This contour plot is the low resolution contour map of the period-amplitude diagram. Note the high concentration of stars near the Oosterhoff I locus. In Figure 6.2, the higher resolution contour map shows some clumps that may be associated with Oosterhoff II. However, it is also clear that there is some population of RRab stars between the Oosterhoff I and II lines.

6.1.2 Distribution of the Groups

To take a closer look at the Oosterhoff groups and the metal-rich group from section 5.4.4, we plot the [Fe/H] distribution with respect to $|Z|$ distance from the plane. In Figure 6.3, each group is identified by a different symbol. We see in this figure the metal-rich stars with [Fe/H] > -1 all appear close to the plane. For the 6 stars that are above this group have their metallicities derived from teh Sandage relation (Equation 4.24). The metallicities may be more uncertain for these stars. The metal-poor stars may exhibit a more extended distribution and may be mostly a halo population. We will argue later that even some of these metal-poor RRab stars are likely to belong to a disk population. We present individual plots of each group

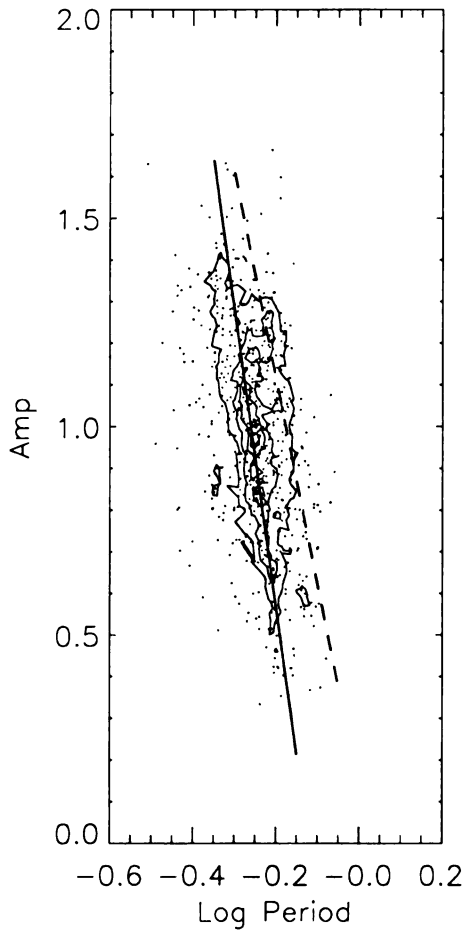

Figure 6.1 Lower resolution contour map of the RRab period-amplitude diagram. Number of contour levels is 5. Note that there is a higher density of stars near the Oosterhoff I locus. The trend lines are the same ones from Figure 5.11.

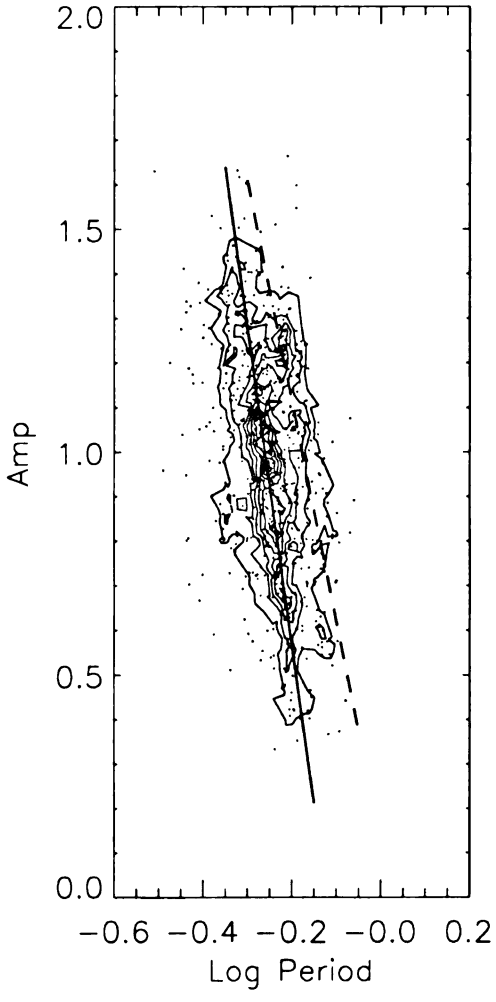

Figure 6.2 Higher resolution contour map of the RRab period-amplitude diagram. Number of contour levels is 10. Note that there is now some clumps associated with Oosterhoff II. The trend lines are the same ones from Figure 5.11.

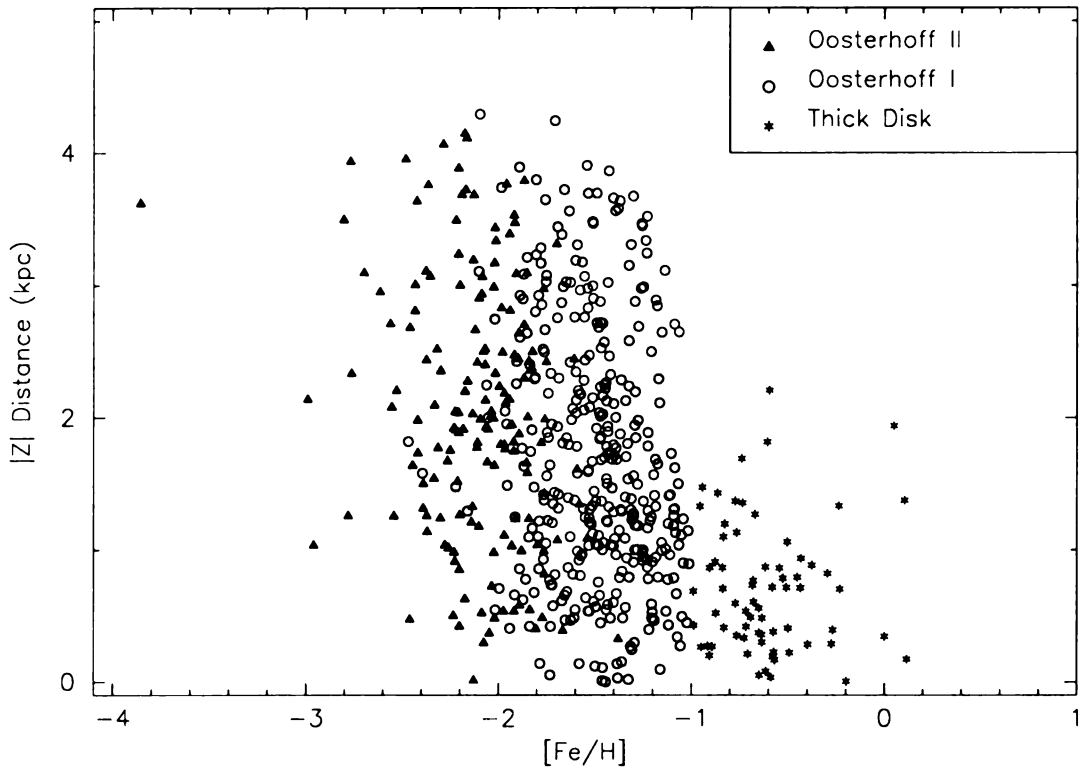

Figure 6.3 [Fe/H] distribution for the three groups with respect to $|Z|$ distance.

in Figures 6.4-6.7.

The Oosterhoff II group's metallicity distribution with $|Z|$ is shown in Figure 6.4. The Oosterhoff II very metal-weak stars ([Fe/H] < -2.5) have an uncertain metallicity since the calibrating stars used from the literature do not go weaker than [Fe/H] ~ -2.5. The stars of this group are found up to 4 kpc from the plane.

In Figure 6.5, the distribution of [Fe/H] of the Oosterhoff I stars with respect to $|Z|$ is shown. These stars are found from close to the plane up to $|Z| \sim 4$ kpc. From the number ratios of Table 6.1, we chose to divide the Oosterhoff I group into 2 subgroups to investigate the large population of these stars. We institute a division of the stars at [Fe/H] $= -1.25$. In Figure 6.6, we see the stars distributed from close to the plane to over 4 kpc. However, when we looked at the number distribution of

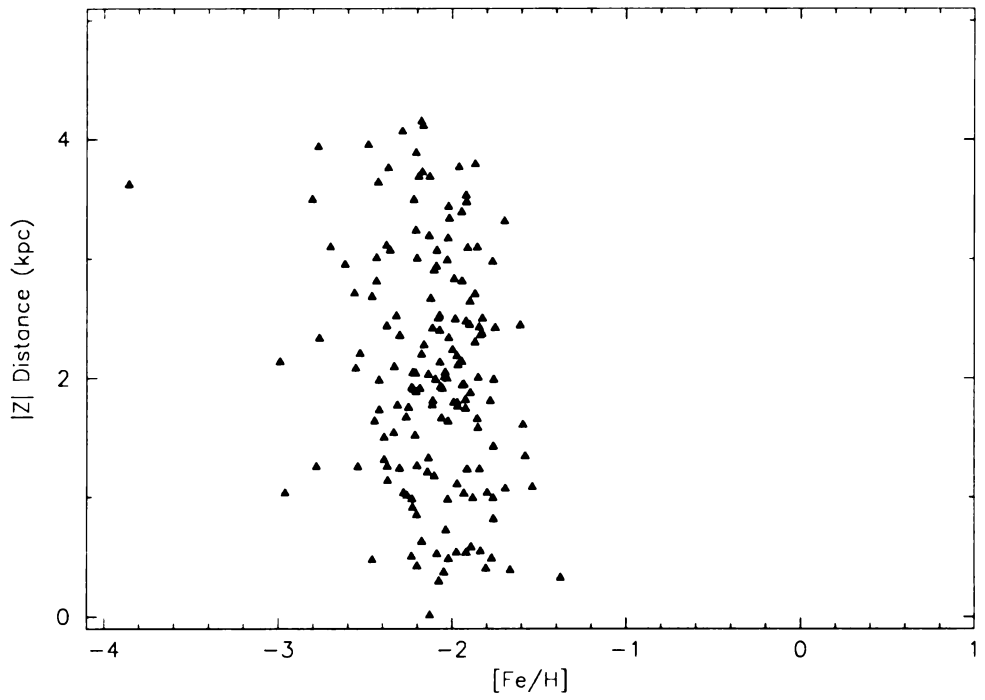

Figure 6.4 Oosterhoff II RRab candidates.

the Oosterhoff I stars, a large fraction of the stars close to the plane were from the metal-rich Oosterhoff I group. Table 6.2 has the number distribution of stars for each Oosterhoff I subgroup. With the subdivision at [Fe/H] = −1.25 in the Oosterhoff I group, we find a clump of stars do exist close to the plane. This could imply that this clump may belong to a disk population that is more metal-weak than the stars in our [Fe/H] > −1.25 sample. However, the spread of stars up to $|Z| \sim 4$ kpc indicates that the halo population is present in this group. One caveat to keep in mind is that the uncertainty of the [Fe/H] measurements may scatter stars into or out of the Oosterhoff I group (similarly, this is also true for the Oosterhoff II and metal-rich group). Because of this scatter, the groups are not as distinct as would be the case if perfect measurements of metallicity were available.

To get a rough answer to whether a metal-weak disk population really exists in this Oosterhoff I group, we look to the number ratios of the Oosterhoff groups at different

Table 6.1 Number of stars of each group per Z bin.

$\|Z\|$ Zone (kpc)	Metal-Rich	Oo I	Oo II	Metal-Rich ($\|b\| > 12°$)	Oo I ($\|b\| > 12°$)	Oo II ($\|b\| > 12°$)
0.0-0.25	13	13	1	1	1	0
0.25-0.5	19	19	9	7	10	3
0.5-0.75	12	28	8	6	19	5
0.75-1.0	11	37	8	7	22	5
1.0-1.25	5	44	14	3	32	9
1.25-1.5	9	41	9	6	29	2
1.5-1.75	1	25	12	0	19	9
1.75-2.0	6	29	22	1	19	16
2.0-2.25	1	25	17	1	21	15
2.25-2.5	0	20	17	0	15	10
2.5-2.75	1	16	8	0	10	5
2.75-3.0	0	21	9	0	18	7
3.0-3.25	1	16	11	0	10	7
3.25-3.5	0	10	7	0	7	5
3.5-3.75	0	12	6	0	11	5
3.75-4.0	0	4	6	0	2	4
4.0-4.25	0	1	3	0	1	3
4.25-4.5	0	1	0	0	0	0
4.5-4.75	0	0	0	0	0	0
4.75-5.0	0	0	0	0	0	0
5.0-5.25	0	0	0	0	0	0
5.25-5.5	0	0	0	0	0	0

Table 6.2 Number distribution of the Oosterhoff I metallicity groups

$\|Z\|$ Zone (kpc)	Oosterhoff I (metal-poor)	Oosterhoff I (metal-rich)
0.0-0.25	12	1
0.25-0.5	11	8
0.5-0.75	24	4
0.75-1.0	24	13
1.0-1.25	32	12
1.25-1.5	31	10
1.5-1.75	20	5
1.75-2.0	27	2
2.0-2.25	24	1
2.25-2.5	18	2
2.5-2.75	13	3
2.75-3.0	18	3
3.0-3.25	14	2
3.25-3.5	9	1
3.5-3.75	11	1
3.75-4.0	4	0
4.0-4.25	1	0
4.25-4.5	1	0
4.5-4.75	0	0
4.75-5.0	0	0
5.0-5.25	0	0
5.25-5.5	0	0

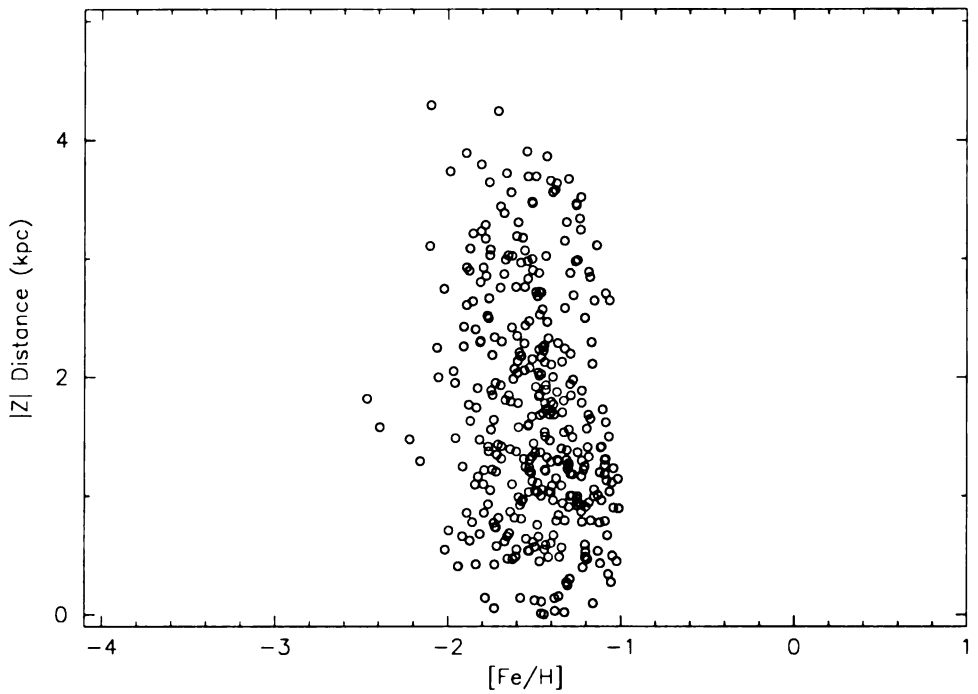

Figure 6.5 Oosterhoff I RRab candidates.

$|Z|$ distance zones. It is assumed that the halo population is best represented by the Oosterhoff II group, but that some thick disk stars may be found in both the more metal-rich and more metal-poor Oosterhoff I groups. We expect the region $2.5 < |Z| < 3.5$ should be dominated by the halo population. The number ratio, N(Oo II)/N(Oo I) in this region is $\approx 0.56 \pm 0.12$ for all [Fe/H] values. Therefore, this shows that the Oosterhoff I stars outnumber the Oosterhoff II by nearly a 2 to 1 ratio. Let us assume this is the Oosterhoff II/Oosterhoff I ratio in the halo near the Sun.

Now we look at the number ratios for the region $0 < |Z| < 2$ kpc, but avoid the Galactic plane by instituting a cutoff in galactic latitude, $|b| > 12°$. Here, we find the N(Oo II)/N(Oo I) ratio to be $\approx 0.32 \pm 0.05$. This result could reflect a change with Z of the halo RR Lyrae population. More likely, however, is that this result shows the existence of a thick disk population in the Oosterhoff I group at low $|Z|$. More than

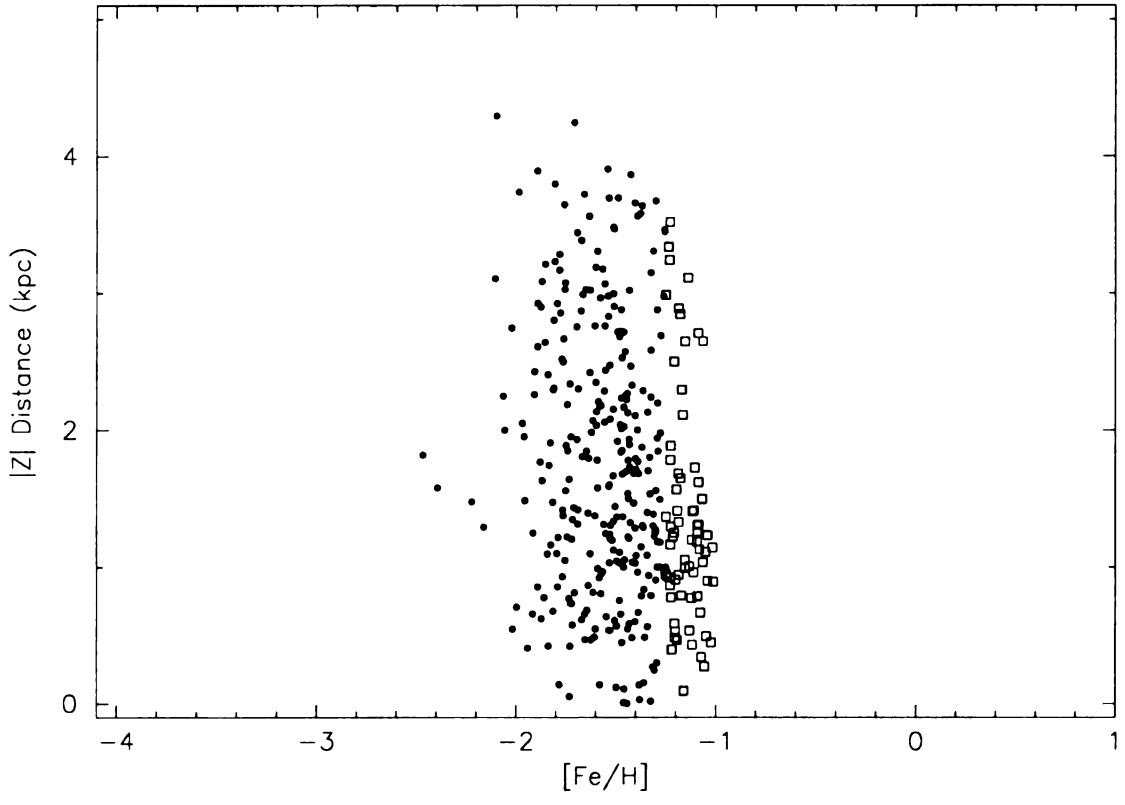

Figure 6.6 Oosterhoff I group of RRab stars. This group is divided into two groups by [Fe/H] = -1.25. The solid circles are those stars with [Fe/H] < -1.25 and the open squares are the stars with [Fe/H] > -1.25. Note the metal richer clump close to the plane of the [Fe/H] > -1.25 group.

a third of all Oosterhoff I RRab stars in the $0 < |Z| < 2$ kpc zone would belong to the thick disk in this interpretation.

Now we can perform the same kind of analysis for the two Oosterhoff I subgroups, again comparing with the Oosterhoff II group. These subgroups, as mentioned above, are separated into a metal-rich ([Fe/H] > -1.25) and a metal-poor ([Fe/H] < -1.25) group. The number ratio of Oosterhoff II to Oosterhoff I-metal-poor at $2.5 < |Z| <$ 3.5 kpc is 0.59. Near the plane, the ratio is 0.41 ± 0.07 (again, only using stars that meet the $|b| > 12°$ criterion). Comparatively, the Oosterhoff II/Oosterhoff I-metal-rich ratio is 6.0 ± 3.2 in the high Z range whereas at the low Z range, it is 1.6 ± 0.4.

Thus, we find from our number ratios that a thick disk component is strong in a metal-rich Oosterhoff I sample. We estimate that approximately 60% of our metal-rich Oosterhoff I group in the low $|Z|$ zone belongs to the thick disk. There is some evidence for a metal-weak thick disk component in our Oosterhoff I group with [Fe/H] < -1.25. For this metal-weak case, the evidence is weaker as it is not quite a 2 sigma result. Again, we must be aware of the fact that the observational uncertainties can scatter some of the metal-rich thick disk stars into the metal-weak sample and vice versa. To avoid this caveat, kinematic information is necessary. The motions of these stars can also provide clear evidence of a disk component in our Oosterhoff I group.

We should note here that the metal-weak thick disk star population in the Oosterhoff I group falls along the period-amplitude relation for halo RR Lyraes, as well as the Oosterhoff I cluster RR Lyraes, of the same metallicity. The metal-rich thick disk stars appear to extend this period-amplitude relation to a shorter period domain. This indicates that there is a continuum of the RR Lyrae properties with metallicity when transitioning from a metal-poor Oosterhoff I RR Lyrae to their metal-rich counterparts. However, there are exceptions to this suggestion (e.g. the metal rich clusters of NGC 6388 and NGC 6441 studied by Pritzl et al. (2000)). The existence of these two cluster may suggest that they have a different history than the thick disk stars.

Figure 6.7 shows the metal-rich distribution of stars with respect to $|Z|$. Note that these stars are found close to the plane of the Galaxy. The combination of the location of the stars in the Galaxy and their high metallicity establishes that they are a part of the thick disk component. Note the interesting feature of the thick disk stars declining toward the plane at [Fe/H] between -1 and 0. This may indicate a component of a thin disk in our thick disk sample.

To check if this trend in the "metal-rich", now "thick disk" group, is real and not

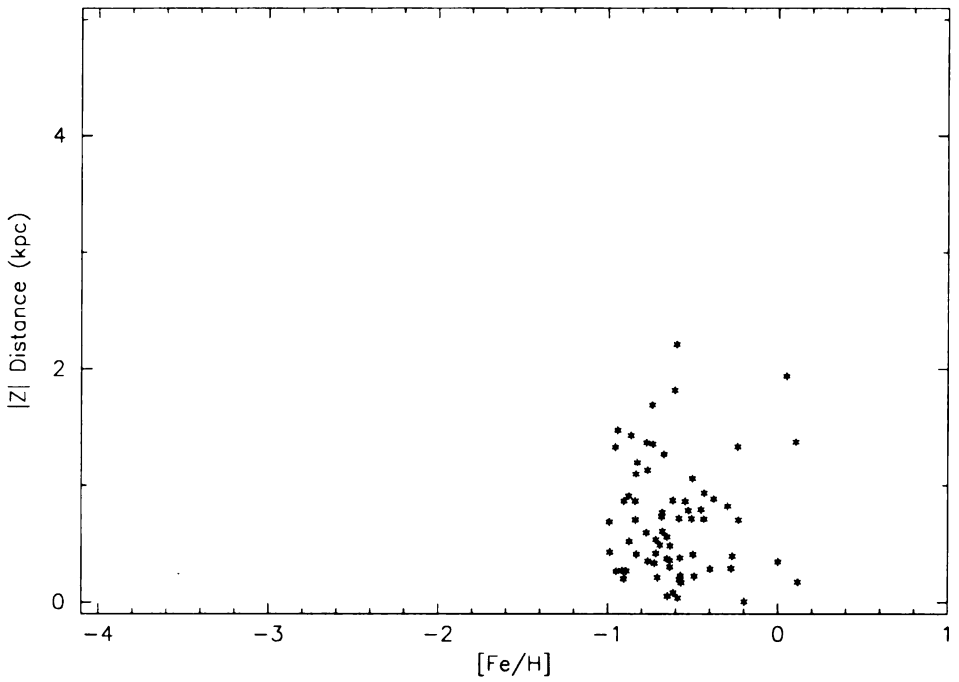

Figure 6.7 Thick disk candidates. Notice the trend that the more metal rich stars are constrained to the plane. This may be indicative of a thin disk component.

an artifact of our adopted M_V-[Fe/H] relation, the $|Z|$ distances were derived again from using fixed absolute magnitudes. Figure 6.8 shows the same group, but with slightly different $|Z|$ distance values. We see that the trend is still present in each calculation, therefore, this declining slope feature is not an artifact.

6.1.3 ΔLog P and the Oosterhoff Dichotomy

In addition to the period-amplitude diagrams, we used the ΔLog P parameter to obtain a clearer picture of the Oosterhoff dichotomy in our sample of RRab's. In Suntzeff et al. (1991), the field RR Lyraes appeared to separate into distinct Oosterhoff groups when the ΔLog P and metallicity were plotted against each other. The ΔLog P, or period shift, is the same parameter that Sandage et al. (1981) had

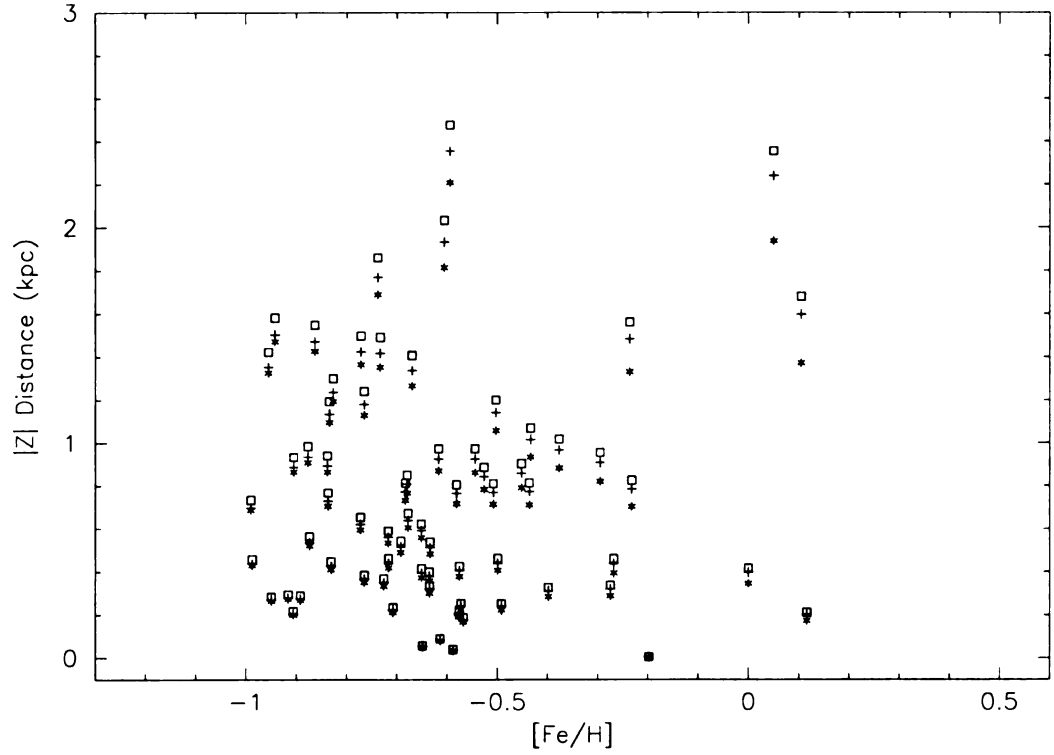

Figure 6.8 This shows the metal-rich thick disk group for different M_V values. The asterisks are for those distances determined from the M_V-[Fe/H] relation. The open squares are for those distances where M_V was fixed to the value of 0.6 and the crosses are for $M_V = 0.7$.

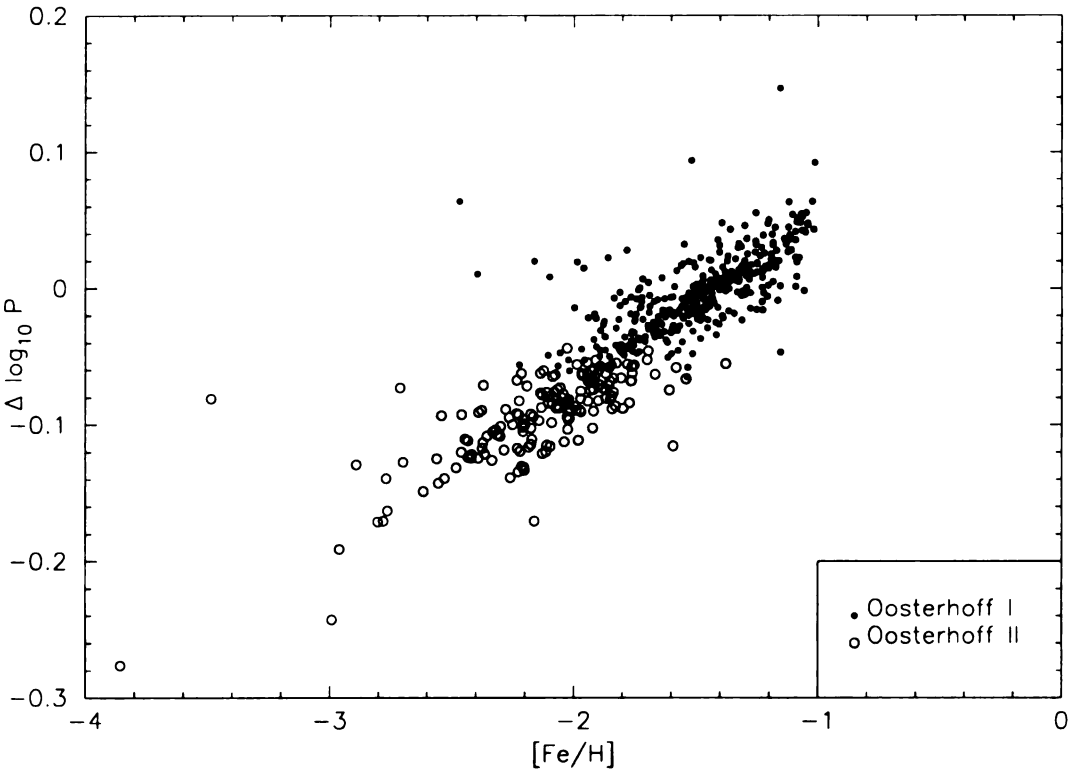

Figure 6.9 The ΔLog P plot. The Oosterhoff groups do not appear to separate in this plot as in Suntzeff et al. (1991)'s figure 8a.

defined in their work with Oosterhoff clusters. Figure 6.9 is our plot of ΔLog P versus [Fe/H]. To help the eye, stars associated with Oosterhoff I are the solid circles and the Oosterhoff II are the open circles. Compared to Suntzeff et al. (1991)'s figure 8a, we do not see a gap at ΔLog P = −0.03. Rather, the stars appear to be continuous from one group to the other.

Knowledge of the kinematics of the RR Lyrae stars would help us relate them to particular Galactic components. For the kinematic information, we would need proper motions and radial velocities. There have been many proper motion surveys where the NSVS stars have already been observed and thus some kinematic information is already available. Therefore obtaining proper motions will be an exercise of cross-correlating our database with the published proper motion catalogs. The radial

velocities are a different story. These motions are not readily available for the NSVS stars since this kinematic information is obtained only through spectroscopy. More on this topic will be discussed in Chapter 7.

6.1.4 Implications for Galactic Evolution

We have shown the dominance of an Oosterhoff I RRab population in the solar neighborhood. At the start of our investigation, we had hoped to test the relative proportions of Oosterhoff I to Oosterhoff II stars as a function of Z distance, as suggested by the work of Lee & Carney (1999). However, the strong contribution of the thick disk stars in our Oosterhoff I sample makes it difficult to test this at the moment. Once the kinematic information is available, we will be able to distinguish more cleanly the halo and disk populations in our Oosterhoff samples and then return to this issue. Our results indicate that the thick disk is an important contribution to the local population of RRab stars, even at [Fe/H] values lower than -1.

However, to make a stronger case, the kinematics of these stars need to be obtained. Through the correlation of the Oosterhoff groups and the kinematics (Lee & Carney 1999), we can specifically identify which stars belong in the halo and disk populations. For now, we rely on the Oosterhoff correlation to the kinematics to make our suggestions of the Galaxy formation scenarios.

6.2 The Thick Disk

In our sample of 608 RRab stars, 70 were found to have an [Fe/H] > -1. As seen in Figure 6.7, these stars also lie close to the plane. We therefore refer to

this subsample as our thick disk sample. We also have convincing evidence that a thick disk component extends down to [Fe/H] $\cong -1.25$. We believe that an even more metal-weak component of the thick disk may exist, but to clearly identify this component the kinematic information is needed. For the remainder of this section, we will discuss only the metal-rich ([Fe/H] > -1) thick disk group.

6.2.1 The Scale Height of the Thick Disk

The scale height of the thick disk is essentially the height above the plane where the number density of the stars falls off by e^{-1}. To derive this structural feature of the Galaxy, we binned our data into an average of either 6 or 10 stars per $|Z|$ bin. The choice of 6 and 10 stars per bin was decided by how many data points were available to determine the scale height and how uncertain those points were. We also implement a limit to the volume in which we calculate the densities in the thick disk. The limits of $|b| > 12°$ and radially 2 kpc from the Sun were used. Therefore, the shape of the volume used to determine the densities was frustrums of a cone. After reaching the height corresponding to 2.0 kpc search radius, the volume was a disk. Once the binning was complete, an exponential function was fitted to the data using an IDL task called CURVEFIT. We assume the exponential function was of the form:

$$F(z) = Ae^{Bz} \tag{6.1}$$

where A and B are parameters from the fit.

For our sample of metal-rich thick disk stars, the scale height parameters from CURVEFIT were $A = 18.1 \pm 6.3$ and $B = -2.3 \pm 0.7$ with a χ^2 value of 0.71 for the fit in the case where we averaged the sample to 10 stars per bin. This yielded

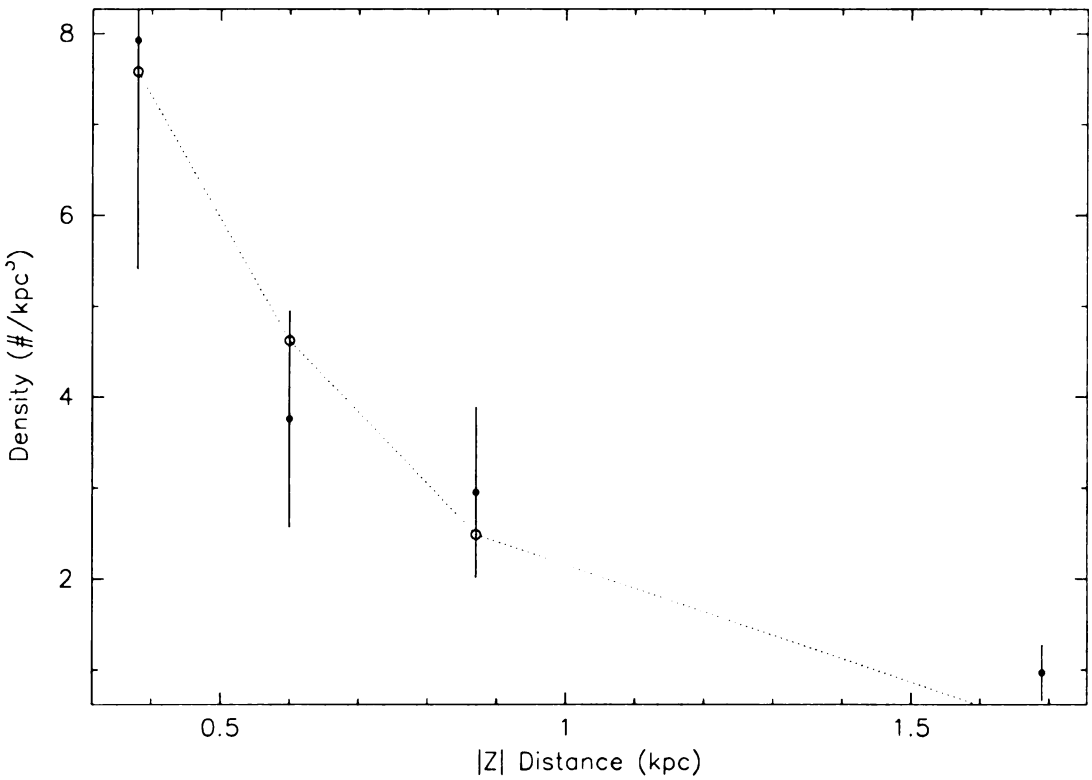

Figure 6.10 Scale height plot derived from using 10 stars per Z bin. Stars here all have [Fe/H]> -1

a scale height of 0.44 ± 0.13 kpc. For the case of 6 stars per bin, the parameters were $A = 23.0 \pm 5.0$ and $B = -2.9 \pm 0.5$ with a χ^2 value of 1.2. The corresponding scale height was determined to be 0.34 ± 0.06 kpc. Figure 6.10 and 6.11 show the exponential fits to the scale height data.

These scale heights are much smaller than the canonical scale height of ~ 1 kpc (Binney & Merrifield 1998). An important reason for the difference may be that our [Fe/H] > -1 RRab sample includes a thin disk component as well as a thick disk component. This is best shown in Figure 6.7 of the thick disk sample in [Fe/H]-$|Z|$ space. The sharp decline of stars toward $|Z|$ may suggest of this thin disk contamination. Layden (1995) had suggested the possibility of an old, thin disk population of RRab stars. Compared to the scale height derived by Layden (1995), which was ≈ 0.7

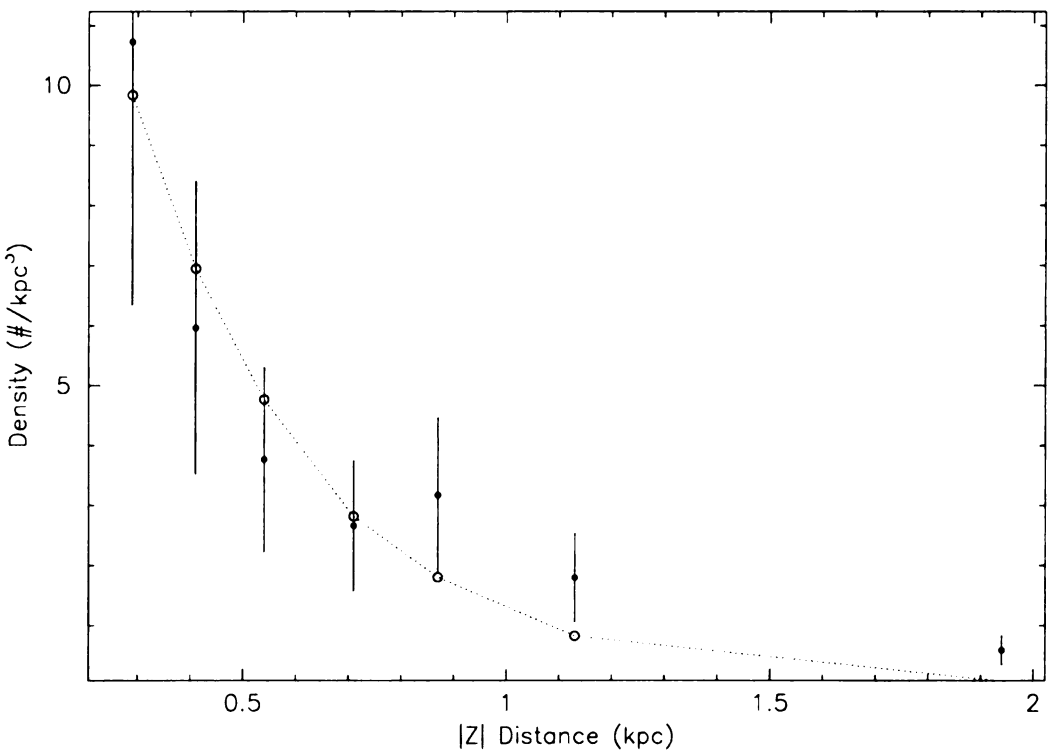

Figure 6.11 Scale height plot derived from using 6 stars per bin. All the stars in the bins have [Fe/H]> -1

kpc, our values are slightly smaller. Layden (1995) commented that for increasing metallicity, the scale heights become smaller. This suggestion seems applicable to our result, although our sample of thick disk stars may contain more metal-rich stars than in Layden's work.

6.2.2 The Metallicity Gradient

Suntzeff et al. (1991) reported a metallicity gradient among the RRab stars as a function of galactocentric distance (R) close to the center of the Galaxy. In their figure 4a, which is a plot of mean [Fe/H] and R distance, the metallicity of their sample decreased in going from $R = 4$ kpc to $R = 10$ kpc. To produce this plot, their sample was averaged into bins containing 20 stars each. Our version of $\langle [Fe/H] \rangle$ as a function of galactocentric distance is presented in Figure 6.12. The stars used for this plot are those stars in the Oosterhoff I and II groups (i.e. [Fe/H] < -1). Our sample is limited to $R \sim 6$ kpc from the Galactic center to about 12 kpc. In the region that overlaps with Suntzeff et al.'s metallicity gradient, we do not see this trend in our plot. In fact, we observe a zero gradient for metallicity in this range of galactocentric distance!

A couple of things can be concluded from our plot. It is plausible that since we do not go down to R = 4 kpc as Suntzeff et al. does, we may not be seeing part of a trend. Another possibility is that our metallicities are on different systems. Suntzeff et al. (1991) derived their [Fe/H] values from the ΔS method (Preston 1959), which uses the spectra of RR Lyraes (specifically the calcium K and Balmer lines). However, both our [Fe/H] and their metallicity values should be on the same system, i.e. the Zinn-West system (Zinn & West 1984). If there are any systematic differences, they should

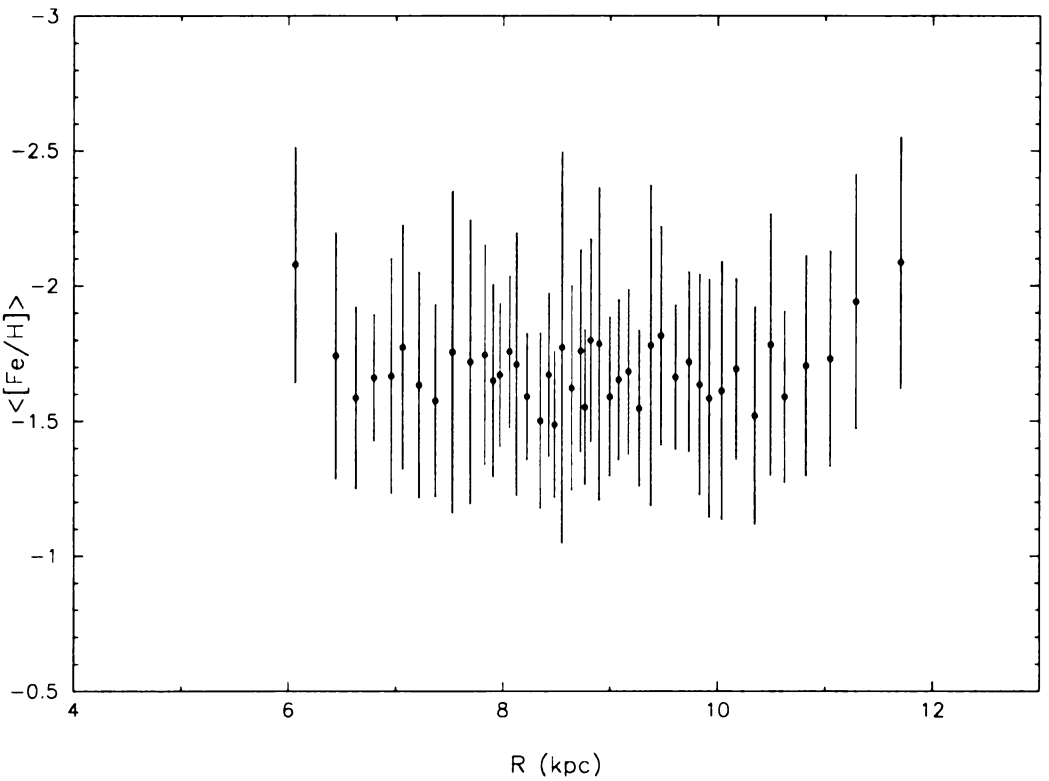

Figure 6.12 The average [Fe/H] distribution with galactocentric distances.

be small and should not erase any metallicity trend. Also, it is possible that despite our exclusion of stars with [Fe/H] > -1, our sample may have more thick disk stars, which can erase our inner halo trends. The sample Suntzeff et al. used contained fainter stars than our sample from the NSVS survey and may be less affected by this problem.

Until we can positively separate out the thick disk stars from the inner halo, we will not be able to make a conclusive statement for or against the observed gradient in Suntzeff et al. (1991). Again, the best solution for this is to obtain kinematic information from spectroscopic observations for our sample of thick disk stars.

Chapter 7

Future Work and Suggested Projects

As one finds interesting results, new questions are always generated. Throughout the work done in this project, various results from MACHO and SDSS (Alcock et al. 2004, Vivas et al. 2004) have appeared, which have guided and/or influenced some of the work here. By no means is this project absolutely complete. There are topics that have not been addressed and many problems that either hindered the project or needed to be resolved by obtaining new data. These points are discussed in this chapter, and it is the hope of this scientist that more people will use the NSVS survey, whether to study the RR Lyraes or gamma ray bursters or to discover asteroids!

7.1 Survey Completeness

The NSVS survey is expected to provide the first kinematically unbiased and

complete RR Lyrae catalog for stars brighter than $V = 15^{th}$ magnitude. However, for the results in this dissertation, only a specific portion of the full catalog was used. Appendix B lists some of the parameters calculated for 608 RRab stars. As mentioned in previous chapters, a magnitude limit was enforced which resulted in the exclusion of stars found at $|Z| > 5$ kpc. The full RR Lyrae catalog should reach to a Z distance of 7 to 9 kpc, depending on the quality of the observation of the faint RR Lyrae candidates.

With the addition of stars found from 5 kpc to the survey limit, we will have a better handle on what the halo region is like within the NSVS survey. However, we must first understand any biases inherent in the use of these fainter stars. We know, for example, we will lose some number of long period RRab stars and any RRc stars. The amplitudes of these stars are low, and the noise in the observations may prevent them from being discovered. These biases will affect any discoveries at these faint magnitudes and possibly influence a correlation with the galactic coordinates l and b. Nonetheless, with a larger sample, we will be able to see if there is a greater dominance of Oosterhoff I at $|Z| = 5$ - 9 kpc or if there is still the same mix of Oosterhoff populations as exists closer to the plane. We will also have more stars for the analysis of the metallicity distribution in the solar neighborhood. With a complete catalog of RR Lyraes, one would also be in a better position to look for clumps of these stars. The clumps could be associated with a tidal stream or subgalactic fragment that is accreting into the Galaxy. In order to interpret any observed clumping in the RR Lyrae distribution, we will need to have a full understanding of all the biases that exist in the sample.

7.2 Need for Kinematic Information

One important and still lacking piece of information needed for the analysis of the RRab stars is a full knowledge of their kinematics. With a combination of their motions, locations, and metallicities, the RR Lyraes can provide deeper clues to the evolution and structure of the Galaxy. This requires knowing the proper motions and radial velocities of these stars. Useful proper motions are available for many of the NSVS RR Lyraes. Unfortunately, there are comparatively few sources for the radial velocities. However, if we do have this kinematic information, we will be able to determine the rotational motion of these stars about the Galactic center. Do we see the prograde motions indicative of a dissipative collapse scenario in our thick disk sample? Are the motions of the metal-weak thick disk group of RRab stars similar to those motions of the metal-rich thick disk stars? Do we see more of a retrograde motion for those stars far from the Galactic plane and center ($z > 5$ kpc and $R > 10$ kpc)? Do those stars show evidence of being part of an accreted system, such as the Sagittarius dwarf's tidal stream (Martínez-Delgado et al. 2004)?

With kinematics to the individual stars, we will have a better handle as to which population (halo or thick disk) these stars belong. As shown with the work done by Lee & Carney (1999), we can also use Oosterhoff groups to study the kinematics of these field stars. With the kinematic information and subsequent classification of the stars to their appropriate Galactic component population, a better assessment of the Galactic structure and evolutionary scenario can be made.

In particular, with kinematic information, the thick disk sample can be reevaluated. Are the clump of stars in the Oosterhoff I group with $-1.25 <$ [Fe/H] < -1 actually a disk component? How many of the Oosterhoff I stars with $-1.25 <$[Fe/H]$<$

-1.6 actually belong to a metal-weak thick disk population? Do all the stars with [Fe/H] > -1 exhibit thick disk kinematics?

7.3 Spectroscopy

Observational astronomy can be split into two camps: photometry and spectroscopy. While the database contains photometric data, spectroscopic data are needed to obtain other useful quantities. Two of these quantities are the radial velocities and the ΔS metallicity.

Obtaining spectra for all the RR Lyraes of a complete catalog will take a large number of observing hours as well as man hours analyzing the data. Large telescopes can cut the exposure times for the fainter stars. Multi-fiber spectrographs are unfortunately not a very efficient way to obtain large numbers of field RR Lyraes in a single run. The RR Lyraes of this survey are too spread out for more than one star to be in a single spectroscopic field of view. The optimal situation at the present time is to use a telescope large enough to have short exposure times for the faint RR Lyrae stars and to use a single slit spectrograph. Perhaps an off-shoot project from this dissertation may be to obtain spectra for a select sample, such as the thick disk candidates, and exclusively study those stars.

7.3.1 Radial velocity measurements

The radial velocities are measured from a Doppler shift of the absorption (or emission) lines found in the spectra of an object with respect to an object at the rest frame. These tiny shifts in the line (in terms of wavelengths) correspond to how fast

the objects are moving toward or away from us. In conjunction with proper motions, which are motions perpendicular to the line of sight, radial velocities can be used to determine statistical parallax distances of the RR Lyraes.

In particular, there are very few statistical parallax solutions for RRc type stars. The NSVS survey should provide a wealth of RRc stars that are good candidates for determining this. However, the kinematics of the field population must be well understood for the calculation of the statistical parallax. Thus, there will be a need for spectroscopic projects to obtain radial velocities to many for the RRc stars found in the NSVS survey.

7.3.2 ΔS Metallicity

Preston (1959) proposed an innovative way to measure the metallicity of an RR Lyrae called the "ΔS" method. This method, which is a rather reliable way to obtain the [Fe/H] values, uses the spectral type of the star based on the calcium K line ($\lambda = 3933\mathring{A}$) and the Balmer lines to find the metallicity. The calcium K and Balmer lines are ordinarily strong in the spectra of RR Lyraes. For this calculation, the RR Lyraes should be observed at minimum light. The ΔS relation is defined as:

$$\Delta S = 10[Sp(H) - Sp(K)] \tag{7.1}$$

where "Sp" stands for the spectral type as determined from the Balmer lines (Sp(H)) and the spectral type from the K line (Sp(K)). The value of ΔS is correlated to the metallicity of the star, with small values being more metal rich and larger values of ΔS being metal poor. The work presented in Layden (1994) is an elaboration of this technique.

Obtaining the ΔS method [Fe/H] value will be useful as a check on the [Fe/H] value we have calculated from the photometric methods. There are many possible ways for the photometric metallicity to be spurious, i.e. the quality of the Fourier parameters or amplitude measurements. As seen in our use of the Jurcsik & Kovacs (1996) method alone, over 200 stars had to be omitted because the [Fe/H] value was either spuriously high or low, or because of an uncertain ϕ_{31} measurement. In addition, stars with the Blazhko Effect could not be analyzed with the Jurcsik & Kovacs method. The ΔS method should not discriminate against these stars, or the double mode RR Lyraes (which also exhibit noisy looking light curves).

7.4 Obstacles Encountered with the RRc Stars

A major problem encountered in this project is the lack of well observed field RRc reference stars in the literature. Kemper (1982) and Bookmeyer et al. (1977) were among the few references that contained good observational parameters for field RRc stars. In addition to the paucity of RRc star research in the literature, some of the reference RRc stars that were observed by the ROTSE-I telescope turned out to have poor ROTSE-I light curves. As a consequence of this, good measurements of amplitude and Fourier decomposition parameters could not be performed. Appendix C is a table of parameters derived for 375 RRc stars.

Even if we had a good sample of RRc stars from NSVS and were able to calibrate parameters, such as amplitude, onto the Johnson V filter system, the relations used for determining [Fe/H] were only developed for RRab stars. For example, the ϕ_{31} parameters are different for the asymmetric light curves of RRab stars and the sinusoidal light curves of the c-types. Thus, the Jurcsik & Kovacs method for determining

[Fe/H] is applicable only to the RRab stars. Until a similar ϕ_{31}-period-[Fe/H] relation (if there is one) is developed for the RRc stars, we are left to determine the metallicity of these stars only through spectroscopy or through multi-color photometric metallicity parameters.

7.5 Other Types of RR Lyraes

As mentioned in section 2.1.1, there are two types of multi-periodic RR Lyraes. These are the double mode RR Lyraes (RRd) and the RR Lyraes with the Blazhko effect. The NSVS survey allows us an opportunity to find these types of stars in the solar neighborhood. Studies of these stars can be excellent side projects from this research.

The RRd and Blazhko RRab stars have very similar looking, messy light curves. The RRd light curves would need to be deconvolved in order to derive the fundamental and first overtone mode periods. Astrophysically, the ratio of these periods can be used to derive stellar masses of the RRd stars (Petersen 1973, Bono et al. 1996). Finding Blazhko effect stars would be useful astrophysically, to study possible non-radial oscillation mechanisms in these stars. A complete survey of Blazhko RR Lyraes in the NSVS sample will be useful to characterize the pulsational properties of the RR Lyraes in the solar neighborhood. In Table 7.1, a list of Blazhko effect and RRd candidates is provided.

Table 7.1 Blazhko Effect and Double-Mode RR Lyrae Candidates.

NSVS id	RA (2000)	DEC (2000)	Period (days)
12962968	136.2020	5.5024	0.496977
14715713	22.2010	-11.4534	0.516926
5207932	240.1340	46.9240	0.469995
5222075	236.6080	44.3125	0.494065
8877855	336.3470	34.8855	0.503446
10806470	256.4160	21.5167	0.613090
15726118	144.3830	-18.2703	0.520967
16240332	230.4710	-12.1128	0.441802
1088956	258.3330	69.1317	0.403212
13439616	233.3780	2.7768	0.575426
16100815	214.1080	-17.0918	0.566316
5152352	223.4170	40.5286	0.353033
10905292	266.4960	10.5037	0.537722
12252066	69.5150	-1.9958	0.579259
12919471	131.9460	-3.6501	0.420834
13961527	283.7150	-0.5452	0.685244
14411401	318.6800	4.4937	0.444705
11559601	316.5430	10.3862	0.557333
12900308	127.6250	-2.7110	0.508529
13144198	175.8840	2.6986	0.595013
13343643	217.0410	6.5455	0.483731
2094282	61.6630	55.4999	0.368768
5377085	273.2430	42.0625	0.442158
9294409	39.7350	8.7423	0.604376

Appendix A

Best Estimate [Fe/H]

This table contains the [Fe/H] values determined from Sandage (2004) and from Jurcsik & Kovacs (1996). The first column is the identification number in the NSVS catalog. Columns 2 and 3 are the [Fe/H] and its uncertainty values from Sandage's relation. Columns 4 and 5 are the [Fe/H] and its uncertainty from the Jurcsik & Kovacs method. The entry 9.99 for either of these columns indicates the [Fe/H] value was not calculated using this method. Columns 6 and 7 are the best estimate [Fe/H] and its corresponding uncertainty.

Table A.1. Photometric Metallicity

NSVS ID	$[Fe/H]_{AP}$	σ_{AP}	$[Fe/H]_{JK}$	σ_{JK}	[Fe/H]	$\sigma_{[Fe/H]}$
47456	-1.47	0.30	-1.84	0.19	-1.73	0.16
95598	-2.17	0.30	-2.32	0.19	-2.28	0.16
219254	-1.16	0.30	9.99	9.99	-1.16	0.30
253438	-1.71	0.30	9.99	9.99	-1.71	0.30
258743	-0.49	0.30	-0.06	0.29	-0.27	0.21
272579	-1.20	0.30	-1.38	0.23	-1.31	0.18
653553	-1.37	0.30	-1.22	0.29	-1.29	0.21
660817	-1.95	0.30	-1.57	0.21	-1.69	0.17
683309	-2.56	0.30	9.99	9.99	-2.56	0.30
768199	-1.86	0.30	-2.44	0.24	-2.22	0.19
777166	-1.83	0.30	-1.64	0.27	-1.73	0.20
877851	-2.18	0.30	-1.79	0.21	-1.92	0.17
887046	-1.63	0.30	-1.27	0.21	-1.39	0.17
933594	-1.47	0.30	-1.57	0.27	-1.53	0.20
972122	-1.20	0.30	-0.71	0.32	[-0.97]	0.22
975558	-2.24	0.30	-1.89	0.23	-2.02	0.18
979936	-1.47	0.30	-1.95	0.29	-1.72	0.21
1048200	-1.51	0.30	-1.33	0.24	-1.40	0.19
1062497	-1.39	0.30	-1.85	0.21	-1.69	0.17
1117769	-1.74	0.30	-1.30	0.29	-1.51	0.21
1127821	-1.49	0.30	9.99	9.99	-1.49	0.30
1132042	-1.57	0.30	-1.50	0.26	-1.53	0.20
1156866	-2.16	0.30	-2.53	0.23	-2.39	0.18
1227428	-0.58	0.30	9.99	9.99	-0.58	0.30
1251329	-2.23	0.30	-1.58	0.21	-1.80	0.17
1328589	-1.87	0.30	-1.90	0.21	-1.89	0.17
1363670	-0.91	0.30	-0.88	0.23	-0.89	0.18
1376650	-0.95	0.30	-0.32	0.25	-0.58	0.19
1412375	-1.59	0.30	-1.46	0.23	-1.51	0.18
1437682	-2.19	0.30	-2.64	0.25	-2.46	0.19
1633417	-1.46	0.30	9.99	9.99	-1.46	0.30
1693393	-1.33	0.30	9.99	9.99	-1.33	0.30
1731449	-0.49	0.30	-0.67	0.21	-0.61	0.17
1751270	-0.49	0.30	9.99	9.99	-0.49	0.30
1945919	-1.82	0.30	-1.68	0.22	-1.73	0.18

Table A.1 (cont'd)

NSVS ID	$[Fe/H]_{AP}$	σ_{AP}	$[Fe/H]_{JK}$	σ_{JK}	[Fe/H]	$\sigma_{[Fe/H]}$
2029729	-1.19	0.30	-0.23	0.27	-0.65	0.20
2132727	-1.78	0.30	9.99	9.99	-1.78	0.30
2198205	-2.29	0.30	-2.11	0.23	-2.17	0.18
2284758	-2.06	0.30	-1.54	0.26	-1.76	0.20
2431223	-1.60	0.30	-1.82	0.22	-1.74	0.18
2462143	-1.37	0.30	-1.57	0.23	-1.50	0.18
2508765	-1.52	0.30	-1.89	0.27	-1.72	0.20
2543920	-1.90	0.30	-2.17	0.24	-2.06	0.19
2549610	-2.47	0.30	-2.32	0.23	-2.38	0.18
2587991	-1.26	0.30	9.99	9.99	-1.26	0.30
2589437	-2.01	0.30	-1.78	0.21	-1.85	0.17
2595352	-1.34	0.30	-1.43	0.23	-1.40	0.18
2601261	-2.42	0.30	9.99	9.99	-2.42	0.30
2610846	-1.71	0.30	-1.64	0.29	-1.67	0.21
2676458	-1.98	0.30	-2.16	0.27	-2.08	0.20
2681536	-1.07	0.30	-1.27	0.22	-1.20	0.18
2696951	-1.81	0.30	-1.74	0.21	-1.76	0.17
2731333	-1.78	0.30	-1.37	0.27	-1.55	0.20
2737869	-1.88	0.30	-2.12	0.24	-2.02	0.19
2745643	-1.61	0.30	-1.52	0.22	-1.55	0.18
2773160	-1.79	0.30	9.99	9.99	-1.79	0.30
2792534	-1.76	0.30	9.99	9.99	-1.76	0.30
2810184	-1.53	0.30	-1.55	0.28	-1.54	0.20
2830505	-1.05	0.30	-1.42	0.28	-1.25	0.20
2909040	-1.77	0.30	9.99	9.99	-1.77	0.30
2927295	-1.11	0.30	9.99	9.99	-1.11	0.30
2927471	-1.31	0.30	-1.63	0.24	-1.50	0.19
2930718	-1.30	0.30	-1.21	0.24	-1.25	0.19
3022099	-0.75	0.30	-1.06	0.22	-0.95	0.18
3030972	-2.08	0.30	-1.79	0.20	-1.88	0.17
3078092	-1.14	0.30	-1.45	0.19	-1.36	0.16
3087037	-1.25	0.30	-0.96	0.25	-1.08	0.19
3117503	-2.19	0.30	-1.95	0.19	-2.02	0.16
3306144	-1.03	0.30	-0.51	0.24	-0.71	0.19
3611791	-0.67	0.30	-0.29	0.24	-0.44	0.19

Table A.1 (cont'd)

NSVS ID	$[Fe/H]_{AP}$	σ_{AP}	$[Fe/H]_{JK}$	σ_{JK}	[Fe/H]	$\sigma_{[Fe/H]}$
3619355	-1.22	0.30	-1.35	0.22	-1.31	0.18
3633663	-2.05	0.30	-2.54	0.22	-2.37	0.18
3713191	-1.64	0.30	-1.90	0.21	-1.82	0.17
3817372	-2.53	0.30	-2.03	0.21	-2.20	0.17
3939459	-1.96	0.30	-0.76	0.31	-1.38	0.22
3962805	-0.85	0.30	-0.53	0.29	-0.68	0.21
3963833	-1.13	0.30	-0.73	0.22	-0.87	0.18
3964415	-2.45	0.30	-3.15	0.23	-2.89	0.18
3994860	-2.26	0.30	-2.76	0.26	-2.54	0.20
4160839	-1.80	0.30	-2.00	0.25	-1.92	0.19
4180591	0.12	0.30	9.99	9.99	0.12	0.30
4241455	-1.40	0.30	-1.37	0.22	-1.38	0.18
4275987	-0.32	0.30	-0.12	0.24	-0.20	0.19
4493602	-1.48	0.30	9.99	9.99	-1.48	0.30
4661441	-1.35	0.30	-1.65	0.25	-1.53	0.19
4694845	-0.83	0.30	-0.67	0.20	-0.72	0.16
4700160	-1.28	0.30	-1.38	0.28	-1.34	0.20
4720404	-1.16	0.30	0.58	0.28	-0.23	0.21
4760770	-0.91	0.30	-2.97	0.17	[-2.47]	0.15
4762874	-1.67	0.30	-2.04	0.27	-1.88	0.20
4820869	-1.44	0.30	9.99	9.99	-1.44	0.30
4828496	-1.38	0.30	-1.51	0.21	-1.47	0.17
4837927	-1.47	0.30	9.99	9.99	-1.47	0.30
4838954	-1.62	0.30	-1.23	0.25	-1.39	0.19
4876765	-1.59	0.30	-1.48	0.26	-1.53	0.20
4930109	-2.48	0.30	-1.90	0.24	-2.13	0.19
4959080	-1.36	0.30	9.99	9.99	-1.36	0.30
4979454	-1.37	0.30	9.99	9.99	-1.37	0.30
4990594	-1.34	0.30	-1.72	0.23	-1.58	0.18
4993764	-2.02	0.30	-1.79	0.21	-1.87	0.17
4996441	-2.43	0.30	-2.08	0.24	-2.22	0.19
4998847	-1.60	0.30	-1.47	0.21	-1.51	0.17
5007979	-1.05	0.30	-0.74	0.26	-0.88	0.20
5013760	-1.50	0.30	-1.58	0.21	-1.56	0.17
5028197	-2.39	0.30	-1.95	0.21	-2.10	0.17

Table A.1 (cont'd)

NSVS ID	$[Fe/H]_{AP}$	σ_{AP}	$[Fe/H]_{JK}$	σ_{JK}	[Fe/H]	$\sigma_{[Fe/H]}$
5034190	-2.19	0.30	-1.78	0.28	-1.97	0.20
5039296	-1.30	0.30	9.99	9.99	-1.30	0.30
5039914	-2.18	0.30	9.99	9.99	-2.18	0.30
5047909	-1.51	0.30	-1.43	0.24	-1.46	0.19
5058465	-1.81	0.30	-1.81	0.27	-1.81	0.20
5089958	-1.20	0.30	-1.61	0.29	-1.41	0.21
5090118	-1.29	0.30	-1.70	0.22	-1.55	0.18
5113606	-2.22	0.30	-1.91	0.22	-2.02	0.18
5120617	-1.55	0.30	-1.49	0.23	-1.51	0.18
5133135	-2.19	0.30	-1.65	0.21	-1.83	0.17
5144530	-1.41	0.30	-1.19	0.28	-1.29	0.20
5149126	-1.50	0.30	-1.54	0.19	-1.53	0.16
5152352	0.26	0.30	9.99	9.99	[0.26]	0.30
5181224	-0.18	0.30	-1.63	0.21	[-1.15]	0.17
5206471	-1.25	0.30	9.99	9.99	-1.25	0.30
5207932	-1.39	0.30	9.99	9.99	-1.39	0.30
5216041	-1.47	0.30	9.99	9.99	-1.47	0.30
5222075	-0.61	0.30	9.99	9.99	-0.61	0.30
5222117	-1.60	0.30	9.99	9.99	-1.60	0.30
5232275	-1.85	0.30	9.99	9.99	-1.85	0.30
5248399	-2.24	0.30	-1.92	0.21	-2.03	0.17
5249019	-2.43	0.30	-2.05	0.22	-2.18	0.18
5249836	-2.41	0.30	-1.67	0.25	-1.98	0.19
5250334	-2.10	0.30	-2.04	0.29	-2.07	0.21
5259122	-1.60	0.30	9.99	9.99	-1.60	0.30
5270815	-1.42	0.30	-1.19	0.23	-1.28	0.18
5288795	-1.92	0.30	-2.29	0.27	-2.12	0.20
5300614	-1.89	0.30	9.99	9.99	-1.89	0.30
5301154	-1.46	0.30	9.99	9.99	-1.46	0.30
5316660	-1.07	0.30	9.99	9.99	-1.07	0.30
5401722	-1.44	0.30	9.99	9.99	-1.44	0.30
5406476	-2.14	0.30	-1.92	0.28	-2.02	0.21
5415960	-1.49	0.30	9.99	9.99	-1.49	0.30
5484202	-1.64	0.30	9.99	9.99	-1.64	0.30
5494745	-1.47	0.30	-1.45	0.23	-1.46	0.18

Table A.1 (cont'd)

NSVS ID	$[Fe/H]_{AP}$	σ_{AP}	$[Fe/H]_{JK}$	σ_{JK}	[Fe/H]	$\sigma_{[Fe/H]}$
5525580	-1.85	0.30	-1.83	0.27	-1.84	0.20
5526812	-1.41	0.30	-1.87	0.21	-1.72	0.17
5568043	-2.57	0.30	-2.00	0.25	-2.23	0.19
5568339	-1.36	0.30	-1.10	0.25	-1.20	0.19
5587647	-1.36	0.30	9.99	9.99	-1.36	0.30
5654619	-0.65	0.30	9.99	9.99	-0.65	0.30
5666134	-1.62	0.30	9.99	9.99	-1.62	0.30
6094124	-2.21	0.30	-1.87	0.20	-1.97	0.17
6231458	-1.69	0.30	-1.62	0.23	-1.65	0.18
6248007	-2.00	0.30	-1.63	0.23	-1.76	0.18
6264114	-1.57	0.30	9.99	9.99	-1.57	0.30
6302329	-0.57	0.30	-0.30	0.23	-0.40	0.18
6392775	-1.50	0.30	-1.64	0.21	-1.59	0.17
6429831	-1.75	0.30	-1.16	0.26	-1.42	0.20
6480339	-0.71	0.30	-1.17	0.22	[-1.01]	0.18
6705217	-0.78	0.30	-0.53	0.25	-0.63	0.19
6808365	-0.91	0.30	9.99	9.99	-0.91	0.30
6860143	-0.73	0.30	-0.51	0.22	-0.59	0.18
6885646	-1.19	0.30	9.99	9.99	-1.19	0.30
6899769	-1.73	0.30	-1.47	0.26	-1.58	0.20
7058441	-0.63	0.30	9.99	9.99	-0.63	0.30
7231539	-0.62	0.30	-0.55	0.20	-0.58	0.17
7235546	-1.89	0.30	-1.48	0.21	-1.61	0.17
7267812	-0.95	0.30	-0.43	0.29	-0.68	0.21
7394810	-1.98	0.30	-1.88	0.20	-1.91	0.17
7404883	-1.34	0.30	-1.75	0.28	-1.56	0.20
7411607	-1.66	0.30	-1.56	0.23	-1.60	0.18
7412670	-1.47	0.30	-1.22	0.23	-1.31	0.18
7454552	-1.51	0.30	9.99	9.99	-1.51	0.30
7458704	-1.70	0.30	-1.98	0.23	-1.87	0.18
7472262	-1.62	0.30	-2.06	0.21	-1.91	0.17
7484923	-1.54	0.30	-1.34	0.23	-1.41	0.18
7496219	-1.37	0.30	-1.37	0.19	-1.37	0.16
7496252	-1.50	0.30	-1.20	0.25	-1.32	0.19
7512212	-1.78	0.30	-1.31	0.23	-1.48	0.18

Table A.1 (cont'd)

NSVS ID	$[Fe/H]_{AP}$	σ_{AP}	$[Fe/H]_{JK}$	σ_{JK}	[Fe/H]	$\sigma_{[Fe/H]}$
7517103	-1.64	0.30	-1.53	0.24	-1.57	0.19
7539425	-1.76	0.30	9.99	9.99	-1.76	0.30
7540718	-1.66	0.30	-1.42	0.20	-1.49	0.17
7554734	-2.37	0.30	9.99	9.99	-2.37	0.30
7564332	-1.79	0.30	-1.34	0.24	-1.51	0.19
7585321	-1.52	0.30	-1.72	0.20	-1.66	0.17
7614129	-1.29	0.30	-1.24	0.23	-1.26	0.18
7635590	-1.95	0.30	-1.77	0.19	-1.83	0.16
7643254	-2.09	0.30	-4.01	0.18	-3.49	0.16
7649368	-1.47	0.30	-1.39	0.25	-1.43	0.19
7654631	-2.07	0.30	-1.76	0.20	-1.86	0.16
7656719	-1.18	0.30	9.99	9.99	-1.18	0.30
7666038	-2.44	0.30	-2.18	0.25	-2.29	0.19
7685674	-1.92	0.30	9.99	9.99	-1.92	0.30
7703549	-1.65	0.30	-1.79	0.20	-1.75	0.17
7706106	-1.73	0.30	-1.97	0.21	-1.89	0.17
7709213	-1.87	0.30	-1.69	0.20	-1.74	0.17
7711863	-1.23	0.30	0.03	0.27	-0.53	0.20
7726595	-1.71	0.30	-1.64	0.23	-1.67	0.18
7741095	-2.07	0.30	-2.27	0.24	-2.19	0.19
7742142	-1.42	0.30	-1.45	0.22	-1.44	0.18
7752384	-1.47	0.30	-1.63	0.19	-1.59	0.16
7753756	-1.38	0.30	9.99	9.99	-1.38	0.30
7755406	-0.47	0.30	-0.53	0.20	-0.51	0.17
7756950	-1.68	0.30	-1.53	0.25	-1.59	0.19
7777447	-2.07	0.30	-1.79	0.27	-1.92	0.20
7783855	-2.17	0.30	-2.49	0.22	-2.38	0.18
7785359	-1.30	0.30	-1.27	0.22	-1.28	0.18
7799920	-1.90	0.30	-1.98	0.19	-1.96	0.16
7818285	-1.36	0.30	-1.47	0.19	-1.44	0.16
7823144	-2.17	0.30	-1.82	0.22	-1.94	0.18
7824713	-1.80	0.30	-1.44	0.23	-1.57	0.18
7826584	-1.89	0.30	-2.01	0.24	-1.96	0.19
7861269	-1.07	0.30	-1.06	0.29	-1.06	0.21
7866619	-2.15	0.30	-2.01	0.21	-2.06	0.17

Table A.1 (cont'd)

NSVS ID	$[Fe/H]_{AP}$	σ_{AP}	$[Fe/H]_{JK}$	σ_{JK}	[Fe/H]	$\sigma_{[Fe/H]}$
7871803	-3.41	0.30	-2.68	0.26	-2.99	0.20
7872648	-1.94	0.30	-2.07	0.22	-2.03	0.18
7912479	-2.43	0.30	9.99	9.99	-2.43	0.30
7919183	-1.54	0.30	-1.97	0.21	-1.83	0.17
7927997	-2.01	0.30	-1.77	0.21	-1.85	0.17
7954067	-1.27	0.30	-1.35	0.18	-1.32	0.16
7962127	-1.19	0.30	9.99	9.99	-1.19	0.30
7970685	-1.17	0.30	-1.27	0.26	-1.23	0.20
7990146	-1.52	0.30	-1.79	0.23	-1.69	0.18
7998286	-0.83	0.30	9.99	9.99	-0.83	0.30
8023769	-0.83	0.30	-0.63	0.20	-0.69	0.17
8050089	-1.52	0.30	-1.16	0.30	-1.34	0.21
8108614	-1.66	0.30	-1.47	0.21	-1.53	0.17
8125354	-1.44	0.30	-0.98	0.32	-1.22	0.22
8160195	-0.73	0.30	9.99	9.99	-0.73	0.30
8179854	-1.79	0.30	-1.40	0.27	-1.57	0.20
8192311	-2.23	0.30	9.99	9.99	-2.23	0.30
8234127	-1.69	0.30	-2.05	0.19	-1.94	0.16
8293251	-2.09	0.30	9.99	9.99	-2.09	0.30
8360536	-2.13	0.30	9.99	9.99	-2.13	0.30
8572436	-0.84	0.30	-1.08	0.24	-0.99	0.19
8651514	-1.36	0.30	-1.40	0.22	-1.38	0.18
8702062	-0.73	0.30	-0.49	0.21	-0.57	0.17
8706200	-2.08	0.30	-1.52	0.27	-1.77	0.20
8724691	-1.72	0.30	-2.00	0.28	-1.87	0.20
8770585	-0.98	0.30	-0.74	0.24	-0.83	0.19
8776606	-0.81	0.30	-0.49	0.27	-0.64	0.20
8782730	-2.14	0.30	9.99	9.99	-2.14	0.30
8783505	-1.70	0.30	-1.90	0.23	-1.83	0.18
8817268	-0.56	0.30	-0.09	0.26	-0.30	0.20
8877855	-1.18	0.30	9.99	9.99	-1.18	0.30
8903282	-1.25	0.30	-2.13	0.20	-1.86	0.17
8909217	-0.73	0.30	-0.80	0.27	-0.77	0.20
8951389	-1.33	0.30	-0.94	0.23	-1.09	0.18
8956174	-1.67	0.30	-1.70	0.21	-1.69	0.17

Table A.1 (cont'd)

NSVS ID	$[Fe/H]_{AP}$	σ_{AP}	$[Fe/H]_{JK}$	σ_{JK}	[Fe/H]	$\sigma_{[Fe/H]}$
9047405	-1.10	0.30	-1.13	0.29	-1.12	0.21
9050491	-2.09	0.30	-1.72	0.24	-1.87	0.19
9063964	-2.90	0.30	-1.43	0.30	-2.16	0.21
9075932	-1.60	0.30	-1.47	0.20	-1.51	0.17
9088465	-2.27	0.30	-1.90	0.22	-2.02	0.18
9091170	-1.76	0.30	9.99	9.99	-1.76	0.30
9130768	-1.89	0.30	-1.32	0.29	-1.60	0.21
9154382	-2.23	0.30	-1.69	0.26	-1.92	0.20
9230082	-1.91	0.30	9.99	9.99	-1.91	0.30
9240847	-0.74	0.30	9.99	9.99	-0.74	0.30
9254455	-1.51	0.30	-1.39	0.28	-1.45	0.21
9310411	-1.94	0.30	-2.14	0.20	-2.08	0.17
9338383	-1.31	0.30	-1.44	0.19	-1.40	0.16
9671363	-1.46	0.30	9.99	9.99	-1.46	0.30
9995853	-1.59	0.30	-1.70	0.19	-1.67	0.16
10083412	-1.40	0.30	9.99	9.99	-1.40	0.30
10141482	-1.39	0.30	-1.46	0.24	-1.43	0.19
10147460	-1.30	0.30	9.99	9.99	-1.30	0.30
10175326	-1.24	0.30	-1.60	0.21	-1.48	0.17
10203057	-2.02	0.30	-1.73	0.23	-1.84	0.18
10228104	-1.61	0.30	-1.08	0.27	-1.31	0.20
10235938	-2.39	0.30	-2.06	0.22	-2.18	0.18
10241977	-1.63	0.30	-1.27	0.26	-1.43	0.20
10329394	-1.54	0.30	9.99	9.99	-1.54	0.30
10332182	-1.24	0.30	-2.09	0.23	-1.78	0.18
10337183	-1.48	0.30	-0.90	0.28	-1.16	0.20
10338359	-2.12	0.30	-1.89	0.22	-1.97	0.18
10347356	-1.49	0.30	9.99	9.99	-1.49	0.30
10350273	-1.91	0.30	-1.97	0.27	-1.94	0.20
10352408	-1.17	0.30	-0.67	0.24	-0.86	0.19
10358221	-1.92	0.30	-1.94	0.24	-1.93	0.19
10360493	-1.48	0.30	-1.31	0.19	-1.36	0.16
10360815	-2.15	0.30	-1.71	0.20	-1.85	0.17
10360975	-1.98	0.30	-1.60	0.27	-1.77	0.20
10363810	-2.35	0.30	-2.00	0.29	-2.17	0.21

Table A.1 (cont'd)

NSVS ID	$[Fe/H]_{AP}$	σ_{AP}	$[Fe/H]_{JK}$	σ_{JK}	[Fe/H]	$\sigma_{[Fe/H]}$
10371698	-1.51	0.30	-1.12	0.30	-1.31	0.21
10395081	-1.64	0.30	-1.20	0.28	-1.41	0.20
10395582	-2.17	0.30	9.99	9.99	-2.17	0.30
10403252	-1.14	0.30	-1.62	0.28	-1.39	0.20
10418706	-1.57	0.30	9.99	9.99	-1.57	0.30
10431935	-0.95	0.30	9.99	9.99	[-0.95]	0.30
10437330	-1.88	0.30	-1.32	0.23	-1.53	0.18
10446172	-1.20	0.30	-1.33	0.20	-1.29	0.17
10451724	-1.55	0.30	-1.27	0.22	-1.37	0.18
10453784	-2.01	0.30	-2.12	0.21	-2.09	0.17
10464169	-1.80	0.30	-1.64	0.24	-1.71	0.19
10488920	-1.85	0.30	-1.84	0.25	-1.84	0.19
10491545	-1.37	0.30	-2.35	0.23	-1.99	0.18
10492034	-1.24	0.30	9.99	9.99	-1.24	0.30
10514624	-2.15	0.30	-1.76	0.22	-1.90	0.18
10530833	-2.07	0.30	9.99	9.99	-2.07	0.30
10531095	-1.84	0.30	-1.73	0.27	-1.78	0.20
10534194	-1.60	0.30	-0.84	0.31	-1.23	0.22
10547760	-1.67	0.30	9.99	9.99	-1.67	0.30
10549959	-2.02	0.30	9.99	9.99	-2.02	0.30
10567739	-2.20	0.30	9.99	9.99	-2.20	0.30
10591456	-1.24	0.30	-1.31	0.19	-1.29	0.16
10614618	-1.55	0.30	9.99	9.99	-1.55	0.30
10614900	-1.32	0.30	9.99	9.99	-1.32	0.30
10628156	-2.28	0.30	-1.83	0.26	-2.02	0.20
10642059	-1.86	0.30	-1.44	0.26	-1.62	0.20
10642884	-1.38	0.30	-0.52	0.23	-0.84	0.18
10647103	-1.56	0.30	-1.04	0.27	-1.28	0.20
10652318	-2.35	0.30	-2.13	0.23	-2.21	0.18
10685785	-1.57	0.30	-1.36	0.22	-1.43	0.18
10706905	-1.26	0.30	-1.46	0.18	-1.40	0.16
10751419	-2.14	0.30	9.99	9.99	-2.14	0.30
10758202	-1.40	0.30	9.99	9.99	-1.40	0.30
10767117	-0.41	0.30	-0.35	0.29	-0.38	0.21
10769204	-1.47	0.30	9.99	9.99	-1.47	0.30

Table A.1 (cont'd)

NSVS ID	$[Fe/H]_{AP}$	σ_{AP}	$[Fe/H]_{JK}$	σ_{JK}	[Fe/H]	$\sigma_{[Fe/H]}$
10773700	-1.04	0.30	9.99	9.99	-1.04	0.30
10781555	-1.57	0.30	-1.80	0.20	-1.73	0.17
10782844	-1.99	0.30	-1.61	0.25	-1.76	0.19
10806470	-2.26	0.30	9.99	9.99	-2.26	0.30
10824625	-1.83	0.30	9.99	9.99	-1.83	0.30
10824661	-1.45	0.30	-1.12	0.21	-1.23	0.17
10869885	-0.54	0.30	9.99	9.99	-0.54	0.30
10885456	-0.45	0.30	9.99	9.99	-0.45	0.30
10887396	-1.58	0.30	9.99	9.99	-1.58	0.30
10891107	-1.08	0.30	9.99	9.99	-1.08	0.30
10905292	-1.79	0.30	9.99	9.99	-1.79	0.30
10955591	-0.11	0.30	-0.85	0.23	-0.58	0.18
10994614	-1.57	0.30	-1.81	0.23	-1.72	0.18
11015121	-1.50	0.30	9.99	9.99	-1.50	0.30
11061928	-1.65	0.30	9.99	9.99	-1.65	0.30
11327182	-1.07	0.30	9.99	9.99	-1.07	0.30
11379204	-0.98	0.30	-1.19	0.21	[-1.12]	0.17
11420828	-1.29	0.30	9.99	9.99	-1.29	0.30
11491796	-0.67	0.30	-0.38	0.25	-0.50	0.19
11527986	-1.23	0.30	-1.28	0.29	-1.25	0.21
11533492	-0.70	0.30	-0.49	0.24	-0.57	0.19
11622871	-1.13	0.30	9.99	9.99	-1.13	0.30
11643237	-1.46	0.30	9.99	9.99	-1.46	0.30
11647104	-2.78	0.30	9.99	9.99	-2.78	0.30
11656645	-0.98	0.30	-1.34	0.23	[-1.21]	0.18
11668678	-1.60	0.30	9.99	9.99	-1.60	0.30
11670319	-2.44	0.30	-2.12	0.22	-2.23	0.18
11672831	-0.41	0.30	-0.21	0.21	-0.27	0.17
11677349	-1.29	0.30	9.99	9.99	-1.29	0.30
11747453	-2.07	0.30	9.99	9.99	-2.07	0.30
11753751	-1.16	0.30	-1.18	0.22	-1.18	0.18
11757688	-1.44	0.30	-1.71	0.18	-1.64	0.16
11762920	-1.59	0.30	9.99	9.99	-1.59	0.30
11770209	-1.92	0.30	9.99	9.99	-1.92	0.30
11772445	-2.05	0.30	-1.36	0.21	-1.58	0.17

Table A.1 (cont'd)

NSVS ID	$[Fe/H]_{AP}$	σ_{AP}	$[Fe/H]_{JK}$	σ_{JK}	[Fe/H]	$\sigma_{[Fe/H]}$
11798849	-1.56	0.30	9.99	9.99	-1.56	0.30
11803133	-1.59	0.30	-1.31	0.23	-1.42	0.18
11828256	-1.91	0.30	9.99	9.99	-1.91	0.30
11840237	-2.43	0.30	9.99	9.99	-2.43	0.30
11864349	-1.93	0.30	-1.17	0.29	-1.54	0.21
11869181	-1.73	0.30	-1.63	0.26	-1.67	0.19
11870671	-2.21	0.30	-1.67	0.21	-1.84	0.17
11872085	-1.97	0.30	-1.62	0.23	-1.75	0.18
11902531	-1.56	0.30	-2.14	0.24	-1.91	0.19
11910764	-1.27	0.30	-1.59	0.27	-1.45	0.20
11929610	-1.69	0.30	9.99	9.99	-1.69	0.30
11951363	-1.14	0.30	9.99	9.99	-1.14	0.30
11967991	-1.38	0.30	-1.49	0.29	-1.43	0.21
11990963	-2.30	0.30	-2.33	0.23	-2.32	0.18
11996470	-1.38	0.30	-1.58	0.23	-1.51	0.18
12007998	-1.41	0.30	-1.46	0.21	-1.44	0.17
12009122	-1.65	0.30	9.99	9.99	-1.65	0.30
12010601	-1.61	0.30	-1.40	0.25	-1.49	0.19
12073505	-2.95	0.30	-2.67	0.29	-2.80	0.21
12096932	-1.31	0.30	-2.31	0.22	-1.96	0.18
12140779	-0.42	0.30	-0.44	0.22	-0.43	0.18
12248877	-1.13	0.30	-0.98	0.28	-1.05	0.20
12250977	-1.21	0.30	9.99	9.99	-1.21	0.30
12252066	-2.45	0.30	9.99	9.99	-2.45	0.30
12370362	-1.50	0.30	9.99	9.99	-1.50	0.30
12678415	-1.40	0.30	-0.80	0.26	-1.06	0.20
12680188	-1.62	0.30	-0.36	0.27	-0.92	0.20
12680351	-2.12	0.30	-2.00	0.23	-2.05	0.18
12728156	-1.25	0.30	-0.32	0.26	-0.72	0.20
12778072	-1.37	0.30	-1.35	0.22	-1.35	0.18
12843002	-1.63	0.30	-2.14	0.19	-2.00	0.16
12871389	-2.25	0.30	9.99	9.99	-2.25	0.30
12872211	-1.47	0.30	9.99	9.99	-1.47	0.30
12880089	-1.26	0.30	-1.14	0.26	-1.19	0.20
12892356	-1.51	0.30	-0.96	0.32	-1.25	0.22

Table A.1 (cont'd)

NSVS ID	$[Fe/H]_{AP}$	σ_{AP}	$[Fe/H]_{JK}$	σ_{JK}	[Fe/H]	$\sigma_{[Fe/H]}$
12900308	-1.31	0.30	-2.80	0.26	-2.16	0.20
12916018	-1.06	0.30	9.99	9.99	-1.06	0.30
12919471	-0.00	0.30	9.99	9.99	-0.00	0.30
12929278	-2.48	0.30	-2.04	0.23	-2.20	0.18
12962968	-0.77	0.30	9.99	9.99	-0.77	0.30
12985723	-1.29	0.30	-1.18	0.27	-1.23	0.20
12990484	-1.69	0.30	-1.73	0.22	-1.72	0.18
13001998	-1.99	0.30	9.99	9.99	-1.99	0.30
13002450	-1.09	0.30	-1.42	0.23	-1.30	0.18
13017408	-2.40	0.30	-1.82	0.24	-2.04	0.19
13039828	-2.76	0.30	9.99	9.99	-2.76	0.30
13094756	-1.55	0.30	-0.98	0.24	-1.21	0.19
13095983	-1.59	0.30	-1.36	0.30	-1.47	0.21
13108142	-2.50	0.30	-2.26	0.20	-2.34	0.17
13124901	-1.85	0.30	9.99	9.99	-1.85	0.30
13151540	-2.02	0.30	-2.34	0.22	-2.22	0.18
13155113	-2.07	0.30	-1.87	0.20	-1.93	0.17
13196916	-1.75	0.30	-1.73	0.22	-1.73	0.18
13197108	-1.54	0.30	9.99	9.99	-1.54	0.30
13197686	-1.58	0.30	-1.75	0.22	-1.69	0.18
13207963	-2.62	0.30	-2.88	0.26	-2.77	0.20
13221776	-1.20	0.30	9.99	9.99	-1.20	0.30
13231809	-1.56	0.30	-1.87	0.18	-1.79	0.16
13236188	-1.81	0.30	9.99	9.99	-1.81	0.30
13264395	-1.95	0.30	-1.71	0.20	-1.78	0.16
13265072	-1.63	0.30	9.99	9.99	-1.63	0.30
13282686	-0.66	0.30	-1.84	0.18	[-1.52]	0.16
13287612	-2.36	0.30	9.99	9.99	-2.36	0.30
13288116	-1.76	0.30	-1.69	0.21	-1.71	0.17
13291329	-1.84	0.30	-2.30	0.26	-2.10	0.20
13294241	-2.48	0.30	9.99	9.99	-2.48	0.30
13302749	-1.46	0.30	9.99	9.99	-1.46	0.30
13311476	-1.94	0.30	9.99	9.99	-1.94	0.30
13322484	-0.92	0.30	-0.80	0.21	-0.83	0.17
13343221	-2.12	0.30	-1.66	0.28	-1.87	0.20

Table A.1 (cont'd)

NSVS ID	$[Fe/H]_{AP}$	σ_{AP}	$[Fe/H]_{JK}$	σ_{JK}	[Fe/H]	$\sigma_{[Fe/H]}$
13350457	-2.10	0.30	9.99	9.99	-2.10	0.30
13362899	-1.59	0.30	-1.93	0.22	-1.81	0.18
13373556	-1.53	0.30	9.99	9.99	-1.53	0.30
13373760	-2.04	0.30	9.99	9.99	-2.04	0.30
13377175	-2.30	0.30	-1.91	0.28	-2.09	0.20
13415461	-1.72	0.30	-1.31	0.22	-1.45	0.18
13419553	-1.61	0.30	-1.63	0.22	-1.63	0.18
13425077	-1.52	0.30	-1.86	0.22	-1.74	0.18
13425719	-1.38	0.30	-1.55	0.29	-1.47	0.21
13436085	-1.80	0.30	-1.91	0.22	-1.87	0.18
13437790	-2.01	0.30	-1.74	0.23	-1.84	0.18
13438360	-2.62	0.30	9.99	9.99	-2.62	0.30
13439616	-1.02	0.30	9.99	9.99	-1.02	0.30
13440706	-1.69	0.30	-1.48	0.29	-1.58	0.21
13444030	-1.45	0.30	-1.40	0.28	-1.42	0.20
13453020	-2.18	0.30	-1.85	0.25	-1.99	0.19
13456880	-2.56	0.30	-2.09	0.23	-2.26	0.18
13466900	-0.59	0.30	9.99	9.99	-0.59	0.30
13467814	-1.09	0.30	9.99	9.99	-1.09	0.30
13479853	-2.44	0.30	-1.84	0.27	-2.11	0.20
13489599	-1.76	0.30	9.99	9.99	-1.76	0.30
13504920	-1.12	0.30	9.99	9.99	-1.12	0.30
13533108	-2.11	0.30	9.99	9.99	-2.11	0.30
13551179	-1.94	0.30	9.99	9.99	-1.94	0.30
13567201	-2.10	0.30	9.99	9.99	-2.10	0.30
13570612	-1.53	0.30	9.99	9.99	-1.53	0.30
13572504	-2.42	0.30	9.99	9.99	-2.42	0.30
13574815	-2.46	0.30	-1.95	0.31	-2.21	0.22
13578753	-1.43	0.30	9.99	9.99	-1.43	0.30
13644720	-1.92	0.30	-1.49	0.25	-1.67	0.19
13667152	-0.59	0.30	-0.86	0.28	-0.73	0.21
13682137	-1.30	0.30	9.99	9.99	-1.30	0.30
13687028	-2.20	0.30	9.99	9.99	-2.20	0.30
13688630	-1.88	0.30	-1.11	0.33	-1.53	0.22
13721372	-1.54	0.30	-1.65	0.26	-1.61	0.20

Table A.1 (cont'd)

NSVS ID	$[Fe/H]_{AP}$	σ_{AP}	$[Fe/H]_{JK}$	σ_{JK}	[Fe/H]	$\sigma_{[Fe/H]}$
13758491	-1.32	0.30	-1.16	0.24	-1.22	0.19
13961527	-1.44	0.30	9.99	9.99	-1.44	0.30
14205594	-0.68	0.30	9.99	9.99	-0.68	0.30
14215652	-1.85	0.30	-2.14	0.25	-2.02	0.19
14266156	-0.62	0.30	9.99	9.99	-0.62	0.30
14279000	-1.32	0.30	9.99	9.99	-1.32	0.30
14284107	-2.03	0.30	-1.71	0.20	-1.81	0.17
14312323	-1.34	0.30	9.99	9.99	-1.34	0.30
14332976	-2.31	0.30	9.99	9.99	-2.31	0.30
14357980	-2.37	0.30	9.99	9.99	-2.37	0.30
14361529	-1.41	0.30	-1.06	0.30	-1.23	0.21
14371460	-1.53	0.30	-0.86	0.22	-1.09	0.18
14378728	-0.94	0.30	9.99	9.99	-0.94	0.30
14411401	-0.50	0.30	9.99	9.99	-0.50	0.30
14412075	-1.25	0.30	-1.66	0.18	-1.55	0.16
14433599	-1.29	0.30	9.99	9.99	-1.29	0.30
14439563	-1.63	0.30	-1.82	0.19	-1.77	0.16
14440338	-1.81	0.30	9.99	9.99	-1.81	0.30
14447741	-1.99	0.30	-2.24	0.25	-2.14	0.19
14487932	-1.38	0.30	1.09	0.33	[-0.26]	0.22
14495865	-1.39	0.30	9.99	9.99	-1.39	0.30
14505896	-1.32	0.30	-1.40	0.23	-1.37	0.18
14512123	-1.60	0.30	-1.37	0.28	-1.48	0.20
14528813	-1.32	0.30	9.99	9.99	-1.32	0.30
14554493	-2.15	0.30	-1.15	0.27	-1.61	0.20
14560814	-1.87	0.30	9.99	9.99	-1.87	0.30
14561489	-3.77	0.30	-3.93	0.27	-3.86	0.20
14564729	-0.12	0.30	9.99	9.99	[-0.12]	0.30
14581148	-1.23	0.30	9.99	9.99	-1.23	0.30
14617414	-1.31	0.30	-0.99	0.20	-1.09	0.17
14629388	-2.08	0.30	-1.66	0.26	-1.84	0.20
14641661	-1.34	0.30	-1.43	0.27	-1.39	0.20
14654206	-2.44	0.30	-2.64	0.24	-2.56	0.19
14669479	-1.26	0.30	9.99	9.99	-1.26	0.30
14682479	-1.09	0.30	9.99	9.99	-1.09	0.30

Table A.1 (cont'd)

NSVS ID	$[Fe/H]_{AP}$	σ_{AP}	$[Fe/H]_{JK}$	σ_{JK}	[Fe/H]	$\sigma_{[Fe/H]}$
14685163	-1.89	0.30	9.99	9.99	-1.89	0.30
14698705	-1.96	0.30	9.99	9.99	-1.96	0.30
14715713	-1.18	0.30	9.99	9.99	-1.18	0.30
14762123	-1.42	0.30	-1.18	0.31	-1.30	0.21
14768130	-1.32	0.30	-1.22	0.20	-1.25	0.17
14782274	-2.21	0.30	9.99	9.99	-2.21	0.30
14791206	-2.21	0.30	9.99	9.99	-2.21	0.30
14818780	-2.29	0.30	-2.30	0.24	-2.30	0.19
14908249	-1.67	0.30	-0.93	0.25	-1.23	0.19
14910117	-1.47	0.30	9.99	9.99	-1.47	0.30
14915325	-1.21	0.30	9.99	9.99	-1.21	0.30
14925915	-2.46	0.30	9.99	9.99	-2.46	0.30
14941696	-1.44	0.30	-1.50	0.21	-1.48	0.17
14943427	-1.95	0.30	-1.87	0.19	-1.89	0.16
14979434	-1.31	0.30	9.99	9.99	-1.31	0.30
14990007	-1.29	0.30	-1.06	0.29	-1.17	0.21
15004446	-1.43	0.30	9.99	9.99	-1.43	0.30
15016349	-1.75	0.30	9.99	9.99	-1.75	0.30
15021359	-1.14	0.30	-0.84	0.30	-0.99	0.21
15206916	-1.02	0.30	9.99	9.99	-1.02	0.30
15218044	-0.76	0.30	9.99	9.99	-0.76	0.30
15657369	-1.52	0.30	-1.81	0.18	-1.73	0.16
15671445	-1.52	0.30	-1.66	0.24	-1.60	0.19
15679506	-1.31	0.30	9.99	9.99	-1.31	0.30
15681945	-1.97	0.30	9.99	9.99	-1.97	0.30
15692808	-2.33	0.30	9.99	9.99	-2.33	0.30
15726118	-1.41	0.30	9.99	9.99	-1.41	0.30
15781327	-1.32	0.30	-1.14	0.22	-1.20	0.18
15806847	-1.08	0.30	-1.14	0.22	-1.12	0.18
15820266	-2.06	0.30	9.99	9.99	-2.06	0.30
15827760	-1.98	0.30	-1.62	0.25	-1.76	0.19
15854954	-0.62	0.30	-0.93	0.20	-0.84	0.16
15889152	-1.96	0.30	-2.35	0.22	-2.21	0.18
15893670	-1.98	0.30	-1.96	0.24	-1.97	0.19
15896141	-2.07	0.30	9.99	9.99	-2.07	0.30

Table A.1 (cont'd)

NSVS ID	$[Fe/H]_{AP}$	σ_{AP}	$[Fe/H]_{JK}$	σ_{JK}	[Fe/H]	$\sigma_{[Fe/H]}$
15897529	-1.75	0.30	9.99	9.99	-1.75	0.30
15901810	-1.90	0.30	9.99	9.99	-1.90	0.30
15972928	-1.98	0.30	-1.83	0.26	-1.89	0.20
15975024	-0.98	0.30	-1.19	0.26	[-1.10]	0.19
15977770	-1.50	0.30	-1.93	0.24	-1.77	0.19
15979689	-1.42	0.30	-1.24	0.29	-1.33	0.21
15985119	-1.70	0.30	9.99	9.99	-1.70	0.30
16053601	-1.28	0.30	9.99	9.99	-1.28	0.30
16100815	-0.96	0.30	9.99	9.99	-0.96	0.30
16109407	-2.53	0.30	9.99	9.99	-2.53	0.30
16117767	-1.63	0.30	9.99	9.99	-1.63	0.30
16127147	-1.17	0.30	9.99	9.99	-1.17	0.30
16155643	-1.71	0.30	-1.54	0.29	-1.62	0.21
16157754	-1.84	0.30	9.99	9.99	-1.84	0.30
16164702	-1.56	0.30	-1.34	0.26	-1.43	0.20
16184196	-1.44	0.30	9.99	9.99	-1.44	0.30
16185842	-1.09	0.30	-1.08	0.30	-1.09	0.21
16197858	-1.47	0.30	9.99	9.99	-1.47	0.30
16224995	-1.48	0.30	9.99	9.99	-1.48	0.30
16238329	-1.43	0.30	9.99	9.99	-1.43	0.30
16239733	-2.23	0.30	9.99	9.99	-2.23	0.30
16240332	-0.77	0.30	9.99	9.99	-0.77	0.30
16241026	-2.04	0.30	9.99	9.99	-2.04	0.30
16244466	-1.65	0.30	9.99	9.99	-1.65	0.30
16258860	-0.72	0.30	9.99	9.99	[-0.72]	0.30
16267747	-2.42	0.30	9.99	9.99	-2.42	0.30
16283172	-1.46	0.30	-0.94	0.28	-1.18	0.20
16292601	-1.51	0.30	9.99	9.99	-1.51	0.30
16304023	-1.41	0.30	-1.31	0.21	-1.34	0.17
16360132	-1.11	0.30	9.99	9.99	-1.11	0.30
16362273	-1.44	0.30	-0.94	0.26	-1.15	0.20
16372425	0.01	0.30	1.94	0.33	[0.88]	0.22
16372447	-1.04	0.30	-1.05	0.20	-1.05	0.17
17011064	-0.65	0.30	9.99	9.99	-0.65	0.30
17022191	-2.30	0.30	9.99	9.99	-2.30	0.30

Table A.1 (cont'd)

NSVS ID	$[Fe/H]_{AP}$	σ_{AP}	$[Fe/H]_{JK}$	σ_{JK}	[Fe/H]	$\sigma_{[Fe/H]}$
17109617	-1.38	0.30	-3.21	0.27	-2.40	0.20
17122030	-1.75	0.30	-1.84	0.30	-1.79	0.21
17130621	-1.63	0.30	9.99	9.99	-1.63	0.30
17147354	-1.64	0.30	9.99	9.99	-1.64	0.30
17176196	-0.24	0.30	9.99	9.99	-0.24	0.30
17212765	-2.02	0.30	-2.36	0.23	-2.23	0.18
17246508	-2.39	0.30	9.99	9.99	-2.39	0.30
17280732	-1.61	0.30	9.99	9.99	-1.61	0.30
17291542	-2.53	0.30	-2.86	0.29	-2.70	0.21
17293210	-2.21	0.30	9.99	9.99	-2.21	0.30
17295262	-2.13	0.30	9.99	9.99	-2.13	0.30
17331060	-1.66	0.30	-1.80	0.23	-1.75	0.18
17344990	-1.50	0.30	-2.02	0.24	-1.81	0.19
17348071	-2.19	0.30	-1.89	0.22	-2.00	0.18
17358579	-2.43	0.30	-1.94	0.22	-2.11	0.18
17368466	-1.96	0.30	-1.53	0.24	-1.70	0.19
17407836	-1.75	0.30	-1.24	0.25	-1.45	0.19
17438804	-1.82	0.30	-0.36	0.33	-1.15	0.22
17474384	-1.66	0.30	9.99	9.99	-1.66	0.30
17478335	-1.54	0.30	9.99	9.99	-1.54	0.30
17510931	-1.48	0.30	-2.50	0.24	-2.10	0.19
17530683	-1.80	0.30	-2.25	0.26	-2.06	0.20
17570707	0.05	0.30	9.99	9.99	0.05	0.30
17572475	-2.08	0.30	-1.84	0.21	-1.92	0.17
17578791	-1.36	0.30	-0.79	0.31	-1.09	0.22
17591359	-1.78	0.30	9.99	9.99	-1.78	0.30
17612485	-1.78	0.30	-2.10	0.25	-1.97	0.19
17620888	-1.27	0.30	9.99	9.99	-1.27	0.30
17633766	-1.35	0.30	-1.45	0.30	-1.40	0.21
17678949	-0.03	0.30	9.99	9.99	[-0.03]	0.30
17702479	-1.34	0.30	-1.14	0.25	-1.23	0.19
17765419	-1.10	0.30	-1.01	0.23	-1.04	0.18
17826311	-1.59	0.30	9.99	9.99	-1.59	0.30
17866005	-2.96	0.30	9.99	9.99	-2.96	0.30
18443369	-1.37	0.30	9.99	9.99	-1.37	0.30

Table A.1 (cont'd)

NSVS ID	$[Fe/H]_{AP}$	σ_{AP}	$[Fe/H]_{JK}$	σ_{JK}	[Fe/H]	$\sigma_{[Fe/H]}$
18473830	-1.34	0.30	9.99	9.99	-1.34	0.30
18479042	-1.82	0.30	9.99	9.99	-1.82	0.30
18551452	-0.67	0.30	9.99	9.99	-0.67	0.30
18552406	0.10	0.30	9.99	9.99	0.10	0.30
18558434	-2.03	0.30	-2.98	0.19	-2.71	0.16
18577666	-2.40	0.30	-0.73	0.31	-1.59	0.22
18621887	-1.33	0.30	9.99	9.99	-1.33	0.30
18688076	-0.97	0.30	9.99	9.99	[-0.97]	0.30
18691062	-1.29	0.30	-1.56	0.28	-1.44	0.21
18714268	-1.16	0.30	-1.11	0.26	-1.13	0.20
19097293	-0.90	0.30	9.99	9.99	-0.90	0.30
19972017	-1.34	0.30	9.99	9.99	-1.34	0.30
19991510	-1.58	0.30	-1.41	0.24	-1.48	0.19

Appendix B

NSVS RRab Parameters

The parameters obtained for the analysis of the RRab stars are listed here. This table contains information for 608 RRab stars from the NSVS database. Column 1 is the identification number of the star in from NSVS. Column 2 and 3 are the galactic coordinates in degrees. Column 4 is the period. Column 5 is the amplitude scaled onto the Johnson V filter system. Column 6 and 7 are the apparent V magnitude and its uncertainty. Column 8 and 9 are the best estimate [Fe/H] value and its uncertainty. Column 10 and 11 are the distance to the star and the Z distance from the Galactic plane in units of kiloparsec. Column 12 and 13 are the absolute magnitude and its uncertainty.

Table B.1. NSVS RRab Properties

NSVS ID	b (o)	l (o)	P (days)	A_V	m_V	σ_{mv}	[Fe/H]	σ_{feh}	D (kpc)	Z (kpc)	M_V	σ_{M_V}
47456	119.501221	21.944254	0.52608	1.07	12.20	0.10	-1.73	0.16	1.13	0.42	0.51	0.12
95598	127.045784	28.588068	0.65198	1.04	12.31	0.11	-2.28	0.16	2.16	1.03	0.41	0.14
219254	123.146973	11.657470	0.64964	0.35	10.32	0.10	-1.16	0.30	0.47	0.09	0.70	0.16
253438	121.905846	17.207481	0.61916	0.84	13.64	0.11	-1.71	0.30	2.75	0.81	0.51	0.13
258743	122.309906	14.121492	0.45749	0.73	13.21	0.11	-0.27	0.21	1.62	0.39	0.94	0.13
272579	124.650543	12.069748	0.51411	0.94	12.46	0.11	-1.31	0.18	1.29	0.27	0.66	0.15
653553	147.079727	21.526051	0.51767	1.04	13.27	0.11	-1.29	0.21	2.73	1.00	0.66	0.15
660817	147.977188	23.166260	0.48044	1.62	12.99	0.11	-1.69	0.17	2.73	1.07	0.51	0.12
683309	146.278351	29.398087	0.80639	0.80	13.63	0.11	-2.56	0.30	4.24	2.08	0.37	0.15
768199	147.864807	34.144066	0.66097	0.79	12.67	0.11	-2.22	0.19	2.63	1.48	0.42	0.14
777166	143.728867	35.420090	0.51871	1.35	13.63	0.11	-1.73	0.20	4.03	2.34	0.51	0.13
877851	133.449478	48.269581	0.66040	1.01	9.78	0.09	-1.92	0.17	0.72	0.53	0.47	0.13
887046	127.266884	47.333412	0.56968	0.99	10.48	0.10	-1.39	0.17	0.91	0.67	0.64	0.15
933594	126.607788	39.309780	0.60309	0.75	13.41	0.11	-1.53	0.20	3.28	2.08	0.54	0.12
972122	115.041275	44.955276	0.54449	0.80	13.64	0.11	[-0.97]	0.22	3.72	2.63	0.75	0.15
975558	113.691597	43.857716	0.65239	1.08	13.16	0.11	-2.02	0.18	3.37	2.34	0.46	0.13
979936	113.875832	40.414055	0.58505	0.82	11.95	0.10	-1.72	0.21	1.86	1.20	0.51	0.13
1048200	112.124062	34.826126	0.49042	1.27	13.60	0.11	-1.40	0.19	3.69	2.11	0.63	0.16
1062497	107.299484	40.443790	0.56961	0.82	12.96	0.11	-1.69	0.17	2.98	1.93	0.51	0.12
1117769	110.446266	31.587154	0.54437	1.18	13.74	0.11	-1.51	0.21	4.11	2.15	0.54	0.12
1127821	109.166328	29.203117	0.54622	0.99	13.73	0.11	-1.49	0.30	3.93	1.92	0.61	0.17
1132042	108.634338	28.253899	0.58900	0.87	12.44	0.11	-1.53	0.20	2.18	1.03	0.54	0.12

Table B.1 (cont'd)

NSVS ID	b (o)	l (o)	P (days)	A_V	m_V	σ_{mv}	[Fe/H]	σ_{feh}	D (kpc)	Z (kpc)	M_V	σ_{M_V}
1156866	113.218933	31.164894	0.69114	0.89	12.93	0.11	-2.39	0.18	2.90	1.50	0.39	0.14
1227428	103.649071	20.206293	0.44771	0.84	13.52	0.11	-0.58	0.30	2.08	0.72	0.85	0.15
1251329	113.071915	25.136835	0.58894	1.32	12.64	0.11	-1.80	0.17	2.44	1.04	0.49	0.13
1328589	106.054108	21.068203	0.55027	1.24	13.14	0.11	-1.89	0.17	2.38	0.86	0.48	0.13
1363670	107.715492	11.981236	0.41663	1.24	13.21	0.11	-0.89	0.18	1.29	0.27	0.77	0.14
1376650	110.919434	11.708086	0.43082	1.19	13.00	0.11	-0.58	0.19	0.94	0.19	0.85	0.14
1412375	116.015244	19.638819	0.48387	1.35	13.36	0.11	-1.51	0.18	1.82	0.61	0.54	0.12
1437682	117.145134	13.919312	0.68039	0.95	13.14	0.11	-2.46	0.19	1.97	0.47	0.38	0.14
1633417	122.473152	2.855022	0.69358	0.40	12.27	0.11	-1.46	0.30	0.17	0.01	0.62	0.17
1693393	126.047432	2.926708	0.60832	0.62	12.61	0.11	-1.33	0.30	0.37	0.02	0.65	0.17
1731449	125.587914	-5.425544	0.41158	0.98	12.12	0.10	-0.61	0.17	0.84	-0.08	0.84	0.13
1751270	129.153076	-6.623267	0.44371	0.80	13.61	0.11	-0.49	0.30	1.93	-0.22	0.88	0.15
1945919	142.779831	-4.290540	0.60708	0.97	12.30	0.11	-1.73	0.18	0.71	-0.05	0.51	0.13
2029729	143.746277	7.891514	0.57205	0.67	11.15	0.10	-0.65	0.20	0.37	0.05	0.83	0.14
2132727	153.606262	6.612230	0.62230	0.88	12.67	0.11	-1.78	0.30	1.22	0.14	0.50	0.13
2198205	149.795959	15.496794	0.66997	1.05	12.99	0.11	-2.17	0.18	2.35	0.63	0.43	0.14
2284758	161.103607	15.550605	0.56446	1.31	13.72	0.11	-1.76	0.20	3.04	0.82	0.50	0.13
2431223	164.635086	32.704151	0.57542	0.94	12.42	0.11	-1.74	0.18	2.26	1.22	0.50	0.13
2462143	150.067535	34.061565	0.59906	0.69	10.80	0.10	-1.50	0.18	1.02	0.57	0.61	0.16
2508765	162.403290	40.002472	0.60428	0.77	12.96	0.11	-1.72	0.20	3.04	1.95	0.51	0.13
2543920	152.476334	43.336571	0.63100	0.93	13.11	0.11	-2.06	0.19	3.28	2.25	0.45	0.13
2549610	151.588394	45.547153	0.61898	1.37	13.12	0.11	-2.38	0.18	3.41	2.44	0.40	0.14

Table B.1 (cont'd)

NSVS ID	b (◦)	l (◦)	P (days)	A_V	m_V	σ_{mv}	[Fe/H]	σ_{feh}	D (kpc)	Z (kpc)	M_V	σ_{M_V}
2587991	152.903366	51.345158	0.63653	0.47	13.59	0.11	-1.26	0.30	3.81	2.98	0.67	0.16
2589437	150.699020	50.908432	0.52425	1.45	13.51	0.11	-1.85	0.17	3.99	3.09	0.48	0.13
2595352	150.114441	54.615074	0.62730	0.56	11.28	0.10	-1.40	0.18	1.33	1.08	0.63	0.15
2601261	144.601303	55.839134	0.72815	0.95	13.63	0.11	-2.42	0.30	4.39	3.64	0.39	0.15
2610846	139.368362	60.014030	0.59309	0.95	13.51	0.11	-1.67	0.21	3.91	3.38	0.52	0.13
2676458	116.106972	57.972610	0.74199	0.60	12.83	0.11	-2.08	0.20	2.95	2.50	0.45	0.13
2681536	109.757332	62.057259	0.46808	1.07	10.81	0.10	-1.20	0.18	1.03	0.91	0.69	0.15
2696951	116.017410	48.530384	0.50375	1.40	13.18	0.11	-1.76	0.17	3.33	2.50	0.50	0.13
2731333	109.020561	55.220936	0.58541	1.02	13.43	0.11	-1.55	0.20	3.74	3.07	0.54	0.12
2737869	104.399849	53.253281	0.60777	1.01	13.17	0.11	-2.02	0.19	3.43	2.75	0.46	0.13
2745643	99.406906	51.209671	0.58869	0.90	11.58	0.10	-1.55	0.18	1.60	1.24	0.54	0.12
2773160	98.244072	47.818634	0.66370	0.74	13.52	0.11	-1.79	0.30	3.95	2.93	0.50	0.13
2792534	94.736938	45.978855	0.63175	0.83	13.71	0.11	-1.76	0.30	4.21	3.03	0.50	0.13
2810184	92.107552	47.690170	0.54223	1.04	13.50	0.11	-1.54	0.20	3.83	2.83	0.54	0.12
2830505	87.386009	40.600391	0.44290	1.19	11.60	0.10	-1.25	0.20	1.50	0.98	0.67	0.15
2909040	82.194786	35.472050	0.64085	0.80	13.75	0.11	-1.77	0.30	4.34	2.52	0.50	0.13
2927295	82.564491	30.261391	0.62532	0.41	13.07	0.11	-1.11	0.30	2.81	1.41	0.71	0.16
2927471	81.760750	30.193151	0.54555	0.87	12.96	0.11	-1.50	0.19	2.87	1.44	0.54	0.12
2930718	88.979736	29.373362	0.57912	0.73	12.20	0.10	-1.25	0.19	1.93	0.95	0.67	0.15
3022099	95.649307	22.499697	0.47653	0.81	10.19	0.10	-0.95	0.18	0.69	0.26	0.75	0.14
3030972	84.343826	25.413269	0.60268	1.16	12.42	0.11	-1.88	0.17	2.31	0.99	0.48	0.13
3078092	88.215256	16.975725	0.46661	1.13	9.65	0.09	-1.36	0.16	0.53	0.15	0.64	0.15

Table B.1 (cont'd)

NSVS ID	b (o)	l (o)	P (days)	A_V	m_V	σ_{mv}	[Fe/H]	σ_{feh}	D (kpc)	Z (kpc)	M_V	σ_{M_V}
3087037	92.023705	16.662127	0.53492	0.88	12.79	0.11	-1.08	0.19	2.33	0.67	0.72	0.15
3117503	97.535233	22.097095	0.59208	1.29	11.13	0.10	-2.02	0.16	1.28	0.48	0.46	0.13
3306144	102.263000	13.622746	0.46787	1.05	12.21	0.10	-0.71	0.19	0.90	0.21	0.82	0.14
3611791	107.782158	-19.511787	0.42161	1.05	12.96	0.11	-0.44	0.19	2.13	-0.71	0.89	0.13
3619355	109.760773	-18.087639	0.61692	0.51	10.54	0.10	-1.31	0.18	0.79	-0.25	0.66	0.15
3633663	112.435997	-20.305910	0.60310	1.14	13.30	0.11	-2.37	0.18	3.27	-1.14	0.40	0.14
3713191	119.661713	-15.607533	0.56730	1.01	12.84	0.11	-1.82	0.17	2.52	-0.68	0.49	0.13
3817372	128.450562	-23.642292	0.72277	1.04	10.68	0.10	-2.20	0.17	1.05	-0.42	0.43	0.14
3939459	136.406784	-10.792614	0.55287	1.29	12.50	0.11	-1.38	0.22	1.74	-0.33	0.64	0.16
3962805	135.312439	-19.124443	0.50686	0.73	12.76	0.11	-0.68	0.21	2.24	-0.73	0.83	0.14
3963833	134.931351	-17.615925	0.48475	1.03	12.17	0.10	-0.87	0.18	1.72	-0.52	0.77	0.14
3964415	135.244156	-18.027645	0.77891	0.81	12.67	0.11	-2.89	0.18	2.68	-0.83	0.31	0.16
3994860	142.429092	-18.247480	0.60688	1.27	13.53	0.11	-2.54	0.20	4.00	-1.25	0.37	0.15
4160839	152.458633	-13.581089	0.54607	1.21	13.24	0.11	-1.92	0.19	2.81	-0.66	0.47	0.13
4180591	152.491104	-7.688322	0.39083	0.69	13.14	0.11	0.12	0.30	1.29	-0.17	1.04	0.14
4241455	152.812195	-3.418465	0.48925	1.19	12.44	0.11	-1.38	0.18	0.51	-0.03	0.64	0.15
4275987	154.928665	-2.273593	0.42555	0.78	10.29	0.10	-0.20	0.19	0.11	-0.00	0.96	0.13
4493602	161.451477	13.870193	0.57979	0.84	13.55	0.11	-1.48	0.30	2.74	0.66	0.61	0.17
4661441	170.079605	22.961758	0.46841	1.27	13.35	0.11	-1.53	0.19	3.18	1.24	0.54	0.12
4694845	176.788269	20.914639	0.39167	1.34	11.90	0.10	-0.72	0.16	1.50	0.53	0.82	0.14
4700160	174.505875	22.598122	0.61773	0.55	12.82	0.11	-1.34	0.20	2.44	0.94	0.65	0.15
4720404	176.143600	27.540829	0.48187	1.06	12.01	0.10	-0.23	0.21	1.52	0.70	0.95	0.13

Table B.1 (cont'd)

NSVS ID	b (o)	l (o)	P (days)	A_V	m_V	σ_{mv}	[Fe/H]	σ_{feh}	D (kpc)	Z (kpc)	M_V	σ_{M_V}
4760770	174.197235	30.435844	0.50044	0.80	13.35	0.11	[-2.47]	0.15	3.59	1.82	0.38	0.14
4762874	170.842682	31.718681	0.57539	0.99	13.24	0.11	-1.88	0.20	3.36	1.77	0.48	0.13
4820869	184.362503	38.118195	0.62532	0.64	13.54	0.11	-1.44	0.30	3.67	2.27	0.62	0.17
4828496	176.069916	41.650879	0.59743	0.70	9.81	0.09	-1.47	0.17	0.67	0.45	0.61	0.16
4837927	181.122620	45.064396	0.57877	0.84	13.71	0.11	-1.47	0.30	4.06	2.88	0.61	0.17
4838954	179.033417	45.607529	0.56211	1.01	12.93	0.11	-1.39	0.19	2.80	2.00	0.63	0.16
4876765	167.964615	47.779037	0.58913	0.88	13.20	0.11	-1.53	0.20	3.34	2.47	0.54	0.12
4930109	162.389313	54.773869	0.64632	1.27	13.76	0.11	-2.13	0.19	4.51	3.68	0.44	0.14
4959080	172.890594	60.983814	0.63568	0.54	12.77	0.11	-1.36	0.30	2.61	2.29	0.64	0.17
4979454	156.119095	70.153717	0.63432	0.55	13.63	0.11	-1.37	0.30	3.87	3.64	0.64	0.17
4990594	155.697891	66.273888	0.53479	0.94	13.17	0.11	-1.58	0.18	3.24	2.96	0.53	0.12
4993764	147.376343	64.868042	0.55905	1.30	13.64	0.11	-1.87	0.17	4.19	3.79	0.48	0.13
4996441	145.702988	66.249275	0.68114	1.12	13.40	0.11	-2.22	0.19	3.81	3.49	0.42	0.14
4998847	145.490799	68.312584	0.50102	1.27	13.47	0.11	-1.51	0.17	3.75	3.48	0.54	0.12
5007979	141.041428	67.861374	0.59957	0.47	10.81	0.10	-0.88	0.20	0.98	0.91	0.77	0.14
5013760	133.134689	68.872162	0.56364	0.93	12.29	0.11	-1.56	0.17	2.21	2.06	0.54	0.12
5028197	139.545792	75.935432	0.69780	1.03	12.08	0.10	-2.10	0.17	2.05	1.99	0.44	0.13
5034190	123.991730	73.351288	0.65387	1.05	11.88	0.10	-1.97	0.20	1.87	1.79	0.47	0.13
5039296	112.749207	76.519165	0.58410	0.70	13.61	0.11	-1.30	0.30	3.78	3.67	0.66	0.16
5039914	109.804016	78.487114	0.68511	0.92	13.61	0.11	-2.18	0.30	4.23	4.15	0.43	0.14
5047909	126.561394	69.433197	0.56249	0.94	12.97	0.11	-1.46	0.19	2.90	2.72	0.62	0.16
5058465	111.644386	68.505112	0.62484	0.89	13.58	0.11	-1.81	0.20	4.08	3.80	0.49	0.13

Table B.1 (cont'd)

NSVS ID	b (o)	l (o)	P (days)	A_V	m_V	σ_{mv}	[Fe/H]	σ_{feh}	D (kpc)	Z (kpc)	M_V	σ_{M_V}
5089958	83.843803	72.625092	0.47858	1.11	11.89	0.10	-1.41	0.21	1.77	1.68	0.63	0.16
5090118	87.091698	71.524384	0.54002	0.88	12.61	0.11	-1.55	0.18	2.57	2.44	0.54	0.12
5113606	91.891922	64.355080	0.61578	1.21	13.34	0.11	-2.02	0.18	3.70	3.34	0.46	0.13
5120617	90.503235	60.089027	0.57065	0.93	13.27	0.11	-1.51	0.18	3.46	3.00	0.54	0.12
5133135	87.727821	58.726974	0.61176	1.20	12.80	0.11	-1.83	0.17	2.78	2.37	0.49	0.13
5144530	68.742462	65.516197	0.58142	0.79	13.20	0.11	-1.29	0.20	3.16	2.88	0.66	0.15
5149126	71.052254	62.851234	0.53227	1.06	11.25	0.10	-1.53	0.16	1.36	1.21	0.54	0.12
5152352	68.847542	61.501141	0.35303	0.83	12.64	0.11	[0.26]	0.30	2.01	1.77	1.08	0.15
5181224	77.042839	55.235344	0.45866	0.51	11.20	0.10	[-1.15]	0.17	1.21	0.99	0.70	0.15
5206471	81.566521	47.898304	0.57175	0.72	13.74	0.11	-1.25	0.30	4.03	2.99	0.67	0.16
5207932	74.104401	48.200279	0.46999	1.28	11.23	0.10	-1.39	0.30	1.29	0.96	0.63	0.17
5216041	79.346565	44.541546	0.60232	0.75	13.48	0.11	-1.47	0.30	3.60	2.53	0.61	0.17
5222075	70.892441	51.129478	0.49406	0.62	12.74	0.11	-0.61	0.30	2.33	1.82	0.85	0.15
5222117	64.344200	51.265274	0.71077	0.44	13.63	0.11	-1.60	0.30	4.09	3.19	0.53	0.13
5232275	65.965652	47.342838	0.60900	0.98	13.72	0.11	-1.85	0.30	4.37	3.21	0.49	0.13
5248399	65.145058	41.647087	0.63033	1.17	12.86	0.11	-2.03	0.17	3.00	1.99	0.46	0.13
5249019	64.494392	41.455597	0.64944	1.23	12.76	0.11	-2.18	0.18	2.89	1.91	0.43	0.14
5249836	70.850655	40.974854	0.62118	1.32	13.40	0.11	-1.98	0.19	3.80	2.49	0.46	0.13
5250334	63.538296	41.018147	0.65355	0.99	13.30	0.11	-2.07	0.21	3.66	2.40	0.45	0.13
5259122	65.930565	38.306431	0.68229	0.54	13.21	0.11	-1.60	0.30	3.28	2.04	0.53	0.13
5270815	75.498230	42.774719	0.60970	0.68	11.93	0.10	-1.28	0.18	1.74	1.18	0.67	0.15
5288795	74.170441	37.237675	0.64109	0.91	13.73	0.11	-2.12	0.20	4.40	2.66	0.44	0.14

Table B.1 (cont'd)

NSVS ID	b (o)	l (o)	P (days)	A_V	m_V	σ_{mv}	[Fe/H]	σ_{feh}	D (kpc)	Z (kpc)	M_V	σ_{M_V}
5300614	74.170441	37.237675	0.64113	0.89	13.72	0.11	-1.89	0.30	4.31	2.61	0.48	0.14
5301154	74.259125	37.064682	0.62249	0.66	13.47	0.11	-1.46	0.30	3.59	2.17	0.62	0.17
5316660	78.855331	32.978035	0.43756	1.23	12.99	0.11	-1.07	0.30	2.75	1.50	0.72	0.16
5401722	79.579475	28.792011	0.55549	0.92	12.78	0.11	-1.44	0.30	2.53	1.22	0.62	0.17
5406476	81.317093	27.876089	0.63414	1.08	13.28	0.11	-2.02	0.21	3.50	1.64	0.46	0.13
5415960	80.136375	25.800640	0.63381	0.64	12.61	0.11	-1.49	0.30	2.40	1.04	0.61	0.17
5484202	66.633545	20.250051	0.60141	0.87	13.70	0.11	-1.64	0.30	4.03	1.39	0.52	0.13
5494745	69.935562	19.374836	0.54550	0.98	13.32	0.11	-1.46	0.18	3.17	1.05	0.62	0.16
5525580	69.867004	13.552402	0.68203	0.71	12.32	0.11	-1.84	0.20	1.80	0.42	0.49	0.13
5526812	73.459137	14.693528	0.52738	1.02	12.62	0.11	-1.72	0.17	2.27	0.58	0.51	0.12
5568043	80.230148	19.053677	0.68722	1.19	12.80	0.11	-2.23	0.19	2.79	0.91	0.42	0.14
5568339	78.904366	18.564575	0.61321	0.63	11.77	0.10	-1.20	0.19	1.52	0.48	0.68	0.15
5587647	78.362907	14.914193	0.54859	0.89	13.42	0.11	-1.36	0.30	3.26	0.84	0.64	0.17
5654619	83.439484	9.840778	0.36000	1.41	13.25	0.11	-0.65	0.30	2.18	0.37	0.83	0.15
5666134	86.614098	9.732788	0.56551	1.00	13.32	0.11	-1.62	0.30	2.76	0.47	0.52	0.13
6094124	93.952812	-14.549849	0.62005	1.19	12.51	0.11	-1.97	0.17	2.13	-0.54	0.46	0.13
6231458	105.111320	-24.910885	0.63045	0.79	11.88	0.10	-1.65	0.18	1.63	-0.69	0.52	0.12
6248007	108.624695	-27.829504	0.53394	1.40	13.11	0.11	-1.76	0.18	3.05	-1.42	0.50	0.13
6264114	103.072250	-30.513044	0.69604	0.47	12.35	0.11	-1.57	0.30	1.90	-0.97	0.53	0.13
6302329	115.725418	-33.082695	0.44230	0.86	9.63	0.09	-0.40	0.18	0.52	-0.28	0.90	0.13
6392775	122.421448	-35.847809	0.55453	0.96	13.09	0.11	-1.59	0.17	3.04	-1.78	0.53	0.12
6429831	126.166321	-28.567034	0.56308	1.10	12.43	0.11	-1.42	0.20	2.17	-1.04	0.63	0.16

Table B.1 (cont'd)

NSVS ID	b (o)	l (o)	P (days)	A_V	m_V	σ_{mv}	[Fe/H]	σ_{feh}	D (kpc)	Z (kpc)	M_V	σ_{M_V}
6480339	137.884659	-27.234627	0.44724	0.93	12.35	0.11	[-1.01]	0.18	1.95	-0.89	0.74	0.14
6705217	161.942429	-16.034155	0.39873	1.26	12.85	0.11	-0.63	0.19	1.75	-0.48	0.84	0.14
6808365	167.760147	-9.579369	0.51574	0.73	13.73	0.11	-0.91	0.30	1.20	-0.20	0.77	0.15
6860143	171.853638	-3.173854	0.45609	0.90	11.62	0.10	-0.59	0.18	0.64	-0.04	0.85	0.13
6885646	179.449127	-12.541998	0.60455	0.55	13.59	0.11	-1.19	0.30	2.15	-0.47	0.69	0.16
6899769	175.757568	-6.806630	0.53951	1.19	13.13	0.11	-1.58	0.20	1.17	-0.14	0.53	0.12
7058441	180.090164	9.818390	0.52769	0.49	13.14	0.11	-0.63	0.30	1.77	0.30	0.84	0.15
7231539	187.447449	19.520897	0.39730	1.16	11.35	0.10	-0.58	0.17	1.13	0.38	0.85	0.13
7235546	183.023575	21.730616	0.57929	1.13	12.41	0.11	-1.61	0.17	2.20	0.81	0.53	0.12
7267812	194.978058	16.125113	0.52311	0.72	12.78	0.11	-0.68	0.21	2.18	0.61	0.83	0.14
7394810	197.886780	31.228720	0.61754	1.04	12.55	0.11	-1.91	0.17	2.38	1.23	0.47	0.13
7404883	196.663483	34.864422	0.50203	1.09	12.48	0.11	-1.56	0.20	2.29	1.31	0.53	0.12
7411607	200.071762	36.715725	0.51017	1.28	13.42	0.11	-1.60	0.18	3.57	2.13	0.53	0.12
7412670	202.303360	36.571804	0.54577	0.98	12.32	0.11	-1.31	0.18	2.06	1.23	0.66	0.15
7454552	190.923523	44.421623	0.52170	1.12	13.68	0.11	-1.51	0.30	4.15	2.90	0.54	0.13
7458704	186.696869	46.245834	0.52615	1.23	13.54	0.11	-1.87	0.18	4.01	2.90	0.48	0.13
7472262	197.494919	43.532116	0.54722	1.08	11.84	0.10	-1.91	0.17	1.81	1.25	0.47	0.13
7484923	198.252838	48.837215	0.59070	0.84	12.15	0.10	-1.41	0.18	1.95	1.47	0.63	0.15
7496219	208.429611	53.103607	0.45240	1.36	10.74	0.10	-1.37	0.16	0.99	0.79	0.64	0.15
7496252	204.561249	53.720707	0.46137	1.40	13.71	0.11	-1.32	0.19	3.91	3.15	0.65	0.15
7512212	195.169235	53.612408	0.55719	1.15	13.28	0.11	-1.48	0.18	3.33	2.68	0.61	0.16
7517103	193.625122	56.022221	0.52442	1.20	12.68	0.11	-1.57	0.19	2.63	2.18	0.53	0.12

Table B.1 (cont'd)

NSVS ID	b (◦)	l (◦)	P (days)	A_V	m_V	σ_{mv}	[Fe/H]	σ_{feh}	D (kpc)	Z (kpc)	M_V	σ_{M_V}
7539425	210.052475	56.666897	0.67471	0.67	13.76	0.11	-1.76	0.30	4.37	3.65	0.50	0.13
7540718	201.300217	57.839439	0.54391	1.12	11.73	0.10	-1.49	0.17	1.61	1.37	0.61	0.16
7554734	201.241287	65.467804	0.79260	0.71	13.55	0.11	-2.37	0.30	4.13	3.76	0.40	0.15
7564332	209.431458	70.512421	0.65340	0.77	11.84	0.10	-1.51	0.19	1.77	1.67	0.54	0.12
7585321	198.788483	71.868042	0.55770	0.96	9.79	0.09	-1.66	0.17	0.69	0.66	0.52	0.12
7614129	208.674561	80.848961	0.46914	1.22	13.46	0.11	-1.26	0.18	3.51	3.46	0.67	0.15
7635590	154.019775	81.090378	0.55861	1.25	12.56	0.11	-1.83	0.16	2.53	2.50	0.49	0.13
7643254	139.957657	79.403259	0.66857	0.92	12.50	0.11	-3.49	0.16	2.80	2.76	0.21	0.17
7649368	116.036880	84.846474	0.51345	1.13	13.62	0.11	-1.43	0.19	3.88	3.86	0.62	0.16
7654631	213.232635	85.841438	0.58658	1.22	11.65	0.10	-1.86	0.16	1.66	1.66	0.48	0.13
7656719	250.768951	86.400177	0.62839	0.44	13.01	0.11	-1.18	0.30	2.85	2.85	0.69	0.16
7666038	343.600281	86.224228	0.66141	1.19	13.52	0.11	-2.29	0.19	4.07	4.06	0.41	0.14
7685674	69.184624	84.377281	0.73739	0.57	13.26	0.11	-1.92	0.30	3.55	3.53	0.47	0.14
7703549	61.611431	77.146461	0.56741	1.01	11.57	0.10	-1.75	0.17	1.60	1.56	0.50	0.13
7706106	76.694511	73.703049	0.54966	1.15	12.94	0.11	-1.89	0.17	3.05	2.93	0.48	0.13
7709213	53.968124	74.508835	0.57325	1.14	11.97	0.10	-1.74	0.17	1.92	1.85	0.50	0.13
7711863	71.811691	70.957581	0.55175	0.79	10.48	0.10	-0.53	0.20	0.83	0.78	0.87	0.14
7726595	28.437370	73.040855	0.55340	1.11	13.05	0.11	-1.67	0.18	3.13	2.99	0.52	0.12
7741095	34.333637	65.824348	0.59117	1.20	13.56	0.11	-2.19	0.19	4.04	3.68	0.43	0.14
7742142	41.927856	65.499634	0.52282	1.05	12.52	0.11	-1.44	0.18	2.34	2.13	0.62	0.16
7752384	62.517723	67.745918	0.51355	1.13	12.46	0.11	-1.59	0.16	2.38	2.21	0.53	0.12
7753756	57.688957	67.637062	0.63956	0.54	13.62	0.11	-1.38	0.30	3.87	3.58	0.64	0.17

Table B.1 (cont'd)

NSVS ID	b (o)	l (o)	P (days)	A_V	m_V	σ_{mv}	[Fe/H]	σ_{feh}	D (kpc)	Z (kpc)	M_V	σ_{M_V}
7755406	50.853001	67.347778	0.37732	1.17	10.36	0.10	-0.51	0.17	0.77	0.71	0.87	0.13
7756950	58.598736	65.971527	0.56433	1.05	13.35	0.11	-1.59	0.19	3.62	3.31	0.53	0.12
7777447	55.365101	59.262951	0.55602	1.35	13.56	0.11	-1.92	0.20	4.04	3.47	0.47	0.13
7783855	33.949596	63.302654	0.66172	1.00	13.21	0.11	-2.38	0.18	3.48	3.11	0.40	0.14
7785359	44.874748	63.508179	0.58140	0.71	11.84	0.10	-1.28	0.18	1.67	1.49	0.66	0.15
7799920	41.337208	56.512096	0.58461	1.11	11.85	0.10	-1.96	0.16	1.78	1.49	0.47	0.13
7818285	56.496567	58.012764	0.45693	1.33	12.29	0.11	-1.44	0.16	2.10	1.78	0.62	0.15
7823144	54.721565	55.969658	0.59521	1.26	13.20	0.11	-1.94	0.18	3.39	2.81	0.47	0.13
7824713	57.392769	55.212971	0.62230	0.89	10.92	0.10	-1.57	0.18	1.16	0.95	0.53	0.12
7826584	53.099026	54.611710	0.71633	0.62	12.63	0.11	-1.96	0.19	2.59	2.11	0.47	0.13
7861269	47.369778	51.443443	0.44863	1.18	13.47	0.11	-1.06	0.21	3.39	2.65	0.72	0.15
7866619	46.279003	49.111233	0.66541	0.98	12.30	0.11	-2.06	0.17	2.20	1.66	0.45	0.13
7871803	46.024120	47.108486	0.92916	1.04	12.74	0.11	-2.99	0.20	2.92	2.14	0.29	0.16
7872648	41.692986	46.069134	0.47574	1.63	13.74	0.11	-2.03	0.18	4.15	2.99	0.46	0.13
7912479	56.618286	43.652096	0.73085	0.95	13.65	0.11	-2.43	0.30	4.36	3.01	0.39	0.15
7919183	60.699646	41.713551	0.52429	1.13	12.63	0.11	-1.83	0.17	2.62	1.74	0.49	0.13
7927997	58.002182	38.988625	0.62386	1.03	12.56	0.11	-1.85	0.17	2.51	1.58	0.49	0.13
7954067	59.582512	34.583504	0.44033	1.36	11.48	0.10	-1.32	0.16	1.40	0.79	0.65	0.15
7962127	61.652435	32.743069	0.45396	1.23	13.32	0.11	-1.19	0.30	3.11	1.68	0.69	0.16
7970685	51.990425	36.666519	0.47276	1.12	13.28	0.11	-1.23	0.20	3.16	1.89	0.68	0.15
7990146	49.175571	30.684275	0.52975	1.08	12.88	0.11	-1.69	0.18	2.78	1.42	0.51	0.12
7998286	51.222157	29.307898	0.46873	0.90	12.91	0.11	-0.83	0.30	2.44	1.19	0.79	0.15

Table B.1 (cont'd)

NSVS ID	b (o)	l (o)	P (days)	A_V	m_V	σ_{mv}	[Fe/H]	σ_{feh}	D (kpc)	Z (kpc)	M_V	σ_{M_V}
8023769	55.873215	24.800865	0.39961	1.29	11.30	0.10	-0.69	0.17	1.17	0.49	0.82	0.13
8050089	61.316631	29.029814	0.64929	0.60	12.49	0.11	-1.34	0.21	2.24	1.09	0.65	0.16
8108614	60.588310	19.978815	0.57711	0.98	11.73	0.10	-1.53	0.17	1.57	0.54	0.54	0.12
8125354	48.721760	20.783705	0.58338	0.80	12.73	0.11	-1.22	0.22	2.20	0.78	0.68	0.15
8160195	53.552132	16.038237	0.57784	0.33	11.58	0.10	-0.73	0.30	1.21	0.33	0.81	0.15
8179854	57.768764	14.369309	0.49744	1.42	13.61	0.11	-1.57	0.20	3.25	0.81	0.53	0.12
8192311	58.986023	12.718218	0.61670	1.22	12.80	0.11	-2.23	0.30	2.28	0.50	0.42	0.14
8234127	62.106895	15.811408	0.51126	1.29	11.64	0.10	-1.94	0.16	1.49	0.41	0.47	0.13
8293251	66.670349	10.678833	0.70296	0.80	13.11	0.11	-2.09	0.30	2.82	0.52	0.45	0.14
8360536	58.625973	3.405887	0.59420	1.23	10.56	0.10	-2.13	0.30	0.18	0.01	0.44	0.14
8572436	68.354561	-9.556754	0.43702	1.08	13.48	0.11	-0.99	0.19	2.59	-0.43	0.74	0.14
8651514	74.546310	-9.629459	0.56070	0.84	11.05	0.10	-1.38	0.18	0.82	-0.14	0.64	0.15
8702062	79.457603	-12.411995	0.41987	1.10	11.53	0.10	-0.57	0.17	1.05	-0.23	0.86	0.13
8706200	79.825867	-12.978333	0.70897	0.78	12.68	0.11	-1.77	0.20	2.17	-0.49	0.50	0.13
8724691	83.727173	-13.120159	0.60410	0.91	13.30	0.11	-1.87	0.20	2.74	-0.62	0.48	0.13
8770585	77.491814	-18.898638	0.55678	0.60	11.69	0.10	-0.83	0.19	1.27	-0.41	0.79	0.14
8776606	77.177155	-20.759872	0.46714	0.90	11.10	0.10	-0.64	0.20	1.01	-0.36	0.84	0.14
8782730	79.629944	-19.965631	0.57208	1.33	13.64	0.11	-2.14	0.30	3.88	-1.33	0.44	0.14
8783505	78.116264	-21.682127	0.56454	1.06	13.19	0.11	-1.83	0.18	3.15	-1.16	0.49	0.13
8817268	84.511093	-24.080667	0.36487	1.31	12.76	0.11	-0.30	0.20	2.01	-0.82	0.93	0.13
8877855	91.849289	-19.024340	0.50345	0.98	13.39	0.11	-1.18	0.30	2.89	-0.94	0.69	0.16
8903282	90.523750	-23.873528	0.53871	0.86	12.16	0.10	-1.86	0.17	1.92	-0.78	0.48	0.13

Table B.1 (cont'd)

NSVS ID	b (o)	l (o)	P (days)	A_V	m_V	σ_{mv}	[Fe/H]	σ_{feh}	D (kpc)	Z (kpc)	M_V	σ_{M_V}
8909217	95.324371	-18.136198	0.46099	0.88	12.74	0.11	-0.77	0.20	1.91	-0.60	0.80	0.14
8951389	89.733879	-27.931662	0.48983	1.14	13.11	0.11	-1.09	0.18	2.80	-1.31	0.72	0.15
8956174	89.474472	-30.449482	0.49582	1.35	12.81	0.11	-1.69	0.17	2.59	-1.31	0.51	0.12
9047405	100.643166	-41.629425	0.52955	0.80	12.58	0.11	-1.12	0.21	2.12	-1.41	0.71	0.15
9050491	101.787338	-42.563652	0.58880	1.23	13.37	0.11	-1.87	0.19	3.40	-2.30	0.48	0.13
9063964	96.136230	-45.121769	0.69417	1.39	13.19	0.11	-2.16	0.21	3.21	-2.28	0.43	0.14
9075932	101.620857	-49.676079	0.56240	1.00	12.01	0.10	-1.51	0.17	1.75	-1.33	0.54	0.12
9088465	109.372108	-52.095524	0.70114	0.93	11.98	0.10	-2.02	0.18	1.24	-0.98	0.46	0.13
9091170	112.610077	-48.547623	0.53139	1.25	13.51	0.11	-1.76	0.30	3.56	-2.67	0.50	0.13
9130768	121.044991	-43.898682	0.54990	1.25	13.33	0.11	-1.60	0.21	3.38	-2.35	0.53	0.12
9154382	125.585434	-55.058842	0.73408	0.80	12.45	0.11	-1.92	0.20	2.21	-1.82	0.47	0.13
9230082	150.693558	-51.478401	0.57622	1.15	13.74	0.11	-1.91	0.30	3.95	-3.09	0.48	0.14
9240847	156.466888	-47.751308	0.46285	0.87	12.86	0.11	-0.74	0.30	2.28	-1.69	0.81	0.15
9254455	147.069778	-38.657055	0.57995	0.87	13.46	0.11	-1.45	0.21	2.72	-1.70	0.62	0.16
9310411	169.083160	-39.838348	0.65130	0.88	9.44	0.09	-2.08	0.17	0.46	-0.30	0.45	0.13
9338383	165.933823	-31.350447	0.45529	1.30	13.00	0.11	-1.40	0.16	2.47	-1.29	0.63	0.15
9671363	200.171249	-8.156617	0.68812	0.42	11.82	0.10	-1.46	0.30	0.76	-0.11	0.62	0.17
9995853	201.842438	22.087044	0.50114	1.27	11.73	0.10	-1.67	0.16	1.64	0.61	0.52	0.12
10083412	202.429688	24.708126	0.60342	0.70	12.71	0.11	-1.40	0.30	2.47	1.03	0.63	0.17
10141482	212.093353	28.380684	0.56347	0.85	11.28	0.10	-1.43	0.19	1.23	0.59	0.62	0.16
10147460	219.265503	27.386021	0.58912	0.68	12.93	0.11	-1.30	0.30	2.72	1.25	0.66	0.16
10175326	218.037827	38.099625	0.54852	0.81	11.80	0.10	-1.48	0.17	1.67	1.03	0.61	0.16

Table B.1 (cont'd)

NSVS ID	b (o)	l (o)	P (days)	A_V	m_V	σ_{mv}	[Fe/H]	σ_{feh}	D (kpc)	Z (kpc)	M_V	σ_{M_V}
10203057	211.728241	42.085018	0.59374	1.16	13.33	0.11	-1.84	0.18	3.52	2.36	0.49	0.13
10228104	226.041321	38.446800	0.60271	0.84	12.58	0.11	-1.31	0.20	2.23	1.39	0.66	0.15
10235938	224.386444	42.669170	0.67384	1.11	13.05	0.11	-2.18	0.18	3.24	2.20	0.43	0.14
10241977	228.926102	43.824474	0.47225	1.44	13.50	0.11	-1.43	0.20	3.56	2.47	0.63	0.16
10329394	232.582748	62.893730	0.59218	0.83	13.22	0.11	-1.54	0.30	3.35	2.98	0.54	0.13
10332182	228.366592	65.588539	0.49966	1.03	13.34	0.11	-1.78	0.18	3.61	3.28	0.50	0.13
10337183	237.586792	66.549026	0.59962	0.76	12.59	0.11	-1.16	0.20	2.30	2.11	0.70	0.15
10338359	234.200394	68.187561	0.62672	1.10	12.40	0.11	-1.97	0.18	2.35	2.18	0.46	0.13
10347356	243.554764	69.877670	0.50248	1.19	13.67	0.11	-1.49	0.30	3.94	3.70	0.61	0.17
10350273	245.540833	71.431038	0.73870	0.56	12.17	0.10	-1.94	0.20	2.05	1.94	0.47	0.13
10352408	230.793777	75.428192	0.54720	0.77	11.70	0.10	-0.86	0.19	1.48	1.43	0.78	0.14
10358221	248.285614	66.299927	0.72682	0.61	12.22	0.10	-1.93	0.19	2.12	1.95	0.47	0.13
10360493	253.440811	66.149864	0.47798	1.31	11.53	0.10	-1.36	0.16	1.41	1.29	0.64	0.15
10360815	254.143265	66.095566	0.59865	1.23	12.32	0.11	-1.85	0.17	2.19	2.00	0.49	0.13
10360975	256.292786	65.288414	0.65052	0.91	13.21	0.11	-1.77	0.20	3.27	2.97	0.50	0.13
10363810	254.461380	68.314301	0.67930	1.07	13.54	0.11	-2.17	0.21	4.01	3.72	0.43	0.14
10371698	270.231659	68.118683	0.53820	1.04	13.47	0.11	-1.31	0.21	3.56	3.31	0.66	0.15
10395081	269.567993	77.239571	0.59841	0.88	13.58	0.11	-1.41	0.20	3.75	3.66	0.63	0.16
10395582	271.055145	77.187874	0.71952	0.80	13.62	0.11	-2.17	0.30	4.22	4.11	0.43	0.14
10403252	282.259674	78.309006	0.43207	1.31	13.52	0.11	-1.39	0.20	3.64	3.56	0.63	0.16
10418706	290.133148	75.563774	0.57442	0.93	13.24	0.11	-1.57	0.30	3.28	3.18	0.53	0.13
10431935	320.200592	75.690735	0.45937	1.03	13.37	0.11	[-0.95]	0.30	3.21	3.11	0.75	0.16

Table B.1 (cont'd)

NSVS ID	b (o)	l (o)	P (days)	A_V	m_V	σ_{mv}	[Fe/H]	σ_{feh}	D (kpc)	Z (kpc)	M_V	σ_{M_V}
10437330	325.013885	70.816566	0.65692	0.82	11.79	0.10	-1.53	0.18	1.70	1.60	0.54	0.12
10446172	342.496826	85.059509	0.46890	1.16	12.43	0.11	-1.29	0.17	2.20	2.20	0.66	0.15
10451724	347.880005	81.244812	0.59893	0.82	11.32	0.10	-1.37	0.18	1.32	1.30	0.64	0.15
10453784	338.640839	77.406013	0.58412	1.19	13.00	0.11	-2.09	0.17	3.14	3.07	0.45	0.13
10464169	11.305488	78.703545	0.55434	1.17	13.74	0.11	-1.71	0.19	4.33	4.24	0.51	0.13
10488920	354.261444	68.809067	0.65088	0.82	10.96	0.10	-1.84	0.19	1.18	1.10	0.49	0.13
10491545	355.218292	67.330376	0.45479	1.35	13.58	0.11	-1.99	0.18	4.05	3.74	0.46	0.13
10492034	359.422760	68.417549	0.53625	0.86	13.51	0.11	-1.24	0.30	3.59	3.34	0.68	0.16
10514624	17.403614	69.401497	0.60906	1.19	12.68	0.11	-1.90	0.18	2.61	2.45	0.48	0.13
10530833	25.991554	64.769646	0.76869	0.58	12.75	0.11	-2.07	0.30	2.79	2.52	0.45	0.14
10531095	17.911552	63.109425	0.56342	1.16	13.10	0.11	-1.78	0.20	3.20	2.85	0.50	0.13
10534194	30.940548	63.866673	0.49262	1.32	13.74	0.11	-1.23	0.22	3.92	3.52	0.68	0.15
10547760	11.289085	62.050667	0.55283	1.09	13.13	0.11	-1.67	0.30	3.25	2.87	0.52	0.13
10549959	6.634994	59.355526	0.75838	0.57	13.55	0.11	-2.02	0.30	3.99	3.43	0.46	0.14
10567739	15.172942	53.650539	0.74830	0.73	13.51	0.11	-2.20	0.30	3.73	3.00	0.43	0.14
10591456	27.551144	56.268166	0.43456	1.37	12.61	0.11	-1.29	0.16	2.33	1.94	0.66	0.15
10614618	27.424004	48.668644	0.63362	0.68	13.48	0.11	-1.55	0.30	3.68	2.76	0.54	0.13
10614900	28.875769	48.956722	0.57358	0.76	13.43	0.11	-1.32	0.30	3.42	2.58	0.65	0.17
10628156	18.450748	48.974583	0.61723	1.24	13.71	0.11	-2.02	0.20	4.20	3.17	0.46	0.13
10642059	20.105104	44.181637	0.51140	1.40	13.04	0.11	-1.62	0.20	2.97	2.07	0.53	0.12
10642884	23.803055	45.231560	0.52207	1.03	10.91	0.10	-0.84	0.18	0.99	0.71	0.78	0.14
10647103	24.462559	43.813869	0.57126	0.93	13.08	0.11	-1.28	0.20	2.86	1.98	0.67	0.15

Table B.1 (cont'd)

NSVS ID	b (o)	l (o)	P (days)	A_V	m_V	σ_{mv}	[Fe/H]	σ_{feh}	D (kpc)	Z (kpc)	M_V	σ_{M_V}
10652318	28.674809	43.357983	0.59715	1.37	12.91	0.11	-2.21	0.18	2.97	2.04	0.42	0.14
10685785	32.769703	42.946533	0.49554	1.28	13.02	0.11	-1.43	0.18	2.78	1.89	0.62	0.16
10706905	35.223679	39.082306	0.45537	1.27	10.68	0.10	-1.40	0.16	0.95	0.60	0.63	0.15
10751419	27.834909	31.737030	0.78759	0.57	12.46	0.11	-2.14	0.30	2.30	1.21	0.44	0.14
10758202	31.325388	31.259958	0.52853	1.01	13.58	0.11	-1.40	0.30	3.46	1.79	0.63	0.17
10767117	34.481865	30.085678	0.35511	1.28	12.58	0.11	-0.38	0.21	1.76	0.88	0.91	0.13
10769204	36.026585	30.090502	0.53961	1.01	13.69	0.11	-1.47	0.30	3.35	1.68	0.61	0.17
10773700	33.545578	28.062008	0.51303	0.83	13.19	0.11	-1.04	0.30	2.62	1.23	0.73	0.16
10781555	32.519276	25.715815	0.55716	1.00	12.21	0.10	-1.73	0.17	1.70	0.74	0.51	0.12
10782844	31.068771	24.823805	0.63831	0.97	12.70	0.11	-1.76	0.19	2.36	0.99	0.50	0.13
10806470	42.306427	32.408207	0.61309	1.25	13.13	0.11	-2.26	0.30	3.12	1.67	0.41	0.14
10824625	45.120922	28.967657	0.55623	1.18	13.64	0.11	-1.83	0.30	3.94	1.91	0.49	0.13
10824661	40.006824	27.389360	0.43605	1.50	12.91	0.11	-1.23	0.17	2.53	1.16	0.68	0.15
10869885	42.161316	20.701864	0.43559	0.88	13.05	0.11	-0.54	0.30	2.44	0.86	0.86	0.15
10885456	37.190937	24.359634	0.37852	1.15	12.66	0.11	-0.45	0.30	1.92	0.79	0.89	0.15
10887396	32.521351	21.771381	0.58568	0.89	13.04	0.11	-1.58	0.30	2.49	0.92	0.53	0.13
10891107	33.036320	21.168482	0.44961	1.18	13.73	0.11	-1.08	0.30	3.13	1.13	0.72	0.16
10905292	35.113121	19.248146	0.53772	1.24	13.16	0.11	-1.79	0.30	2.60	0.86	0.50	0.13
10955591	39.167610	11.970716	0.43591	0.58	11.42	0.10	-0.58	0.18	0.94	0.19	0.85	0.13
10994614	44.150360	16.547720	0.52234	1.15	12.95	0.11	-1.72	0.18	2.57	0.73	0.51	0.13
11015121	48.059158	14.635036	0.59966	0.77	12.97	0.11	-1.50	0.30	2.25	0.57	0.61	0.17
11061928	53.036594	11.636043	0.53723	1.15	12.94	0.11	-1.65	0.30	2.33	0.47	0.52	0.13

Table B.1 (cont'd)

NSVS ID	b (o)	l (o)	P (days)	A_V	m_V	σ_{mv}	[Fe/H]	σ_{feh}	D (kpc)	Z (kpc)	M_V	σ_{M_V}
11327182	50.852222	-7.636373	0.48074	1.01	13.51	0.11	-1.07	0.30	2.57	-0.34	0.72	0.16
11379204	54.212822	-14.954093	0.44278	1.14	12.26	0.11	[-1.12]	0.17	1.67	-0.43	0.71	0.15
11420828	58.240215	-10.052041	0.61643	0.57	12.39	0.11	-1.29	0.30	1.72	-0.30	0.66	0.16
11491796	67.599960	-13.922969	0.43408	0.98	12.36	0.11	-0.50	0.19	1.69	-0.41	0.88	0.13
11527986	59.708134	-16.845942	0.47619	1.14	13.48	0.11	-1.25	0.21	3.18	-0.92	0.67	0.15
11533492	58.469673	-18.844734	0.47260	0.79	9.86	0.10	-0.57	0.19	0.52	-0.17	0.86	0.13
11622871	68.838654	-21.424620	0.56235	0.68	11.85	0.10	-1.13	0.30	1.47	-0.54	0.70	0.16
11643237	69.906799	-22.600559	0.54724	0.97	12.93	0.11	-1.46	0.30	2.60	-1.00	0.62	0.17
11647104	70.568718	-23.083731	0.85273	0.82	13.12	0.11	-2.78	0.30	3.20	-1.26	0.33	0.16
11656645	72.979012	-23.521858	0.57584	0.51	11.94	0.10	[-1.21]	0.18	1.47	-0.59	0.68	0.15
11668678	76.493279	-23.680206	0.56287	1.00	13.56	0.11	-1.60	0.30	3.42	-1.37	0.53	0.13
11670319	75.939964	-24.722748	0.64808	1.24	12.59	0.11	-2.23	0.18	2.35	-0.98	0.42	0.14
11672831	77.443382	-24.053720	0.39039	1.05	10.42	0.10	-0.27	0.17	0.71	-0.29	0.94	0.13
11677349	72.799309	-29.791384	0.56021	0.80	12.79	0.11	-1.29	0.30	2.38	-1.18	0.66	0.16
11747453	75.047089	-30.073528	0.62105	1.08	13.55	0.11	-2.07	0.30	3.84	-1.93	0.45	0.14
11753751	78.627480	-28.867075	0.43481	1.31	13.54	0.11	-1.18	0.18	3.41	-1.65	0.69	0.15
11757688	78.421295	-30.413668	0.48839	1.23	11.83	0.10	-1.64	0.16	1.71	-0.87	0.52	0.12
11762920	82.233391	-28.387510	0.56953	0.96	13.29	0.11	-1.59	0.30	3.32	-1.58	0.53	0.13
11770209	82.304024	-30.970781	0.64254	0.90	13.30	0.11	-1.92	0.30	3.39	-1.74	0.47	0.14
11772445	80.245827	-33.867294	0.49672	1.60	12.64	0.11	-1.58	0.17	2.41	-1.34	0.53	0.12
11798849	86.286514	-35.274506	0.55999	0.98	13.69	0.11	-1.56	0.30	3.95	-2.28	0.54	0.13
11803133	85.614380	-38.356049	0.64099	0.68	10.35	0.10	-1.42	0.18	0.78	-0.48	0.63	0.16

Table B.1 (cont'd)

NSVS ID	b (o)	l (o)	P (days)	A_V	m_V	σ_{mv}	[Fe/H]	σ_{feh}	D (kpc)	Z (kpc)	M_V	σ_{M_V}
11828256	80.244354	-44.102306	0.49326	1.52	13.40	0.11	-1.91	0.30	3.48	-2.43	0.48	0.14
11840237	89.125107	-42.349823	0.60103	1.42	13.72	0.11	-2.43	0.30	4.17	-2.81	0.39	0.15
11864349	93.098686	-37.302723	0.69023	0.74	12.55	0.11	-1.54	0.21	1.79	-1.09	0.54	0.12
11869181	92.414474	-41.393284	0.60180	0.92	12.85	0.11	-1.67	0.19	2.73	-1.81	0.52	0.12
11870671	93.099632	-41.453117	0.60738	1.24	11.99	0.10	-1.84	0.17	1.86	-1.23	0.49	0.13
11872085	94.542740	-40.369217	0.54574	1.33	13.47	0.11	-1.75	0.18	3.74	-2.42	0.50	0.13
11902531	84.038559	-59.311455	0.64502	0.64	12.68	0.11	-1.91	0.19	2.63	-2.26	0.48	0.13
11910764	85.319984	-66.262276	0.52884	0.92	12.68	0.11	-1.45	0.20	2.43	-2.22	0.62	0.16
11929610	100.269516	-57.342876	0.57902	0.99	13.64	0.11	-1.69	0.30	4.09	-3.44	0.51	0.13
11951363	118.251160	-57.434704	0.52108	0.86	13.65	0.11	-1.14	0.30	3.69	-3.11	0.70	0.16
11967991	119.017403	-67.149017	0.56670	0.83	13.39	0.11	-1.43	0.21	3.28	-3.02	0.62	0.16
11990963	128.064438	-57.365791	0.67358	1.05	12.87	0.11	-2.32	0.18	2.99	-2.52	0.41	0.14
11996470	134.171585	-60.224842	0.45167	1.37	13.68	0.11	-1.51	0.18	4.00	-3.47	0.54	0.12
12007998	143.544189	-59.891407	0.55298	0.91	9.70	0.09	-1.44	0.17	0.63	-0.55	0.62	0.15
12009122	143.794373	-58.369900	0.64672	0.70	13.35	0.11	-1.65	0.30	3.56	-3.03	0.52	0.13
12010601	142.728668	-54.028740	0.54784	1.07	13.41	0.11	-1.49	0.19	3.36	-2.72	0.61	0.16
12073505	167.148605	-50.901009	0.64530	1.60	13.68	0.11	-2.80	0.21	4.50	-3.50	0.32	0.15
12096932	175.795975	-51.694885	0.54807	0.86	12.62	0.11	-1.96	0.18	2.49	-1.95	0.47	0.13
12140779	180.098206	-38.530781	0.36997	1.19	12.54	0.11	-0.43	0.18	1.50	-0.93	0.89	0.13
12248877	196.023392	-30.393412	0.48778	1.02	12.69	0.11	-1.05	0.20	2.20	-1.11	0.73	0.15
12250977	200.710785	-31.948706	0.63058	0.46	12.69	0.11	-1.21	0.30	2.30	-1.22	0.68	0.16
12252066	198.201797	-30.317051	0.57926	1.51	13.09	0.11	-2.45	0.30	3.24	-1.64	0.38	0.15

Table B.1 (cont'd)

NSVS ID	b (o)	l (o)	P (days)	A_V	m_V	σ_{mv}	[Fe/H]	σ_{feh}	D (kpc)	Z (kpc)	M_V	σ_{M_V}
12370362	201.943268	-10.289137	0.47911	1.31	12.54	0.11	-1.50	0.30	0.67	-0.12	0.61	0.17
12678415	210.258347	9.520493	0.61582	0.64	11.99	0.10	-1.06	0.20	1.65	0.27	0.72	0.15
12680188	214.289429	7.816315	0.57141	0.97	12.64	0.11	-0.92	0.20	2.01	0.27	0.76	0.14
12680351	212.600723	8.693817	0.62546	1.10	13.00	0.11	-2.05	0.18	2.45	0.37	0.45	0.13
12728156	214.433640	15.350633	0.55053	0.81	11.91	0.10	-0.72	0.20	1.58	0.42	0.82	0.14
12778072	220.891632	12.494733	0.51319	1.06	12.55	0.11	-1.35	0.18	2.24	0.49	0.64	0.15
12843002	219.856308	19.301691	0.50171	1.29	12.19	0.10	-2.00	0.16	2.14	0.71	0.46	0.13
12871389	219.110428	25.158173	0.68353	0.98	13.60	0.11	-2.25	0.30	4.12	1.75	0.42	0.14
12872211	222.298553	23.870424	0.56148	0.91	13.42	0.11	-1.47	0.30	3.38	1.37	0.61	0.17
12880089	223.706985	25.457478	0.50596	1.02	13.36	0.11	-1.19	0.20	3.28	1.41	0.69	0.15
12892356	221.772720	30.318052	0.63647	0.64	12.31	0.11	-1.25	0.22	1.98	1.00	0.67	0.15
12900308	227.332733	20.538494	0.50853	1.04	13.35	0.11	-2.16	0.20	3.68	1.29	0.43	0.14
12916018	226.921646	24.829767	0.53703	0.74	12.78	0.11	-1.06	0.30	2.47	1.04	0.72	0.16
12919471	230.605087	23.749748	0.42083	0.59	10.75	0.10	-0.00	0.30	0.86	0.35	1.01	0.14
12929278	233.779251	24.955757	0.75422	0.91	12.02	0.10	-2.20	0.18	2.01	0.85	0.43	0.14
12962968	224.097656	32.049026	0.49698	0.72	12.60	0.11	-0.77	0.30	2.13	1.13	0.80	0.15
12985723	231.993164	35.208866	0.63429	0.50	11.79	0.10	-1.23	0.20	1.50	0.87	0.68	0.15
12990484	230.415604	38.181911	0.52390	1.23	12.33	0.11	-1.72	0.18	2.18	1.35	0.51	0.12
13001998	234.106995	41.933163	0.53091	1.40	13.72	0.11	-1.99	0.30	4.23	2.83	0.46	0.14
13002450	233.030991	42.713589	0.48740	0.99	12.63	0.11	-1.30	0.18	2.30	1.56	0.66	0.15
13017408	239.861679	35.394211	0.64947	1.20	13.35	0.11	-2.04	0.19	3.53	2.05	0.45	0.13
13039828	245.444962	43.004093	0.77894	1.02	13.14	0.11	-2.76	0.30	3.42	2.33	0.33	0.16

Table B.1 (cont'd)

NSVS ID	b (o)	l (o)	P (days)	A_V	m_V	σ_{mv}	[Fe/H]	σ_{feh}	D (kpc)	Z (kpc)	M_V	σ_{M_V}
13094756	257.014374	44.039722	0.50350	1.23	13.56	0.11	-1.21	0.19	3.60	2.50	0.68	0.15
13095983	255.871216	45.782803	0.60461	0.82	13.19	0.11	-1.47	0.21	3.12	2.23	0.61	0.16
13108142	262.990173	49.061378	0.67287	1.19	12.10	0.10	-2.34	0.17	2.04	1.54	0.40	0.14
13124901	256.410339	53.492592	0.68480	0.70	13.22	0.11	-1.85	0.30	3.28	2.64	0.48	0.13
13151540	273.722809	62.766136	0.76776	0.55	12.19	0.10	-2.22	0.18	2.14	1.91	0.42	0.14
13155113	265.312378	57.063427	0.62633	1.06	10.98	0.10	-1.93	0.17	1.23	1.03	0.47	0.13
13196916	286.550079	62.276196	0.58700	1.00	11.93	0.10	-1.73	0.18	1.85	1.64	0.51	0.13
13197108	281.455933	69.513725	0.54570	1.03	13.60	0.11	-1.54	0.30	3.94	3.69	0.54	0.13
13197686	286.891815	63.276314	0.54300	1.07	12.64	0.11	-1.69	0.18	2.58	2.30	0.51	0.12
13207963	295.017822	68.774353	0.68155	1.24	13.53	0.11	-2.77	0.20	4.22	3.94	0.33	0.15
13221776	295.379639	60.226074	0.63706	0.42	12.07	0.10	-1.20	0.30	1.80	1.57	0.69	0.16
13231809	304.658783	57.400116	0.52579	1.13	11.40	0.10	-1.79	0.16	1.44	1.22	0.50	0.13
13236188	309.571106	61.904587	0.57226	1.10	13.38	0.11	-1.81	0.30	3.66	3.23	0.49	0.13
13264395	323.410919	67.520699	0.56455	1.23	12.07	0.10	-1.78	0.16	1.96	1.81	0.50	0.13
13265072	325.407257	68.666328	0.52776	1.17	13.52	0.11	-1.63	0.30	3.82	3.56	0.52	0.13
13282686	340.319702	64.834595	0.47111	0.78	11.23	0.10	[-1.52]	0.16	1.32	1.20	0.54	0.12
13287612	319.714020	56.376869	0.65153	1.17	13.33	0.11	-2.36	0.30	3.69	3.07	0.40	0.15
13288116	319.858368	55.736679	0.57642	1.05	11.81	0.10	-1.71	0.17	1.73	1.43	0.51	0.12
13291329	321.789581	54.286030	0.60935	0.98	13.45	0.11	-2.10	0.20	3.83	3.11	0.44	0.13
13294241	328.308624	60.485836	0.76082	0.89	13.76	0.11	-2.48	0.30	4.54	3.95	0.38	0.15
13302749	330.143829	53.462772	0.62355	0.66	12.70	0.11	-1.46	0.30	2.52	2.03	0.62	0.17
13311476	336.068085	52.203205	0.55808	1.25	13.73	0.11	-1.94	0.30	4.29	3.39	0.47	0.14

Table B.1 (cont'd)

NSVS ID	b (o)	l (o)	P (days)	A_V	m_V	σ_{mv}	[Fe/H]	σ_{feh}	D (kpc)	Z (kpc)	M_V	σ_{M_V}
13322484	346.373291	53.652008	0.41081	1.28	11.59	0.10	-0.83	0.17	1.36	1.10	0.78	0.14
13343221	351.615326	57.272148	0.63386	1.07	13.11	0.11	-1.87	0.20	3.21	2.70	0.48	0.13
13350457	354.162933	56.145138	0.68563	0.87	13.27	0.11	-2.10	0.30	3.50	2.90	0.44	0.14
13362899	358.603088	51.720634	0.53030	1.13	12.96	0.11	-1.81	0.18	2.94	2.31	0.49	0.13
13373556	347.554443	49.816856	0.60048	0.80	12.45	0.11	-1.53	0.30	2.08	1.59	0.54	0.13
13373760	347.006439	49.234749	0.68279	0.84	12.89	0.11	-2.04	0.30	2.65	2.01	0.45	0.14
13377175	347.980988	48.022697	0.61271	1.28	13.65	0.11	-2.09	0.20	3.95	2.93	0.44	0.13
13415461	1.875560	49.706699	0.49582	1.38	13.12	0.11	-1.45	0.18	2.95	2.25	0.62	0.16
13419553	7.088809	50.512054	0.46506	1.46	13.61	0.11	-1.63	0.18	3.92	3.02	0.52	0.12
13425077	11.090534	50.078346	0.54797	1.01	12.90	0.11	-1.74	0.18	2.85	2.19	0.50	0.13
13425719	5.774812	47.300579	0.55742	0.87	13.59	0.11	-1.47	0.21	3.70	2.72	0.61	0.16
13436085	7.225332	45.427967	0.52678	1.29	12.41	0.11	-1.87	0.18	2.29	1.63	0.48	0.13
13437790	6.156682	44.097824	0.71409	0.71	10.10	0.10	-1.84	0.18	0.78	0.55	0.49	0.13
13438360	7.896868	44.773785	0.79835	0.86	13.60	0.11	-2.62	0.30	4.19	2.95	0.36	0.15
13439616	7.894747	44.255661	0.57543	0.54	11.95	0.10	-1.02	0.30	1.64	1.14	0.74	0.16
13440706	8.608793	44.192329	0.59643	0.92	13.15	0.11	-1.58	0.21	3.13	2.18	0.53	0.12
13444030	10.337668	43.761627	0.46347	1.36	13.45	0.11	-1.42	0.20	3.36	2.33	0.63	0.16
13453020	10.907901	40.564697	0.64707	1.07	13.05	0.11	-1.99	0.19	2.76	1.79	0.46	0.13
13456880	18.037943	42.451427	0.74655	0.99	11.43	0.10	-2.26	0.18	1.50	1.01	0.42	0.14
13466900	6.136125	42.413097	0.46069	0.78	13.67	0.11	-0.59	0.30	3.27	2.21	0.85	0.15
13467814	3.881129	40.707649	0.51756	0.85	12.64	0.11	-1.09	0.30	2.00	1.30	0.72	0.16
13479853	7.589994	38.294613	0.62598	1.32	13.22	0.11	-2.11	0.20	2.92	1.81	0.44	0.14

Table B.1 (cont'd)

NSVS ID	b (o)	l (o)	P (days)	A_V	m_V	σ_{mv}	[Fe/H]	σ_{feh}	D (kpc)	Z (kpc)	M_V	σ_{M_V}
13489599	6.378333	33.625187	0.59134	0.99	13.31	0.11	-1.76	0.30	2.48	1.38	0.50	0.13
13504920	9.709496	30.448288	0.62396	0.42	12.35	0.11	-1.12	0.30	1.53	0.78	0.71	0.16
13533108	21.651941	37.866859	0.59284	1.23	13.60	0.11	-2.11	0.30	3.94	2.42	0.44	0.14
13551179	19.474808	33.417191	0.63938	0.93	13.60	0.11	-1.94	0.30	3.88	2.14	0.47	0.14
13567201	20.325811	29.456038	0.63521	1.05	12.59	0.11	-2.10	0.30	2.39	1.18	0.44	0.14
13570612	19.432436	28.125971	0.63073	0.67	12.96	0.11	-1.53	0.30	2.77	1.30	0.54	0.13
13572504	22.711609	29.254160	0.72644	0.95	13.44	0.11	-2.42	0.30	3.54	1.73	0.39	0.15
13574815	24.495834	29.515583	0.77875	0.81	13.18	0.11	-2.21	0.22	3.08	1.52	0.42	0.14
13578753	24.255520	28.421713	0.59903	0.73	13.05	0.11	-1.43	0.30	2.54	1.21	0.62	0.17
13644720	21.412170	18.860125	0.66778	0.81	12.24	0.10	-1.67	0.19	1.20	0.39	0.52	0.12
13667152	25.423300	25.524029	0.36510	1.34	13.70	0.11	-0.73	0.21	3.14	1.35	0.81	0.14
13682137	29.759157	24.347685	0.50969	1.03	13.53	0.11	-1.30	0.30	3.09	1.27	0.66	0.16
13687028	25.288321	21.269785	0.73576	0.77	13.52	0.11	-2.20	0.30	3.48	1.26	0.43	0.14
13688630	24.206963	20.415380	0.73770	0.55	12.10	0.10	-1.53	0.22	1.54	0.54	0.54	0.12
13721372	26.128742	16.453974	0.59823	0.81	12.38	0.11	-1.61	0.20	1.72	0.49	0.53	0.12
13758491	22.836477	16.643322	0.45035	1.34	12.12	0.10	-1.22	0.19	1.39	0.40	0.68	0.15
13961527	32.836761	-1.009987	0.68524	0.42	10.99	0.10	-1.44	0.30	0.05	-0.00	0.62	0.17
14205594	39.906250	-21.498280	0.51519	0.58	12.75	0.11	-0.68	0.30	2.09	-0.77	0.83	0.15
14215652	42.864716	-22.072023	0.72469	0.57	11.74	0.10	-2.02	0.19	1.45	-0.55	0.46	0.13
14266156	48.719170	-18.498653	0.45052	0.85	13.28	0.11	-0.62	0.30	2.74	-0.87	0.84	0.15
14279000	46.276936	-20.670000	0.61870	0.58	12.82	0.11	-1.32	0.30	2.24	-0.79	0.65	0.17
14284107	45.629635	-22.040789	0.57804	1.23	10.95	0.10	-1.81	0.17	1.07	-0.40	0.49	0.13

Table B.1 (cont'd)

NSVS ID	b (o)	l (o)	P (days)	A_V	m_V	σ_{mv}	[Fe/H]	σ_{feh}	D (kpc)	Z (kpc)	M_V	σ_{M_V}
14312323	54.473141	-22.814650	0.56685	0.80	13.69	0.11	-1.34	0.30	3.61	-1.40	0.65	0.17
14332976	39.997299	-25.917233	0.68975	1.00	13.60	0.11	-2.31	0.30	4.05	-1.77	0.41	0.15
14357980	42.937115	-30.604195	0.68496	1.06	12.51	0.11	-2.37	0.30	2.47	-1.26	0.40	0.15
14361529	45.276924	-30.278885	0.58137	0.79	12.28	0.11	-1.23	0.21	1.83	-0.93	0.68	0.15
14371460	48.740299	-31.334873	0.46340	1.41	11.80	0.10	-1.09	0.18	1.51	-0.79	0.72	0.14
14378728	51.799431	-31.893711	0.48948	0.88	13.25	0.11	-0.94	0.30	2.79	-1.47	0.76	0.16
14411401	55.488701	-28.916634	0.44471	0.81	12.86	0.11	-0.50	0.30	2.19	-1.06	0.87	0.15
14412075	51.314747	-31.471144	0.45930	1.24	11.24	0.10	-1.55	0.16	1.22	-0.64	0.54	0.12
14433599	54.621769	-34.015480	0.48066	1.16	13.40	0.11	-1.29	0.30	3.30	-1.85	0.66	0.16
14439563	57.897449	-34.008324	0.53570	1.14	11.77	0.10	-1.77	0.16	1.66	-0.93	0.50	0.13
14440338	56.799084	-34.891403	0.59832	1.00	13.66	0.11	-1.81	0.30	4.01	-2.29	0.49	0.13
14447741	60.587196	-35.073334	0.58697	1.17	13.40	0.11	-2.14	0.19	3.53	-2.03	0.44	0.14
14487932	53.249748	-44.332264	0.57115	0.81	12.20	0.10	[-0.26]	0.22	1.66	-1.16	0.94	0.14
14495865	59.906624	-44.358536	0.58832	0.74	12.84	0.11	-1.39	0.30	2.41	-1.68	0.64	0.17
14505896	56.219135	-50.725349	0.46968	1.23	12.70	0.11	-1.37	0.18	2.42	-1.87	0.64	0.15
14512123	63.410767	-38.934597	0.54950	1.05	13.08	0.11	-1.48	0.20	2.93	-1.84	0.61	0.16
14528813	70.897186	-40.641930	0.54275	0.89	13.69	0.11	-1.32	0.30	3.44	-2.24	0.65	0.17
14554493	78.179100	-47.295483	0.53624	1.49	13.43	0.11	-1.61	0.20	3.32	-2.44	0.53	0.12
14560814	62.620159	-49.883759	0.54732	1.25	13.64	0.11	-1.87	0.30	4.03	-3.09	0.48	0.13
14561489	65.340767	-48.763741	0.85390	1.49	13.74	0.11	-3.86	0.20	4.81	-3.62	0.14	0.19
14564729	60.773281	-52.886078	0.36479	1.02	12.38	0.11	[-0.12]	0.30	1.81	-1.44	0.98	0.14
14581148	72.871597	-56.347710	0.49097	1.07	13.76	0.11	-1.23	0.30	3.90	-3.24	0.68	0.16

Table B.1 (cont'd)

NSVS ID	b (o)	l (o)	P (days)	A_V	m_V	σ_{mv}	[Fe/H]	σ_{feh}	D (kpc)	Z (kpc)	M_V	σ_{M_V}
14617414	75.484924	-65.235069	0.48187	1.17	11.38	0.10	-1.09	0.17	1.30	-1.18	0.71	0.14
14629388	56.861462	-69.306274	0.65519	0.96	12.64	0.11	-1.84	0.20	2.59	-2.43	0.49	0.13
14641661	73.271080	-75.084595	0.60602	0.65	12.02	0.10	-1.39	0.20	1.83	-1.77	0.63	0.16
14654206	85.067947	-70.758591	0.74082	0.92	12.76	0.11	-2.56	0.19	2.87	-2.71	0.36	0.15
14669479	105.366844	-75.794510	0.43723	1.36	13.49	0.11	-1.26	0.30	3.56	-3.45	0.67	0.16
14682479	102.473526	-77.646324	0.57362	0.60	11.36	0.10	-1.09	0.30	1.29	-1.26	0.72	0.16
14685163	98.012337	-83.907196	0.56532	1.19	13.49	0.11	-1.89	0.30	3.91	-3.89	0.48	0.14
14698705	157.011749	-78.460747	0.62115	1.01	13.46	0.11	-1.96	0.30	3.84	-3.76	0.47	0.14
14715713	153.981033	-72.034561	0.51693	0.91	13.22	0.11	-1.18	0.30	3.04	-2.89	0.69	0.16
14762123	177.327194	-64.403786	0.62322	0.63	10.77	0.10	-1.30	0.21	1.00	-0.91	0.66	0.15
14768130	178.210236	-60.337986	0.51065	1.04	11.76	0.10	-1.25	0.17	1.57	-1.37	0.67	0.15
14782274	193.359528	-58.074860	0.69256	0.92	13.44	0.11	-2.21	0.30	3.81	-3.24	0.42	0.14
14791206	200.085190	-63.018288	0.74472	0.75	13.71	0.11	-2.21	0.30	4.36	-3.88	0.42	0.14
14818780	198.898804	-54.451916	0.64867	1.14	12.88	0.11	-2.30	0.19	2.89	-2.36	0.41	0.14
14908249	205.182846	-33.579369	0.48169	1.42	13.55	0.11	-1.23	0.19	3.22	-1.78	0.68	0.15
14910117	206.000061	-33.187031	0.65995	0.53	13.51	0.11	-1.47	0.30	3.38	-1.85	0.61	0.17
14915325	209.230576	-32.524971	0.64028	0.42	12.84	0.11	-1.21	0.30	2.32	-1.25	0.68	0.16
14925915	213.503464	-39.237862	0.65690	1.22	13.61	0.11	-2.46	0.30	4.24	-2.68	0.38	0.15
14941696	218.822296	-34.360752	0.56991	0.86	11.40	0.10	-1.48	0.17	1.34	-0.76	0.61	0.16
14943427	221.109558	-34.368797	0.58148	1.16	10.65	0.10	-1.89	0.16	1.03	-0.58	0.48	0.13
14979434	211.662262	-26.940224	0.56859	0.77	13.38	0.11	-1.31	0.30	2.78	-1.26	0.66	0.16
14990007	216.275253	-25.570761	0.56000	0.80	12.40	0.11	-1.17	0.21	1.84	-0.79	0.69	0.15

Table B.1 (cont'd)

NSVS ID	b (o)	l (o)	P (days)	A_V	m_V	σ_{mv}	[Fe/H]	σ_{feh}	D (kpc)	Z (kpc)	M_V	σ_{M_V}
15004446	216.122910	-23.392466	0.53649	0.99	13.71	0.11	-1.43	0.30	3.33	-1.32	0.62	0.17
15016349	219.166138	-20.997637	0.59941	0.95	13.26	0.11	-1.75	0.30	2.93	-1.05	0.50	0.13
15021359	219.608063	-19.681362	0.51895	0.87	12.86	0.11	-0.99	0.21	2.04	-0.69	0.74	0.15
15206916	225.273300	-10.745565	0.40861	1.37	13.59	0.11	-1.02	0.30	2.40	-0.45	0.73	0.16
15218044	232.068527	-11.891831	0.53743	0.53	12.45	0.11	-0.76	0.30	1.70	-0.35	0.80	0.15
15657369	238.032578	22.951389	0.48900	1.28	12.12	0.10	-1.73	0.16	1.98	0.77	0.51	0.12
15671445	239.771927	25.932220	0.53729	1.05	11.14	0.10	-1.60	0.19	1.25	0.55	0.53	0.12
15679506	244.978455	24.938131	0.53225	0.93	13.27	0.11	-1.31	0.30	3.09	1.30	0.66	0.16
15681945	245.033981	25.707674	0.61124	1.05	13.66	0.11	-1.97	0.30	4.06	1.76	0.47	0.14
15692808	243.502518	28.681847	0.64624	1.17	13.71	0.11	-2.33	0.30	4.36	2.09	0.40	0.15
15726118	251.459000	24.664467	0.52097	1.05	13.58	0.11	-1.41	0.30	3.51	1.47	0.63	0.17
15781327	254.263016	34.403996	0.53769	0.92	10.80	0.10	-1.20	0.18	0.94	0.53	0.69	0.15
15806847	258.114380	43.380939	0.50340	0.91	12.02	0.10	-1.12	0.18	1.74	1.20	0.71	0.15
15820266	264.241364	31.849098	0.61793	1.09	13.42	0.11	-2.06	0.30	3.62	1.91	0.45	0.14
15827760	265.607086	34.606625	0.59778	1.11	13.41	0.11	-1.76	0.19	3.50	1.99	0.50	0.13
15854954	275.991516	40.471840	0.41201	1.07	11.57	0.10	-0.84	0.16	1.33	0.87	0.78	0.14
15889152	276.268463	48.578545	0.62233	1.00	12.69	0.11	-2.21	0.18	2.72	2.04	0.42	0.14
15893670	278.867401	49.487835	0.73283	0.63	11.37	0.10	-1.97	0.19	1.46	1.11	0.46	0.13
15896141	279.104095	52.239491	0.74832	0.64	12.76	0.11	-2.07	0.30	2.70	2.13	0.45	0.14
15897529	280.837158	51.137188	0.54382	1.18	13.58	0.11	-1.75	0.30	3.95	3.08	0.50	0.13
15901810	275.644775	42.792259	0.66438	0.81	13.56	0.11	-1.90	0.30	3.89	2.64	0.48	0.14
15972928	300.160370	50.781483	0.68115	0.80	12.57	0.11	-1.89	0.20	2.42	1.88	0.48	0.13

Table B.1 (cont'd)

NSVS ID	b (o)	l (o)	P (days)	A_V	m_V	σ_{mv}	[Fe/H]	σ_{feh}	D (kpc)	Z (kpc)	M_V	σ_{M_V}
15975024	301.499237	54.515896	0.51049	0.81	12.45	0.11	[-1.10]	0.19	2.12	1.73	0.71	0.15
15977770	303.469147	52.610065	0.55340	0.97	11.89	0.10	-1.77	0.19	1.78	1.42	0.50	0.13
15979689	304.800507	51.559258	0.59717	0.74	12.59	0.11	-1.33	0.21	2.30	1.80	0.65	0.15
15985119	296.372009	43.614815	0.55296	1.11	13.67	0.11	-1.70	0.30	3.99	2.75	0.51	0.13
16053601	321.917419	50.425144	0.65861	0.40	11.42	0.10	-1.28	0.30	1.30	1.00	0.66	0.16
16100815	330.349548	41.211075	0.56632	0.54	12.61	0.11	-0.96	0.30	2.01	1.33	0.75	0.16
16109407	331.490051	36.899616	0.79526	0.81	13.47	0.11	-2.53	0.30	3.67	2.21	0.37	0.15
16117767	328.358765	46.083988	0.51986	1.21	13.43	0.11	-1.63	0.30	3.36	2.42	0.52	0.13
16127147	332.439301	44.332298	0.56618	0.69	13.54	0.11	-1.17	0.30	3.28	2.29	0.69	0.16
16155643	345.575195	43.711353	0.64395	0.75	13.09	0.11	-1.62	0.21	2.87	1.98	0.52	0.12
16157754	346.614258	43.529667	0.68360	0.70	13.46	0.11	-1.84	0.30	3.49	2.40	0.49	0.13
16164702	335.632721	42.193077	0.52178	1.15	12.95	0.11	-1.43	0.20	2.58	1.73	0.62	0.16
16184196	341.979126	38.864986	0.53936	0.99	12.84	0.11	-1.44	0.30	2.45	1.54	0.62	0.17
16185842	340.687195	36.543964	0.46246	1.12	13.23	0.11	-1.09	0.21	2.72	1.62	0.72	0.15
16197858	343.304291	33.608208	0.45272	1.43	13.69	0.11	-1.47	0.30	3.63	2.01	0.61	0.17
16224995	348.454956	41.169312	0.51642	1.12	13.37	0.11	-1.48	0.30	3.10	2.04	0.61	0.17
16238329	354.703278	40.597260	0.51413	1.10	13.33	0.11	-1.43	0.30	2.97	1.93	0.62	0.17
16239733	349.752533	35.692989	0.63471	1.14	13.57	0.11	-2.23	0.30	3.50	2.04	0.42	0.14
16240332	350.792267	36.415791	0.44180	1.01	13.08	0.11	-0.77	0.30	2.30	1.37	0.80	0.15
16241026	355.841553	40.441933	0.77896	0.52	10.97	0.10	-2.04	0.30	1.11	0.72	0.45	0.14
16244466	352.330475	36.039570	0.58166	0.95	13.51	0.11	-1.65	0.30	3.14	1.85	0.52	0.13
16258860	359.039490	37.428608	0.45521	0.90	13.64	0.11	[-0.72]	0.30	2.96	1.80	0.82	0.15

Table B.1 (cont'd)

NSVS ID	b (o)	l (o)	P (days)	A_V	m_V	σ_{mv}	[Fe/H]	σ_{feh}	D (kpc)	Z (kpc)	M_V	σ_{M_V}
16267747	1.188146	35.755470	0.75685	0.85	13.62	0.11	-2.42	0.30	3.39	1.98	0.39	0.15
16283172	345.807648	28.647741	0.49310	1.22	13.32	0.11	-1.18	0.20	2.77	1.33	0.69	0.15
16292601	347.505737	26.940298	0.47813	1.33	13.07	0.11	-1.51	0.30	2.48	1.12	0.54	0.13
16304023	353.862793	28.835241	0.53391	0.99	11.57	0.10	-1.34	0.17	1.17	0.56	0.65	0.15
16360132	4.147345	29.629766	0.54865	0.72	12.88	0.11	-1.11	0.30	1.95	0.96	0.71	0.16
16362273	3.324018	28.395050	0.54078	0.98	13.23	0.11	-1.15	0.20	2.22	1.05	0.70	0.15
16372425	7.900294	28.445274	0.39704	0.72	10.64	0.10	[0.88]	0.22	0.48	0.23	1.25	0.14
16372447	4.384451	25.975040	0.44900	1.16	11.85	0.10	-1.05	0.17	1.13	0.49	0.73	0.14
17011064	23.312609	-16.567329	0.37290	1.33	12.73	0.11	-0.65	0.30	1.96	-0.56	0.83	0.15
17022191	22.510883	-18.953867	0.71564	0.91	13.70	0.11	-2.30	0.30	3.82	-1.24	0.41	0.15
17109617	36.498825	-22.643702	0.51957	1.04	13.62	0.11	-2.40	0.20	4.10	-1.58	0.39	0.14
17122030	32.352455	-27.145754	0.66737	0.69	12.54	0.11	-1.79	0.21	2.41	-1.10	0.49	0.13
17130621	32.352661	-27.145672	0.66756	0.61	12.57	0.11	-1.63	0.30	2.41	-1.10	0.52	0.13
17147354	37.481529	-28.978630	0.51227	1.25	13.53	0.11	-1.64	0.30	3.71	-1.80	0.52	0.13
17176196	30.036282	-30.366259	0.40499	0.84	13.18	0.11	-0.24	0.30	2.63	-1.33	0.95	0.15
17212765	28.105206	-41.759926	0.60057	1.13	12.88	0.11	-2.23	0.18	2.88	-1.92	0.42	0.14
17246508	44.674866	-37.167240	0.79719	0.71	12.55	0.11	-2.39	0.30	2.17	-1.31	0.39	0.15
17280732	32.576530	-42.620033	0.54271	1.09	13.74	0.11	-1.61	0.30	4.08	-2.76	0.53	0.13
17291542	35.853813	-45.897892	0.66155	1.25	13.63	0.11	-2.70	0.21	4.31	-3.10	0.34	0.15
17293210	33.787334	-47.047890	0.80026	0.58	12.62	0.11	-2.21	0.30	2.57	-1.88	0.42	0.14
17295262	31.398708	-48.384190	0.68630	0.89	13.71	0.11	-2.13	0.30	4.27	-3.19	0.44	0.14
17331060	48.930229	-49.758087	0.55196	1.08	12.62	0.11	-1.75	0.18	2.47	-1.89	0.50	0.13

Table B.1 (cont'd)

NSVS ID	b (o)	l (o)	P (days)	A_V	m_V	σ_{mv}	[Fe/H]	σ_{feh}	D (kpc)	Z (kpc)	M_V	σ_{M_V}
17344990	56.607376	-51.479397	0.52597	1.09	13.41	0.11	-1.81	0.19	3.58	-2.80	0.49	0.13
17348071	54.625187	-53.825741	0.60884	1.22	12.88	0.11	-2.00	0.18	2.77	-2.24	0.46	0.13
17358579	55.397545	-58.822548	0.69408	1.07	12.15	0.10	-2.11	0.18	2.07	-1.77	0.44	0.13
17368466	39.342537	-58.853577	0.52573	1.41	13.54	0.11	-1.70	0.19	3.87	-3.31	0.51	0.12
17407836	64.011528	-64.963341	0.51892	1.29	12.99	0.11	-1.45	0.19	2.84	-2.57	0.62	0.16
17438804	2.047993	-76.221588	0.61690	0.93	12.91	0.11	-1.15	0.22	2.72	-2.65	0.70	0.15
17474384	91.202820	-87.168976	0.57127	1.00	13.43	0.11	-1.66	0.30	3.73	-3.72	0.52	0.13
17478335	176.852097	-88.742424	0.52065	1.14	13.57	0.11	-1.54	0.30	3.91	-3.91	0.54	0.13
17510931	207.928604	-82.927299	0.45167	1.44	13.67	0.11	-2.10	0.19	4.33	-4.29	0.44	0.13
17530683	256.057617	-77.666779	0.63696	0.84	12.06	0.10	-2.06	0.20	2.05	-2.00	0.45	0.13
17570707	217.897049	-63.529995	0.37043	0.86	12.76	0.11	0.05	0.30	2.16	-1.94	1.02	0.14
17572475	222.846970	-62.819401	0.60308	1.16	12.75	0.11	-1.92	0.17	2.78	-2.47	0.47	0.13
17578791	224.519470	-59.187309	0.55292	0.88	13.26	0.11	-1.09	0.22	3.15	-2.71	0.72	0.15
17591359	237.141769	-59.230789	0.60851	0.94	13.40	0.11	-1.78	0.30	3.69	-3.17	0.50	0.13
17612485	215.756607	-55.337986	0.62965	0.86	12.51	0.11	-1.97	0.19	2.49	-2.05	0.47	0.13
17620888	219.872604	-51.472561	0.55982	0.79	13.38	0.11	-1.27	0.30	3.44	-2.69	0.67	0.16
17633766	223.902512	-47.181042	0.60239	0.66	12.60	0.11	-1.40	0.21	2.34	-1.71	0.63	0.16
17678949	224.554642	-37.871883	0.33543	1.15	13.61	0.11	[-0.03]	0.30	3.17	-1.94	1.00	0.14
17702479	229.919495	-31.811018	0.53658	0.93	12.70	0.11	-1.23	0.19	2.46	-1.30	0.68	0.15
17765419	233.208206	-23.435892	0.46872	1.09	12.60	0.11	-1.04	0.18	2.26	-0.90	0.73	0.14
17826311	244.297546	-23.173033	0.59330	0.87	12.79	0.11	-1.59	0.30	2.52	-0.99	0.53	0.13
17866005	232.868744	-14.517106	0.87118	0.89	13.59	0.11	-2.96	0.30	4.12	-1.03	0.30	0.16

Table B.1 (cont'd)

NSVS ID	b (o)	l (o)	P (days)	A_V	m_V	σ_{mv}	[Fe/H]	σ_{feh}	D (kpc)	Z (kpc)	M_V	σ_{M_V}
18443369	266.088501	21.980890	0.56614	0.83	13.32	0.11	-1.37	0.30	3.07	1.15	0.64	0.17
18473830	270.053162	28.038099	0.46772	1.26	13.65	0.11	-1.34	0.30	3.62	1.70	0.65	0.17
18479042	272.672791	27.398193	0.57501	1.10	13.24	0.11	-1.82	0.30	3.20	1.47	0.49	0.13
18551452	274.096252	29.396816	0.48917	0.69	13.11	0.11	-0.67	0.30	2.58	1.27	0.83	0.15
18552406	274.832397	28.876301	0.36551	0.86	13.52	0.11	0.10	0.30	2.84	1.37	1.04	0.14
18558434	275.350037	31.735121	0.65154	0.94	12.95	0.11	-2.71	0.16	3.01	1.58	0.34	0.15
18577666	279.878113	34.637508	0.67823	1.10	12.98	0.11	-1.59	0.22	2.83	1.61	0.53	0.12
18621887	289.114075	25.568596	0.41644	1.53	13.73	0.11	-1.33	0.30	3.56	1.54	0.65	0.17
18688076	297.233887	38.751743	0.53693	0.68	13.35	0.11	[-0.97]	0.30	2.93	1.84	0.75	0.16
18691062	298.571930	36.076412	0.57738	0.72	12.88	0.11	-1.44	0.21	2.55	1.50	0.62	0.16
18714268	297.845154	28.289732	0.51412	0.91	12.57	0.11	-1.13	0.20	2.12	1.01	0.70	0.15
19097293	346.734070	22.368542	0.46363	0.98	13.05	0.11	-0.90	0.30	2.27	0.86	0.77	0.15
19972017	4.805492	-66.688400	0.59345	0.69	12.52	0.11	-1.34	0.30	2.32	-2.13	0.65	0.17
19991510	35.761162	-69.063492	0.63377	0.70	11.06	0.10	-1.48	0.19	1.19	-1.11	0.61	0.16

Appendix C

NSVS RRc Parameters

The parameters obtained for the RRc stars are presented here. This table contains information for 375 RRc stars from the NSVS database. Column 1 is the ID of the star in the NSVS database. Column 2 and 3 are the galactic coordinates in degrees. Column 3 is the period of the RRc star. Column 4 is the amplitude scaled onto the Johnson V filter system. Column 5 is the intensity weighted mean magnitude in the ROTSE-I magnitude system.

Table C.1. NSVS RRc Properties

NSVS id	l °	b °	P days	A_V	m
100670	129.270416	29.883783	0.27721	0.83	13.67
100771	129.917755	31.728859	0.29152	0.40	12.59
274511	126.721222	19.011028	0.23642	0.51	12.71
275145	126.022820	15.614045	0.22690	0.44	12.55
358966	126.314789	11.221107	0.23345	0.68	13.61
431054	131.741852	14.718515	0.33096	0.43	12.44
445756	133.383270	19.140774	0.31800	0.53	13.44
530227	138.539963	16.372107	0.38671	0.40	10.68
576841	135.617981	20.534494	0.29355	0.43	11.80
644472	141.356979	19.842054	0.33203	0.76	13.99
766402	142.179657	30.800709	0.26704	0.51	11.89
1045426	117.731552	33.386520	0.23623	0.51	13.48
1046926	113.273239	34.792645	0.24004	0.60	13.28
1048405	112.257011	34.701321	0.30951	0.40	13.48
1089620	102.383820	32.977276	0.23980	0.41	10.90
1132768	114.020813	25.860584	0.32676	0.54	12.31
1136059	108.439919	27.273951	0.25858	0.41	12.12
1184638	102.028183	29.995337	0.22852	0.48	11.91
1206915	101.185959	24.201981	0.26089	0.53	11.94
1221668	104.933861	21.801950	0.27972	0.64	12.31
1228707	102.879326	19.745369	0.32675	0.63	13.57
1230621	104.143295	19.597635	0.35713	0.37	11.77
1274340	112.659676	19.836754	0.24674	0.61	13.70
1293676	110.970345	25.083467	0.31116	0.14	13.73
1357112	106.880234	12.709002	0.31425	0.51	12.92
1411823	118.355530	21.920290	0.30347	0.54	12.10
1420035	118.840981	19.869600	0.42677	0.60	13.33
1487938	115.718384	2.980748	0.43508	0.46	12.45
1961900	144.270157	-1.629497	0.34256	0.56	12.20
1996966	139.009735	3.613680	0.34733	0.66	12.77
2005448	139.510651	5.893476	0.27258	0.29	11.63
2099913	151.333603	1.205521	0.38150	0.43	13.27
2273941	155.765778	15.256597	0.30468	0.38	12.87
2354674	152.651657	26.209362	0.41883	0.69	13.62

Table C.1 (cont'd)

NSVS id	l °	b °	P days	A_V	m
2355916	152.101929	26.718040	0.26703	0.36	12.78
2388495	155.538605	29.288443	0.42274	0.55	12.25
2389900	151.971161	29.595310	0.39395	0.33	11.51
2413271	159.193298	27.554525	0.34031	0.35	12.40
2468181	151.919724	36.162468	0.25239	0.45	12.90
2506354	160.916275	38.739815	0.34527	0.54	11.62
2545934	148.834305	43.009747	0.29850	0.46	11.21
2672695	119.577309	59.516796	0.23332	0.38	11.93
2733101	104.792572	57.222061	0.27428	0.29	11.83
2812349	88.509232	47.751503	0.40645	0.52	13.36
2823966	83.755150	44.021393	0.30629	0.44	11.81
2829408	83.623642	42.031776	0.28345	0.46	13.13
2880024	95.594063	36.101936	0.34178	0.61	13.76
2941753	84.019463	26.787584	0.23929	0.53	13.44
2957161	93.016953	31.605032	0.27618	0.46	13.32
3014041	94.175804	23.955090	0.34808	0.33	11.60
3037032	88.018242	25.212988	0.29869	0.33	9.31
3041762	87.580826	23.990103	0.29551	0.35	11.82
3117162	97.232666	22.090036	0.35856	0.60	13.09
3143986	98.425873	17.204224	0.38812	0.61	13.03
3197352	98.581642	13.100430	0.40417	0.32	12.04
3224111	90.872154	11.626518	0.39673	0.33	11.61
3275156	95.585999	4.372744	0.42894	0.61	10.15
3310907	99.226440	10.250599	0.22612	0.62	12.77
3625232	109.985779	-22.342701	0.28277	0.49	13.46
3652211	116.345078	-18.681414	0.26020	0.74	13.65
3732137	118.991379	-13.529486	0.39196	0.69	12.46
3778236	119.446762	-22.456173	0.22561	0.93	13.82
3795183	123.323280	-20.559044	0.28617	0.38	13.25
3802178	125.153069	-22.948662	0.25348	0.54	13.06
3867878	128.791397	-14.353570	0.30542	0.59	12.83
3871660	129.671204	-16.243986	0.37919	0.38	12.72
3936667	135.261688	-9.242709	0.49010	0.46	12.90
3962006	134.249710	-17.003263	0.23681	0.35	12.14

Table C.1 (cont'd)

NSVS id	l °	b °	P days	A_V	m
3964811	137.846313	-23.845339	0.28778	0.74	13.68
3965004	135.512466	-18.338594	0.30612	0.33	12.61
4173293	155.768494	-13.889706	0.31275	0.81	13.49
4180588	153.414734	-8.826829	0.29741	0.64	12.42
4248644	151.404312	0.311229	0.24987	0.38	12.48
4291961	158.074448	-1.146471	0.26831	0.52	12.98
4330579	160.262268	-4.489732	0.33799	0.58	11.38
4497479	162.263184	14.304114	0.25770	0.60	13.56
4511557	170.483322	4.301557	0.42967	0.87	13.29
4515424	172.028641	4.303196	0.41016	0.52	13.44
4696344	179.106812	20.683613	0.34197	0.67	13.76
4721053	174.765060	28.021643	0.33961	0.48	11.66
4830676	178.798431	42.409698	0.31036	0.46	11.70
4832302	180.630783	42.926617	0.22951	0.36	11.57
4854765	169.949371	43.032730	0.24062	0.50	13.70
4878614	162.192307	47.161285	0.35565	0.39	11.10
4894894	180.365723	49.428013	0.35877	0.52	13.50
4909939	175.016754	56.116264	0.36000	0.56	13.66
4934543	157.345261	55.663219	0.34942	0.55	11.53
4959078	173.677475	61.183609	0.28845	0.54	12.72
4966884	173.532013	65.779640	0.31801	0.47	11.85
4969618	164.758789	65.519691	0.23804	0.39	11.68
5071531	100.690086	69.154335	0.30541	0.41	12.28
5082447	100.099426	73.423172	0.27669	0.37	12.09
5225506	68.098763	49.855972	0.31710	0.41	11.48
5253581	71.334785	39.730148	0.33974	0.38	10.52
5258665	64.146767	38.476971	0.38488	0.63	13.13
5271037	73.944229	42.837440	0.23834	0.41	12.92
5334748	66.803291	34.532963	0.23564	0.49	11.22
5339632	69.376541	33.561829	0.46012	0.47	12.45
5394110	78.225723	30.559233	0.23409	0.38	12.33
5396898	76.539467	29.710617	0.29483	0.41	12.68
5403828	74.857765	27.902426	0.28024	0.65	12.95
5414485	75.463776	25.678295	0.29777	0.72	13.19

Table C.1 (cont'd)

NSVS id	l °	b °	P days	A_V	m
5422752	79.899796	24.342773	0.26912	0.65	13.43
5423881	76.987450	23.841221	0.27085	0.51	12.58
5445163	75.716408	22.944822	0.35511	0.39	12.42
5497311	71.201775	19.366034	0.31983	0.64	13.46
5526732	69.485527	13.190183	0.23691	0.40	12.01
5597754	78.800728	13.355254	0.22898	0.40	12.56
5602108	78.362946	12.452659	0.52312	0.38	12.56
5645451	81.266396	10.122531	0.33032	0.47	10.94
5649335	81.512070	9.580833	0.31438	0.45	12.17
5856839	93.123497	1.179625	0.35597	0.45	12.34
6117001	99.946220	-12.188179	0.49062	0.52	12.52
6129647	99.705017	-16.594318	0.40695	0.85	13.94
6176482	102.614426	-10.657374	0.38046	0.53	12.92
6202363	108.889923	-7.890906	0.31233	0.45	12.73
6218057	110.822098	-9.777617	0.32823	0.66	13.45
6254694	110.471527	-28.154781	0.22567	0.40	12.95
6259045	99.873497	-34.215569	0.36721	0.41	12.96
6304258	116.072739	-34.739391	0.28256	0.94	13.96
6326608	114.285416	-28.895668	0.23733	0.45	13.21
6335770	116.564079	-30.082813	0.27172	0.50	10.34
6364806	122.093323	-26.826324	0.38759	0.37	12.29
6371473	124.015739	-27.041729	0.24528	0.65	13.45
6391062	121.758667	-36.284412	0.33825	0.75	13.80
6396811	124.115730	-36.961384	0.24532	0.34	12.81
6410297	129.592896	-38.159473	0.39034	0.51	10.47
6429575	125.946930	-26.660509	0.26835	0.54	12.17
6441014	129.835052	-30.907660	0.21714	0.67	13.52
6455098	134.183701	-31.575314	0.35388	0.29	12.01
6504379	140.855545	-36.956890	0.24022	0.48	12.54
6551824	144.825974	-27.980558	0.24118	0.55	11.87
6566467	147.907349	-25.504044	0.33164	0.36	11.25
6624543	155.811295	-27.048969	0.32828	0.57	11.83
6687550	159.131775	-14.885459	0.45362	0.60	12.09
6734929	166.790756	-23.197241	0.41144	0.62	13.51

Table C.1 (cont'd)

NSVS id	l °	b °	P days	A_V	m
6737414	164.945816	-20.646034	0.23025	0.40	11.70
6855021	171.807343	-4.192020	0.30841	0.47	13.39
6911093	176.230270	-4.493929	0.26441	0.52	12.98
7175575	181.169540	13.058206	0.43945	0.61	13.68
7195883	181.027100	17.070852	0.31482	0.48	11.76
7235165	187.793808	20.237804	0.32414	0.44	12.41
7237529	185.228622	21.542217	0.23678	0.50	12.64
7272542	195.537552	16.891264	0.33220	0.76	13.86
7280723	195.045837	18.877190	0.27460	0.54	13.25
7343080	190.306610	27.514090	0.23900	0.31	12.43
7365267	190.005569	31.873558	0.26073	0.51	12.89
7416581	198.126633	39.134239	0.33744	0.47	12.21
7444716	186.544769	43.331841	0.24700	0.38	11.90
7459875	188.210327	46.720387	0.39017	0.49	12.66
7483757	206.451904	47.214970	0.30905	0.48	12.97
7577789	185.807037	69.155823	0.33970	0.48	13.10
7619767	231.008728	83.606888	0.32243	0.68	13.46
7651368	113.287689	79.992416	0.30815	0.40	10.52
7662319	321.271332	89.103676	0.25603	0.36	10.62
7676759	46.874016	81.376518	0.42500	0.51	12.11
7723298	47.463070	75.230606	0.32907	0.48	11.64
7724334	29.338892	74.380234	0.32004	0.64	13.87
7736895	38.129833	68.043030	0.30599	0.71	13.64
7848125	55.024960	49.004917	0.24567	0.57	12.79
7866630	46.140427	49.089909	0.31534	0.63	13.98
7903602	47.516312	36.756310	0.46531	0.55	13.76
7961459	61.754261	32.944923	0.37308	0.72	12.55
7962118	56.824986	31.810413	0.31587	0.65	12.79
8011261	49.696148	25.817089	0.23411	0.37	12.60
8044823	57.971466	29.571711	0.22624	0.68	13.50
8047300	63.018482	29.966068	0.27267	0.44	10.76
8102280	65.115730	22.736937	0.28645	0.33	11.38
8104613	62.104633	21.282692	0.30331	0.41	11.16
8160526	52.887600	15.705971	0.23608	0.32	13.01

Table C.1 (cont'd)

NSVS id	l °	b °	P days	A_V	m
8187518	56.348953	12.489247	0.24464	0.43	12.04
8251846	68.551468	15.005470	0.52466	0.58	10.13
8508217	76.626305	-0.503263	0.29910	0.78	12.30
8554140	70.110695	-4.600965	0.22522	0.56	11.34
8559749	67.484940	-7.712886	0.23991	0.34	12.78
8588794	68.650909	-12.337778	0.33606	0.75	12.03
8681429	81.184387	-10.291162	0.25338	0.63	12.39
8693990	82.303886	-7.547287	0.23188	0.47	9.52
8711606	83.581680	-10.211844	0.38417	0.42	12.11
8794962	79.273788	-23.261797	0.30081	0.53	12.24
8795419	82.887459	-19.725647	0.26018	0.38	11.96
8806325	80.680511	-24.817566	0.38523	0.78	13.68
8808550	83.446083	-22.655369	0.24173	0.33	12.47
8845503	89.551147	-13.224326	0.23335	0.37	12.48
8868525	89.580856	-19.085112	0.23913	0.37	12.85
8868558	91.229416	-17.183275	0.32862	0.46	12.38
8902831	92.360771	-20.799198	0.32073	0.38	12.54
9005333	98.876770	-22.635584	0.38116	0.40	13.29
9006322	98.724716	-23.336769	0.30046	0.31	12.51
9052484	103.672058	-40.635361	0.26842	0.41	11.26
9069445	98.918617	-46.519657	0.25486	0.53	12.99
9104210	110.805115	-39.686264	0.25162	0.36	12.32
9108069	111.490372	-44.075348	0.27661	0.47	12.75
9116801	116.302307	-43.345966	0.32459	0.55	12.73
9160913	130.119568	-52.222069	0.35195	0.46	12.38
9184496	130.943527	-41.443817	0.28669	0.64	12.47
9186812	131.950943	-40.626926	0.28778	0.46	11.21
9255199	147.454330	-38.590065	0.37469	0.63	13.67
9294293	158.191818	-41.100468	0.27939	0.33	12.24
9311873	170.865982	-40.319599	0.23197	0.44	12.16
9313163	169.543869	-38.194382	0.28932	0.48	10.87
9469890	182.316589	-14.069934	0.25993	0.40	11.69
9480935	185.738815	-22.312019	0.33121	0.72	12.84
9481703	186.415894	-22.448172	0.23253	0.72	13.90

Table C.1 (cont'd)

NSVS id	l °	b °	P days	A_V	m
9484367	189.368423	-23.337019	0.26079	0.55	13.05
9485503	187.265701	-21.639187	0.44008	0.73	13.64
9486446	186.592361	-20.894581	0.27852	0.76	13.93
9927549	199.626419	10.973780	0.39139	0.50	12.71
9984319	202.956223	18.949072	0.27153	0.46	12.07
10080683	200.374664	24.779287	0.35201	0.53	12.79
10085444	204.301056	24.539936	0.23049	0.40	12.24
10086452	200.299057	26.250927	0.34409	0.56	12.46
10123418	204.092941	33.455822	0.22930	0.58	13.09
10147580	211.705490	30.349247	0.26092	0.39	12.10
10160266	215.518097	33.173321	0.40620	0.39	11.70
10169623	216.495697	36.472832	0.31783	0.53	13.61
10180261	222.951645	38.080631	0.31676	0.43	11.07
10207146	215.972046	42.685646	0.29703	0.65	12.86
10223742	210.146011	49.702747	0.42224	0.34	12.47
10235317	221.664581	43.344654	0.28889	0.41	11.03
10323641	244.010910	66.136841	0.34565	0.54	12.32
10332963	230.258057	65.629097	0.42128	0.59	13.85
10346621	241.079361	69.984459	0.36283	0.53	11.91
10471644	1.023201	72.226959	0.23804	0.37	12.21
10502199	3.303787	63.435036	0.38629	0.79	13.75
10548943	10.844966	61.338264	0.27900	0.75	13.72
10556949	17.241270	59.329361	0.28188	0.58	12.27
10568869	12.773267	52.310093	0.34080	0.57	11.43
10585624	24.019337	58.033188	0.34007	0.58	12.96
10606707	27.938969	52.209923	0.31308	0.51	12.98
10618445	35.712620	49.147488	0.27906	0.81	13.77
10626169	19.616404	50.262951	0.33523	0.69	13.40
10631442	24.238859	49.640526	0.31701	0.66	13.93
10706395	38.368664	40.218548	0.32937	0.63	13.76
10713473	36.855305	37.456886	0.31458	0.34	11.68
10733284	23.900723	35.380604	0.26698	0.40	12.28
10774934	32.809776	27.483202	0.30979	0.37	11.42
10806788	39.635838	31.522345	0.22912	0.39	11.48

Table C.1 (cont'd)

NSVS id	l °	b °	P days	A_V	m
10812050	42.118481	30.949932	0.36286	0.33	11.80
10826152	39.984615	27.047895	0.32386	0.57	12.82
10851353	39.993771	23.606880	0.26879	0.63	12.54
10897604	32.822731	19.708948	0.32010	0.40	12.38
10907674	35.256382	18.842327	0.24507	0.65	12.32
10915546	35.179249	17.288055	0.22819	0.42	10.20
10939618	41.372036	15.699781	0.36838	0.63	13.55
11039298	47.618771	12.887670	0.35159	0.61	12.75
11062878	48.221699	9.143929	0.28932	0.54	12.42
11087999	41.420021	10.672621	0.30142	0.64	12.83
11216261	50.880520	1.606691	0.24683	0.42	12.13
11369857	50.122723	-15.536270	0.31770	0.57	12.72
11453654	63.576683	-9.674345	0.25418	0.33	11.81
11464227	60.655930	-13.752760	0.23879	0.41	12.47
11577968	60.127472	-27.774405	0.22683	0.50	12.80
11621286	71.004814	-19.387995	0.34005	0.59	11.45
11623858	69.877548	-20.859077	0.24818	0.44	12.57
11649451	69.982460	-24.233786	0.42980	0.39	12.26
11698983	69.592484	-28.107746	0.28855	0.57	11.52
11725468	71.255241	-36.350800	0.28969	0.54	13.37
11757787	80.467873	-28.427000	0.25250	0.43	12.57
11857987	89.668961	-37.759232	0.26223	0.48	12.05
11879431	96.460945	-42.858765	0.32950	0.55	13.47
11906467	87.822990	-60.046894	0.27687	0.58	12.59
11963569	112.625015	-66.796928	0.34457	0.73	13.40
11990107	126.982407	-56.003624	0.32774	0.68	13.12
12017790	151.363556	-56.503864	0.30161	0.53	13.43
12034782	162.110748	-63.234550	0.30149	0.50	12.37
12046016	167.950302	-57.758030	0.32172	0.52	11.00
12149036	184.826996	-37.055897	0.22594	0.46	12.59
12167526	192.179779	-41.029232	0.24545	0.63	12.50
12209023	193.308502	-31.752964	0.24372	0.42	12.99
12267781	201.252701	-26.459351	0.37567	0.68	13.23
12353908	200.849594	-13.951427	0.23999	0.71	13.84

Table C.1 (cont'd)

NSVS id	l o	b o	P days	A_V	m
12369230	203.603531	-11.522971	0.27460	0.70	13.51
12380585	204.410599	-18.186193	0.42615	0.35	10.67
12453519	204.926636	-9.210847	0.37149	0.53	13.55
12694915	214.695679	10.350087	0.32186	0.57	11.73
12731514	215.389542	15.571384	0.39644	0.62	10.59
12967357	226.682434	32.349972	0.23614	0.61	11.42
13000052	236.707275	39.560318	0.23277	0.42	10.37
13009628	236.866974	33.922630	0.28220	0.45	12.75
13036186	248.927719	38.748844	0.31369	0.46	11.31
13079296	245.522186	53.159607	0.25511	0.48	13.48
13087665	249.339996	45.366241	0.31662	0.57	12.63
13093893	256.448029	43.921864	0.30583	0.34	11.89
13095859	253.526199	47.513908	0.36333	0.79	13.78
13240381	313.264801	60.297836	0.40686	0.67	13.96
13266377	321.576935	61.795872	0.33975	0.63	12.97
13291516	325.051422	59.433193	0.23684	0.37	12.45
13320653	343.322998	52.414982	0.28964	0.65	13.60
13340275	347.153503	56.308456	0.40640	0.36	12.20
13341685	354.635742	59.910160	0.32534	0.67	13.67
13366719	345.269775	52.419621	0.33437	0.80	13.76
13370177	345.115875	49.889870	0.38076	0.60	13.41
13375187	348.334015	49.467781	0.22937	0.44	11.74
13400513	358.205261	43.064568	0.31690	0.57	11.77
13472973	3.287261	38.329628	0.49645	0.29	11.44
13503007	8.770260	30.468061	0.29747	0.43	12.29
13557030	19.093407	31.544914	0.35044	0.34	11.64
13570725	22.115299	29.422520	0.51541	0.33	12.09
13573565	25.865915	30.438231	0.29314	0.30	11.07
13600796	15.968682	27.352701	0.22706	0.62	13.66
13602900	13.747386	25.516621	0.26189	0.54	12.21
13704508	31.174009	22.233915	0.22680	0.43	11.53
13713798	29.543032	19.585894	0.27038	0.35	11.61
13922338	39.917992	2.994995	0.26918	0.33	10.80
14180830	38.607605	-17.254089	0.22860	0.53	10.66

Table C.1 (cont'd)

NSVS id	l °	b °	P days	A_V	m
14300598	49.212009	-23.369699	0.26789	0.35	11.94
14307859	47.768051	-25.661430	0.25678	0.56	12.08
14438283	55.001221	-35.276958	0.21556	1.00	13.71
14453645	62.972698	-35.648949	0.43574	0.39	11.42
14539755	67.066093	-46.989979	0.23866	0.57	12.32
14541901	70.442497	-45.861233	0.29919	0.42	9.84
14559767	64.403938	-48.313282	0.25476	0.62	12.62
14621398	81.396339	-65.644630	0.24071	0.44	10.71
14654114	78.278465	-73.444740	0.52726	0.41	11.14
14705456	134.187531	-74.781601	0.29327	0.38	10.50
14729341	171.963501	-68.946083	0.31030	0.65	13.88
14764485	185.941376	-65.612328	0.32369	0.57	11.99
14781930	192.958328	-58.177902	0.22854	0.39	12.28
14795340	206.172897	-61.483536	0.22941	0.48	12.71
14842973	204.712814	-45.165657	0.23231	0.61	13.48
14978941	211.267700	-26.932749	0.29721	0.53	11.39
14991786	212.463516	-23.585995	0.38348	0.35	12.18
15011994	215.439072	-20.786266	0.32698	0.41	12.39
15016085	217.333450	-20.273819	0.35242	0.42	12.38
15023875	218.002884	-18.242340	0.35186	0.48	11.42
15025254	214.496796	-16.237423	0.39405	0.70	13.14
15050581	221.178497	-21.091024	0.37677	0.55	13.41
15119318	221.964279	-15.036404	0.32008	0.43	12.06
15543698	233.198990	17.234991	0.42320	0.51	13.33
15544076	238.007584	14.104473	0.29579	0.30	10.88
15595338	241.334732	14.063331	0.23258	0.42	10.95
15686648	243.451218	28.464273	0.27135	0.42	11.23
15692686	241.929123	29.795527	0.40306	0.72	12.66
15708493	247.827560	31.840040	0.29397	0.39	13.19
15729930	250.731186	26.646395	0.22588	0.67	13.57
15863238	264.853271	43.760876	0.37696	0.58	12.57
15902803	276.642914	42.060917	0.23185	0.41	12.82
15955497	290.422241	51.627125	0.23257	0.40	13.01
15974125	300.917938	52.180897	0.33994	0.39	11.36

Table C.1 (cont'd)

NSVS id	l °	b °	P days	A_V	m
16018678	313.694458	41.739189	0.23924	0.60	10.56
16166066	331.316681	35.591228	0.32669	0.56	12.83
16194218	340.596008	32.168770	0.29107	0.72	13.61
16227319	348.924164	40.462734	0.30647	0.93	13.93
16283847	348.319061	30.736151	0.41656	0.40	11.77
16309498	351.261719	24.674549	0.34379	0.39	11.83
16376359	7.460183	26.933979	0.32324	0.70	13.60
16394081	7.018230	22.772858	0.23674	0.58	12.95
16989220	32.024185	-17.849466	0.46488	0.39	11.60
17002449	19.758013	-16.422264	0.26265	0.49	13.05
17048204	22.126772	-24.500483	0.45608	0.52	12.02
17116519	33.204647	-25.590487	0.23823	0.61	12.74
17135302	35.831547	-26.902031	0.39448	0.60	12.95
17151684	37.791306	-29.898062	0.33711	0.62	12.86
17212680	35.381809	-39.516193	0.27344	0.53	11.56
17265263	40.846790	-43.426998	0.20746	0.54	13.10
17269781	42.396095	-44.464317	0.22590	0.31	11.51
17285380	29.807364	-44.991295	0.33843	0.69	12.78
17287608	31.605921	-45.433327	0.36182	0.65	13.63
17382133	47.676540	-64.497932	0.31421	0.49	12.68
17386234	54.971199	-65.197739	0.23505	0.38	10.21
17573448	223.055145	-62.259953	0.39312	0.54	13.11
17577125	218.708984	-59.753479	0.26334	0.40	10.36
17638053	226.400406	-45.503700	0.24039	0.39	11.88
17675110	229.249939	-40.073483	0.26532	0.39	12.50
18318050	257.396454	16.238852	0.24192	0.45	12.78
18433211	262.634399	22.002930	0.26221	0.73	13.38
18440572	263.592957	23.588711	0.35549	0.46	12.75
18458089	264.556000	27.165705	0.27267	0.48	12.68
18501806	275.353973	17.750219	0.22919	0.58	13.11
18563622	277.448639	31.715849	0.27605	0.61	12.57
18720155	299.633087	31.741343	0.35076	0.47	12.03
19101566	349.918701	23.798420	0.25418	0.55	11.76
19937092	28.336639	-56.363834	0.22799	0.63	13.00

Table C.1 (cont'd)

NSVS id	l °	b °	P days	A_V	m
19989934	30.672920	-68.631020	0.30562	0.47	12.36

BIBLIOGRAPHY

Akerlof, C., Alcock, C., Allsman, R., Axelrod, T., Bennett, D. P., Cook, K. H., Freeman, K., Griest, K., Marshall, S., Park, H.-S., Perlmutter, S., Peterson, B., Quinn, P., Reimann, J., Rodgers, A., Stubbs, C. W., & Sutherland, W. 1994, ApJ, 436, 787

Akerlof, C., Amrose, S., Balsano, R., Bloch, J., Casperson, D., Fletcher, S., Gisler, G., Hills, J., Kehoe, R., Lee, B., Marshall, S., McKay, T., Pawl, A., Schaefer, J., Szymanski, J., & Wren, J. 2000b, AJ, 119, 1901

Akerlof, C., Balsano, R., Barthelemy, S., Bloch, J., Butterworth, P., Casperson, D., Cline, T., Fletcher, S., Frontera, F., Gisler, G., Heise, J., Hills, J., Kehoe, R., Lee, B., Marshall, S., McKay, T., Miller, R., Piro, L., Priedhorsky, W., Szymanski, J., & Wren, J. 1999, Nature, 398, 400

Akerlof, C., Balsano, R., Barthelmy, S., Bloch, J., Butterworth, P., Casperson, D., Cline, T., Fletcher, S., Frontera, F., Gisler, G., Heise, J., Hills, J., Hurley, K., Kehoe, R., Lee, B., Marshall, S., McKay, T., Pawl, A., Piro, L., Szymanski, J., & Wren, J. 2000a, ApJ, 532, L25

Alcock, C., Allsman, R., Alves, D. R., Axelrod, T., Becker, A., Bennett, D., Clement, C., Cook, K. H., Drake, A., Freeman, K., Geha, M., Griest, K., Kovács, G., Kurtz, D. W., Lehner, M., Marshall, S., Minniti, D., Nelson, C., Peterson, B., Popowski, P., Pratt, M., Quinn, P., Rodgers, A., Rowe, J., Stubbs, C., Sutherland, W., Tomaney, A., Vandehei, T., & Welch, D. L. 2000, ApJ, 542, 257

Alcock, C., Allsman, R. A., Axelrod, T. S., Bennett, D. P., Cook, K. H., Freeman, K. C., Griest, K., Marshall, S. L., Peterson, B. A., Pratt, M. R., Quinn, P. J., Reimann, J., Rodgers, A. W., Stubbs, C. W., Sutherland, W., & Welch, D. L. 1995, AJ, 109, 1653

Alcock, C., Alves, D. R., Axelrod, T. S., Becker, A. C., Bennett, D. P., Clement, C. M., Cook, K. H., Drake, A. J., Freeman, K. C., Geha, M., Griest, K., Lehner, M. J., Marshall, S. L., Minniti, D., Muzzin, A., Nelson, C. A., Peterson, B. A., Popowski, P., Quinn, P. J., Rodgers, A. W., Rowe, J. F., Sutherland, W., Vandehei, T., & Welch, D. L. 2004, AJ, 127, 334

Arp, H. C. 1955, AJ, 60, 317

Bailey, S. I. 1902, Annals of Harvard College Observatory, 38, 1

Bekki, K. & Chiba, M. 2001, ApJ, 558, 666

Benedict, G. F., McArthur, B. E., Fredrick, L. W., Harrison, T. E., Lee, J., Slesnick, C. L., Rhee, J., Patterson, R. J., Nelan, E., Jefferys, W. H., van Altena, W., Shelus, P. J., Franz, O. G., Wasserman, L. H., Hemenway, P. D., Duncombe, R. L., Story, D., Whipple, A. L., & Bradley, A. J. 2002, AJ, 123, 473

Bertin, E. & Arnouts, S. 1996, A&AS, 117, 393

Binney, J. & Merrifield, M. 1998, Galactic Astronomy (Princeton, NJ : Princeton University Press)

Blažko, S. 1907, Astronomische Nachrichten, 175, 325

Bono, G., Caputo, F., Castellani, V., & Marconi, M. 1996, ApJ, 471, L33+

Bono, G., Caputo, F., Castellani, V., Marconi, M., Storm, J., & Degl'Innocenti, S. 2003, MNRAS, 344, 1097

Bookmeyer, B. B., Fitch, W. S., Lee, T. A., Wisniewski, W. Z., & Johnson, H. L. 1977, Revista Mexicana de Astronomia y Astrofisica, 2, 235

Cacciari, C. & Clementini, G. 2003, Lecture Notes in Physics, Berlin Springer Verlag, 635, 105

Cacciari, C., Clementini, G., & Fernley, J. A. 1992, ApJ, 396, 219

Carney, B. W., Laird, J. B., Latham, D. W., & Aguilar, L. A. 1996, AJ, 112, 668

Carretta, E., Gratton, R. G., Clementini, G., & Fusi Pecci, F. 2000, ApJ, 533, 215

Carroll, B. W. & Ostlie, D. A. 1996, An introduction to modern astrophysics (Reading, Mass. : Addison-Wesley Pub.)

Catelan, M. 2004, astro-ph/0310159

Chaboyer, B. 1999, in ASSL Vol. 237: Post-Hipparcos cosmic candles, 111–+

Chiba, M. & Beers, T. C. 2000, AJ, 119, 2843

Clement, C. M., Muzzin, A., Dufton, Q., Ponnampalam, T., Wang, J., Burford, J., Richardson, A., Rosebery, T., Rowe, J., & Hogg, H. S. 2001, AJ, 122, 2587

Clement, C. M. & Rowe, J. 2000, AJ, 120, 2579

Cousens, A. 1983, MNRAS, 203, 1171

Eggen, O. J., Lynden-Bell, D., & Sandage, A. R. 1962, ApJ, 136, 748

Fernley, J. A., Skillen, I., Jameson, R. F., & Longmore, A. J. 1990, MNRAS, 242, 685

Hartwick, F. D. A. 1987, in Proceedings of the NATO ASIC : The Galaxy (Dordrecht: D. Reidel Publishing Co.), 281–290

Heiser, A. M. 1996, AJ, 112, 2142

Hoeg, E., Bässgen, G., Bastian, U., Egret, D., Fabricius, C., Großmann, V., Halbwachs, J. L., Makarov, V. V., Perryman, M. A. C., Schwekendiek, P., Wagner, K., & Wicenec, A. 1997, A&A, 323, L57

Jameson, R. F. 1986, Vistas in Astronomy, 29, 17

Jin, H., Kim, S.-L., Kwon, S.-G., Youn, J.-H., Lee, C.-U., Lee, D.-J., & Kim, K.-S. 2003, A&A, 404, 621

Jurcsik, J. & Kovacs, G. 1996, A&A, 312, 111

Kehoe, R., Akerlof, K., Balsano, R., Barthelmy, S., Bloch, J., Butterworth, P., Casperson, D., Cline, T., Fletcher, S., Frontera, F., Gisler, G., Heise, J., Hills, J., Hurley, K., Lee, B., Marshall, S., McKay, T., Pawl, A., Piro, L., Priedhorsky, B., Szymanski, J., & Wren, J. 2001, in Supernovae and Gamma-Ray Bursts: the Greatest Explosions since the Big Bang, eds. Mario Livio, Nino Panagia, and Kailash Sahu (Cambridge, UK: Cambridge University Press), 47–66

Kemper, E. 1982, AJ, 87, 1395

Kholopov, P. N. 1985, Obschii katalog peremennykh zvezd : chetvertoe izdanie, soderzhashchee svedeniia O peremennykh zvezdakh, otkrytykh i oboznachennykh do 1982 g. / P. (Obschii katalog peremennykh zvezd : chetvertoe izdanie, soderzhashchee svedeniia o peremennykh zvezdakh, otkrytykh i oboznachennykh do 1982 g. / P. N. Kholopov. Moskva : Nauka, 1985-1995.)

King, D. S. & Cox, J. P. 1968, PASP, 80, 365

King, I., Gilmore, G., & van der Kruit, P. C. 1990, The Milky Way As Galaxy (Mill Valley, California:University Science Books)

Kinman, T. D., Suntzeff, N. B., & Kraft, R. P. 1994, AJ, 108, 1722

Kolenberg, K. 2004, Communications in Asteroseismology, 145, 16

Kovács, G. 2001, in Stellar pulsation - Nonlinear Studies, eds. Mine Takeuti and Dimitar D. Sasselov, Vol. 257 (Dordrecht:Kluwer Academic Publishers), 61–101

Kovacs, G. & Kanbur, S. M. 1998, MNRAS, 295, 834

LaCluyzé, A., Smith, H. A., Gill, E.-M., Hedden, A., Kinemuchi, K., Rosas, A. M., Pritzl, B. J., Sharpee, B., Wilkinson, C., Robinson, K. W., Baldwin, M. E., & Samolyk, G. 2004, AJ, 127, 1653

Landolt, A. U. 1992, AJ, 104, 340

Layden, A. C. 1994, AJ, 108, 1016

—. 1995, AJ, 110, 2288

—. 1998, AJ, 115, 193

Layden, A. C., Hanson, R. B., Hawley, S. L., Klemola, A. R., & Hanley, C. J. 1996, AJ, 112, 2110

Layden, A. C. & Sarajedini, A. 2000, AJ, 119, 1760

Lee, J. & Carney, B. W. 1999, AJ, 118, 1373

Lee, Y., Demarque, P., & Zinn, R. 1990, ApJ, 350, 155

Lomb, N. R. 1976, Ap&SS, 39, 447

Longair, M. S. 1998, Galaxy formation (New York:Springer)

Lub, J. 1977, A&AS, 29, 345

Martínez-Delgado, D., Gómez-Flechoso, M. Á., Aparicio, A., & Carrera, R. 2004, ApJ, 601, 242

Mizerski, T. & Bejger, M. 2002, Acta Astronomica, 52, 61

Moskalik, P. 1986, Acta Astronomica, 36, 333

Norris, J. E. 1994, ApJ, 431, 645

Oosterhoff, P. T. 1939, The Observatory, 62, 104

—. 1944, Bull. Astron. Inst. Netherlands, 10, 55

Peacock, J. A. 1999, Cosmological physics (Cambridge, UK:Cambridge University Press)

Pena, J. H., Diaz, L. M., & Peniche, R. 1990, Revista Mexicana de Astronomia y Astrofisica, 20, 139

Petersen, J. O. 1973, A&A, 27, 89

Petit, M. 1987, Variable stars (Chichester, England and New York:John Wiley and Sons)

Popowski, P. 2001, MNRAS, 321, 502

Poretti, E. 2001, A&A, 371, 986

Press, W. H. & Rybicki, G. B. 1989, ApJ, 338, 277

Press, W. H., Teukolsky, S. A., Vetterling, W. T., & Flannery, B. P. 1992, Numerical recipes in FORTRAN. The art of scientific computing 2nd ed. (Cambridge, UK:Cambridge University Press)

Preston, G. W. 1959, ApJ, 130, 507+

Pritzl, B., Smith, H. A., Catelan, M., & Sweigart, A. V. 2000, ApJ, 530, L41

Reimann, J. D. 1994, Ph.D. Thesis

Rice, J. A. 1995, Mathematical Statistics and Data Analysis (Belmont, California:Duxbury Press)

Rich, R. M. 1998, in ASP Conf. Ser. 147: Abundance Profiles: Diagnostic Tools for Galaxy History, eds .D. Friedli,M. Edmunds, C. Robert, and L. Drissen, Vol. 147 (San Francisco, ASP), 36–+

Rucinski, S. M. 1993, PASP, 105, 1433

—. 1997, AJ, 113, 407

Sandage, A. 2004, AJ, 128, 858

Sandage, A., Katem, B., & Sandage, M. 1981, ApJS, 46, 41

Scargle, J. D. 1982, ApJ, 263, 835

Schlegel, D. J., Finkbeiner, D. P., & Davis, M. 1998, ApJ, 500, 525

Schwarzenberg-Czerny, A. 1989, MNRAS, 241, 153

—. 1998, Baltic Astronomy, 7, 43

Searle, L. & Zinn, R. 1978, ApJ, 225, 357

Simon, N. R. 1979, A&A, 74, 30

Simon, N. R. & Teays, T. J. 1982, ApJ, 261, 586

Skillen, I., Fernley, J. A., Stobie, R. S., Marang, F., & Jameson, R. F. 1993, South African Astronomical Observatory Circular, 15, 90

Smith, H. A. 1995, RR Lyrae stars (Cambridge Astrophysics Series, Cambridge, New York: Cambridge University Press)

Sommer-Larsen, J., Beers, T. C., Flynn, C., Wilhelm, R., & Christensen, P. R. 1997, ApJ, 481, 775

Stellingwerf, R. F. 1978, ApJ, 224, 953

Stetson, P. B. 1987, PASP, 99, 191

—. 1996, PASP, 108, 851

Suntzeff, N. B., Kinman, T. D., & Kraft, R. P. 1991, ApJ, 367, 528

Szymanski, M., Kubiak, M., & Udalski, A. 2001, Acta Astronomica, 51, 259

van Albada, T. S. & Baker, N. 1973, ApJ, 185, 477

van Leeuwen, F., Evans, D. W., Grenon, M., Grossmann, V., Mignard, F., & Perryman, M. A. C. 1997, A&A, 323, L61

Vivas, A. K., Zinn, R., Abad, C., Andrews, P., Bailyn, C., Baltay, C., Bongiovanni, A., Briceño, C., Bruzual, G., Coppi, P., Della Prugna, F., Ellman, N., Ferrín, I., Gebhard, M., Girard, T., Hernandez, J., Herrera, D., Honeycutt, R., Magris, G., Mufson, S., Musser, J., Naranjo, O., Rabinowitz, D., Rengstorf, A., Rosenzweig, P., Sánchez, G., Sánchez, G., Schaefer, B., Schenner, H., Snyder, J. A., Sofia, S., Stock, J., van Altena, W., Vicente, B., & Vieira, K. 2004, AJ, 127, 1158

Welch, D. L. & Stetson, P. B. 1993, AJ, 105, 1813

Wils, P. 2001, Informational Bulletin on Variable Stars, 5134, 1

Woźniak, P. R., Vestrand, W. T., Akerlof, C. W., Balsano, R., Bloch, J., Casperson, D., Fletcher, S., Gisler, G., Kehoe, R., Kinemuchi, K., Lee, B. C., Marshall, S., McGowan, K. E., McKay, T. A., Rykoff, E. S., Smith, D. A., Szymanski, J., & Wren, J. 2004, AJ, 127, 2436

Zinn, R. 1993, in ASP Conf. Ser. 48: The Globular Cluster-Galaxy Connection, eds. Graeme H. Smith, and Jean P. Brodie (San Francisco: Astronomical Society of the Pacific (ASP)), 38–+

Zinn, R. & West, M. J. 1984, ApJS, 55, 45